INFORMATION TO USERS

This manuscript has been reproduced from the microfilm master. UMI films the text directly from the original or copy submitted. Thus, some thesis and dissertation copies are in typewriter face, while others may be from any type of computer printer.

The quality of this reproduction is dependent upon the quality of the copy submitted. Broken or indistinct print, colored or poor quality illustrations and photographs, print bleedthrough, substandard margins, and improper alignment can adversely affect reproduction.

In the unlikely event that the author did not send UMI a complete manuscript and there are missing pages, these will be noted. Also, if unauthorized copyright material had to be removed, a note will indicate the deletion.

Oversize materials (e.g., maps, drawings, charts) are reproduced by sectioning the original, beginning at the upper left-hand corner and continuing from left to right in equal sections with small overlaps. Each original is also photographed in one exposure and is included in reduced form at the back of the book.

Photographs included in the original manuscript have been reproduced xerographically in this copy. Higher quality 6" x 9" black and white photographic prints are available for any photographs or illustrations appearing in this copy for an additional charge. Contact UMI directly to order.

UMI

A Bell & Howell Information Company
300 North Zeeb Road, Ann Arbor MI 48106-1346 USA
313/761-4700 800/521-0600

Université d'Ottawa · University of Ottawa

AN INTERPRETATION OF HIGH RESOLUTION AEROMAGNETIC DATA OVER THE MANITOUWADGE GREENSTONE BELT, ONTARIO, CANADA

by

Warner Frederick Miles

A thesis submitted to the School of Graduate Studies and Research

in partial fulfillment of the requirements

for the degree of M.Sc. in Earth Sciences

OTTAWA-CARLETON GEOSCIENCE CENTRE

AND

UNIVERSITY OF OTTAWA

OTTAWA, CANADA

ABSTRACT

The aim of this study is to interpret aeromagnetic data using 3D techniques. The data consist of eleven high resolution surveys over the Manitouwadge greenstone belt of the Superior Province, Ontario. The interpretation was calibrated to the detailed geological mapping of the area by Zaleski et. al. (1995)

The study has three components. First, the data and grid quality were maximized to maintain as much of the high frequency component of the flight line data as possible while minimizing levelling e rors and gridding artefacts. Second, a number of 3D interpretation techniques was investigated. Third, the 3D interpretation techniques were applied to the data over the Manitouwadge study area.

Grid improvement techniques, particularly micro-levelling and trend reinforcement, were found to be necessary to maximize grid quality.

The 3D interpretation techniques used included apparent magnetic susceptibility mapping, analytic signal, horizontal gradient of pseudo-gravity, potential field tilt and Euler deconvolution as well as first and second vertical derivatives. Each method enhances a different component of the total field intensity and complemented each other when interpreted in combination. The apparent susceptibility map combined with the horizontal gradient of pseudo-gravity maxima produced an image that approximates the mapped geology.

Calibrating the magnetic interpretation to the known geology allowed the extrapolation of supracrustal rock units into areas of limited geological mapping. The presence of supracrustal units in the engulfing Black Pic tonalitic batholith extends the geological mapping and illustrates regional deformation.

STATEMENT OF ORIGINAL CONTRIBUTION

This thesis reports the results of an original study, carried out by the author. It involves the processing and interpretation of high resolution aeromagnetic data sets that had not previously been analysed in a quantitative manner, in order to improve the understanding of the structure and physical properties of the Manitouwadge region. The study makes extensive use of computers to manipulate, filter, analyse and visualize geophysical data. Naturally, existing computer programs at the Geological Survey of Canada (GSC) were used whenever possible to accomplish routine tasks. In many cases, these programs had to be adapted by the author in order to handle high resolution data, and in other cases completely new algorithms were written. This statement intends to provide an accurate representation of the original contributions made by the author to the software development.

Routine programs for gridding, frequency domain filtering and displaying potential field data were all written by GSC staff, and used as basic tools by the author. The author routinely supports development of improved software in discussions with GSC colleagues. Significant programming efforts by the author were spent on routines to handle the high resolution profile data, including format conversion routines to import the data, profile data manipulation software including arithmetic functions and International Geomagnetic Reference Field removal, as well as programs to calculate statistics on point, profile and gridded data sets.

In order to manipulate the grids a number of programs were written by the author. These include programs that: perform functions using two input grids including arithmetic, nulling and matching functions; adjust grid values by addition, multiplication, and the application of logarithmic functions; fit a polynomial of user-specified order to a grid; extract a grid to exact

boundaries plus or minus a user-specified distance (the author added this functionality to a pre-existing program).

A program was written to calculate the apparent magnetic susceptibility from a grid of magnetic data that has been reduced to the pole and downward continued to the Earth's surface. To calibrate the apparent susceptibility grid to measured susceptibilities, a program to interpolate values from a grid at given locations was written. The trend reinforcement software written by Pierre Keating was adapted by the author to use standard format data and to run in a UNIX environment. A program to calculate the analytic signal from grids of the three orthogonal derivatives was also written by the author based on the published mathematical derivation. The Euler deconvolution software was altered to correct horizontal location errors and to output the depth solutions formatted for use in display software as dots colour keyed to the depth.

TABLE OF CONTENTS

LIST OF TABLES

LIST OF FIGURES

ACKNOWLEDGEMENTS

This thesis was supervised by Dr. Walter Roest and Dr. Keith Benn. I am grateful to my co-workers at the Geological Survey of Canada including Dr. Roest, Greg Boyce, Regis Dumont, Frank Kiss, Dr. Pierre Keating, Dr. Mark Pilkington, James Rupert and Dr. Mike Thomas for their helpful suggestions and support. This work would not have been possible without the support of Ms. Joan Tod, Head, Regional Geophysics, Geological Survey of Canada, who provided access to computing facilities, permission to use the magnetic data, and encouragement.

Dr. Eva Zaleski of the Continental Geoscience Division, Geological Survey of Canada, offered many helpful insights into the geology, initiated the acquisition of the magnetic data, and always has time to discuss the work. Many, many thanks.

Noranda Exploration Company Ltd. are acknowledged for their contribution of the high resolution aeromagnetic data to the National Aeromagnetic Data Base. Thanks to Mr. Larry Petrie for facilitating the release of these data.

This thesis was completed because: Jennifer showed it could be done within the gene pool, Fred took the kids while I did field work in Nevada, Sandra provided all ceramics used in this work, Sue gave up noodle lunches, Andy recommended alcohol beverages to get past the rough spots, Matt helped with the drinking, and Norm started it. Thanks.

Alison Elizabeth and Hayley Flossie Miles are acknowledged and thanked for their patience and cooperation.

Laurie Miles, as usual, organized the party.

INTRODUCTION

Eleven high resolution, detailed aeromagnetic surveys over the Manitouwadge greenstone belt of the Wawa subprovince, Superior Province, Ontario, were released to the Geological Survey of Canada for public distribution by Noranda Exploration Company Limited in January, 1997. The availability of these data coupled with the release of detailed geological mapping of part of that area by Zaleski et al. (1995) provided an opportunity to perform a calibrated interpretation using 3D (grid-based) methods.

The aims of this study were: to process, rationalize and evaluate the data; to interpret the data in a systematic manner employing 3D analytic techniques; and to address questions arising out of the preliminary interpretation of the data and the detailed geological mapping.

The general geology is summarized from the detailed mapping of Zaleski et al. (1995), which was supported by preliminary versions of the high resolution magnetics.

The eleven aeromagnetic surveys used in this thesis were improved with micro-levelling, levelling to the national datum and trend reinforcement techniques. The final levelled data set was released as Geological Survey of Canada Open File 3447.

The systematic interpretation of the magnetic data involved 3D (gridded data) techniques including apparent susceptibility mapping, analytic signal maxima, horizontal gradient of pseudo-gravity maxima, potential fields tilt method, and Euler deconvolution. Most of these methods have been developed within the last 10 years. Published model studies using these methods usually employ lower resolution, well conditioned, gridded data sets. The utility of these methods using data gridded to maximize resolution is a sub-text to this thesis. In places, 2.5 D profile modelling supported the 3D methods. These techniques were used to place semi-

quantitative constraints on the interpretation of magnetics, as opposed to simple pattern recognition in the preliminary interpretations of the detailed surveys. The interpretation was calibrated to the mapping of Zaleski et al. (1995).

The interpretation aim included investigating a number of specific questions about the preliminary interpretation and its relationship to the known geology: the nature of east-west oriented linear magnetic highs and lows within the area underlain by Quetico subprovince metasedimentary rocks; the nature of curvilinear magnetic features within the Black Pic batholith northwest of the Manitouwadge greenstone belt; folding of the Nama Creek pluton by the Blackman Lake antiform (the magnetic signature of the area is at odds with the geological interpretation); the nature and boundaries of non-exposed units north of the Loken Lake pluton; the relationship between the Manitouwadge greenstone belt and the Schreiber-Hemlo and Faries Lake greenstone belts.

1. GEOLOGY

1.1 REGIONAL GEOLOGY

The Manitouwadge greenstone belt (MGB) is located in the Wawa subprovince of the Superior Province. The Superior Province is an Archean craton that is subdivided into granite-greenstone, metasedimentary, plutonic and high grade gneiss subprovinces (Fig. 1.1). High grade gneiss subprovinces to the north and south bracket alternating granite-greenstone (volcano-plutonic) and metasedimentary subprovinces. The subprovinces young to the south with intervening metasedimentary subprovinces slightly younger than adjacent granite greenstone subprovinces. Ages range from 3.0 Ga to about 2.7 Ga (Card,1990, p.99).

The Wawa subprovince is a granite-greenstone terrane bounded to the north by the metasedimentary Quetico subprovince, to the south by the Minnesota River Valley high grade gneiss terrane, to the east by the Kapuskasing Structural Zone and to the west by the Trans-Hudson Orogen (Fig. 1.2). The granite-greenstone terrane is composed of two linear concentrations of greenstones intruded and separated by granitoid rocks where the granitoids comprise 70 to 80% of the subprovince. The northern concentration of greenstones include the Manitouwadge greenstone belt (Fig. 1.3), as well as the Dayohessarah-Kabinakagami, Hornepayne (Moshkinabi), and Schreiber-Hemlo greenstone belts. The Manitouwadge greenstone belt is adjacent to the boundary between the Wawa and Quetico subprovinces.

1.2 DETAILED GEOLOGY

Detailed geological mapping of the Manitouwadge greenstone belt has been performed by several authors (Pye, 1957, Milne, 1974 and Zaleski et al., 1995). Pye worked without the benefit of aeromagnetic data, Milne incorporated regional (800m line spacing)

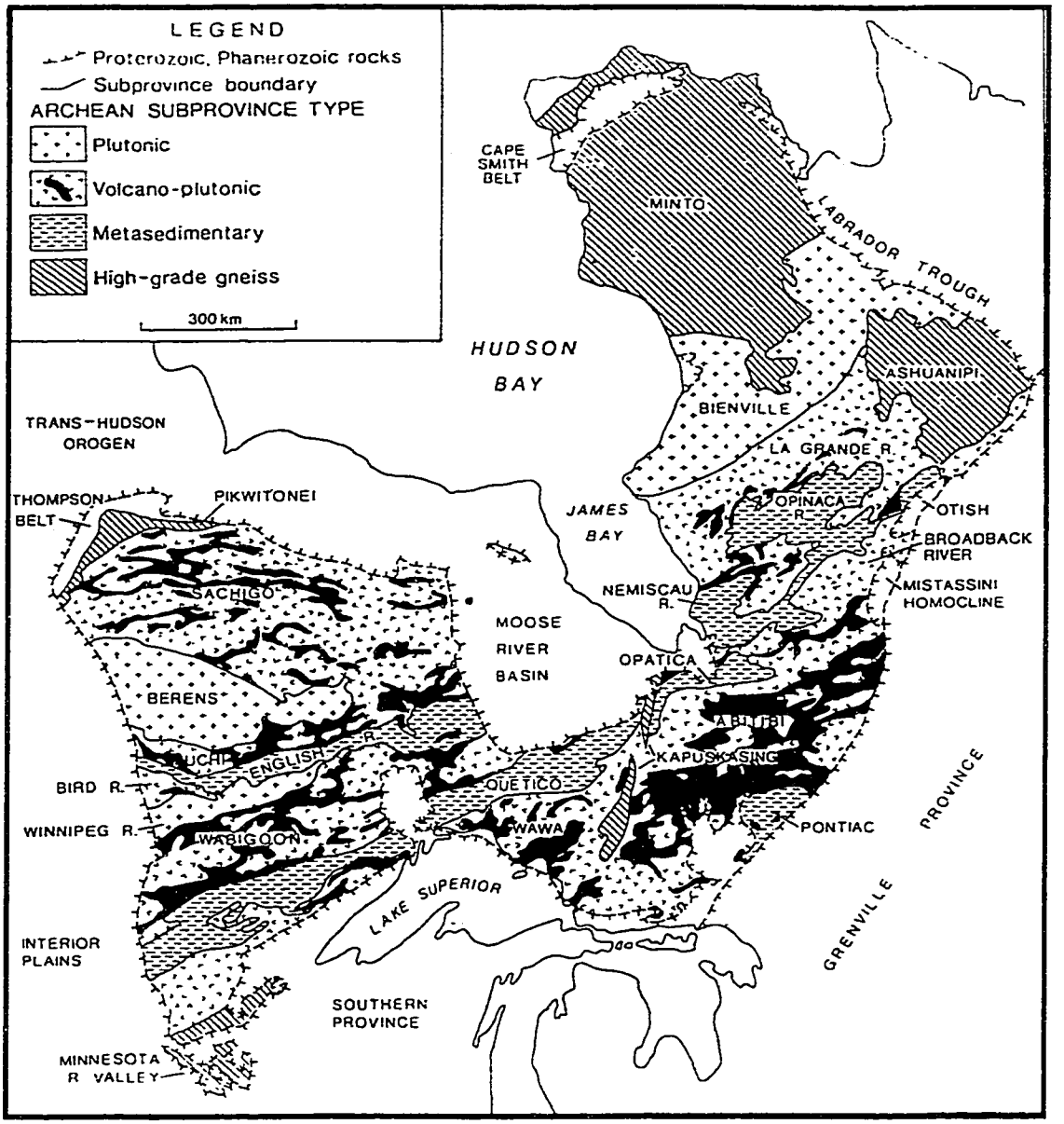

Fig. 1.1. Subprovinces of the Superior Province (from Card, 1990).

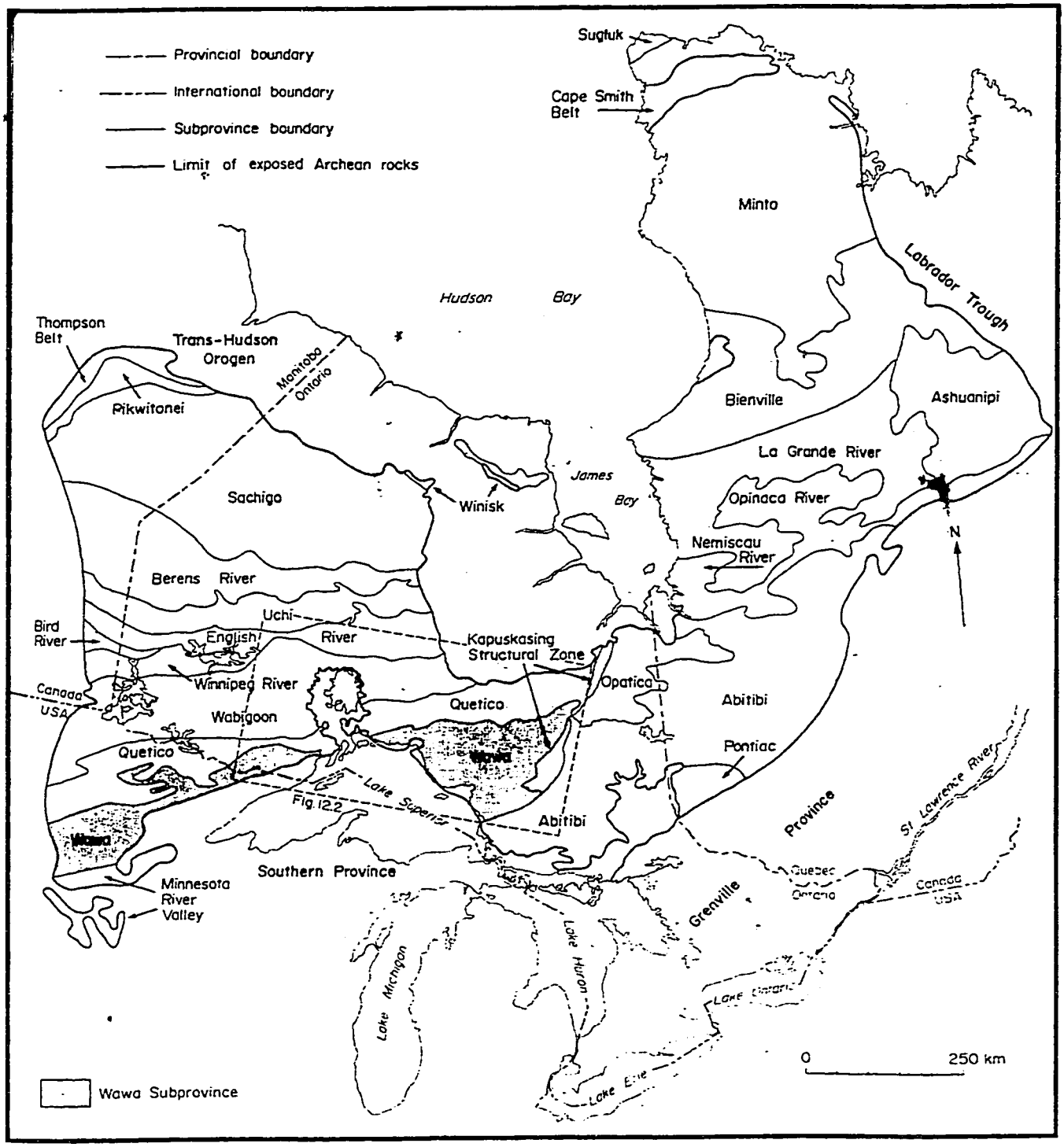

Fig. 1.2. Location of the Wawa Subprovince (from Williams et al., 1991)

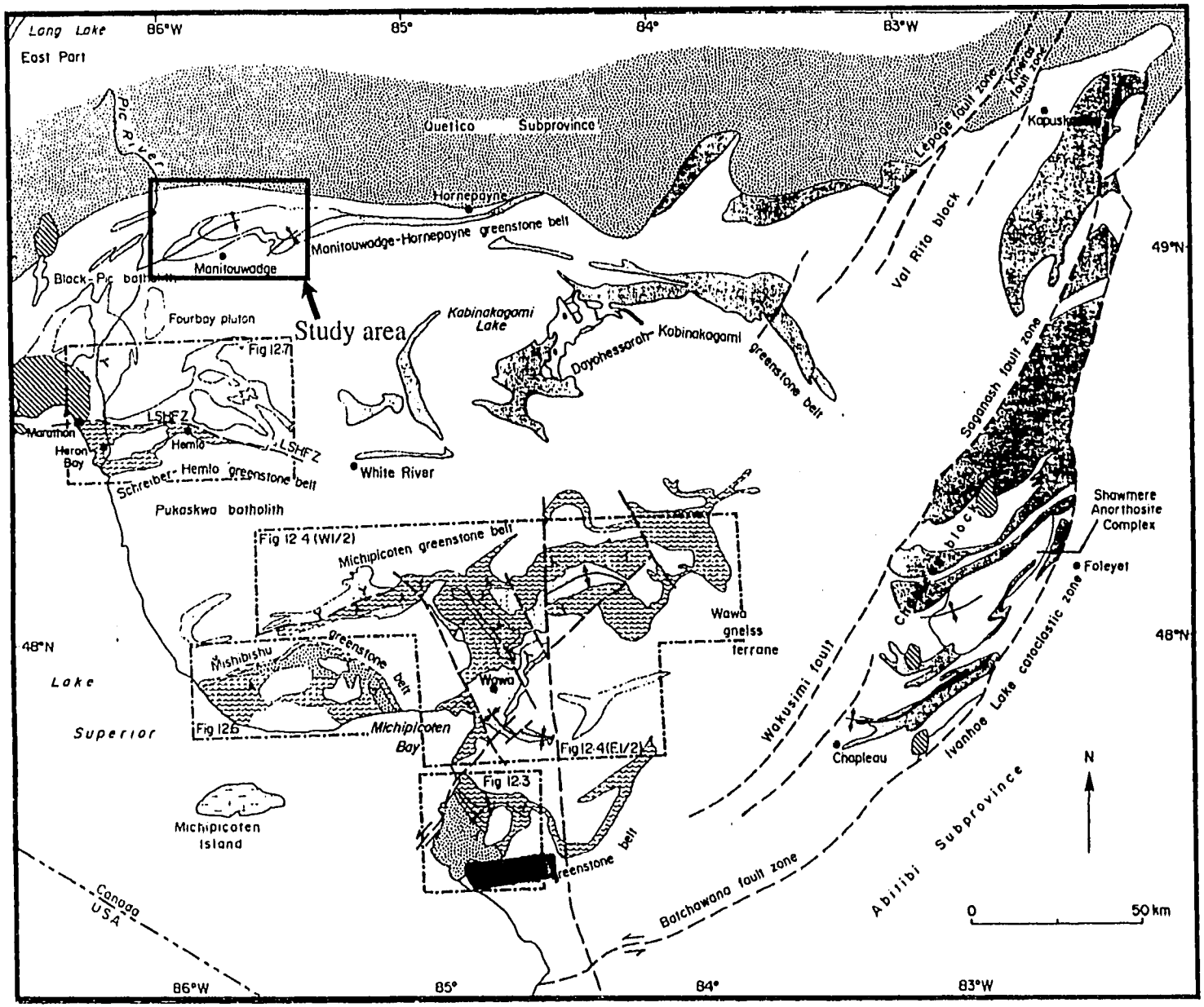

Fig. 1.3. Greenstone belts of the Wawa Subprovince (from Williams et al., 1991)

aeromagnetic data, as blackline contour maps, into his interpretation and Zaleski et al.(1995) made use of the high resolution total field and first vertical derivative maps also used in this study. The detailed geology, geochemistry, metamorphism, structural geology, description of ore deposits and geochronology in this section are summarized from Zaleski et al., 1995. Units described below are keyed to the mapped units on the Geological Survey of Canada's Open File 3034 'Geology of the Manitouwadge greenstone belt overlain on shaded relief of total field magnetics', Zaleski and Peterson, 1995 (see Map 1 attached to this thesis).

The Manitouwadge greenstone belt consists of a mafic to felsic succession of volcanic rocks and associated synvolcanic intrusions (Fig. 1.4). The greenstone belt is engulfed by syn- to post-tectonic granitoid intrusions. The geological map is dominated by D_3 folding, most notably the Manitouwadge synform, with greatest thicknesses of volcanics in the hinge regions. An inner and an outer volcanic belt (IVB and OVB, respectively) are also defined as volcanics lying north and south, respectively, of a unit of metasediments along the southern limb of the Manitouwadge synform. To the north, the greenstone belt is infolded with migmatitic metasediments of the Quetico subprovince. These Archean supracrustal and intrusive rocks are cut by three generations of Proterozoic dykes and numerous faults.

Mafic metavolcanic rocks (unit 3) are strongly foliated, fine grained homogeneous to thinly layered schists usually interleaved with medium to coarse grained metagabbro. This unit may be locally pillowed, although not suitable for accurate younging and structural facing determinations. The protolith to these intensely deformed mafic rocks is difficult to determine. The typical mineral assemblage of these mafic schists includes hornblende-plagioclase±garnet±biotite±clinopyroxene with quartz, magnetite, titanite, sulphide minerals

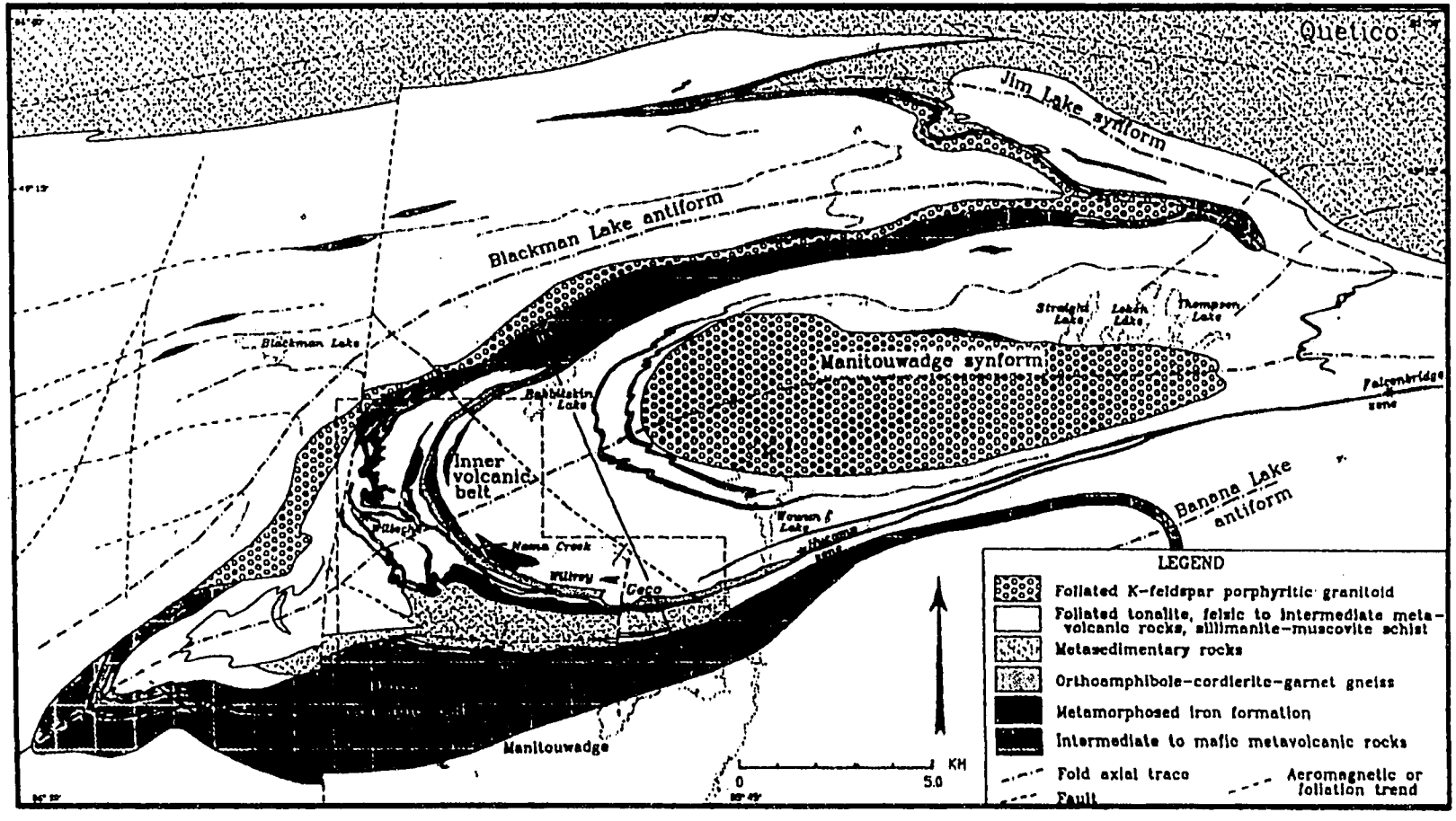

Fig. 1.4. Generalized Archean geology of the Manitouwadge greenstone belt (study area). (from Zaleski et al., 1995)

and apatite in accessory or trace amounts. In the outer volcanic belt, zones of up to 40% garnet including quartz, magnetite and cummingtonite are common. The outer belt mafic metavolcanics are folded to the west around the Manitouwadge synform and thin to the east and possibly are folded to the south toward the Faries Lake greenstone belt around the Banana Lake antiform.

Mixed mafic and felsic metavolcanic rocks (unit 4) consist of mafic and felsic layers either extruded at the same time or tectonically interleaved. The dominant mafic layers are strongly foliated hornblende-plagioclase schist similar to the mafic volcanic rocks of unit 3. Magnetite may be a component. Felsic layers are schists containing plagioclase and biotite with phenocrysts of quartz, magnetite and garnet. Calc-silicate rocks in some areas were intepreted as altered felsic volcanics with interleaved mafic volcanic layers. This unit is found exclusively in the hinge zone of the Manitouwadge synform in the inner volcanic belt. It is important to keep in mind when interpreting the magnetic intensity of these geologic units that there may be variable chemistry or alteration histories. Mappable units may not be geochemically or magnetically homogeneous.

Intermediate to mafic metavolcanic rocks (unit 5) are a mappable unit of a mixed group of rocks that are mostly hornblende-plagioclase, hornblende-plagioclase-biotite, and hornblende-plagioclase-garnet±clinopyroxene±magnetite schists. This unit is found in the inner volcanic belt, but can be traced through the major D_3 folds (Manitouwadge synform, Blackman Lake antiform and Jim Lake synform). The unit is only seen north of the Manitouwadge synform axial surface trace, except within the synvolcanic trondhjemite where it is referred to as the Dead Lake suite.

Intermediate to mafic metavolcanics are a strongly magnetic unit mapped in areas of poor exposure based on its magnetic signature. This mappable unit is characterized somewhat differently in 4 sub-areas.

From the Cadawaja fault to Rabbitskin Lake, mafic to intermediate and some felsic schist is homogeneous, laminated or layered and cut by many foliated pegmatite, granite and intrusions. Garnetiferous zones are common with garnet (30-40%) and magnetite (less than 10%).

South of Fox Lake, unit 5 is seen on both sides of the Nama Creek pluton and as inclusions in that pluton. Here the unit is fine grained, mafic to intermediate metavolcanic with hornblende-plagioclase±clinopyroxene±quartz±biotite with accessory titanite, magnetite and apatite. To the southeast of Fox Lake, interleaved pegmatitic granite and felsic schists grade locally to garnetiferous gneiss containing up to 50% garnet porphyroblasts in a fine grained matrix of hornblende, clinopyroxene and magnetite. These rocks are strongly magnetic.

Traced through the Blackman Lake and Jim Lake folds, the unit is thinly layered, fine to medium grained mafic to intermediate metavolcanics, foliated diorite and gabbro, the latter possibly being recrystallized mafic volcanic rock. The unit also contains interleaved iron formation. The unit here is characterized by mappable zones of highly magnetic metavolcanic screens in foliated tonalite and pegmatite.

The Dead Lake suite contains metavolcanics mapped as unit 5. The suite is found at the western end of the Loken Lake pluton within the synvolcanic trondhjemite and are folded to the north and south through the series of map-scale D_3 folds. Mappable units of the Dead

Lake suite are also seen within trondhjemite at the eastern end of the Loken Lake pluton. The suite is described as interleaved foliated gabbro, diorite and layered mafic to intermediate rocks that may be supracrustal. The assemblage is hornblende-magnetite±plagioclase ±garnet±clinopyroxene±sulphides. Quartz as eyes or lenticules can be 50% of the rock locally. The rocks are fine to medium grained and homogeneous in hand sample. Layered rocks are associated with magnetitic quartzites, interpreted as metachert or with mafic metavolcanics. The origin of these rocks is interpreted as metamorphosed and digested chert. Modified bedding and geochemistry support a supracrustal origin for the Dead Lake suite.

Unit 6 is termed felsic to intermediate metavolcanics but in fact consists of a number of difficult to map transitional rock types. Unit 6 occupies the hinge zone of the Manitouwadge synform in both the inner and outer volcanic belts. Rock types include fragmental rocks, calc-silicate, sillimanite-muscovite and felsic to intermediate schists, straight gneiss and . In the inner volcanic zone, the predominant rocks of this unit are homogeneous to weakly layered quartz-phyric to aphyric felsic schists with minor biotite±muscovite. The fragmental rocks have these felsic enclaves in a biotite±hornblende±garnet±magnetite matrix. The fragmental appearance may not be a primary feature. In the outer volcanic belt, unit 6 is largely felsic to intermediate metavolcanics and biotite schist intruded by foliated .

Aphyric felsic metavolcanic rocks (unit 7) occur in three areas around the outer volcanic belt either as breccias or laminated rocks. Highly deformed monolithic felsic breccia with fine grained to aphanitic felsic clasts in a biotite-muscovite or garnet-hornblende schist matrix are seen in 50m thick units folded around the Manitouwadge synform axial trace.

These rocks are associated with iron formation and disseminated sulphides (including pyrrhotite). Brecciated aphyric felsic schists interpreted as volcaniclastic rocks are mapped north of Gaug Lake between mafic metavolcanics and metasedimentary rocks. White, laminated quartz-rich felsic schist is mapped south of the Agam Lake fault on both sides of the Fox Creek fault and is interpreted as either volcanic or intrusive.

Quartz phyric felsic volcanics (unit 7) associated with the known mineral deposits (Geco-Willroy, Nama and Willecho deposits) and are interleaved with iron formation, volcanogenic massive sulphide deposits and sillimanite-muscovite quartz schist. Unit 7 occurs as homogeneous schists and as breccias and contain up to 20% quartz phenocrysts in a fine grained biotite-felsic to leucofelsic matrix of quartz, plagioclase, microcline and biotite with accessory muscovite, epidote and garnet. Porphyroblasts of magnetite are prominent. Locally magnetite is part of the matrix. The muscovite and microcline are interpreted as due to potassic alteration. Towards the contact with iron formation there is an increase in calc-silicate mineral abundance, interpreted as metasomatic alteration.

Metamorphosed iron formation (unit 9) is mapped as three sub-units. Quartz-magnetite IF (unit 9a) is the most abundant IF and consists of alternating coarse grained white quartz layers with dark magnetite±grunerite±actinolite±garnet±clinopyroxene layers. The percentage of Fe minerals is variable and magnetite may be absent. Layering varies from dark laminae in a quartz rich rock to dark and light layers upto 10cm wide. Fe silicates are ususally medium to very coarse grained. The IF may be tectonically fragmented. Silicate IF (unit 9b) is dark and homogeneous and is more or less equivalent to the dark layers of the quartz-magnetite IF. It is found mainly near contacts with unit 9a. Unit 9c is sulphidic IF

and is similar to 9a except with disseminated or stringer pyrite, pyrrhotite or sphalerite. It occurs as a transition from quartz-magnetite IF to volcanogenic massive sulphide deposits. All three iron formations are associated with the known VMS deposits and can be mapped along the northern and southern limbs of the Manitouwadge synform. It can also be found in association with mafic metavolcanics in the hinge of the Blackman Lake antiform and as inclusions in the Black Pic north of the north limb of the Jim Lake synform and west of Kern Lake.

Metasedimentary rocks (unit 10) are homogeneous, grey, foliated, fine grained layered metagreywackes represented by biotite-quartz-feldspar±hornblende±muscovite schists with more pelitic layers containing garnet and/or sillimanite. Unit 10 is located between the inner and outer volcanic belts. It is geochemically indistinguishable from Quetico metasediments, although of lower metamorphic grade.

Unit 11 is a straight gneiss or laminated felsic gneiss interpreted as an annealed mylonite lying on early ductile faults. It is a fine grained to aphanitic felsic rock with quartz-feldspar and, locally, micaceous or hornblende-rich lamellae. The gneiss is observed in outcrop to be transitional to pegmatite. It is mapped between quartz-phyric felsic rocks in the Willroy area and between IF and metasomatically altered rocks in the Willecho area and south of Wowun Lake.

Unit 2 is a metasomatically altered rock termed orthoamphibole-garnet±cordierite gneiss and is defined by the presence of orthoamphibole. The two main assemblages are garnet±cordierite±sillimanite±plagioclase and cummingtonite±hornblende±plagioclase±garnet. Layers of hornblende-

plagioclase±cummingtonite±garnet represent layers of lower intensity hydrothermal alteration of mafic volcanics. Quartz and magnetite are constant accessory minerals. The unit is characterized by two type of layering: domains of varying degrees of alteration and remnants of primary structures. The unit wraps around the trondhjemite and can be mapped through the hinge and limbs of the Manitouwadge synform and is interpreted, from its magnetic signature, to continue to the southern limb of the Blackman Lake antiform, where it outcrops. Unit 2 is associated with the Dead Lake suite rocks at the eastern end of the Loken Lake pluton. It also outcrops in the outer volcanic belt on the southern limb of the Manitouwadge synform in mafic metavolcanics near the contact with felsic volcanics and metasedimentary rocks. These rocks are interpreted to be zones of synvolcanic hydrothermal alteration later metamorphosed to upper amphibolite facies.

Unit 1 represents metasomatically altered felsic volcanics as sillimanite-muscovite-quartz schist south of the VMS deposits at the Willroy and Geco properties and sillimanite-knot felsic schist around and to the north of the Willecho deposits. These two rock types are end members of the same unit with transitional quartzites and micacious schists. The unit may also have minor plagioclase, biotite, K-feldspar, garnet and magnetite. Unit 1 is closely associated with protolithic felsic volcanics and the VMS deposits. Similar to unit 2, unit 1 is interpreted to represent zones of synvolcanic hydrothermal alteration later metamorphosed to upper amphibolite facies.

Unit 12 consists of foliated trondhjemite to hornblende-granodiorite containing supracrustal screens including the Dead Lake suite rocks. It is characterized by abundant coarse grained quartz, disseminated magnetite porphyroblasts (1-3mm) and minor biotite

with weak to moderately developed foliation. It appears to be limited to the inner volcanic belt and is folded around the Manitouwadge synform, Blackman Lake antiform and Jim Lake synform. It intrudes mafic and mixed mafic-felsic metavolcanic units as well as the metasomatically altered orthoamphibole-cordierite-garnet gneiss at its outer contact and contacts the Loken Lake pluton in the inner core. Unit 12 is interpreted to be a synvolcanic intrusion.

Unit 13 is foliated K-feldspar porhyritic granitoid and is represented by two discrete intrusions; the Nama Creek pluton and Loken Lake pluton.

The Nama Creek pluton is a foliated hornblende-biotite granitoid with 1 to 2cm microcline phenocrysts (0-25%) and a tonalitic to granitic matrix. It has a moderate to strong tectonic fabric folded around the Blackman Lake antiform indicating the intrusion is pre- to syn-D_2. The Nama Creek pluton extends from the northern limb of the Manitouwadge synform between supracrustal rocks of the greenstone belt and Black Pic , although in at least one place it is mapped between layers of intermediate to mafic metavolcanics (near Fox Lake). It is also observed to have inclusions of the same metavolcanics.

The Loken Lake pluton is also a microcline phenocrystic granitoid and it intrudes the core of the Manitouwadge synform, surrounded by the synvolcanic trondhjemite (unit 12). It is similar to the Nama Creek pluton except it has larger microcline phenocrysts (5-15cm) and is more leucocratic. Large areas are non-porphyritic and resemble the synvolcanic trondhemite, but are about 30 Ma younger. A strong tectonic fabric appears to be folded about the D_3 Manitouwadge synform indicating this intrusion is also pre- to syn-D_2.

Unit 14 consists of undivided foliated intrusive rocks and is represented by the multiphase

Black Pic batholith and various foliated tonalitic intrusions within the supracrustal and subvolcanic rocks. The Black Pic batholith engulfs the Manitouwadge greenstone belt and is largely tonalitic varying to diorite, granodiorite and granite. The contact with mafic metavolcanics of the outer volcanic belt is interleaved and folded. The oldest phase of the batholith is a medium to coarse grained foliated hornblende-biotite diorite to monzodiorite (quartz 5-20%, microcline <2-15% and hornblende+biotite 15-30%) containing plagioclase augen. Septa of strongly magnetic mafic to intermediate metavolcanics and quartz-magnetite iron formation are mapped within the northwest of the main greenstone belt. The Black Pic batholith is involved in D_3 folding. The is migmatized toward the Quetico boundary. A younger phase of foliated monzodiorite is distinguished from the main batholith north of the Banana Lake antiform, separating the inner and outer volcanic zones of the greenstone belt. This unit is also represented by a large irregular body within the hinge of the Manitouwadge synform as a granodiorite- with inclusions of units 6 and 10. Contacts are gradational and their position not well constrained. Smaller irregular tonalitic bodies and dykes intrude all supracrustal units and crosscut early folds and the straight gneiss but have foliations parallel to the dominant fabric of the host rocks indicating that they are syn-D_2 bodies.

Unit 15 includes pegmatites, aplites and foliated granites. Generally this unit is represented by many small undivided leucocratic intrusions of various ages with quartz, K-feldspar, plagioclase and accessory muscovite and biotite. The largest of these intrusions is north of the Geco deposit intruding many supracrustal units and the synvolcanic trondhjemite. Elsewhere, this unit is transitional to straight gneiss (unit 11).

Alkalic rocks form dykes and small irregular bodies within the greenstone belt and consist

of hornblende syenite, hornblendite and lamprophyre. Syenite-hornblendites are pink and green, leucocratic to melanocratic, up to 80-90% hornblende and less foliated than host rocks. Hornblende phenocrysts are typically up to 15mm with inclusions of biotite. Skeletal or corroded phenocrysts of clinopyroxene are minor. These rocks are interpreted as mixtures of leucocratic and melanocratic material. This unit is of interest for its tectonic implications, late emplacement and, in one locality, a massive sulphide clast within an alkalic intrusion breccia indicating the possibility of massive sulphide deposits, in this case, away from the area of known deposits.

Metasedimentary rocks (unit 10q) of the Quetico subprovince are migmatized equivalents to the metasediments of the Manitouwadge synform (unit 10). The metagreywackes are composed of pelitic and psammitic layers. The pelitic layers commonly contain garnet and sillimanite and preferentially have pegmatitic and tonalitic leucosome migmatitic segregations. The southern extent of these metasedimentary rocks mark the Wawa-Quetico subprovince boundary. The transition from upper amphibolite to granulite metamorphic facies is seen just north of Jim Lake with the occurrence of an orthopyroxene-biotite-garnet assemblage. Within the metasediments, to the east of Anna Lee Lake, mafic metavolcanics have been mapped (OGS Map 2219). Sheeted gabbroic and dioritic intrusions are interlayered with the metasediments west of Appelle Lake and have been grouped together as the Everest Lake pluton and, alternatively, have been grouped with the Black Pic batholith.

Three generations of Proterozoic dykes intrude the study area. Northwest trending dykes are interpreted by Zaleski et al.(1995) to belong to the Matachewan swarm, dated at 2454±2

	Inner volcanic belt (IVB)	Outer volcanic belt (OVB)	Dead Lake (DL)	One Otter–Banana (OB)	Eastern extension (E)	Jim–Davis (JD)	Noranda suite
Felsic metavolcanic rocks	(2)	(3)					
Quartz–phyric felsic rocks	(6)						(3)
Trondhjemite–granodiorite	(8)		(7)	(2)	(1)	(1)	
Mafic metavolcanic rocks	(6)	(7)	(5)	(4)			(3)
Hornblende–magnetite–garnet rocks/magnetite quartzite		(1)	(3)				

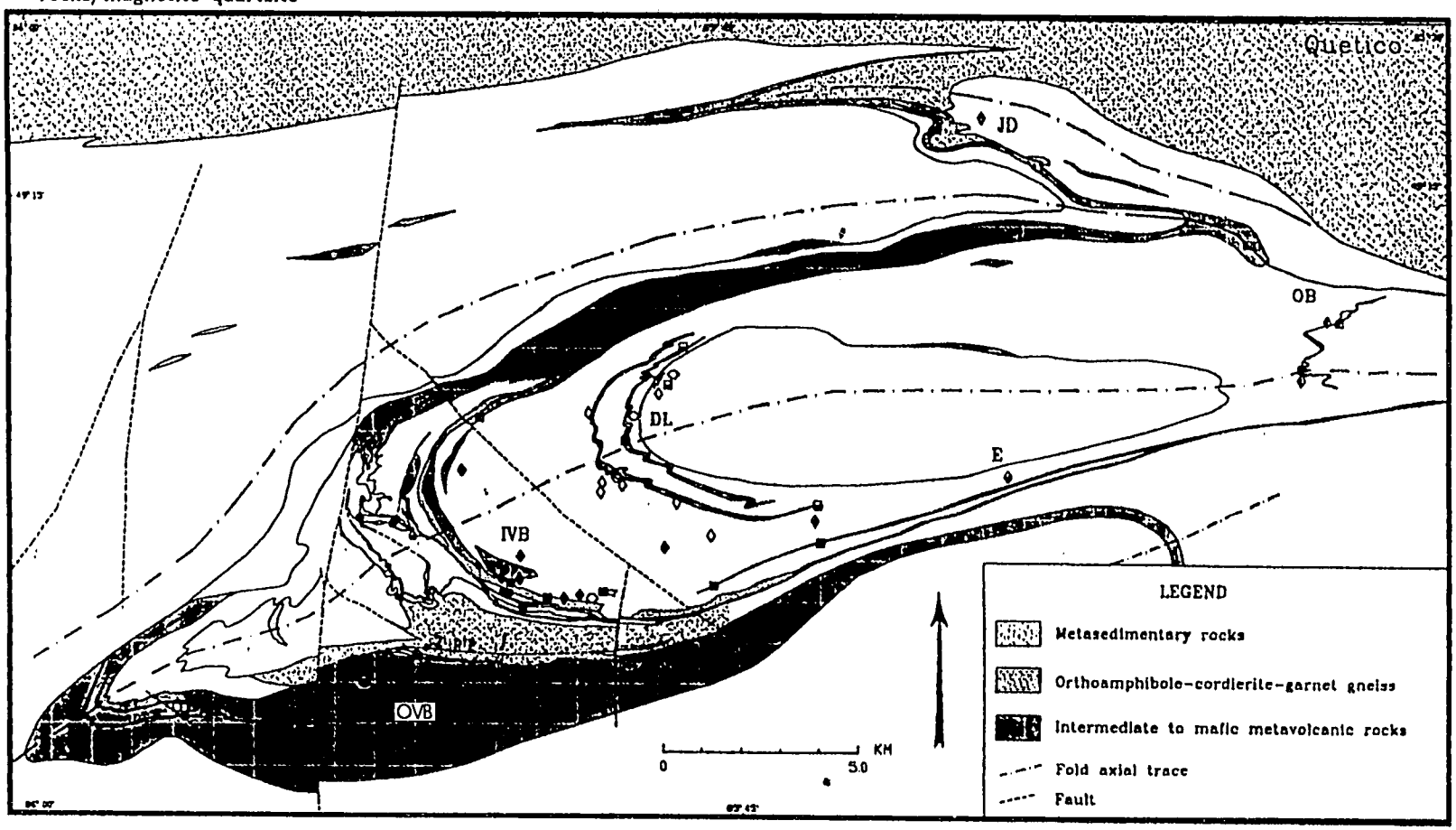

Fig. 1.5. Geochemical sample locations (from Zaleski et al., 1995)

Ma (Heaman, 1988). Northeast trending dykes represent the Biscotasing swarm, dated at 2166.7±1.4 Ma (Buchan et al.,1993). North trending dykes probably represent the Marathon swarm, dated at 2170 Ma (Fahrig and West, 1986).

1.3 GEOCHEMISTRY

Major element and REE geochemical studies were carried out by Zaleski et al.(1995) in support of detailed geological mapping. The sampled rock types were aphyric felsic metavolcanics (unit 7), quartz-phyric felsic metavolcanics (unit 8), foliated trondhjemite (unit 12), mafic volcanics (unit 3) and hornblende-magnetite-garnet rocks (unit 1.5). Figure 1.5 shows sample locations.

Mafic metavolcanic rock analyses indicate these rocks, throughout the Manitouwadge greenstone belt, are tholeiites as defined by Jensen's (1976) classification (Fig. 1.6). These compositions indicate the rocks are most likely derived from a common magma system. Mafic rocks of the inner volcanic belt have abundances of TiO_2 >1% and FeO_t >10%.

Felsic metavolcanics and trondhjemite are transitional calc-alkaline to tholeiitic rhyolites and dacites (Fig. 1.6). Trondhjemite sampled throughout the belt has a narrow compositional range, suggesting the rocks are comagmatic. Two analyses of the trondhjemite, sampled near the Dead Lake suite rocks, have elevated Fe contents and more calcic compositions, suggesting the latter contaminated the former. Felsic rocks of the IVB can be distinguished from mafic volcanics by their abundances of TiO_2 <0.4% and FeO_t <8%. These relatively immobile elements can be used to determine the protolith to metasomatically altered rocks as either felsic or mafic volcanics..

Unaltered metavolcanics in the MGB have undergone extensive alkali exchange. The

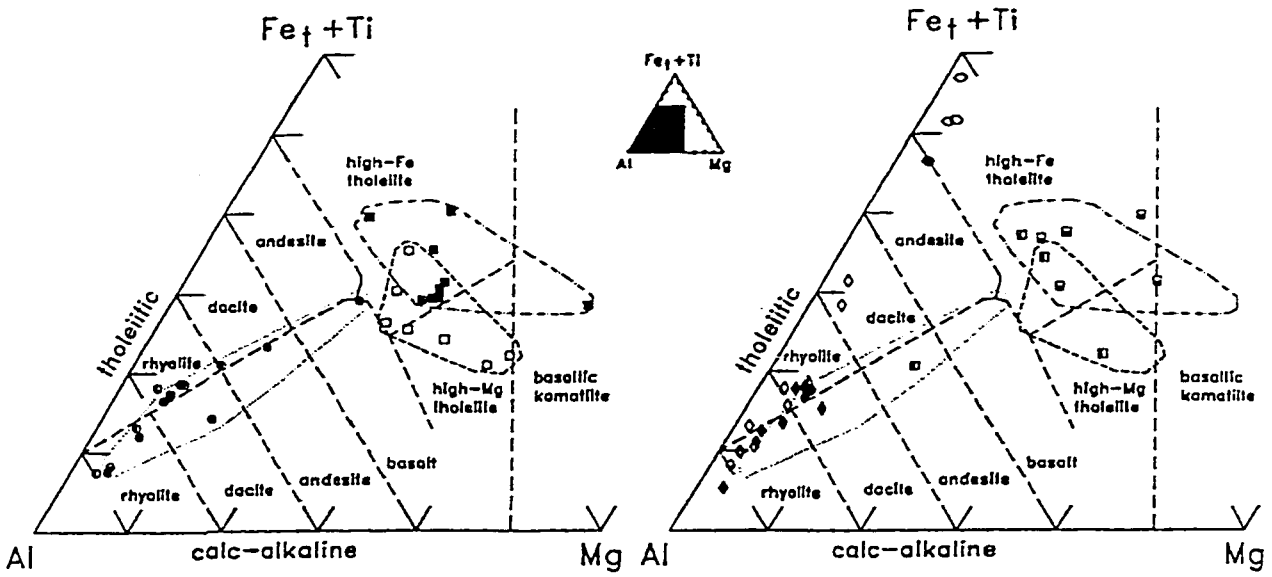

Fig. 1.6. Rock compositions based on Jensen's (1976) definitions (from Zaleski et al., 1995)

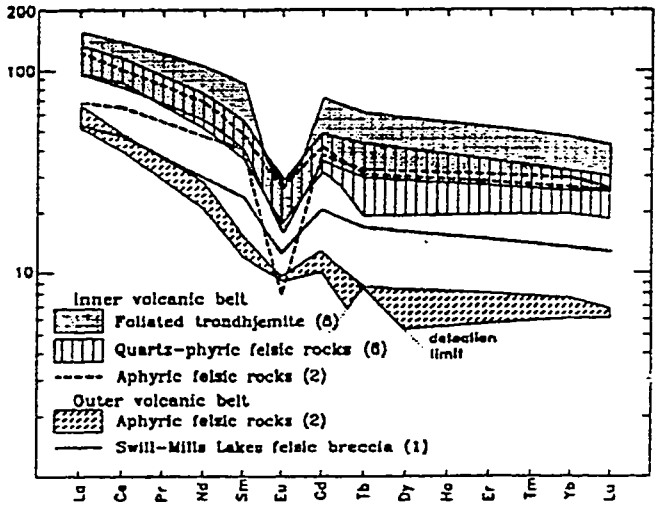

Fig. 1.7. Chondrite-normalized REE abundances in Manitouwadge greenstone belt rocks (from Zaleski et al.,1995)

quartz-phyric felsic metavolcanic rocks are potassic while the synvolcanic trondhjemite is sodic. This indicates the former have been exposed to low temperature seafloor alteration and the latter have not.

REE analyses (Fig. 1.7) show that IVB felsic volcanics and trondhjemite, compared to OVB felsic volcanics, have higher total REE abundances, more gently sloping patterns and more pronounced Eu anomalies. The similarity between the IVB rock REE analyses is interpreted by Zaleski et al.(1995) to indicate the trondhjemite was a reservoir for quartz-phyric felsic volcanics.

1.4 STRUCTURAL GEOLOGY

The Manitouwadge greenstone belt has been subjected to 4 phases of deformation. D_1 is largely interpreted from faults deformed by D_2 folds. D_2 is recognized from dominant foliations and lineations and interpreted map scale folds. D_3 was responsible for the major map-scale east west trending folds. D_4 is interpreted from deflections of D_3 axial traces.

D_1 is largely obscured by later deformation and metamorphism and includes as all pre-D_2 events. The straight gneiss (unit 11) is interpreted as annealed mylonite lying on discontinuities related to early ductile faults. It is seen north of the Willecho deposits where pegmatite is transitional to straight gneiss (Fig. 1.8). Within the Willecho area, the straight gneiss is adjacent to truncated and boudinaged iron formation and in the Willroy-Geco area straight gneiss is in contact with highly strained, straight laminated iron formation. The straight gneiss layering is interpreted to be related to D_1 gneissosity folded by a D_2 fold southwest of the Nama deposit (Fig. 1.8). D_1 is interpreted to suggest thrust faulting by

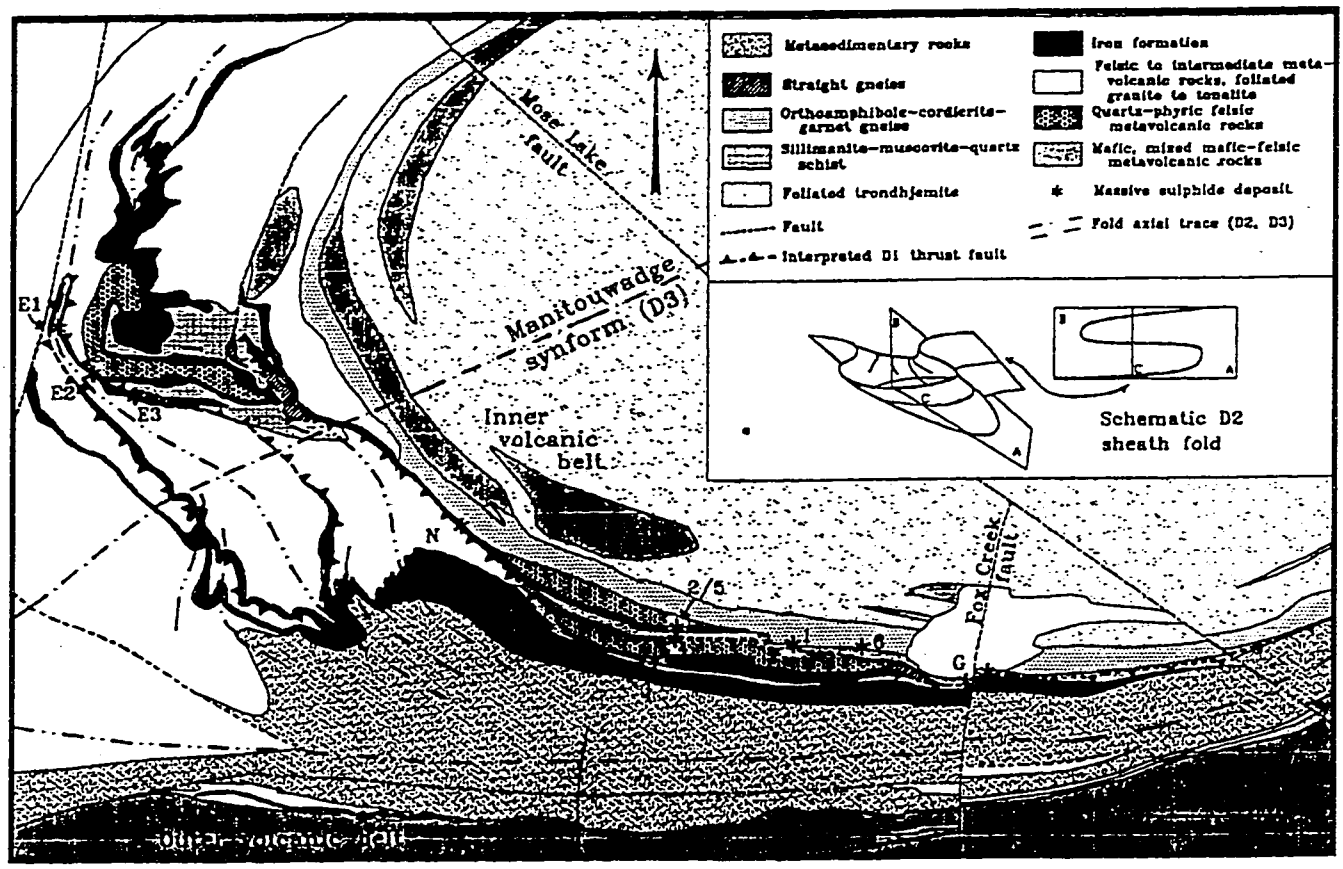

Fig. 1.8. Manitouwadge synform geology. D_2 folding of a D_1 fault in map view between the Nama creek deposit (N) and the Willecho deposits (E1,E2,E3) and in the inset as a schematic view (from Zaleski et al., 1995).

Zaleski et. al. (1995)

D_2 produced the dominant planar and linear fabrics in the belt. The D_2 foliation is a moderate to strong schistosity defined by micas, amphiboles and also quartz and feldspars. It is interpreted to be a composite D_2/D_1 fabric and is largely parallel to lithological contacts. Dominant planar fabrics in the Quetico metasedimentary rocks are deformed by D_3 folds and are equated with the D_2 fabrics of the greenstone belt. D_2 lineations are defined by sillimanite, amphiboles and micas, all minerals of the upper amphibolite facies. The generally have an ENE plunge. The relationship between D_2 lineations and later folding is variable. In many places D_2 lineations and D_3 fold axes are coaxial, but in the inner volcanic belt the orientation of lineations varies systematically from the hinge region of the D_3 Manitouwadge synform to the southern limb.

D_2 folding is important to the economic geology of the belt as it repeats VMS deposits. A D_2 syncline repeats the volcanic and sedimentary sequences across the southern limb of the D_3 Manitouwadge synform. There is a repetition of the sequence: mafic metavolcanics, felsic metavolcanics interlayerd with iron formation, and metasediments. The axial trace of the D_2 fold is within the metasediment unit on the southern limb (Fig. 1.9). Figure 1.9 shows the axial traces of other D_2 folds and Figure 1.10 illustrates these folds before D_3 deformation. The refolding to D_2 folds offers a mechanism to explain the Dead Lake suite rocks as equivalent to inner/outer volcanic belt units.

D_3 is most obviously seen in the folding of D_2 fabrics into the major mapscale folds: the Jim Lake and Manitouwadge synforms and the Blackman Lake and Banana Lake antiforms. The D_3 folds display a Z-asymmetry. From north to south the hinge zones become broader

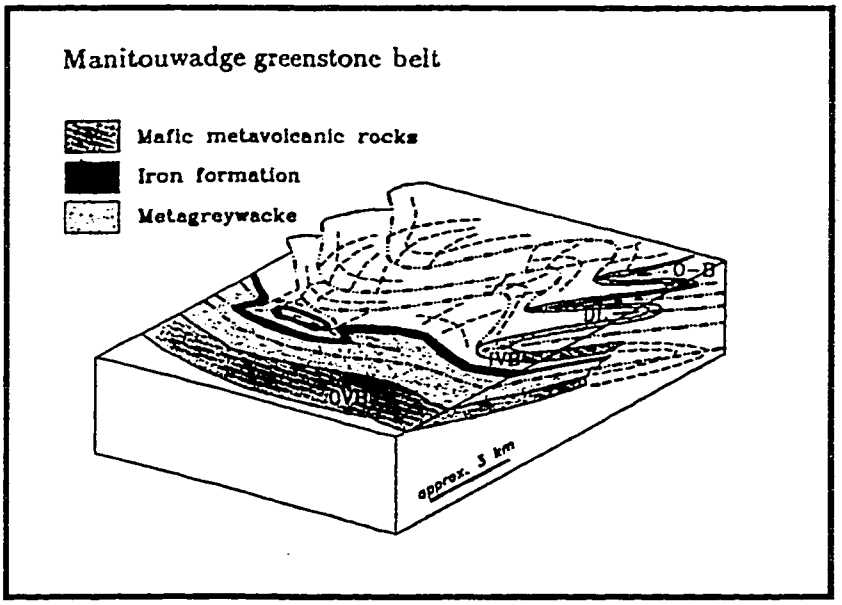

Fig. 1.9. Block diagram showing schematic pre-D_3 relationships of supracrustal rocks, repeated by D_2 folds. The fold trace in the metagreywacke between inner and outer volcanic belts represents the D_2 Manitouwadge syncline.. The D_2 sheath fold, illustrated in Figure 1.8, is represented in the iron formation on the right side of the diagram. DL = Dead Lake suite, O-B = One Otter-Banana area.

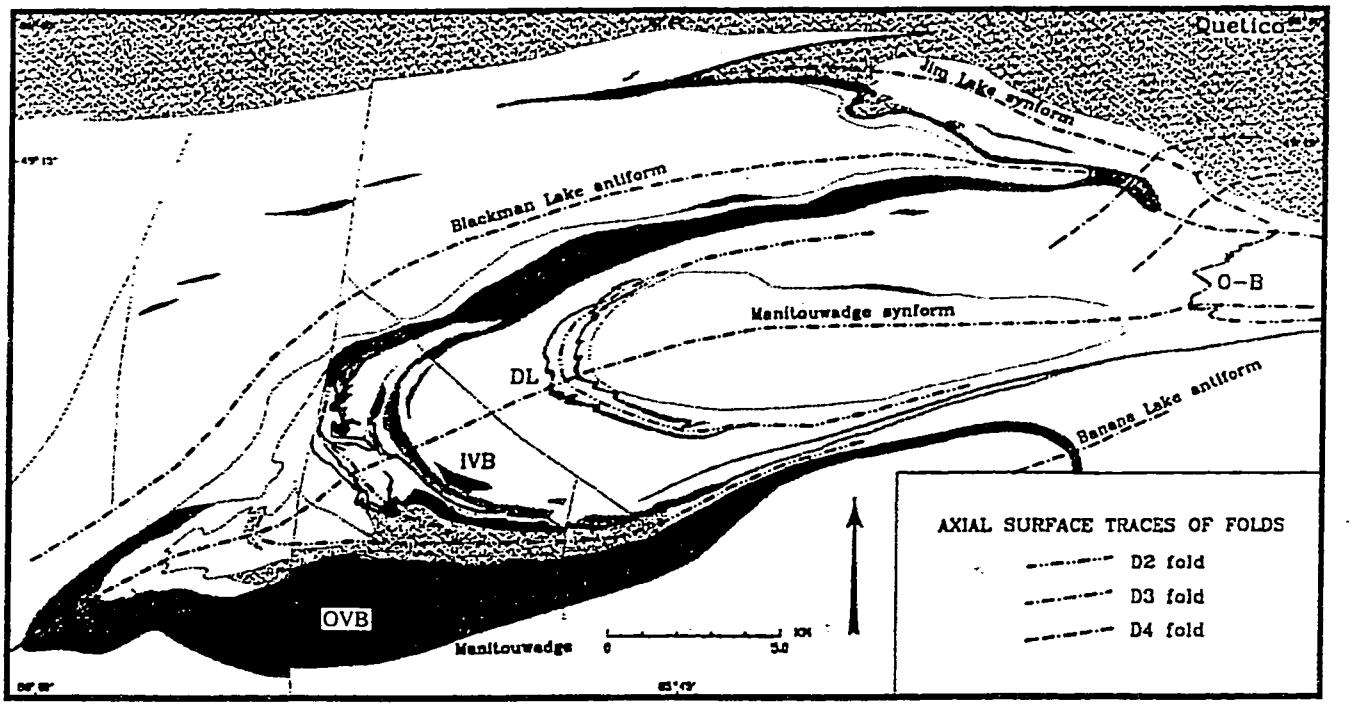

Fig. 1.10. Axial traces of D_2 synclines, D_3 and D_4 folds (from Zaleski et al., 1995)

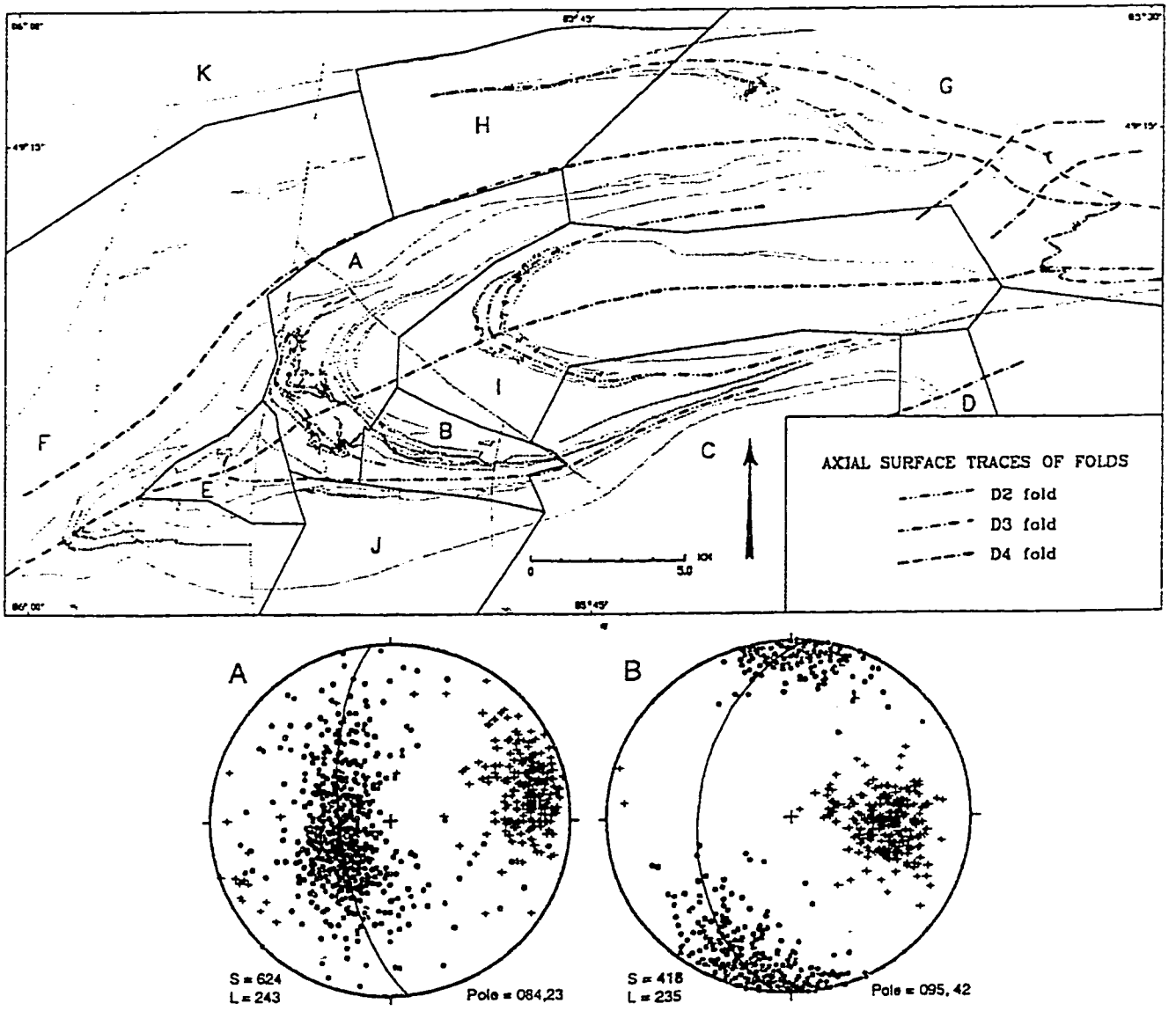

Fig. 1.11. Structural subareas of the Manitouwadge area with accompanying stereonets for area A and B. The equal area nets show the distribution of the dominant D_2 planar (filled circle) and linear (cross) fabric elements The great circle and pole (filled square) is the cylindrical best fit for planar data (from Zaleski et al., 1995).

and the axial traces of the D_3 folds, although curved, become less east-west and more northeast trending (Fig. 10). This is interpreted as indicating a response to oblique, dextral transpression at the Wawa-Quetico subprovince boundary by Zaleski et. al. (1995).

D_3 folds strongly reorient D_1 and D_2 fabrics. In the Manitouwadge synform the inner hinge is broad and rounded and the outer hinge is tighter. In the inner hinge zone, the fold axis has a shallow to moderate northeast plunge and the axial surface dips to the south. D_2 planar fabrics between the Willecho and Geco deposits, plotted on a sterographic projection (Fig. 1.11), define a girdle with a moderate to shallow easterly plunging axis. In the outer hinge region, D_2 foliations define a girdle with a moderately northeast plunging pole. D_2 lineations consistently plunge northeast. The earlier fabrics are strongly transposed by D_3 folding.

It is important to note that the Blackman and Jim Lake D_3 folds are described as being defined largely by folded mafic to intermediate screens and inclusions in foliated Black Pic plutonic material. The Black Pic batholith north and west of the greenstone belt contains enough included mafic material, presumably included supracrustal material, to illustrate folding even if it is not a mappable unit at 1:25 000 scale.

D_3 is also seen in minor map-scale and outcrop-scale folds deforming D_2 schistosity. Around the Manitouwadge synform, outcrop-scale folds have Z-asymmetry on the southern limb, M-asymmetry in the hinge and S-asymmetry on the northern limb.

D_4 is defined by deflections in the Blackman Lake antiform, Jim Lake synform and the Wawa-Quetico boundary (Fig. 1.10, NE corner). A northeast trending shear zone, marking the western limit of supracrustal rocks in the outer volcanic belt north of the Manitouwadge

synform's axial trace, may also represent D_4 as it reorients D_3 structures. Kink folds and crenulations cleavages are also attributed to D_4. The D_4 structures are consistent with ongoing dextral transpression at the local subprovince boundary.

Several late faults have been mapped. The Mose Lake fault strikes to the northwest across the Manitouwadge synform through the thickest section of synvolcanic trondhjemite. The northerly striking Cadawaja fault shows obvious sinistral offset as it crosses the hinge zone of the Manitouwadge synform west of the Willecho deposits. The Slim Lake fault also strikes to the north (west of the main supracrustal belt) and the Fox Creek fault cuts the Geco deposit with 60 metres of sinistral displacement and east side up vertical displacement. The Agam Lake fault occurs within the metasediments on the southern limb of the Manitouwadge synform and strikes east-west.

1.5 METAMORPHISM

There is a regional metamorphic gradient across the MGB, ranging from amphibolite facies in the Schreiber-Hemlo greenstone belt south of the MGB (Corfu and Muir, 1989b) to upper amphibolite facies within the MGB (Zaleski et al., 1995) to granulite facies in the Quetico metasediments north of Manitouwadge (Williams and Breaks, 1989) .

Pan and Fleet (1992, p.1375) report upper amphibolite facies with peak temperatures of 600-700°C and pressures of 3-6 kb in the MGB. The metamorphic grade increases toward the north. D_2 fabrics are defined by upper amphibolite facies minerals indicating D_2 was synchronous with peak metamorphism. Metasediments within the MGB are foliated and contain local garnet-biotite-sillimanite, but unlike their Quetico equivalents, show no migmatitic segregations.

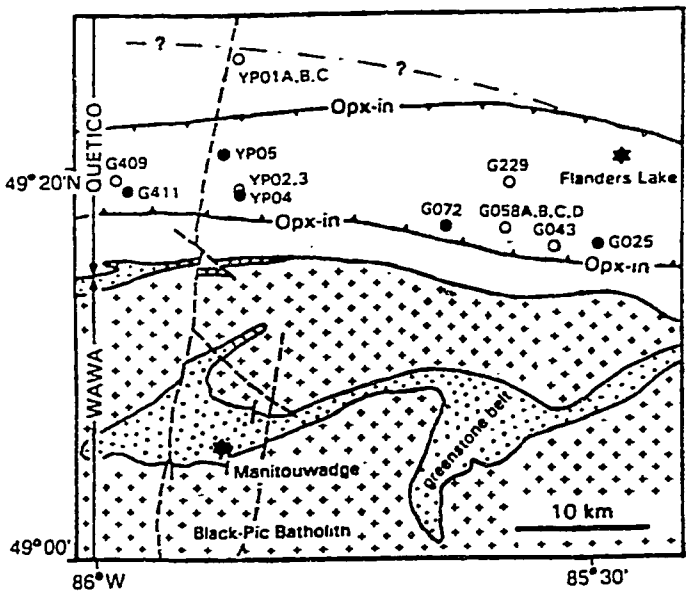

Fig. 1.12. Orthopyroxene-in isograd showing the granulite zone in Quetico metasedimentary rock north of the Manitouwadge greenstone belt (from Pan and Fleet, 1994).

The granulite facies zone within the Quetico subprovince reflects peak temperatures of 680-770°C and 4-6 kb pressures (Pan and Fleet, 1994, p.1427). The zone is defined by the presence of orthopyroxene (Fig. 1.12). It extends 100km from Manitouwadge to Hornepayne and is about 10km wide. The zone is predominantly migmatized metasedimentary rocks with volumetrically insignificant folded amphibolitic mafic layers. All rocks of the zone are characterised by abundant magnetite making it a prominent magnetic anomaly (Pan and Fleet, 1994, p.1428).

The Quetico subprovince is described as having a symmetric metamorphic zonation, with low grade margins and high grade migmatites in the central areas (Percival, 1989). North of the MGB, however, this trend is reversed, with granulite facies preserved near the margin grading northward to central amphibolite facies.

1.6 GEOCHRONOLOGY

Geochronological work on rocks of the Manitouwadge greenstone belt clarifies relationships between volcanic, intrusive and sedimentary rocks and allows dating of deformational and metamorphic events. Figure 1.13 shows sample locations. All ages are from Zaleski et al. (1995), unless otherwise stated.

Dating of felsic volcanic units indicate extrusion at about 2720 Ma. Dates include an aphyric felsic breccia in the outer volcanic belt at 2722±2 Ma and a muscovite schist around the Geco deposit at 2720±2 Ma (Davis et al., 1994, p.427). A foliated trondhjemite yielded an age of 2720±3Ma, indicating the intrusion is indeed synvolcanic.

The metagreywackes of the southern limb of the Manitouwadge synform yielded ages between 2719±2 Ma and 2679±11 Ma with a more accurate younger date at 2692±1. These

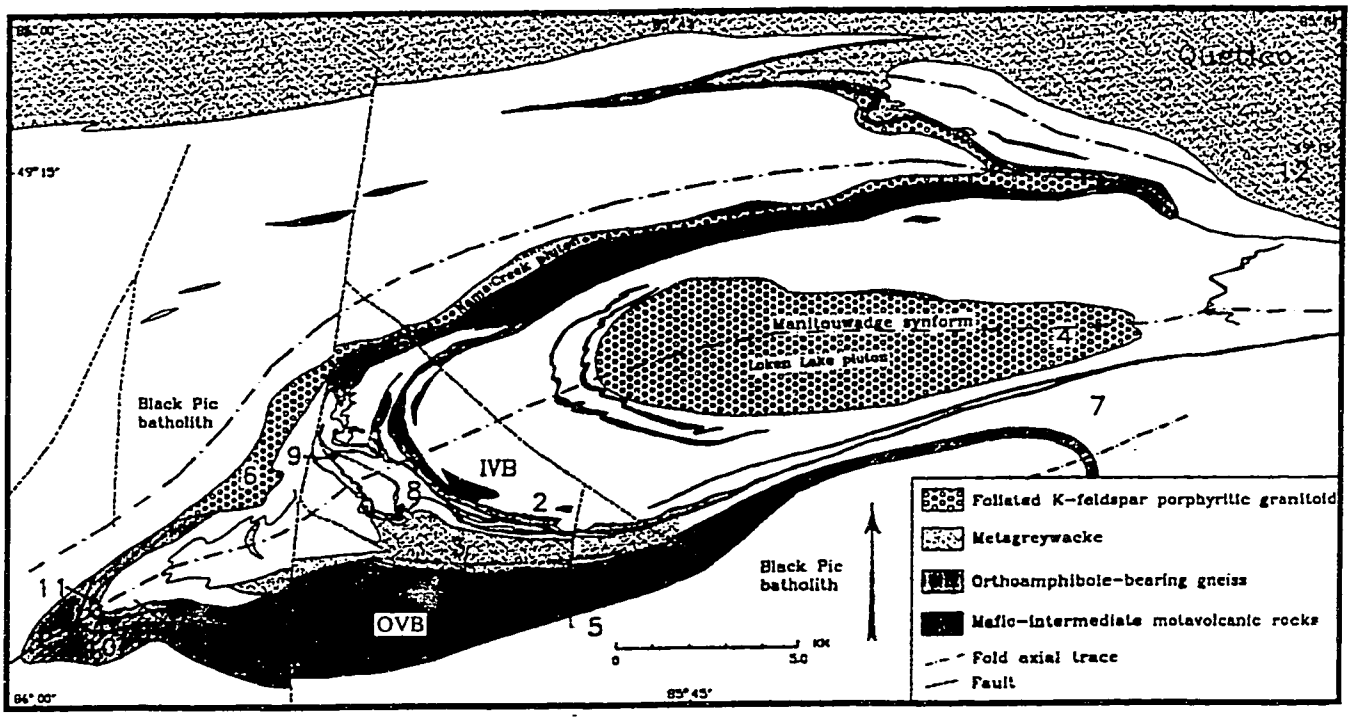

Fig. 1.13. Locations of geochronological samples (from Zaleski et al., 1995)

rocks were deposited no earlier than 2693 Ma and are at least 25 Ma younger than the local volcanic rocks. The age of the oldest zircon at 2719±2 Ma suggests that the sediments may have a local source.

The timing of D_1 deformation is provided by dating of a pegmatite dyke transitional to straight gneiss at 2669±3 Ma. A syn-D_2 dyke has an age of 2671±3Ma which is similar to both the D_1 pegmatite and a 2675±1 Ma (Davis et al., 1994, p.427) age for metamorphic monazite in the Geco mine. A Quetico muscovite-biotite granite dyke, interpreted as late D_3 to D_4 was determined to be 2642±2 Ma.

Pre- to syn-D_2 Nama Creek pluton and Loken Lake pluton yield dates of 2680±3 Ma and 2687+2/-3 Ma, respectively. The Black Pic batholith's oldest dioritic phase was dated at 2687+3/-2 Ma (within error the age of the Loken Lake pluton). A foliated monzodiorite sample from the Black Pic batholith between the inner and outer volcanic belts in the area of the Banana Lake antiform hinge (Sample 7, Fig. 1.13) has an age of 2677±2Ma, 10 Ma younger than the other sample. The foliation could be D_2 or D_3 fabric.

1.7 ORE DEPOSITS

The Manitouwadge greenstone belt hosts volcanogenic massive sulphide deposits. Four mines have exploited a number of deposits. Between 1957 and 1995 over 55 million tonnes of ore were produced. The deposits occupied the southern limb and hinge of the Manitouwadge synform. From Fox Creek along the southern limb towards the hinge were the Geco, Willroy, Nama Creek and Willecho deposits. All known deposits are within the IVB.

The deposits are categorized into three main types on the basis of the proportions of copper, zinc and lead, by the nature of the mineralization and by the deposits relationship to iron formation. Type 1 deposits are Cu-rich stringer and disseminated orebodies either

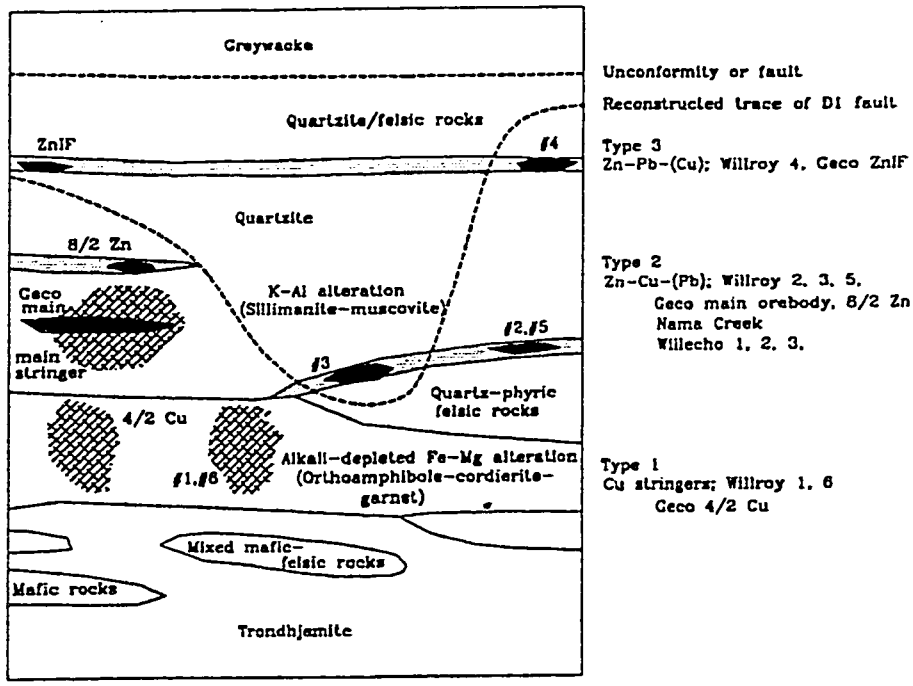

Fig. 1.14. Schematic reconstructed section of probable relationships between orebodies. Stringer/disseminated zones are shown as cross-hatching, and iron formations are stippled. (from Zaleski et al., 1995).

hosted by orthoamphibole-cordierite-garnet gneiss or enveloping the main Geco orebody in sillimanite-muscovite-quartz schist. Type 2 are massive and semi-massive orebodies with dominant Zn and Cu with or without Pb. Type 2 deposits are associated with iron formation that is interleaved with sillimanite-muscovite-quartz schist or quartz-phyric felsic metavolcanics. Type 3 deposits are massive and semi-massive with, in decreasing proportions, Zn and Pb with or without Cu. These orebodies are hosted by iron formation south of sillimanite-muscovite-quartz schists. Generally, the trend is to increasing Zn and Pb in the deposits toward the south. Sulphide mineralogy is simple and consists of pyrite, pyrrhotite, chalcopyrite, sphalerite and galena.

Figure 1.14 is a section of the mineralized zone reconstructed to its pre-D_2 state. It illustrates the relationships between deposit types and host rocks. There is a strong association of VMS deposits with iron formation and metasomatically altered rock. The increase in Zn/Cu ratio to the south within orebodies indicates younging in that direction. D_2 fold repetition of sequences across the southern limb of the Manitouwadge synform include the VMS deposits and they should be repeated in the OVB. Orthoamphibole-garnet-cordierite mafic rocks found in the OVB are correlated with VMS-hosting altered rocks in the IVB.

1.8 DISCUSSION

The Manitouwadge greenstone belt represents a single cycle of volcanism intruded by synvolcanic trondhjemite and syntectonic -granodiorite. The four phases of deformation include two major folding events that produced the major map-scale features.

The synvolcanic trondhjemite was the heat engine for the extensive stratabound metasomatic alteration of volcanic rocks, including the VMS deposits, as well as being the

reservoir for the IVB felsic volcanics. As a result of its map extent, inclusions of supracrustal septa and style of alteration, the trondhjemite is interpreted to be a sill, laccolith or a series of semi-concordant intrusions.

Early D_1 faulting, associated with repetition of sequences and low angle truncations is interpreted by Zaleski et al. (1995) to suggest thrusting. D_2 fabrics, defined by upper amphibolite facies minerals, were synchronous with peak metamorphism. D_2 folding produced the repetition of units defining the IVB and the OVB and may be responsible for the presence of Dead Lake suite volcanics deep within the trondhjemite. D_3 folded the belt and the Wawa-Quetico boundary with dominantly Z-asymmetry. Together with other dextral kinematic indicators, D_3 and D_4 are interpreted by Zaleski et al. (1995) to be the result of progressive dextral transpression at the Wawa-Quetico boundary.

The Wawa-Quetico boundary is structurally as well as lithologically transitional. From the boundary south through the MGB, tight D_3 folds and dominantly east-west structures gradually change to more rounded, broader D_3 fold hinges and northeast trending axial traces. MGB metasediments are indistinguishable from Quetico metasediments, except for metamorphic grade. The maximum age for a MGB metasediment zircon is the same as for local felsic volcanics indicating D_1 uplift of MGB volcanics may have provided a source for the sediments. The MGB metasediments overlie the volcanics unconformably or are allochthonous, tectonically emplaced possibly by D_1 thrusting. The Wawa-Quetico subprovince boundary to the west of the MGB can be seen as a fault contact (Percival, 1989) and to the east the metasediments and metavolcanics are interbedded along the boundary (Berger, 1985). Zaleski et al. (1995) interpret the boundary north of the MGB as transitional between a conformable and a faulted contact.

2. MAGNETICS

2.1 BASIC CONCEPTS

A magnetic field is a consequence of the flow of electrical current. Ampère's Law gives the magnetizing field ($\boldsymbol{H}$) resulting at a point, p, from a current passed through a conductor of length l, as;

$$\boldsymbol{H} = (\boldsymbol{I}l)\left(\frac{\boldsymbol{r}_l}{4\pi r^2}\right) \tag{1}$$

where $\boldsymbol{I}$ is the current, r is the distance from the conductor to p and $\boldsymbol{r}_l$ is the unit vector in that direction, measured with respect to the axis of the conductor (Fig. 2.1).

Circular orbitals of electrons in atoms create magnetic dipole moments. Molecules may also be magnetic dipoles. These dipoles can be aligned by an external magnetic field by the process of magnetic induction, causing an ancillary field, $\boldsymbol{M}$, augments the magnetizing field, $\boldsymbol{H}$. $\boldsymbol{M}$ is proportional to, and aligned with, $\boldsymbol{H}$ for low intensity magnetic fields. Magnetic susceptibility (k) is the ability of a body to be magnetized by induction and is given by;

$$\boldsymbol{M} = k\boldsymbol{H} \tag{2}$$

k is a dimensionless unit as $\boldsymbol{M}$ and $\boldsymbol{H}$ have the same units. If $\boldsymbol{M}$ and $\boldsymbol{H}$ have units in Amperes/meter, k is designated as k_{SI}. If $\boldsymbol{M}$ and $\boldsymbol{H}$ are given in oersteds (cgs-emu units), then k is designated k_{emu}. The two measures of susceptibility are related by;

$$k_{SI} = 4\pi k_{emu} \tag{3}$$

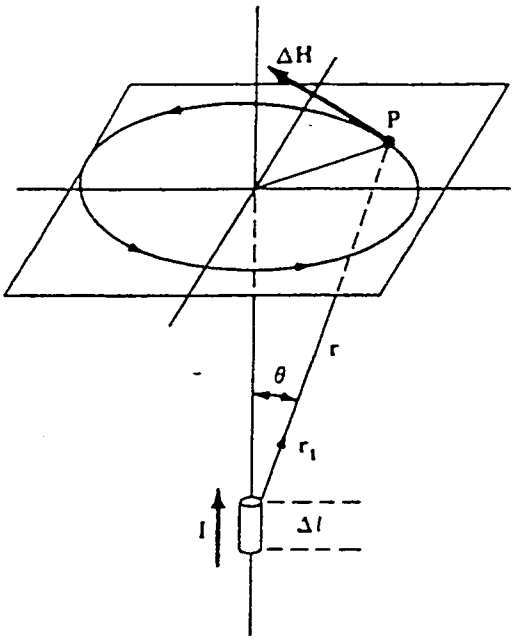

Fig. 2.1. Ampère's law. A current, ***I***, through a length of conductor, *l*, creates a magnetizing field, ***H***, at a point, *P* (from Telford et al., 1990).

k_{SI} units are used here throughout. The magnetic induction field ($\boldsymbol{B}$) is the total magnetic field and is given for SI by;

$$\boldsymbol{B} = \mu_0(\boldsymbol{H}+\boldsymbol{M}) = \mu_0(1+k)\boldsymbol{H} = \mu\mu_0\boldsymbol{H} \quad (4)$$

or in cgs-emu,

$$\boldsymbol{B}' = \boldsymbol{H}' + 4\pi\boldsymbol{M}' = (1 + 4\pi k')\boldsymbol{H}' = \mu\boldsymbol{H}' \quad (5)$$

where μ_0 is the magnetic permeability of free space (a constant), k is the magnetic susceptibility or air (assume a value of zero) and μ is the magnetic permeability of air (μ=1). B and H are linearly related by μ. B is the measured magnetic field but under the above assumptions can be treated as equal to the Earth's field, H. The unit of magnetic induction is the nanoTesla (nT).

Figure 2.2 is a graphic depiction of the orientation of the magnetic field. The Earth's total magnetic field, $\boldsymbol{H}_e$, is fully described by its magnitude ($\boldsymbol{F}_e$), inclination (I), and declination (D). Inclination is the dip from horizontal of the Earth's field and declination is its angle in the horizontal plane from true geographic north.

Airborne magnetometers measure the total intensity of the Earth's magnetic field. This field is the result of three main sources; the core field, the induced field, and the remanent field. The core field is Earth's primary magnetic field.

The induced magnetic field is the product of the intensity of the geomagnetic field and magnetic susceptibility (k) of the rock (Eqn. 2). k is a property of a material reflective of its

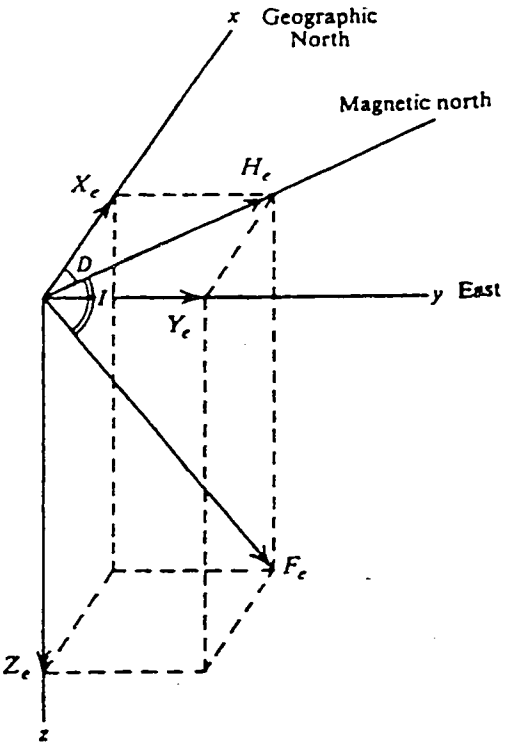

Fig. 2.2. Elements of the Earth's magnetic field. From Telford et al., (1990).

magnetic content and character. Diamagnetism is the weak magnetization all substances generate in the presence of an external magnetic field, opposing that field, and is, therefore, negative with k on the order of -10^{-5} SI. Paramagnetism is the due to the spin of uncompensated electrons of the transition elements. In the presence of an external magnetic field, the randomly oriented magnetic forces align parallel that field and is, therefore, positive and k is on the order of $+10^{-3}$ to $+10^{-5}$. Ferromagnetism is the property of spontaneously coupling of neighbouring paramagnetic atoms in a parallel orientation, usually within a preferred crystal lattice. In ferromagnetic minerals, k can range from 10^2 to 10^5 SI and overwhelm the diamagnetic and paramagnetic effects. Magnetite is the principal phase responsible for ferromagnetic susceptibility, although pyrrhotite and some members of the titanohematite series may contribute significantly to a rock's magnetic susceptibility. The percentage of magnetite (V), although not the only magnetic mineral present in crustal rock, can be estimated from k by the empirical relationship;

$$V = 21.8k^{0.9}(SI) \qquad (6)$$

(McGrath, 1996).

Remanent magnetization is also a property of crustal rock and is the magnetic field present in the absence of the core field. Remanence is the record of a paleogeomagnetic field preserved in a rock by orientation of ferromagnetic grains within that field that have become frozen in the rock. The intensity of the remanent magnetization of a rock body depends on the proportion of ferromagnetic minerals present, the strength of the geomagnetic field at the time of origin of the remanence and the geological history of the rock (Sharma, 1978). The ratio of remanent

magnetization to induced magnetization (Koenigsberger ratio) for a variety of crustal rock types are shown in Figure 2.3, apparently indicating dominance of remanence over induction. However, as a result of unstable remanence that realigns with the induced field, and of the general heterogeneity of the remanent magnetization, induced magnetization is usually dominant. Thus, when interpreting magnetic anomalies, the remanent effect can usually be ignored.

2.2. TEMPORAL VARIATIONS OF THE GEOMAGNETIC FIELD

The Earth's magnetic field varies with time, in a variety of ways characterized by their period of duration.. Even calibrated and highly accurate magnetometers cannot compensate for changes in the primary field intensity that, in turn, vary the intensity of the induced field. These temporal variations must be understood and minimized to ensure the magnetic signature is due only to the induced field.

Gauss, using spherical harmonic analysis, demonstrated that the source of the Earth's magnetic field is internal (Telford et al., 1990). The main field is proposed to be due to convection currents of conductive material in the molten outer core about the solid, iron-nickel core, creating a self-excited dynamo or a large, natural electromagnet. The main field has, at many times in geologic history, reversed the orientation of its axis. The geomagnetic axis has always, except for geologically instantaneous periods of transition, been sub-parallel to the geographic, rotational axis. For this reason, there is a suspected coupling between the Earth's spin and outer core currents. The main field wanders about its axis very slowly, on the order of 10° of inclination and 35° of declination over the last 400 years (Telford et al., 1990, p. 72). This gradual change alters the field's inclination, declination and total intensity and is referred to as

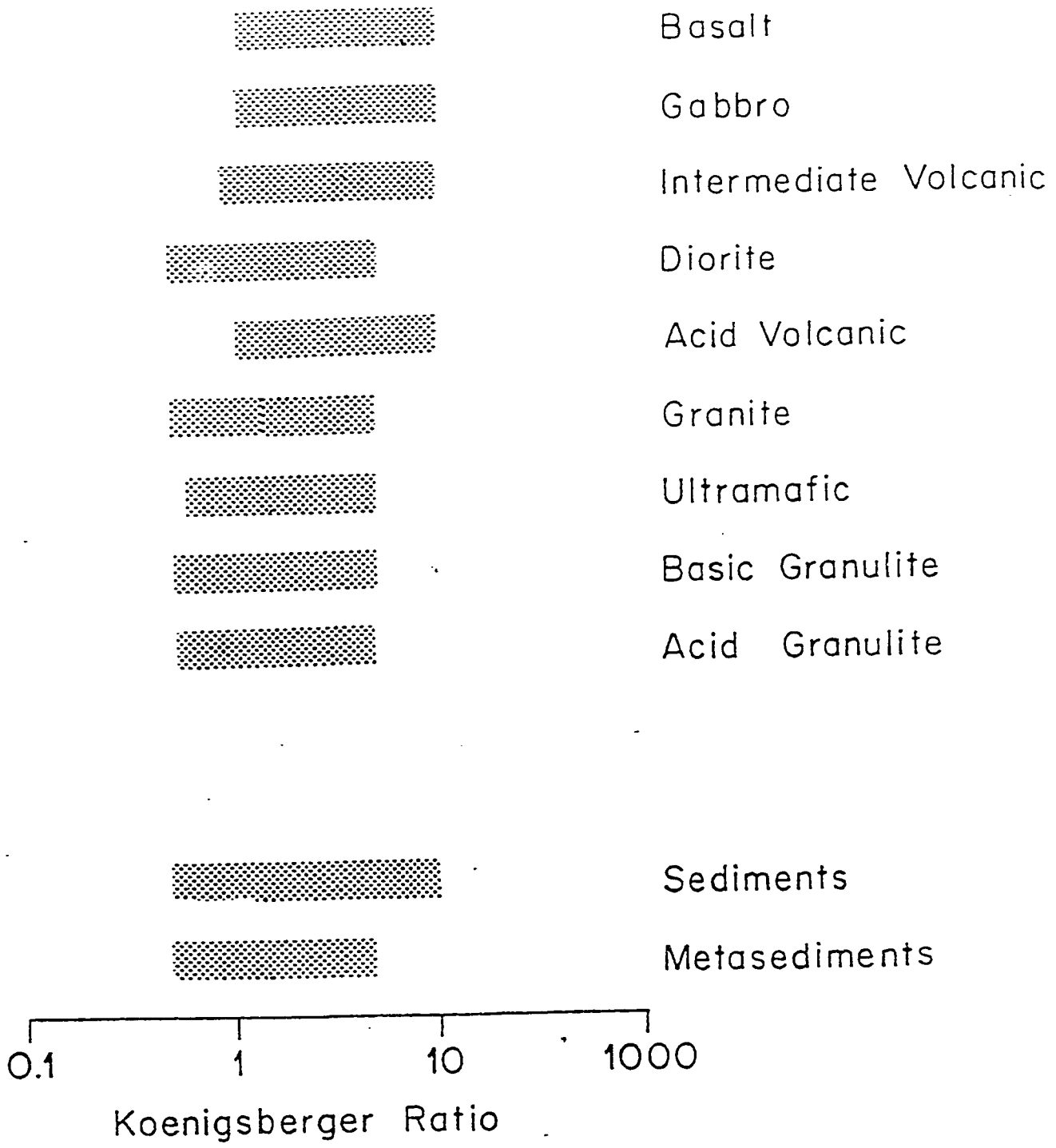

Fig. 2.3. Common range of ratios of remanent to induced magnetization intensity (Koenigsberger ratio), from Clark (1983).

secular variation.

Apart from the secular variation, all other temporal variations of the geomagnetic field have an origin external to the Earth, mostly due to cosmic interactions with the Earth's ionosphere. These variations have a much shorter period than the secular variation and are commonly (and incorrectly) referred to as diurnal variations.

Solar and lunar variations in the field have periods of one year and one month, respectively. They are the result of the disturbance of the Earth's magnetic field by the orbit of the Earth around the Sun and the moon around the Earth.

True diurnal variations or daily effects have a period up to 24 hours and amplitudes to 50nT (Luyendyk, 1997). They are due to the rotation of the Earth about its axis, relative to the Sun (Fig. 2.4) and the interaction of solar wind on the ionosphere.

Magnetic storms are due to changes in the flux of cosmic rays or solar wind interacting with the Earth's magnetic field. The fluctuations in the solar wind corresponds to sunspot or solar flare activity and the interaction with the Earth's ionosphere is visually manifested in the Aurora Borealis. These disturbances have amplitudes of tens of nanoTeslas and periods of hours to weeks. Magnetic data acquisition should be curtailed during these conditions.

Pulsations are randomly occurring temporal variations with period of 1 to 300 seconds and amplitudes generally less than 10 nT (Luyendyk, 1997).

Temporal or diurnal variations cause the Earth's magnetic field strength to vary over time. As a consequence, the induced magnetic field is proportionately varied with time. Aeromagnetic surveys collect magnetic data over time periods affected by the temporal variations. Hence, an understanding of these variations is critical to minimizing these sources of error in aeromagnetic

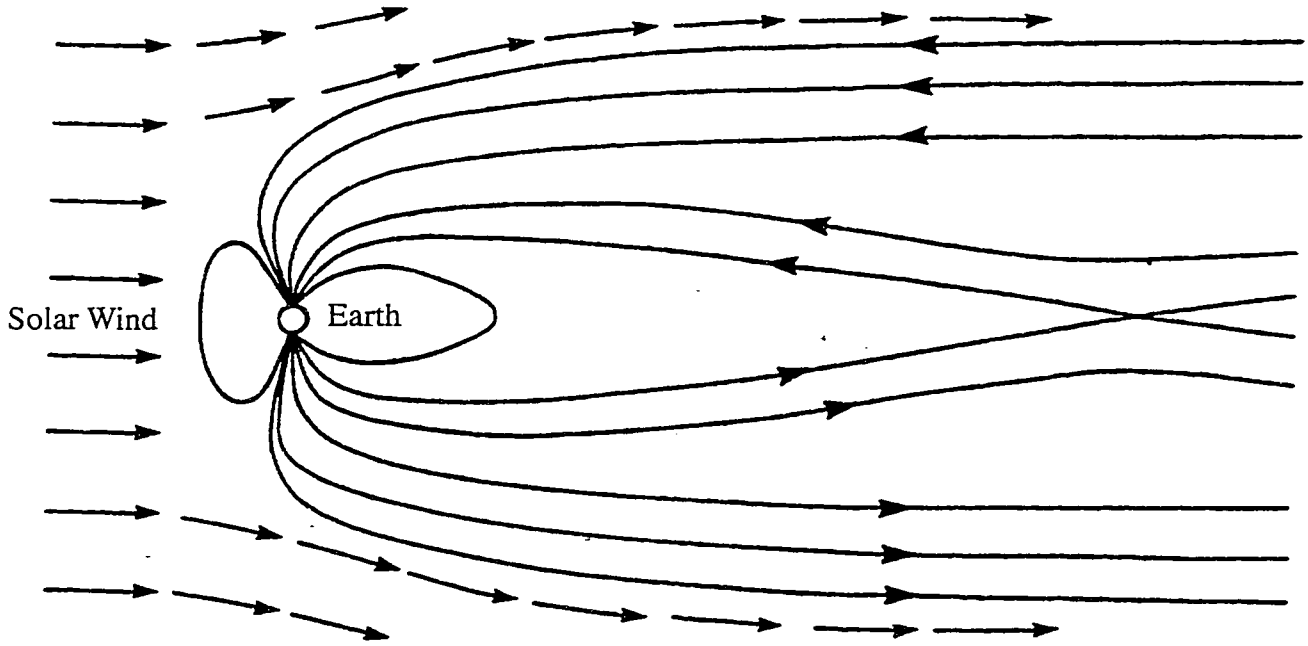

Fig. 2.4. Schematic vertical section of distortion of the geomagnetic field due to the solar wind (from Burch, 1974).

data.

3. DATA AND DATA PROCESSING

The optimum resolution, quality and integrity of an aeromagnetic data set are governed by the original survey specifications and the data processing applied to it. The frequency content and the resolution of the data are governed by the spacing of the flight lines and the flying height above the magnetic sources. Post-acquisition processing is aimed at reducing the effects of temporal variations in the Earth's magnetic field on the data set. These include tie-line levelling techniques, micro-levelling and survey-to-survey levelling. In order to perform some of the levelling techniques, the 2D flight line data must be represented as a 3D grid. For that reason, gridding is considered here as part of the data processing procedure.

3.1. SURVEY SPECIFICATIONS

The aeromagnetic data interpreted in this study were originally flown for Noranda Exploration Company, Ltd. by DIGHEM Surveys and Processing Ltd. The coverage extends from N48°45' to N49° 25' and from W85° to W86°45'; from the Schreiber-Hemlo greenstone belt northwest to the Manitouwadge greenstone belt and the Wawa-Quetico subprovince boundary and east to the Moshkinabi greenstone belt.

The surveys were conducted in two phases. DIGHEM survey #1056AG was flown between December 10 and December 15, 1988. DIGHEM survey #1073 was flown between June 1 and September 16, 1989. The survey specifications are essentially identical. Both surveys were helicopter-borne and acquired frequency-domain electromagnetic/resistivity, magnetic and VLF data. Only the magnetic data were available for this study.

The magnetic data were acquired with an optically pumped Cesium vapour Picodas 3000 magnetometer with a sensitivity of 0.01 nanoTeslas. The total magnetic field intensity was

sampled at 10 Hz (10 readings per second), although processed at 5 Hz, resulting in an average data point spacing of about 7.5m. The magnetometer was towed in a bird 15m beneath the helicopter, which was flown at a mean terrain clearance of 45m, resulting in a sensor-surface separation of 30m. This low altitude was used to accommodate the limited depth penetration of the electromagnetic component of the survey.

The magnetic base stations used were a Geometrics G-826a (Survey 1056AG) and a G-803A digital recording proton precession magnetometers, both with sensitivities of 0.50 nT and a sampling rate of 0.20 Hz (1 sample every 5 seconds). Although not explicitly stated in DIGHEM's technical report for the surveys, it is reasonable to assume the base stations were in close proximity to the survey areas given the well developed local road network. The base station information was synchronized with the airborne magnetometer to allow monitoring and/or removal of diurnal drift.

The mean terrain clearance of the aircraft was monitored and recorded with radar altimetry. The aircraft was an Aerospatiale AS350B turbine helicopter flying with an average airspeed of 110 km/h.

The surveys used a UHF electronic positioning system (Del Norte model 547). This pre-GPS system required ground-based transponder stations to transmit distance information to the helicopter. An arbitrary coordinate system is based on the line joining ground stations (ordinate axis) and a base line flown perpendicular to it, establishing the abscissa. On-board processing fixed the location of the aircraft in these arbitrary coordinates in real time. In post-flight processing, the positions are converted to UTM coordinates by correlation with known fiducial points observed on the helicopter's video tracking system. The system has a sensitivity of 1m,

but the accuracy is controlled by the quality of the correlation of the coordinate system with known points. Although not as accurate as differential GPS, the positioning system should provide more than adequate control.

The survey traverse and control lines are plotted in Figure 3.1. Table 3.1 lists the DIGHEM survey number, corresponding GSC survey number, flight altitude, flight orientation and line spacing. The flight altitude is a constant 30m for all surveys. The finer line spacing of 150m is limited to areas of known, continuous greenstone belt supracrustal rock. The orientations are perpendicular to the local average geologic strike. These high resolution, detailed aeromagnetic surveys provide significant detail about the underlying rock. The different orientations of the flight lines between survey blocks maximizes the utility of the magnetics but requires that the surveys be levelled to each other, both in long wavelength and in the high frequency differences at their mutual boundaries.

The most important issues in data quality with the surveys are the flight line spacing and the mean terrain clearance altitude of the sensor. As the area is largely underlain by igneous rock, as opposed to magnetically homogeneous sediments, the flying height above ground is the distance to source or the source/sensor separation (h). The ratio of h to the linespacing, Δx, is crucial.

The ability of a magnetic survey to represent the magnetic field can be quantified. The Nyquist wavelength (λ_N) is the shortest spatial wavelength that can be identified from samples of the field at line spacing Δx, and is given by:

$$\lambda_N = 2\Delta x \qquad (1)$$

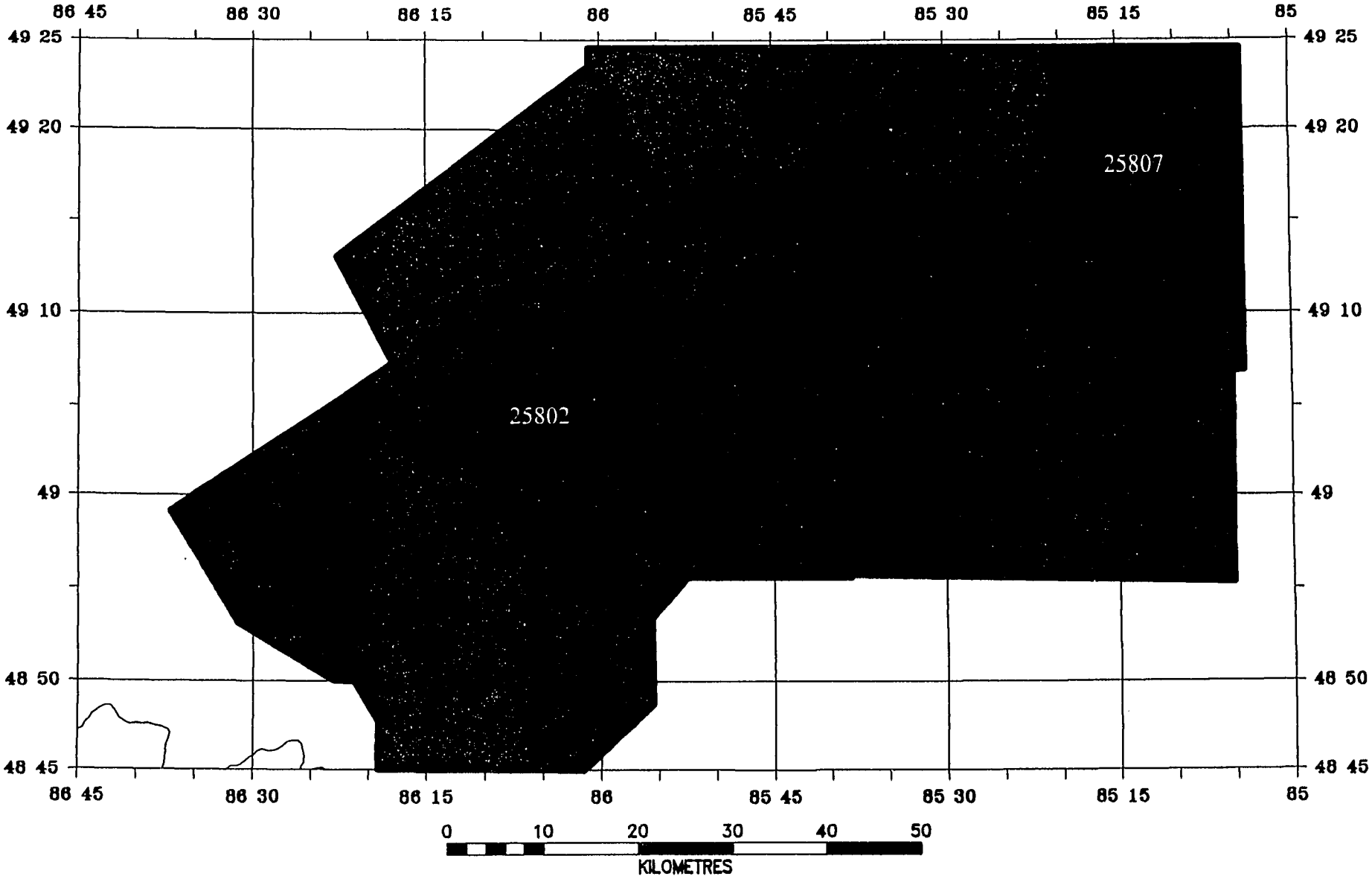

Fig. 3.1. Manitouwadge area aeromagnetic surveys. Numbers in coloured areas correspond to GSC project numbers. Double ended arrows indicate the traverse flight line orientation.

DIGHEM Number	G.S.C. Number	Year	Altitude	Direction	Line Spacing
1073 A	25801	1989	30m	180°	150m
1073 B	25802	1989	30m	150°	150m
1073 C	25803	1989	30m	090°	150m
1073 D	25804	1989	30m	148°	200m
1073 E	25805	1989	30m	151°	200m
1073 F	25806	1989	30m	180°	200m
1073 G	25807	1989	30m	180°	200m
1073 H	25808	1989	30m	136°	200m
1073 I	25809	1989	30m	160°	200m
1056 A	25810	1988	30m	173°	200m
1056 G	25811	1988	30m	155°	200m

Table 3.1. Survey numbers and flight specifications.

Any wavelength shorter that λ_N is aliased into a wavelength larger than λ_N (Reid, 1980, p. 974), distorting the power spectrum. The Nyquist wavenumber, r_N, is given by:

$$r_N = 2\frac{\pi}{\lambda_N} = \frac{\pi}{\Delta x} \tag{2}$$

F_t, the fraction of the power that is aliased, is given by:

$$F_t = \exp(-2\pi\frac{h}{\Delta x}) \tag{3}$$

For the 150m line spacing data used in this study;

$$F_{t_{150}} = \exp(-2\pi\frac{30m}{150m}) = 0.2846 \tag{4}$$

or 28.5% and for the 200m linespacing data;

$$F_{t_{200}} = \exp(-2\pi\frac{30m}{200m}) = 0.3896 \tag{5}$$

or 39%. The large amounts of power aliased are magnified when the vertical derivative is taken. Reid (1980) derives the amount of power aliased for the first vertical derivative case as:

$$F_g = [2(\frac{\pi h}{\Delta x})^2 + 2\frac{\pi h}{\Delta x} + 1] \exp(-2\frac{\pi h}{\Delta x}) \tag{6}$$

which yields an F_g for the 150m data of 86.7% and for the 200m data of 93%. Reid (1980) considers that the aliased power should not be greater than 5%. This would suggest that the appropriate height should be 95m and 71.5m for the 200m and 150m linespacing data,

respectively. These, however, are optimum conditions rarely met in multiparameter airborne geophysical surveys. As well, the choice of $h/\Delta x$ is a compromise between anomaly separation/definition and aliasing. Generally, an $h/\Delta x$ of 1/2.5 is acceptable (Teskey and Irvine, 1995, p. 9). As there is a pronounced geological strike and efforts have been made to orient the flight lines perpendicular to those strikes, the $h/\Delta x$ ratio can be relaxed (Reid, 1980, p. 978).

The visual effect of the choice of line spacing and flying height can be seen in Figure 3.2. It shows the magnetic anomalies expected at various altitudes above a dyke. It is readily seen that any interpolation scheme will better approximate the smoother, higher altitude anomaly shape than the sharper, nearer source anomaly shape. By analogy, a sensor too close to the source for a given line spacing will be as effective in representing the magnetic field as trying to read a billboard with one's nose pressed against it. The fine detail where you touch the billboard may be clear, but the big picture is blurry. If $h/\Delta x$ is too low, grids of the data will have sharp anomalies where supported by the data and smoother ones between lines, giving a segmented appearance to linear anomalies.

The $h/\Delta x$ ratios of the surveys dictate that some action be taken to improve the data. Reinforcing linear trends will help in producing a reasonable 3D representation from the magnetic profile data. Upward continuation of the data by 30m to 60m should bring the data to an acceptable amount of aliasing. The continuation can be thought of as a low pass filter that attempts to limit the shortest spatial wavelength to the Nyquist wavelength.

3.2. LEVELLING

Temporal or diurnal variations in the geomagnetic field are the major cause of line-to-line level shifts in magnetic survey data. Other causes include navigational error and directional, or

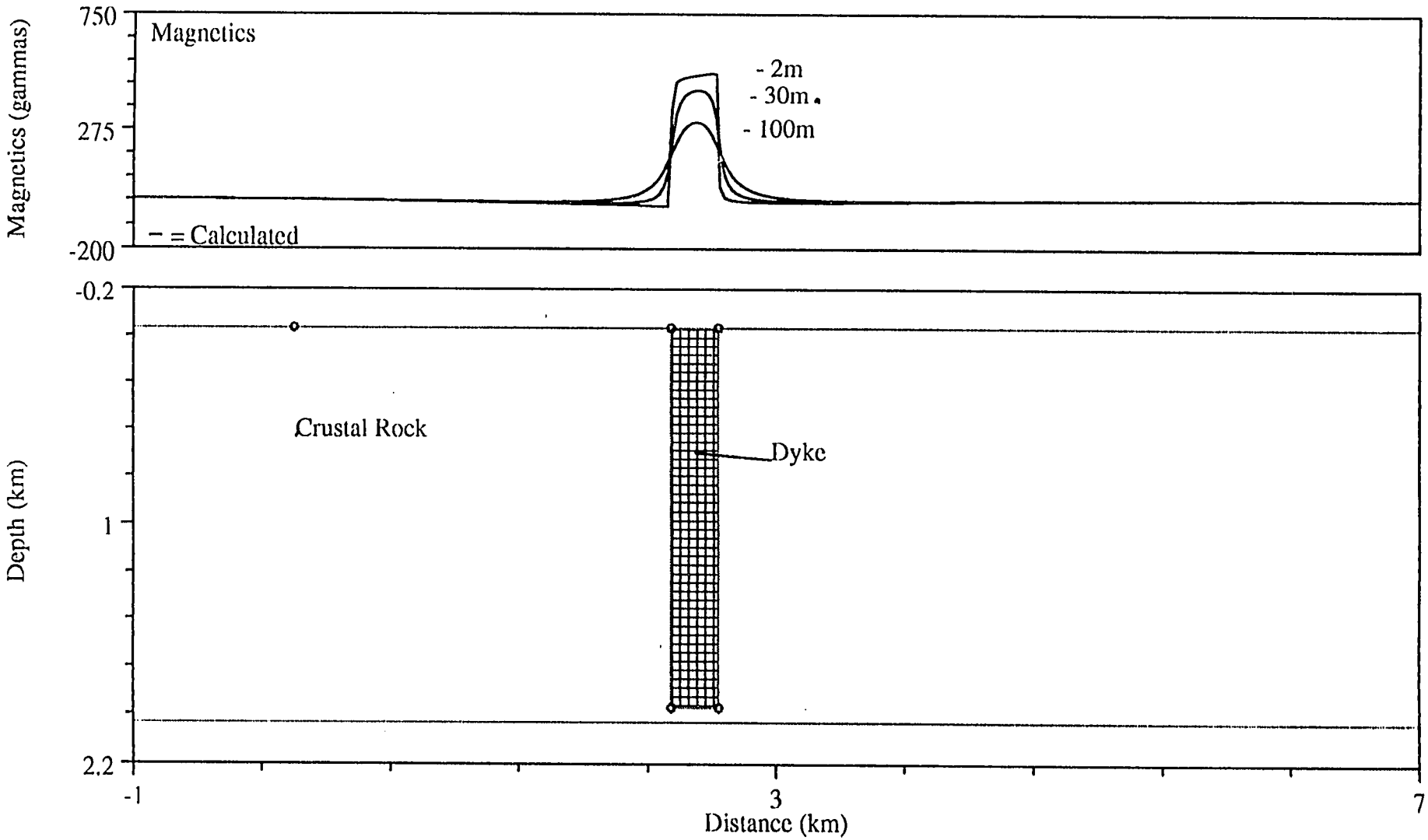

Fig. 3.2. Effect of altitude on magnetic anomalies. The superimposed profiles represent magnetic anomalies calculated at three different altitudes above source (2m, 30m and 100m).

heading, effects due to the magnetization of the aircraft. The temporal variations are monitored by the base station magnetometer and are corrected usually by some form of control line-based levelling. The exact method of levelling used in the surveys of this study is unknown as full technical reports were unavailable and, as well, geophysical contractors consider many of their data processing techniques as trade secrets. However, the method likely resembles the standard tie-line levelling methods of the Australian Geological Survey Organization as described by Luyendyk (1997).

The line-to-line, or tie-line, levelling method revolves around the differences at intersections between tie or control lines (hereafter referred to as 'ties') and traverse lines (hereafter referred to as 'lines', see Fig. 3.3). Lines are grouped into 'flights', where lines are flown consecutively during one flight. The method is a four-stage process; levelling the ties, drifting the lines by flight to the ties, drifting the lines individually to the ties and, finally, drifting the ties individually to the lines.

Levelling the ties begins by choosing a principal tie on which all levelling will be based. The principal tie is chosen as the one which best fits the following criteria. It should cross as many lines as possible, preferably all. To minimize drift within the tie, it should be acquired during a quiet diurnal period (as monitored by the base station magnetometer) and be acquired over an area of low magnetic gradient. Finally, to spread the effects of levelling evenly, the tie should be in the middle of as many lines as possible. In fact, the entire set of ties should be ranked and sequenced based on these criteria as the earlier a tie is used in the levelling process, the greater its effect will be on the quality of the levelling process.

The levelling proceeds in an iterative manner. Preliminary drift curves are estimated for

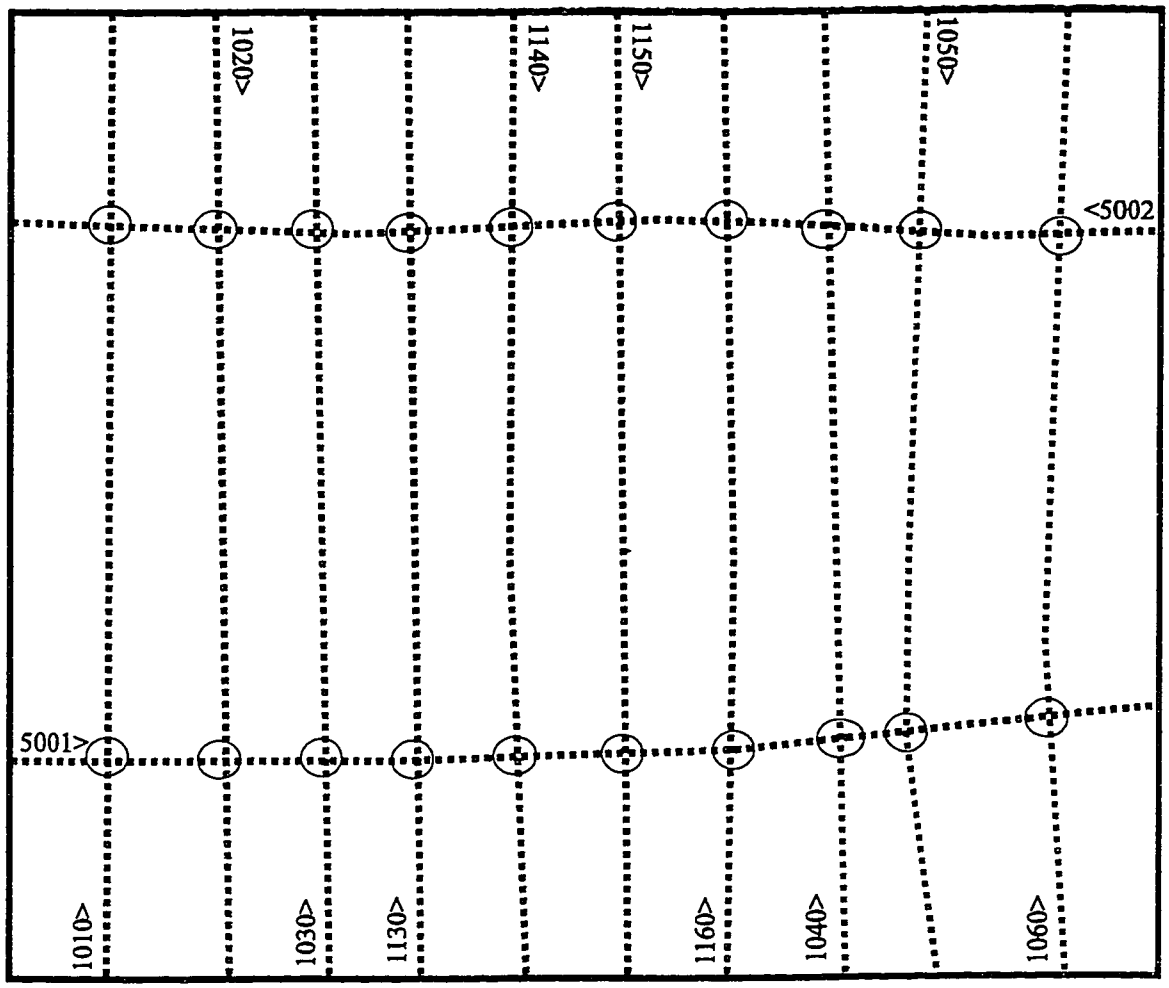

Fig. 3.3. Aeromagnetic survey design. North-south lines are traverse lines. Lines are grouped into flights by colour. East-west lines are tie lines. Line label arrows indicate flight line direction. The intersections of traverse and tie lines are circled.

flights by fitting a polynomial to intersection errors between the principal tie and the lines of the flights. Unlevelled ties are then levelled, one at a time, by subtracting the drift curve (due to line error only) from the intersection error, giving the component of intersection error due to that tie. Once all the flights have been processed for an individual tie, the complete set of intersection errors attributable to the tie are fitted to a polynomial as a function of time. The polynomial corrects the magnetic value at each intersection along the tie, thereby levelling it. This procedure is repeated for each tie resulting a set of ties, levelled to the principal tie, whose drift is assumed to be nil.

All intersection error can now be attributed to the lines. A polynomial is fitted to the errors of each flight as a function of time. These corrections are now applied to the intersection points for each flight. This should correct for flight-specific drift. This procedure is repeated for each line individually to remove line-specific drift and heading errors.

The survey is now levelled, however, small residual errors may exist and are removed by relevelling the ties to the lines and then the lines to the ties. The corrections are now applied to all the line and tie data completing the tie-line levelling of the data.

The least squares method of polynomial fitting of the error at intersections minimizes the difference between the polynomial and the data being fitted but does not honour every data point. This ensures random noise (navigation error, micro pulsations) is not introduced into the data. The degree of the polynomial fitted must be chosen carefully and is governed by the number of data points. The choice of degree of polynomial is crucial, as too low an order will give simplistic results and poorly fit the error, while too high an order polynomial will tend to honour the data points and introduce other errors to the levelling process. As bad data points can have

undue influence on the polynomial, the data are usually first fit to a preliminary polynomial which is used to reject errors greater than two standard deviations for the final polynomial fit. Furthermore, poor fits to polynomials are expected at the ends of flights, lines and ties as they are not constrained.

Tie-line levelling will produce a smooth, continuous representation of the data, although the absolute level will be only as good as the principal tie, which may be subject to drift itself. Despite all that can be done to minimize levelling errors, there may be level shifts introduced. Furthermore, this type of levelling is unable to remove errors of wavelength less than twice the control line spacing and, for the data used in this study, the control line spacing is roughly equal to the length of the longest lines. Also, the survey has lost its absolute level because it is based on the level of the principal tie and any associated drift. In the larger picture, to compare one survey to another, the secular variation of the geomagnetic field must also be removed.

3.3. GRIDDING

Aeromagnetic surveys sample a continuous surface or field along regularly spaced, parallel flight lines, with spacing between lines much greater than sampling along the line. Gridding is the interpolation of non-regularly spaced point observations to a regularly spaced array of X and Y locations in an attempt to recreate the continuous surface sampled by the survey. A reasonable grid allows accurate contouring, 3D map presentations and a large number of filtering and interpretation techniques. However, gridding cannot recreate the original field perfectly. Limitations of the interpolation technique used must be understood and minimized to optimize the utility of the final grid.

A grid can take on two types of values; real values interpolated from observed data and null

or dummy values. Nulls are usually set to a constant outside the range of possible real values. For example, the grids used in this study have null values set to -9999. Null values are usually disregarded in processing or filtering and set to white or no value on maps. They represent data voids and areas outside the original observed data set.

A number of gridding algorithms are available for processing aeromagnetic data, however, the minimum curvature method of Briggs (1974) is widely accepted and is the method used to generate grids used in this study.

The basic requirement of a grid is that it defines a continuous function in x and y based on a sampled data set and that grid point values tend to observed point values when the observed point's position tends to the grid point position. The minimum curvature method generates grid values that approach, within a specified tolerance, the smoothest surface passing through, or honouring, the input data points.

Briggs (1974) notes that the cubic spline for the piece-wise polynomial fit of two dimensional data provides both control at observed points as well as optimum smoothness between observations. The smoothness and data point honouring of the spline fit can be achieved in one or two dimensions by solving the differential equations equivalent to a third order spline. These equations describe the displacement of a thin sheet under the influence of point loads. Boundary conditions include observed data points as well as the edges of the interpolation. This forces the solution of the equation to have observed point values at observed point positions. Briggs (1974) developed difference equations for all seven possible boundary conditions; away from edges and observations, along edges and away from corners, one row from the edge, at the corners, next to the corners, and edges next to corners. The set of equations are solved iteratively. Assigning

approximate values to U(I,J), a new set of U(I,J) is determined and recycled back into the equations. This procedure continues until the grid values at the observed data points are within a user-specified limit.

Swain (1976) introduced a scheme for reducing the number of iterations required by Briggs' difference equations to reach an acceptable solution. The solution of the difference equations is more efficient if the input points are as close as possible to the final solution. The method involves the progressive reduction of the grid spacing by a factor of two, with an iterative solution computed for each spacing, and using the results of the previous interpolation to constrain the next.

The start of the procedure involves loading the input profile data into memory. The grid is represented as an N x M array (U(I,J)) and every L^{th} element (where usually L=8 for the first stage and is halved for each subsequent stage) is given a weighted mean value using points within a user-specified 'line spacing' or search radius. Based on the input data, an iterative solution of Briggs difference equations for this grid spacing (L) is computed. L is reduced by a factor of 2 and the value determined for U(I,J) in the previous stage is assigned to the new grid values U(I+L,J), U(I,J+L), U(I+L,J+L), as well as the new U(I,J). A new iterative solution of the minimum curvature surface is found with only U(I,J) fixed. This new solution is based only on the control points and the computation converges more quickly because the input grid points are closer to the real solution than an arbitrary starting point. This procedure is repeated until L=1, giving the desired grid spacing. Convergence of the solution is tested by noting the largest change in U that occurs in one iteration and a solution is considered acceptable when this change is less than a user specified threshold or grid tolerance value.

Minimum curvature gridding generates reasonable, 3D representations of the input 2D data, provided that the user-specified parameters have been properly chosen. The user-specified parameters are; grid interval, search radius, blanking radius, and grid tolerance.

The optimum grid spacing is generally accepted to be 1/4 to 1/5 the line spacing and is a compromise between undersampling and oversampling of the flight line data. A larger grid interval effectively filters out high frequency information along the flight line. A smaller grid interval, while preserving high frequency information, will tend to isolate anomalies that should be continuous across flight lines (Keating, 1997).

The search radius limits the distance around a grid point within which data are used for the local interpolation. This is usually chosen to be twice the actual flight line spacing to ensure the local interpolation is not only based on data along a single line, but across lines as well.

The blanking radius is the maximum distance a grid value can be from a real observation point without being set to a null value. It is usually chosen to be three times the flight line spacing. If the blanking radius is too large, the grid will contain values not supported by the original data. If the blanking radius is too small, the grid will contain nulls where grid cells are not supported by an observed data point, defeating the purpose of gridding in the first place.

The threshold value controls how closely the final grid will honour the input points. The threshold or grid tolerance value should be related to the accuracy of the input data. It is not necessary to grid data to a tolerance less than its measurement accuracy. Conversely, a smooth grid, not representative of the frequency content of the input data, will result if the threshold value is much greater than the data accuracy.

Two limitations with gridding in general and with minimum curvature methods in particular,

should be recognized. First, linear magnetic trends that are intersected by the survey flight lines at a low angle can appear as series of circular anomalies (Fig. 3.4, 'bull's eyes', 'string-of-pearls' etc). This is a direct result of the combination of undersampling of data across flight lines and the minimum curvature method; the minimum curvature surface without data constraints will tend to that of a sphere, resulting in circles in two dimensions (Keating, 1997). The isolating of anomalies in this manner are considered the result of choosing too fine a grid interval. Second, reasonable grids of profile data represent only a fraction of that data. Data are sampled along the flight line usually at distances (between 5m and 15m) an order of magnitude less than the flight line spacing. As a flight line spacing of 150m will dictate a grid interval of 30m to 40m, the grid will be represent only a third of the input data.

3.4. MICRO-LEVELLING

Micro-levelling is a technique used to reduce errors in the line-to-line levelling of aeromagnetic data. It attempts to reduce the effects of variations in the Earth's magnetic field that occur over a period less than the time taken to fly along traverse lines between control lines. It will also correct for heading errors not previously removed. These minor errors can be significant when high pass and derivative filters are applied to the data.

The technique is based on the assumption that errors in the data will be observed on grids as spurious anomalies elongated in the flight line direction along individual lines and that all lines are subparallel with a fairly constant flight line spacing. Micro-levelling corrections are usually less than 5-10nT (Luyendyk, 1997) and, in fact, the method is not effective on errors much greater than this amount. The strategy is to isolate the spurious anomalies from the gridded data by filtering to produce a correction grid. Chapter 4.2 of this thesis discusses the basic concepts

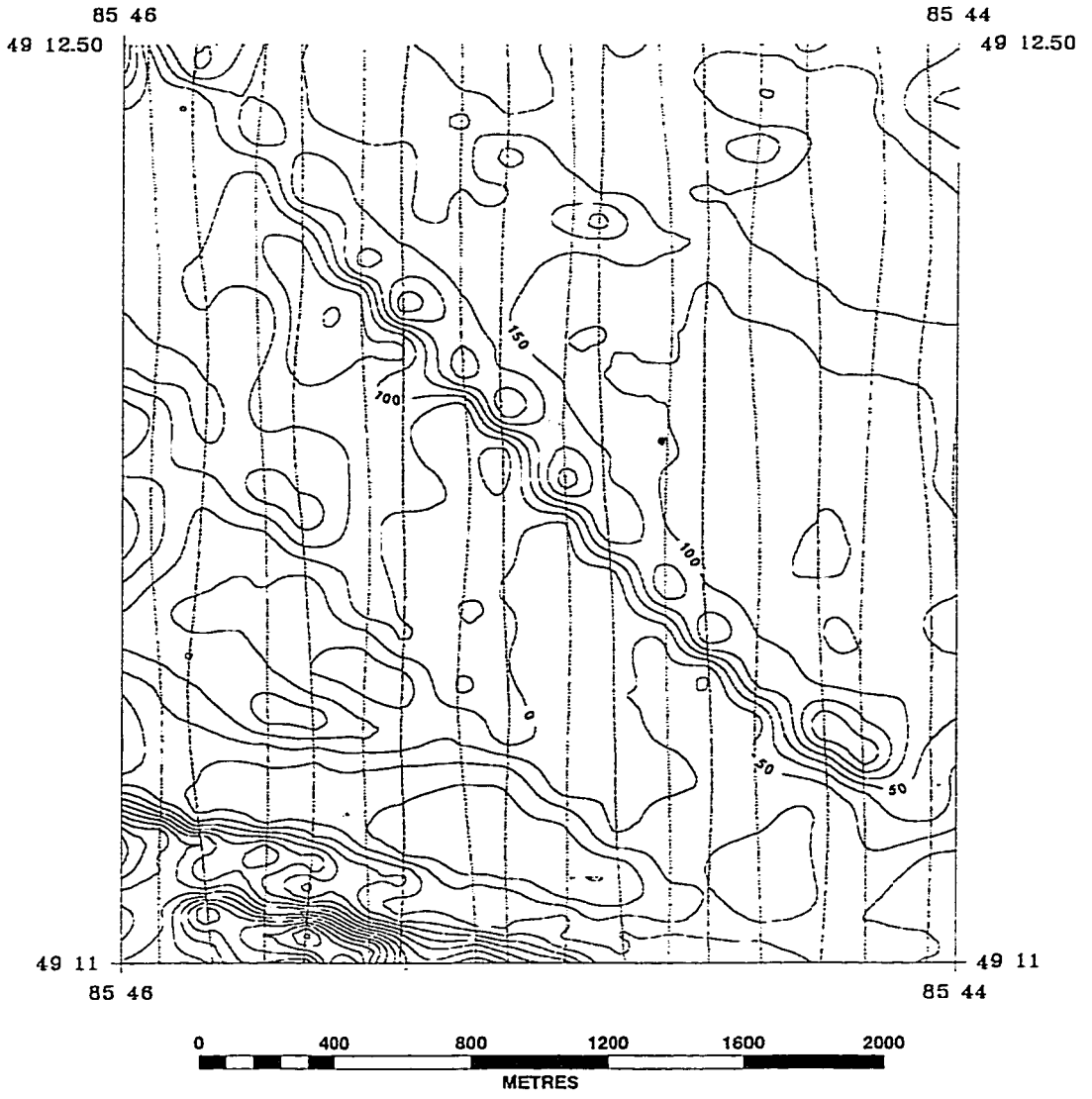

Fig. 3.4. Linear magnetic trend at low angle to flight lines represented as a series of circular anomalies. North trending lines represent the flight lines.

of filtering of gridded data, as well as individual filters, in detail.

Isolating the along line errors is achieved by the combination of a Butterworth high pass filter and a directional cosine filter. The Butterworth high pass filter is given a cut off value of four times the flight line spacing, limiting the wavelength of the anomalies under consideration. The directional cosine filter passes only those wavenumbers parallel the flight line direction. This produces a preliminary correction grid (Fig. 3.5a). It is obvious that the grid contains geologically significant magnetic information, as not all features of the grid are parallel to the flight line direction. To reduce this component of the grid, a second directional cosine filter is applied to the correction grid with the results rejected, leaving the component that is not parallel to the flight line direction in the filtered grid (Fig 3.5b), which is then subtracted from the correction grid. If the grid correction grid contains corrections greater than an amount deemed reasonable for the method, they can be set to that limit at this stage. The final correction grid (Fig. 3.5c) is then interpolated at each magnetic value in the profile data and subtracted from that value generating a micro-levelled value.

From Figure 3.5, it is clear that the final correction grid contains error corrections that are parallel to the flight lines and that the corrections are very small relative to the total field. All grids used in this study have been micro-levelled to improve the over-all levelling and improve the appearance and quality of derivative grids and images.

3.5. SURVEY-TO-SURVEY LEVELLING

To produce one continuous, seamless master grid and to facilitate processing, survey-to-survey levelling was performed on the eleven, tie-line levelled, sub-surveys. The data were then included in the National Aeromagnetic Data Base of the Geological Survey of Canada.. The

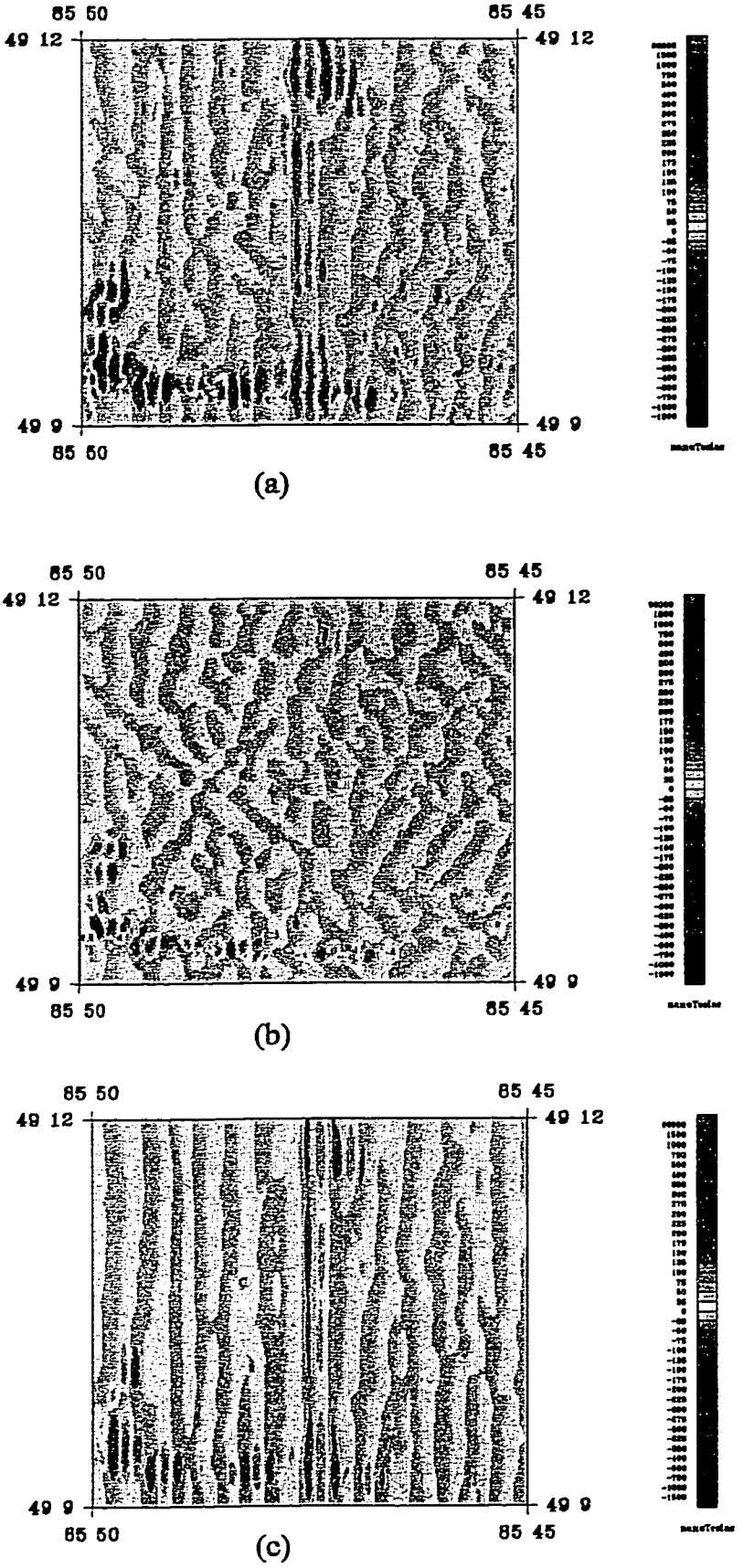

Fig. 3.5. Microlevelling filtering steps. a) preliminary correction grid, b) second directional cosine filtered grid, c) final correction grid.

levelling involves removing the effects of secular variations in the magnetic field between surveys, modifying the long wavelength component of the data to match regional coverage and correcting for high frequency edge effects.

Secular variations in the geomagnetic main or core field are monitored by geomagnetic observatories. The International Geomagnetic Reference Field (IGRF) is a model of these measured secular variations. From models of the field based on earth and satellite-based magnetic observatories, the Earth's core field intensity can be calculated for a given height above mean sea level, the horizontal position and the date of the survey. As the field varies slowly with time, an average survey date is usually used in these calculations. As the topographic relief is generally relatively low in the Manitouwadge area, and as the vertical gradient of the field is on the order of 0.025 nT/m (Luyendyk, 1997), a constant height above mean sea level is used for IGRF calculations. In fact, the choice of a constant height is made necessary by the lack of adequate vertical positioning. The constant height was calculated for each survey from the average topographic elevation in the individual survey area plus the mean terrain clearance of the survey (30m).

Removal of the IGRF from the magnetics is performed on the profile data. It allows the removal to the deep earth source component of the field and leaves the component due to induction and remanence. This remainder, the residual total magnetic field, reflects the lateral and vertical variations in magnetic properties within the crust. The residual field can now be compared with other data sets acquired at different times, which is integral to survey-to-survey levelling.

The data were levelled to the national datum. This was done largely to include the data in the

Geological Survey of Canada's National Aeromagnetic Data Base, but also to bring the magnetic field of the surveys to a recognized and familiar level. As added benefits to levelling and storing the data in this manner, data access and was simplified and permanent archiving was achieved.

The national datum is represented locally by a survey flown between May and October, 1962. This survey was flown with north-south traverse lines at a mean terrain clearance of 305m (1000 feet) and with a line spacing of 805m (half mile). The data were acquired as analogue profiles which were transcribed to 1:63 360 scale maps and hand contoured at a 10 nanoTesla interval. In the late 1970's, these maps were digitized along the flight lines at the intersections with contour lines (Dods et al., 1985). Figure 3.6 shows the digitized points superimposed on the colour contours of the residual total magnetic field. Gridded versions of the data were originally levelled to the national datum using control lines flown specifically for this purpose. The control lines flown in 1984 (Teskey and Hood, 1991) from Winnipeg, Manitoba to Sept-Isles, Quebec in the east-west direction and from Lake Ontario to James Bay in the north-south direction. Base stations set up at 400km intervals along the profiles monitored the diurnal variations. These profiles were the basis of the long wavelength levelling of the regional data gridded to 812.8m interval. In the late 1980's, the profile data of the National Aeromagnetic Data Base were gridded to a 200m interval and a levelling adjustment was derived from the difference between the 200m grids and the 812.8m grids regridded to a 200m interval (Reford et al., 1990). The resulting levelled 200m master grid was used to interpolate levelled magnetic values at the location of the profile data. This effectively low pass filtered the data at 200m. Levelling of other parts of the country avoided this filtering by interpolating values from the adjustment grid and adding the interpolated values to the profile data values.

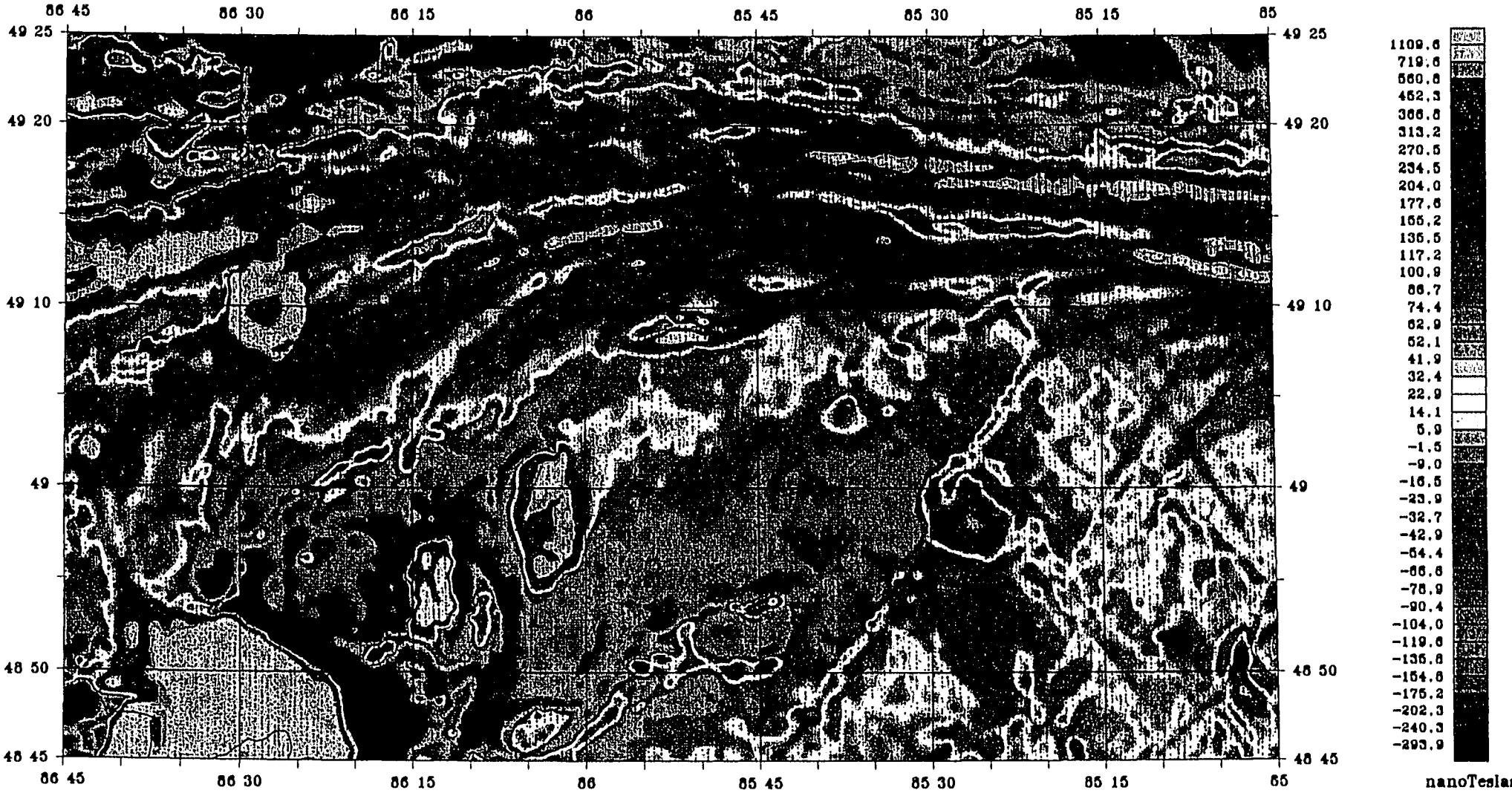

Regional Residual Total Field Magnetics

0 10 20 30 40 50

KILOMETRES

Fig. 3.6. Regional residual total field magnetics levelled to the national datum. Flight line spacing is 805m. Black dots represent data points digitized from the intersection of flight lines and contour lines on 1:63 360 contour maps.

In order to level the high resolution Manitouwadge data to the national datum, both data sets were gridded to a 100m interval. The high resolution data grid was subtracted from the regional grid to generate a difference grid. The difference grids were fitted to a first order surface to remove any high frequency effects. This was considered more reasonable than a low pass filter as most of the surveys were smaller than the wavelengths we wanted to compare. The first order surface grids were interpolated to the profile data and added to the tie-line levelled, IGRF removed, residual total magnetic field data, adjusting the survey to the national datum. This procedure retains all the high frequency information contained in the tie-line levelled data.

As the individual sub-area surveys of the Manitouwadge survey were flown in different directions to maximize the amount of data flown perpendicular to the strike of the local geology, there are high frequency differences between the sub-areas at there boundaries where there are flight line mismatchs. These differences at the boundary can be due to line-to-line levelling or merely the detection of an anomalous source too small to be detected by both surveys. These boundaries can appear noisy in grid form and introduce artefact linear features (seams). To produce seamless grids suitable for the filtering required for many of the interpretation techniques used in this study, a high frequency adjustment scheme was devised. All sub-areas were gridded to the final minimum gridding interval of 25m, extracted to their mutually exclusive boundaries and merged into a master grid. One by one, the sub-areas were targeted for levelling. The area of the target survey was set to null in the master grid (Fig.3.7a). The target survey was extracted from its original grid with a two grid cell boundary overlap and subtracted from the master grid to generate a difference grid, a band two grid cells wide around the perimeter of the target survey. The target survey was extracted from its original grid with the

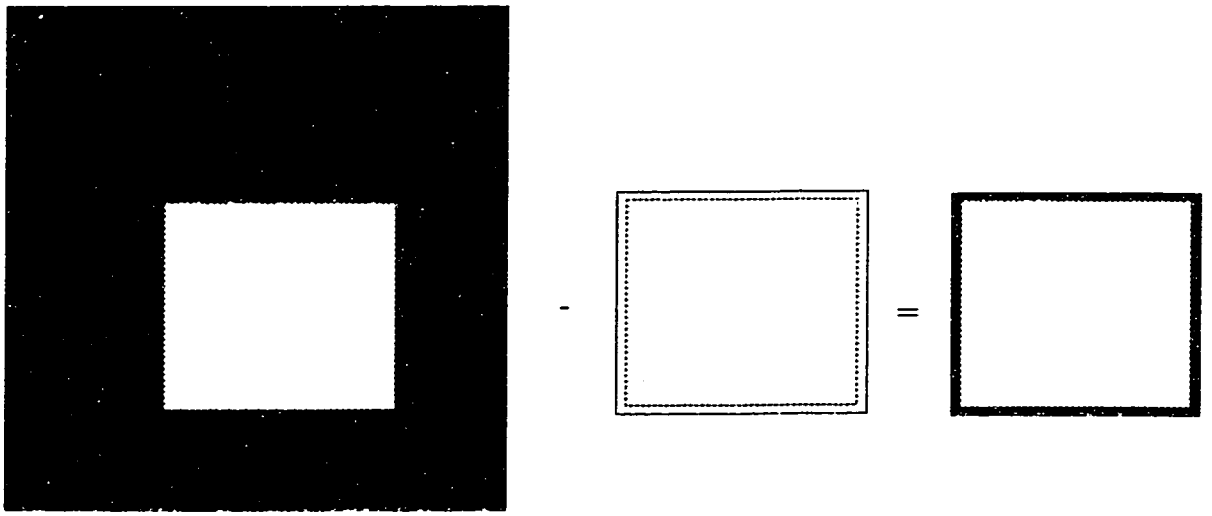

Master grid with target survey area nulled - Target survey with 2 grid cell overlap = Difference grid

a)

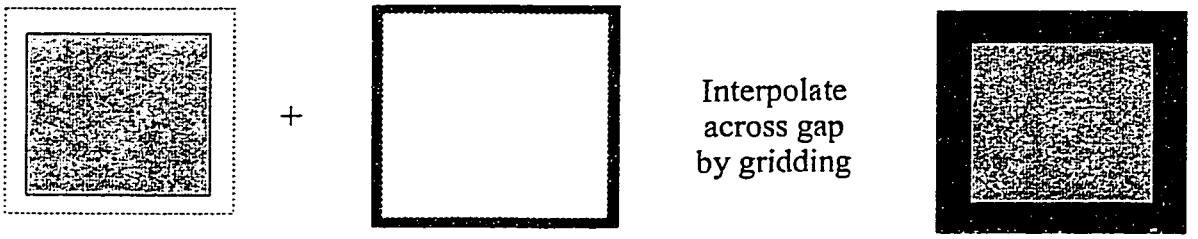

Target grid trimmed by 6 grid cells and set to zero (grey area) + Difference grid — Correction grid

b)

Fig. 3.7. High frequency levelling at survey boundaries. a) Area of survey to be corrected is nulled in a master grid of all local surveys. Target survey area with two grid cell overlap is subtracted from the master grid producing a difference grid. b) Target area grid is trimmed around perimeter by six grid cells and all non-null grid values are set to zero. This grid is merged with the difference grid and regridded to interpolate correction values across the six grid cell gap.

six outer most grid cells trimmed away (Fig. 3.7b). The non-null values of the extracted grid were set to zero. The zeroed grid and the difference grid were regridded using a minimum curvature algorithm with a small search radius, a loose grid adjustment value and no blanking to fill the six grid cell null zone with high frequency correction values. Six grid cells were chosen for this correction zone as it corresponds to a distance less than or equal to the line spacing of the data. It was felt this offered maximum smoothness of transition without altering an excessive proportion of the data. The grid of correction values was interpolated to the profile data and added to the tie-line levelled, IGRF removed, datum levelled magnetic data. The high frequency edge adjusted data were then gridded and the master grid updated. This process was repeated for each survey to create the seamless profile and gridded data sets that have been published as Geological Survey of Canada Openfile 3447. Figure 3.8 presents the final levelled residual total field magnetics for the Manitouwadge area, with the study area outlined.

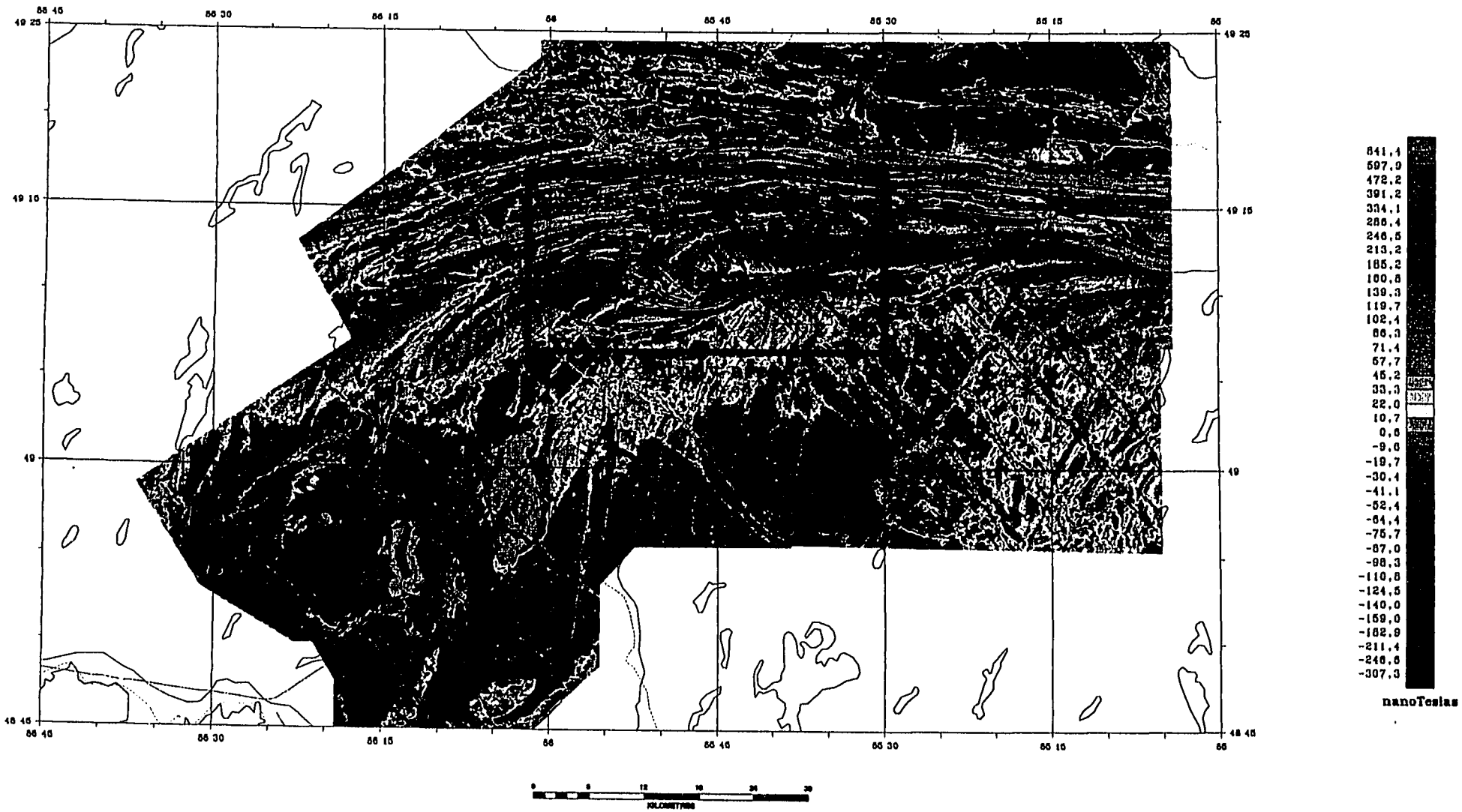

Fig. 3.8. Final levelled residual total field magnetics, Manitouwadge greenstone belt.

4.0. DATA ENHANCEMENT

Following the completion of the levelling of the aeromagnetic data, enhancements to the gridded versions of the data will aid in the interpretation. Trend reinforcement is an attempt to improve the quality of a grid before wavelength filtering is applied. Most filtering of 3D gridded data is performed in the frequency domain and most 3D interpretation tools are based on filtered grids.

4.1 TREND REINFORCEMENT

Two major concerns in representing the magnetic data in grid form, namely circular artefacts and the loss of high frequency information, can be somewhat alleviated by reinforcing local trends and gridding at a finer interval. Keating (1997) develops an automated trend reinforcement technique that improves the interpolation of linear features that intersect the flight lines at low angles. The method allows the grid to be interpolated at higher resolution.

The method is based on nearest neighbour analysis (Davis, 1976) applied to local maxima and minima of a grid generated using the minimum curvature algorithm. The technique can be viewed as a five step process (Fig. 4.1). First, all local maxima and minima with an amplitude greater than a user-specified minimum are located from a preliminary grid. These local anomalies are only then located on the flight line data. This ensures that no trend reinforcement is performed on maxima or minima that are already well represented by the grid. Second, each flight line maximum or minimum is correlated with a corresponding maximum or minimum on the nearest adjacent flight line (B to C, Fig. 4.1). The selection criteria for connecting maxima or minima are that connection can only be made between adjacent lines and the angle between connecting points and the flight line cannot be less than a user-specified minimum (exclusion

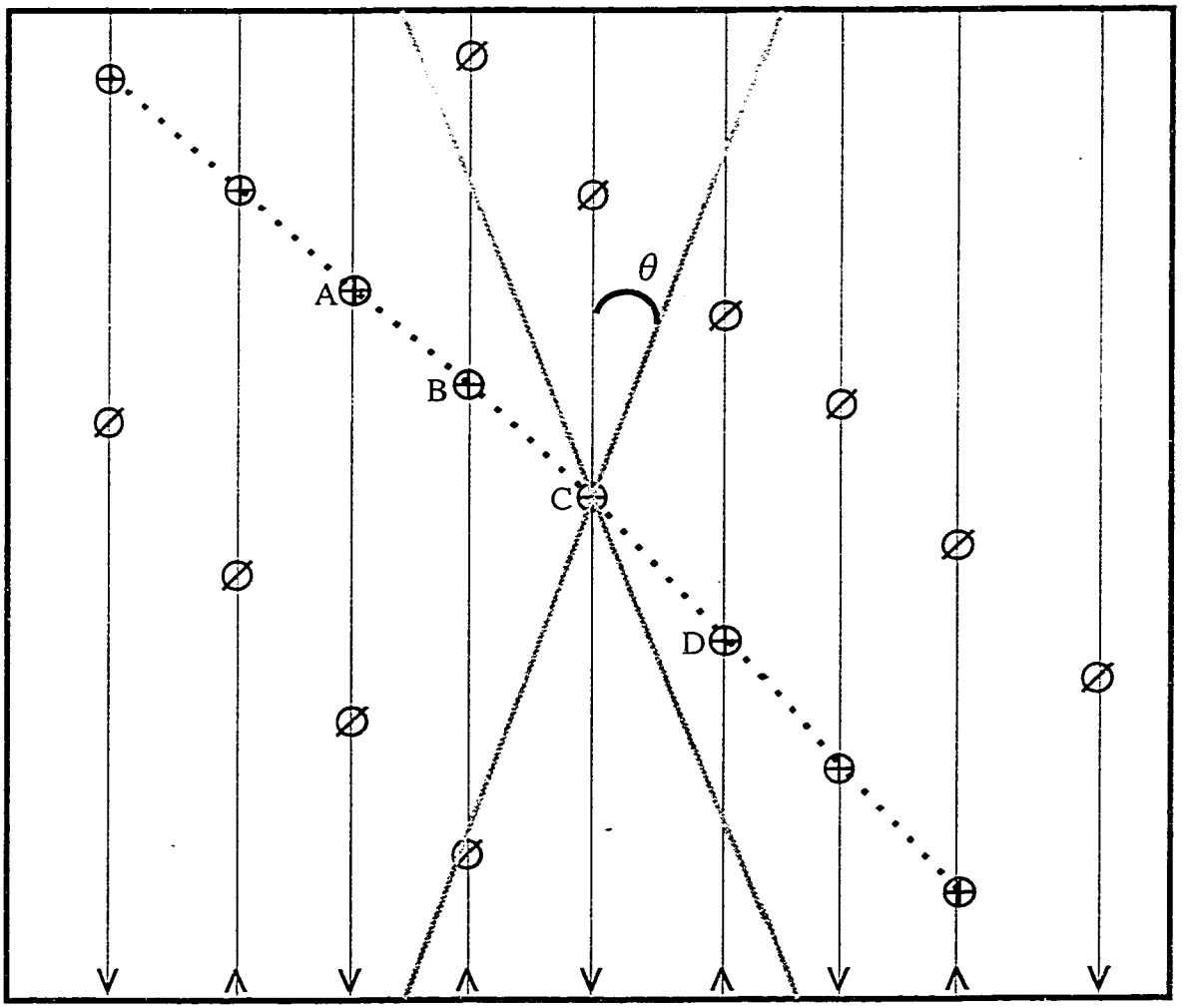

Fig. 4.1. Geometry of Keating's trend reinforcement technique. Crosses within circles represent local maxima, diagonal slashes within circles are local minima, theta is the exclusion angle and black dots between local maxima are the interpolated, trend-reinforcing points.

angle, Fig.4.1). The minimum angle can be estimated from inspection of the preliminary grid linear trend intersections with flight lines. Third, once a connecting pair of points have been accepted, the nearest neighbour search continues in the opposite direction (B to A, Fig. 4.1), ensuring the complete connection of a long string of local maxima or minima. Fourth, intersecting maxima and minima trends are deleted to avoid generating artefacts in the grid. Finally, having met all the previous criteria, a linear interpolation of data points is made between the connecting maxima or minima. A linear interpolation is favoured over other methods, such as cubic spline interpolation, as it constrains the values between known points. The interpolated points, between maxima or minima, are then added to the original flight line data and regridded, producing a trend reinforced grid.

This automated trend reinforcement method improves the quality of the grid representation of aeromagnetic data even when more than one regional trend exists. The method performs the required trend reinforcement reasonably well and is relatively quick and automated. The method is not restricted to any one trend, but reinforces all local trends that meet the criteria. However, any artificial augmentation of a data set puts the integrity of the data set at risk. To minimize this risk, the interpolated data points generated by the method can be plotted and visually inspected. User-specified parameters can then be adjusted to achieve reasonable results.

The data used in this study were trend reinforced using Keating's (1997) method. An exclusion angle of 30° was chosen after inspecting a preliminary grid of the data that indicated that Matachewan dykes intersect the flight lines at about that angle. A smaller angle would have reinforced all parts of the Matachewan dykes as well as the NE trending Biscotasing dykes and possibly the NNE trending Marathon dykes. However, exclusions angles less than 30° allowed

undesirable connections of maxima and minima that generated unrealistic anomalies. Figure 4.2 shows the trend reinforcing points for sub-area 25801. The utility of the method is indicated by the way the trend reinforcing points mimic the major trends; the east-west striping of the Quetico metasediments in the north-east, the folded supracrustals of the Manitouwadge synform as well as the Proterozoic dykes. Figure 4.3 is a trend-reinforced version of Figure 3.4. The major NW trending linear feature is the magnetic expression of a Matachewan dyke. Although the feature has not been completely connected into a continuous anomaly, this image does illustrate that the method improves the gridding algorithm's ability to represent the profile data as a 3D surface. The image also shows that, even where the dyke anomaly has been reinforced, the gridding algorithm still generates a 'pinch and swell' pattern, with pinches at flight lines and swells in between. There is still an undersampling problem between flight lines and away from trend-reinforcing points.

The residual total field magnetic data grids used in this study were trend-reinforced using a 30° exclusion angle.

4.2. FILTERING

Most methods used to interpret magnetic data require some type of filter. These filters include: low pass filters for the removal of the regional components for modelling; high pass filters to accentuate the high frequency component of the data; reduction to the pole; horizontal and vertical derivatives for pattern recognition and various automated interpretation techniques; upward continuation to attenuate high frequency noise; apparent susceptibility computations; and directional filters for the removal of unwanted or artifact signal. Filtering is usually performed on gridded data transformed from the space domain to the frequency domain. The fundamental

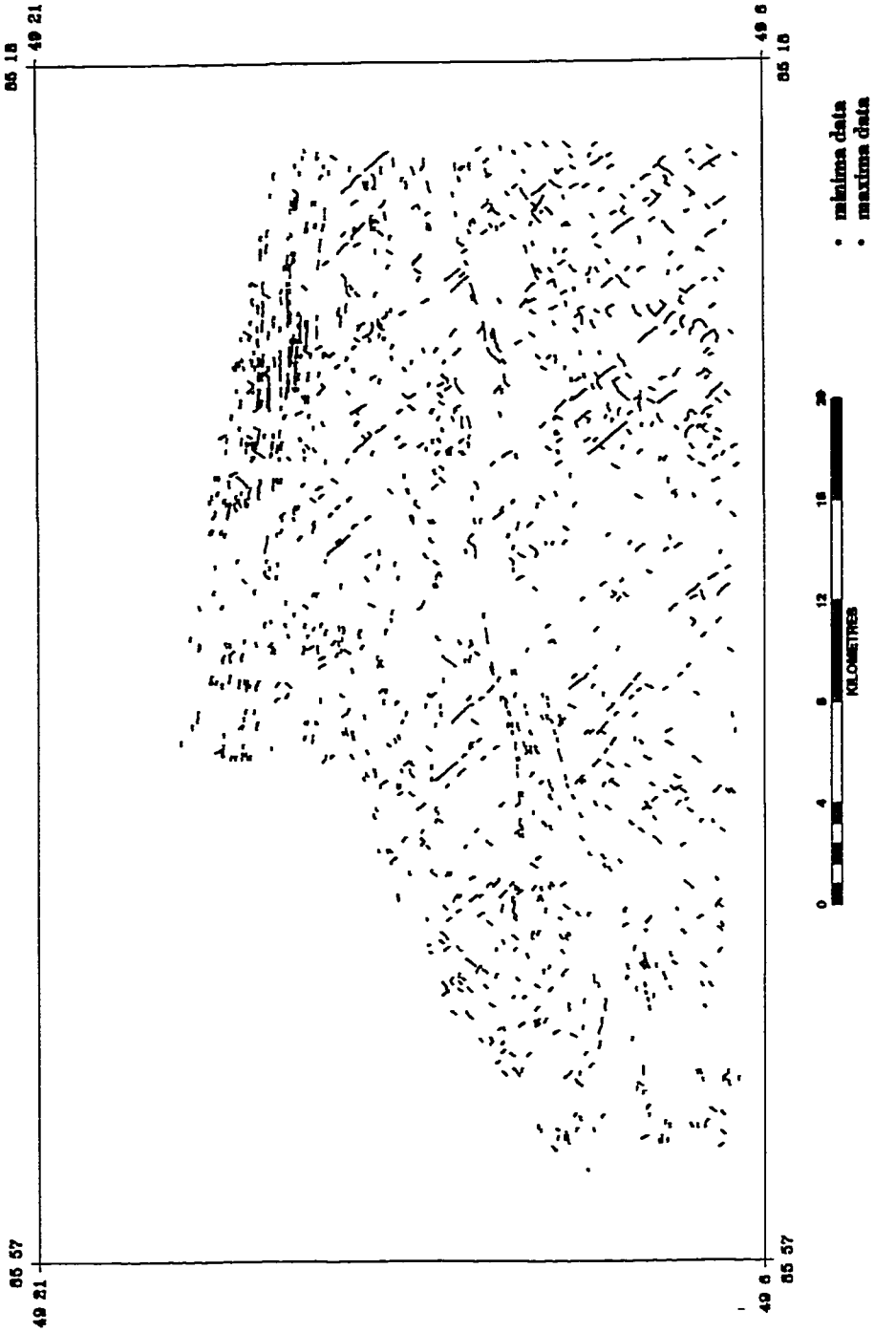

Fig. 4.2. Trend-reinforcing interpolated data points for sub-area 25801. Red dots represent interpolations between maxima and blue dots represent interpolations between minima.

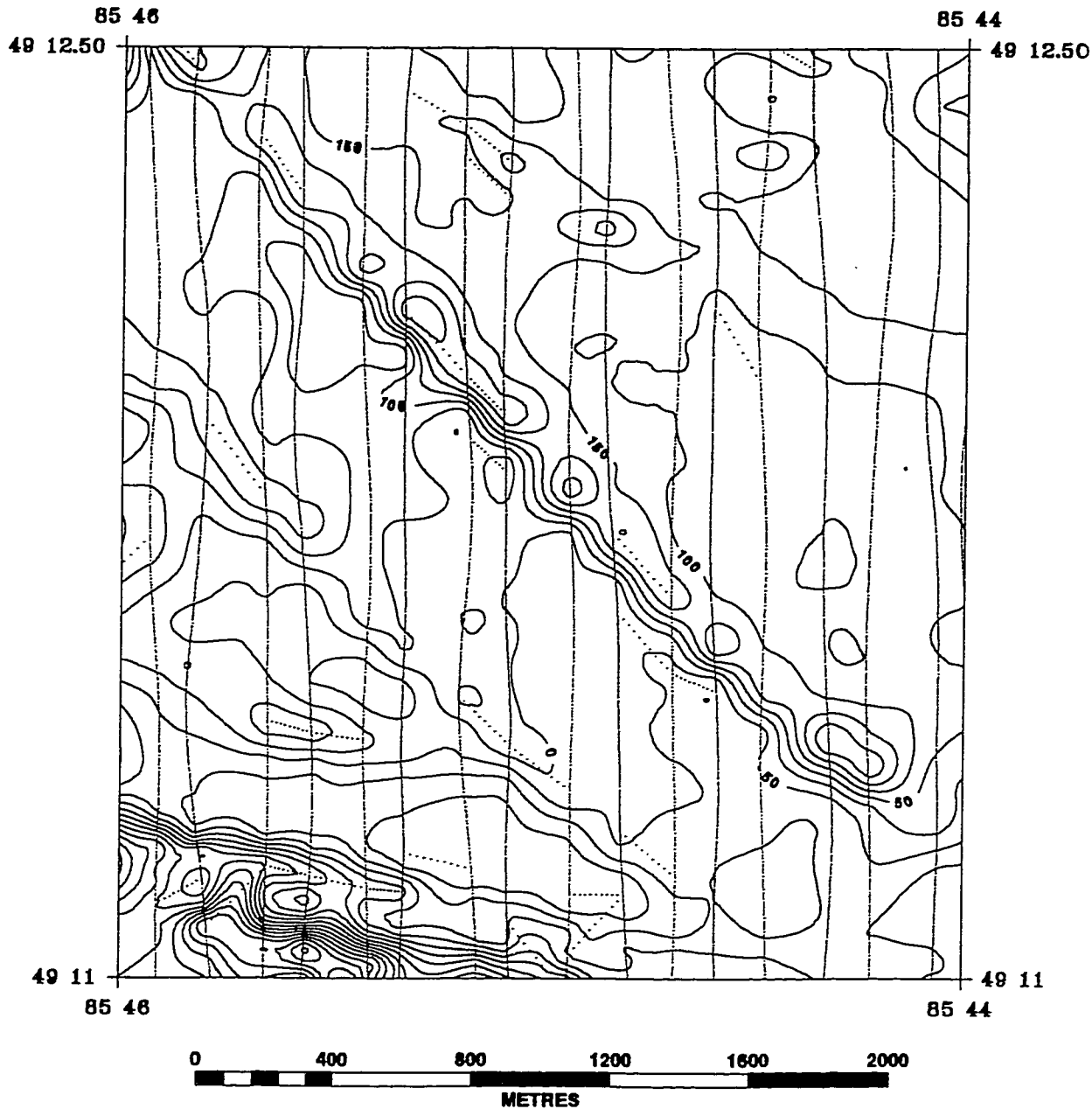

Fig 4.3. Trend reinforced magnetic data (See Fig. 3.4 for non-reinforced version). Red north-south lines represent flight data and the red dots between these lines represent the values interpolated across lines between adjacent maxima and minima.

advantage of filtering data in this way is the simplification achieved in manipulating a grid's frequency content.

The Fourier transform is a method of converting spatial functions to the frequency or wavenumber domain. The Fourier transform has the effect of breaking down a waveform into a set of component sinusoids of different frequencies. The sinusoids sum to the original waveform. Figure 4.4 demonstrates the Fourier transform of a simple waveform. The two sinusoids add together to equal the original waveform and are said to be the Fourier transform of the waveform. The Fourier transform, S(f), of a simple waveform or function, s(t), is given by:

$$S(f)=\int_{-\infty}^{\infty} s(t)e^{-j2\pi ft}dt \qquad (1)$$

where j is the square root of -1. S(f) contains exactly the same information as the original function, s(t). After a filtering manipulation has been performed, the filtered function can be returned to the spatial domain by applying an inverse Fourier transform which, for the simple waveform case, is given by:

$$s(t)=\int_{-\infty}^{\infty} S(f)e^{j2\pi ft}df \qquad (2)$$

A rectangular grid of interpolated data points can be considered a discrete representation of the continuous function. The frequency content of the data can be considered as spatial

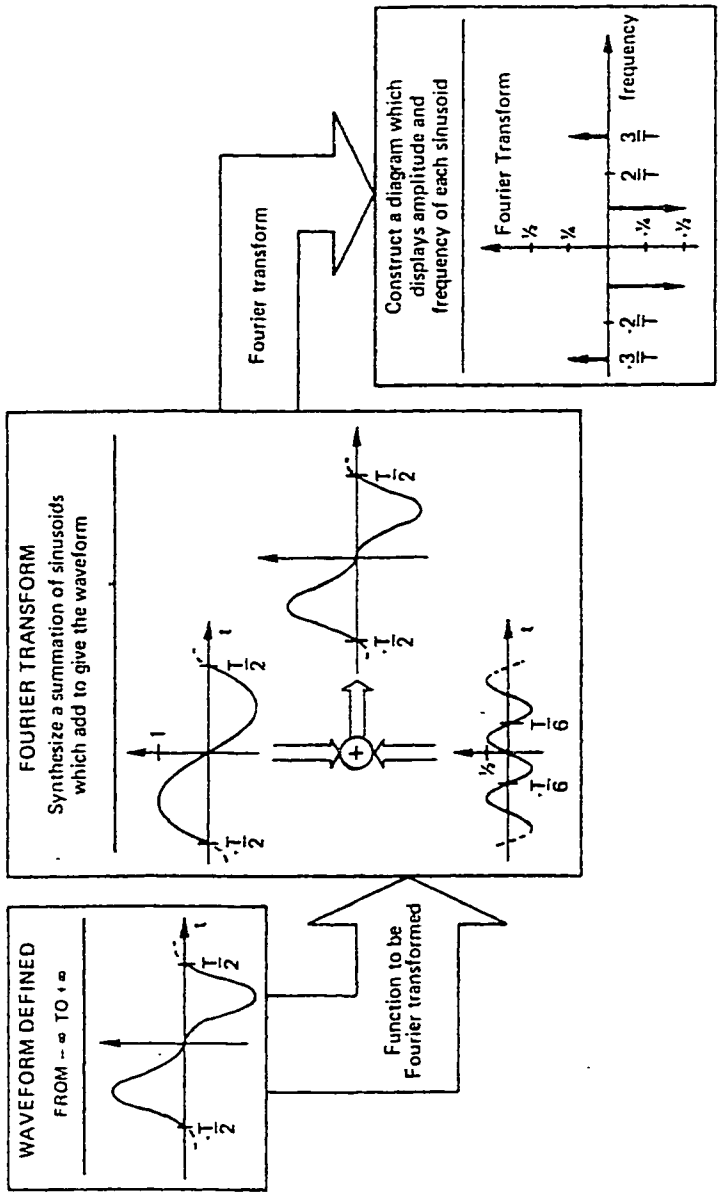

Fig. 4.4. Graphic representation of the Fourier transform from Brigham, 1974.

frequency, in units of radian per grid interval, or by wavenumber, in units of cycles per grid interval. The highest resolvable wavenumber, or Nyquist number, in a square grid is equal to one-half the grid interval, giving a range of wavenumbers between 0 (constant component) and 0.5 cycles per grid cell. The spatial data, f(x,y), is converted to the wavenumber domain by applying a 2D Fourier transform to the data, given by;

$$F(u,v)=\int_{-\infty}^{\infty}\int_{-\infty}^{\infty} f(x,y)\cdot e^{i(ux-vy)}dxdy \qquad (3)$$

where F(u,v) is the Fourier transform of f(x,y), u and v are the wavenumbers in the x and y directions and i is the square root of -1. The transformed frequency domain grid retains the information of the spatial domain grid but is described not by positions in space but by its component frequencies. In the frequency domain, filtering is achieved by multiplying by a transfer function designed to enhance or affect certain frequency or wavenumber ranges. The grid is returned to the spatial domain by applying an inverse Fourier transform;

$$f(x,y)=\frac{1}{4\pi^2}\int_{-\infty}^{\infty}\int_{-\infty}^{\infty} F(u,v)\cdot e^{i(ux-vy)}dudv \qquad (4)$$

The above equations were derived for continuous functions and their continuous transform functions. Similar integrals have been developed for the discrete or sampled cases, generally suitable for digital computer analysis and specifically for sampled data sets such as magnetic flight line data and gridded data sets. The fast Fourier transform of Cooley and Tukey (1965)

provides a quick and efficient means of transforming sampled data into the frequency domain.

Filtering in the frequency domain is achieved by multliplying the wavenumbers by a transform function. This is best illustrated by analysing the wavenumber or frequency domain spectrum. The energy spectrum, E(u,v), of the wavenumber spectrum is defined as;

$$E(u,v)=a^2+b^2 \tag{5}$$

where a is the real part of F(u,v) representing amplitude and b is the imaginary part (terms containing i) representing the phase infomation. Figure 4.5 is a plot of the energy spectrum showing the varying frequency content of different directions within the data. The amplitude of the spectrum, shown in colour, reflects the energy and is a function of the magnetization. Wavenumbers increase outward from the centre left of the image along the directions. Energy spectra averaging by direction allows presentation of the energy spectra independent of direction. This is the average radial energy of the spectrum and the radial wavenumber is given by:

$$r^2=u^2+v^2 \tag{6}$$

Plotting the log of the average radial energy versus the radial wavenumber gives a readily interpretable representation of the frequency content of the grid (Fig. 4.6). Higher wavenumbers correspond to higher frequencies. Note that the largest wavenumber corresponds to the Nyquist frequency. The change in slope of the radial energy spectrum at 0.4 cycles/km illustrates the long wavelength regional component and the short wavelength, high frequency residual component of the data. A transfer function is designed to either attenuate or augment a particular

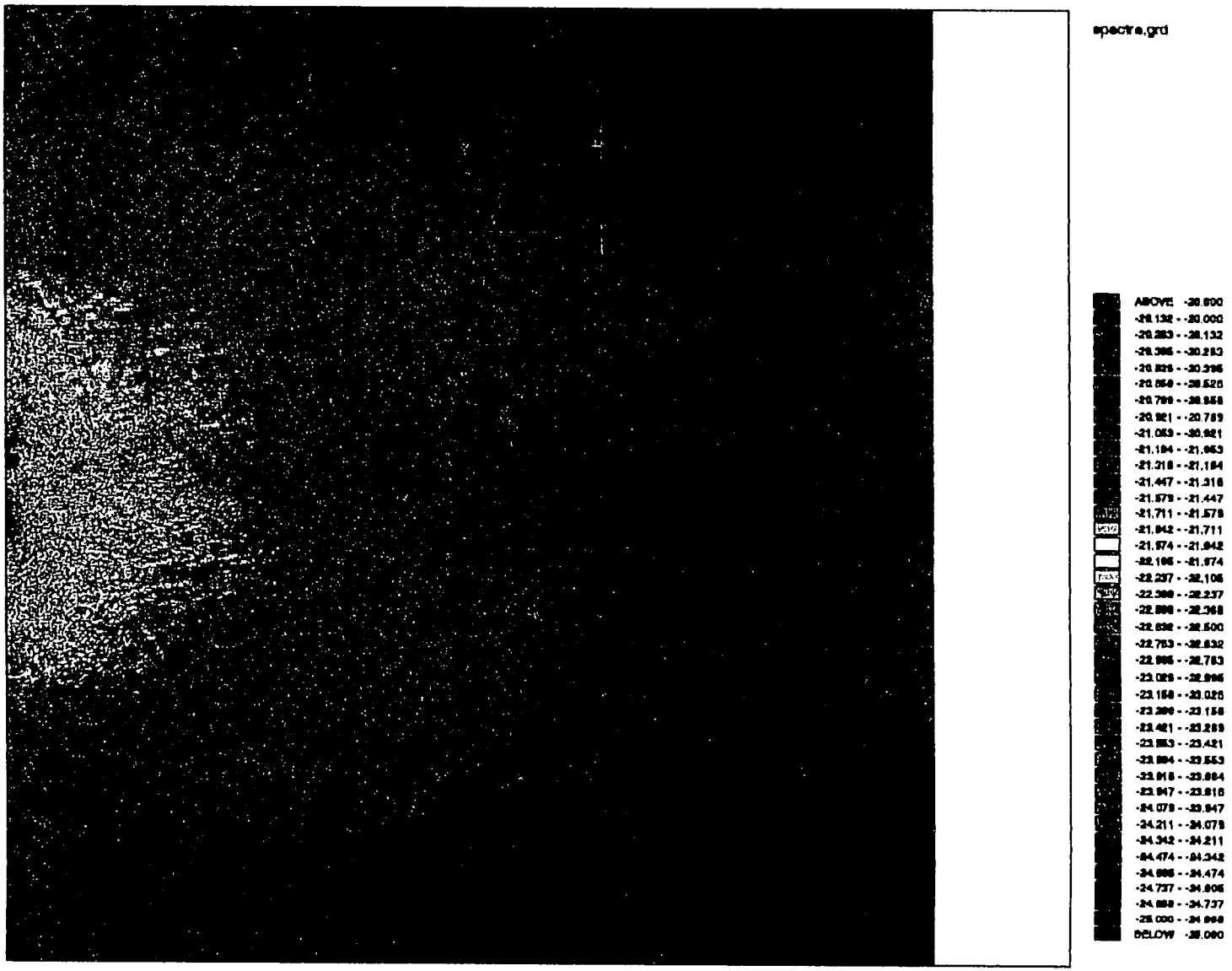

Fig. 4.5. The energy (or power) spectrum of a 40m grid of magnetic data over the Manitouwadge greenstone belt. Energy is represented by the blue to red (low to high energy) colour range as a function of direction and wavenumber.

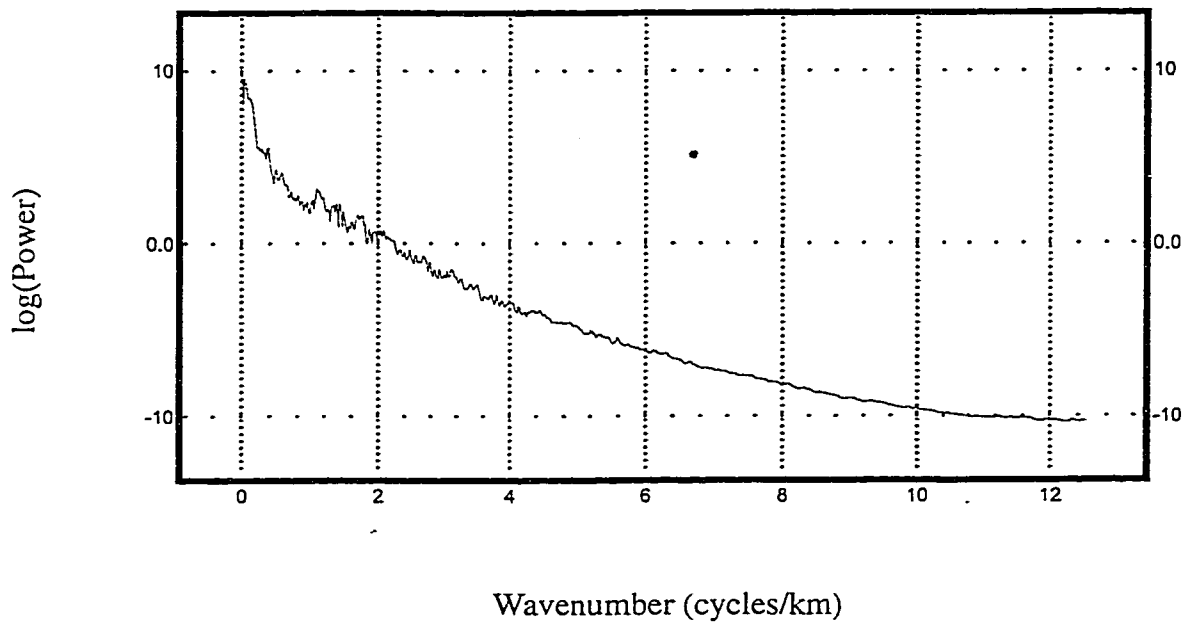

Fig. 4.6. The radially averaged energy (or power) spectrum of a 40m grid of magnetic data over the Manitouwadge greenstone belt.

frequency range in the data. The wavenumber of magnetic data in the frequency domain is related to depth to source and high wavenumbers correspond to higher frequencies and nearer surface anomalies in the data grid. By applying a transform function that attenuates higher wavenumbers, a low pass filter is achieved so that the regional or background component of the field is retained.

Frequency domain filtering has many applications. The filtering is achieved by the application of a transfer function to the data in the frequency domain.

The Butterworth filter is a smooth transfer function used for high and low pass filtering based on a user specified cut off wavelength. It is used to separate a grid's frequency content into high and low components, which translate into short and long wavelength, respectively. This filter has application in micro-levelling where it is used to restrict the wavelength of anomalies under consideration. It has the form;

$$L(k)=\frac{1}{[1+(\frac{k}{k_c})^n]} \quad , \qquad k=\frac{r}{2\pi} \tag{7}$$

where k is the wavenumber and k_c is the central (cut off) wavenumber in cycles per metre and n is the degree of the function. L(k) is the response of the filter varying between 0.0 and 1.0. For a given wavenumber, k, the response of the filter function is L(k). n controls the amount of roll off; a decrease in n increases the amount of roll off (Fig. 4.7).

Derivative filters enhance near surface anomalies by enhancing high wavenumbers

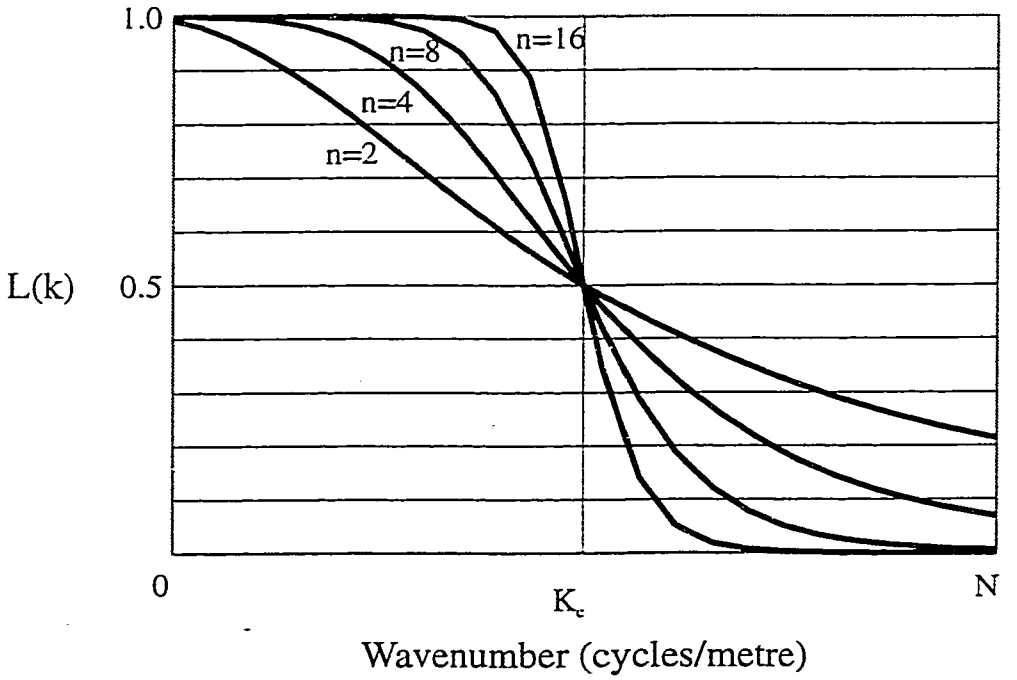

Fig. 4.7. Butterworth filter transfer function response versus wavenumber for various degrees (n). L(k) is the response, K_c is the cut off wavenumber and N is the Nyquist frequency.

preferentially over low wavenumbers. The filters can be used to calculate the rate of change of the magnetic field in the X, Y or Z directions. These three orthogonal derivatives are used in the computation of 3D interpretation techniques including Euler deconvolution, analytic signal and the geophysical TILT (these methods are discussed in detail later in this chapter). The vertical (Z direction) derivative transform function is given by;

$$L(r) = r^{n} \tag{8}$$

where r is the radial wavenumber and n is the order of the vertical derivative (1, 2, 3 etc.). With n=1, the response versus wavenumber of this function plots as a straight line with positive slope, enhancing higher wavenumbers and producing the first vertical derivative (also known as the vertical gradient). For n=2, the second vertical derivative, the transform becomes quadratic with corresponding greater enhancement of the higher wavenumbers.

The first vertical derivative is the rate of change of the magnetic field in the vertical direction and is equivalent to measuring the field at two vertically separated magnetometers and dividing the difference by the separation distance. The filter removes the long wavelength component and helps resolve closely spaced, even superposed anomalies. The derivative operation also enhances noise in the data which limits the utility of higher order derivatives. The zero value of the first vertical derivative coincides with vertical contacts of magnetic domains (Hood, 1965).

The horizontal rate of change of the magnetic field can be calculated in the X and Y directions in the frequency domain quite simply. The horizontal derivative with respect to X is produced by the transfer function:

$$L(u)=(ui)^n \quad (9)$$

and with respect to Y by:

$$L(v)=(vi)^n \quad (10)$$

where u and v are the wavenumbers in the X and Y directions, respectively and n is the order of the derivative. The horizontal derivative maxima occur roughly over the contacts between differently magnetized bodies.

The inverse of the vertical derivative filter is the vertical integration filter. The integral of the input transform is calculated with the simple transfer function;

$$L(r)=(r)^{-1} \quad (11)$$

The integration enhances lower frequencies and longer wavelengths. Due to Poisson's relation, a reduced to the pole magnetic field can be integrated to produce a pseudo-gravity field, which assumes a direct relationship between bulk volume of magnetite and rock density.

A continuation filter calculates the field at a different altitude or elevation than the one at which it was acquired. Upward continuation enhances the lower frequencies (deeper sources) and suppresses smaller, near surface anomalies while downward continuation enhances the higher (near surface) frequencies. The transform function for continuation is;

$$L(r)=(e)^{hr} \quad (12)$$

where h is the distance of continuation in grid cells, h being negative for upward continuation and positive for downward continuation, and r is the radial wavenumber. The effect of the transform function on the wavenumber increases exponentially with the positive distance (+h, Fig. 4.8a). For example, if h=1, no different response is given for low and high wavenumbers, but as h increases the response for higher wavenumbers increases exponentially.

A directional cosine filter is used to remove or retain anomalies parallel to a specific direction, usually the flight line direction. The filter transfer function takes the form;

$$L(u,v)=|\cos^{n}(\alpha-\theta)+\frac{\pi}{2}| \qquad \textbf{(13)}$$

which rejects anomalies parallel α, or;

$$L(u,v)=1-|\cos^{n}(\alpha-\theta)+\frac{\pi}{2}| \qquad \textbf{(14)}$$

which passes anomalies parallel the user specified direction α, and n is the degree of the cosine function. Increasing the degree, n, of the cosine function increases the sharpness of the filter.

The variations in inclination and declination of the core field cause magnetic anomaly patterns of identical bodies to be different at different positions on the earth, notably an asymmetry to the northwest at the magnetic latitude of this study (Fig. 4.9). This can make anomaly pattern recognition somewhat confusing. Reduction to the pole is a frequency domain technique that converts all anomalies to those seen in a vertical orientation of the geomagnetic field, as at the magnetic poles. Reduced to the pole magnetic bodies with vertical sides have anomalies centred over them. This complex, asymmetric transform function varies depending

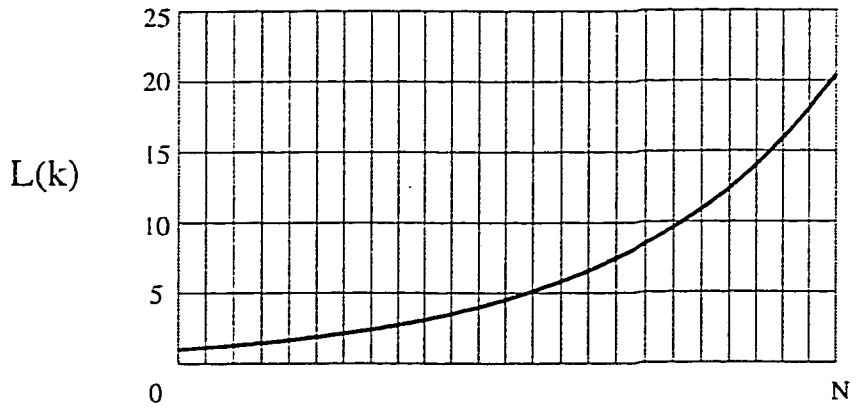

(a) Downward continuation

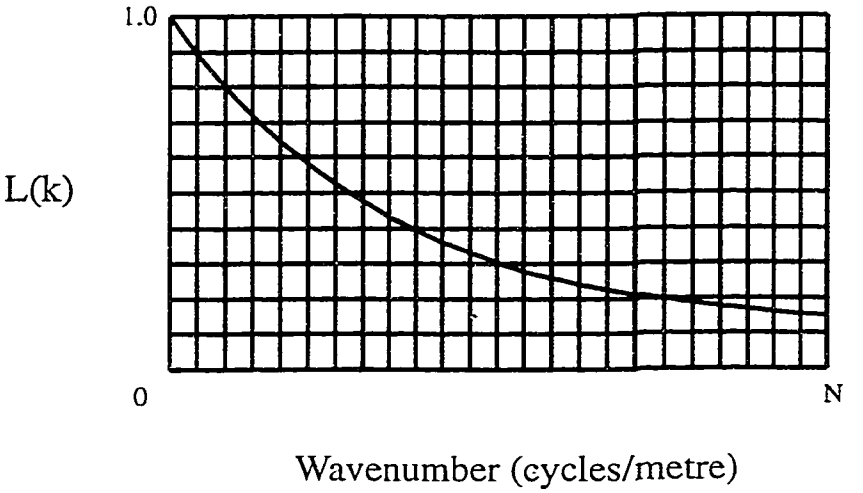

(b) Upward continuation

Fig. 4.8. Continuation filter transfer function response versus wavenumber; a) downward continuation, b) upward continuation. L(k) is the response and N is the Nyquist frequency.

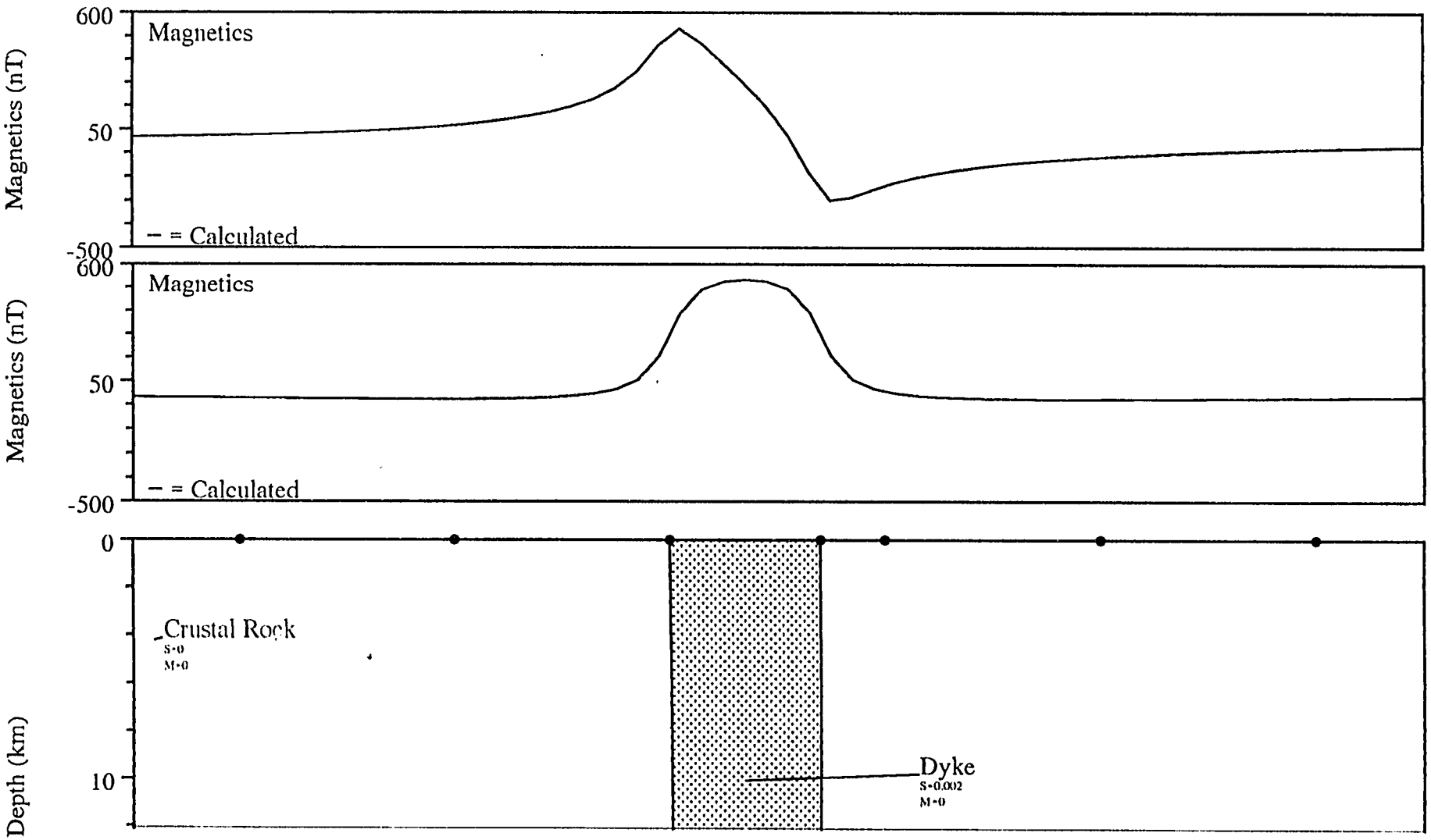

Fig. 4.9. The effect of inclination of the core field on the symmetry of an anomaly. Both profiles represent the magnetic anomaly along a north trending profile due to a dyke with an east-west strike. The upper profile is the anomaly induced by the core field at an inclination of 60° and the lower profile represents the same profile at the magnetic north pole where the inclination is 90°.

on the inclination and declination of the field, assumes anomalies are caused by induced magnetization only and that the bodies are approximated by vertical right rectangular prisms. The transfer function is defined as;

$$L(\theta) = \frac{1}{[\sin(I) + i\cos(I)\cdot\cos(D-\theta)]^2} \qquad \textbf{(15)}$$

where I is the inclination of magnetic field, D is the declination. Gunn (1997, p.65) notes that if significant remanent magnetization is present, reduced to the pole maps will have distorted or smeared anomalies.

When filtering in the frequency domain, it is important to remember that the Fourier transform is defined for continuous functions and discrete representations of continuous functions. Discontinuities in the data are not handled well by the transform and produce oscillations or ringing (Gibb's phenomenon) emanating from the discontinuity. Discontinuities can be due to level shifts at survey boundaries or sharp local anomalies. Close visual inspection of filtered grids is required, although the ringing may be imperceptible, depending on the presentation of the data. It is important that the data be well conditioned by both long wavelength levelling and high frequency edge fitting between separate surveys. The ringing effects due to local anomalies can be minimized by the judicious application of a low pass filter. Sharp discontinuities can also be caused by the transfer (filter) function itself if it is too abrupt. Transfer functions must be designed with adequate gentle transitions or roll-off. Also, edge effects at grid data limits can produce poor filtering reponses. This is diminished by tapering or

padding the edges of the grid with reasonable, if fictitious, values. The width of the padding around the edges of the grid is a function of the wavelength of the desired filter product; a wider taper is required for long wavelength, low pass filtering than for short wavelength, high pass filtering. A taper of about 10% of the maximum extent of the grid is a rule of thumb.

4.2.1. APPARENT MAGNETIC SUSCEPTIBILITY

A total field magnetic data grid can be processed to produce the theoretical magnetic susceptibility of the sources, provided certain assumptions about the sources are valid. The processed data field is referred to as the apparent magnetic susceptibility. The main benefit of this technique to interpretation is that the apparent susceptibilities can be related to a measurable physical property of the source rocks.

The theoretical derivation of reduction of the total magnetic field to its apparent magnetic susceptibility was developed by Spector and Grant (1970) and presented in the form described below by Yunsheng et al., (1985). The total magnetic field in the frequency domain, $(T(u,v)$, due to a vertical prism (Fig. 4.10), is given by;

$$T(u,v) = 2KT_0M(u,v)H(u,v)S(u,v)D(x,y;u,v), \tag{16}$$

where;

$$\begin{aligned} M(u,v) = [&-lLu^2 - mM^2 + nN(u^2+v^2) \\ &(-Lm+Ml)uv + i(Ln+Nl)u(u+v^2) \\ &+ i(Mn+Nm)v(u^2+v^2)](u^2+v^2)^{-1} \\ &(\textit{the magnetization factor}) \\ H(u,v) = &\exp[-h(u^2+v^2)^{1/2} \\ &(\textit{the depth factor}) \end{aligned} \tag{17}$$

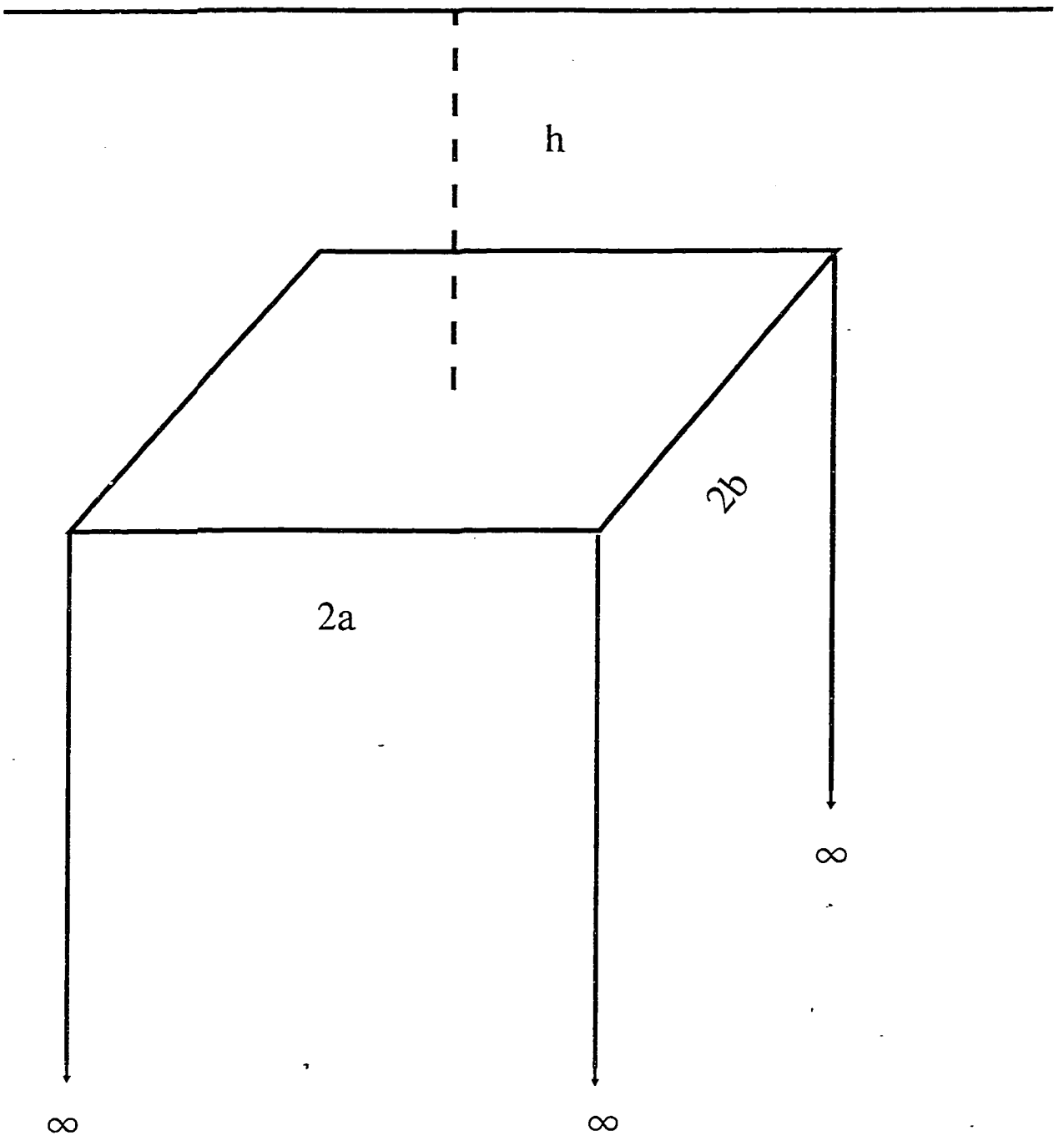

Fig. 4.10. Vertical prism model used in the apparent susceptibility method. h is the depth to source, 2a and 2b are the prism dimensions in x and y directions and the depth extent of the prism is infinite. (After Yunsheng et al., 1985).

$S(u,v) = 4\sin(ua)\sin(vb)$
(the size factor)
$D(x,y,;u,v) = \exp[-i(vx+vy)]$
(the displacement factor)
K = *susceptibility*
T_0 = *intensity of the Earth's field*
l,m,n = *the direction cosines of the Earth's magnetic field*
L,M,N = *direction cosines of the total polarization vector*
a,b = *half-width sides of the prisms*
u,v = *wavenumbers*

Assuming no remanent magnetization (all magnetization is induced) then the Earth's magnetic field orientation and the polarization vector are the same, giving the magnetization factor;

$$M(u,v) = [-\frac{l^2u^2 - m^2v^2}{(u^2+v^2)} + n^2 - \frac{2lmuv}{u^2+v^2)} + i\frac{2lnu + 2mnv}{(u^2+v^2)^{1/2}}] \qquad \textbf{(18)}$$

Further assuming that the geology can be represented by independent prisms of infinite depth extent and with dimensions equal to the grid interval so that the total magnetic field is the sum of the magnetic effects due to each prism, the total field is given by;

$$T(u,v) = 2\pi T_0 \sum_{j=1}^{n} K_j M_j(u,v) H_j(u,v) S_j \times (u,v) D_j(x,y;u,v) \qquad \textbf{(19)}$$

where n is the number of prisms or grid cells. As we have assumed the prisms are the all the same, the magnetization (M), depth (H) and the size (S) of the prisms can be considered constants outside the summation;

$$T(u,v) = 2\pi T_0 M(u,v) H(u,v) S(u,v) \sum_{j=1}^{n} K_j D_j(x,y;u,v) \quad \textbf{(20)}$$

Dividing by M, H and S;

$$T_n(u,v) = 2\pi T_0 \sum_{j=1}^{n} K_j D_j(x,y;u,v) \quad \textbf{(21)}$$

The inverse Fourier transform is then;

$$T_n(x,y) = 2\pi T_0 \sum_{j=1}^{n} K_j d_j(u,v;x,y) \quad \textbf{(22)}$$

given that $d_j(u,v;x,y)$ is the inverse Fourier transform of $D_j(u,v;x,y)$. As a result of reduction to the pole, removal of the shape factor and downward continuation to the surface and by making the centre of the grid cell coincide with the vertical axis of the prism;

$$T_n(x,y) = 2\pi T_0 K(x,y) \quad \textbf{(23)}$$

Finally, dividing by $2\pi T_0$, the resultant grid will represent the apparent susceptibility of the sources.

The first of the two main assumptions of the apparent susceptibility method is that all magnetization is induced. Generally, it is accepted in magnetic interpretation that induced magnetization predominates over remanent magnetization (McGrath, 1996) and that significant

remanence is rare (Gunn, 1997). Smearing of remanent-dominated anomalies by the reduction to the pole filter was not observed. Furthermore, a paleomagnetic study of rocks of the Manitouwadge greenstone belt by Mah (1994, unpublished thesis) indicates that remanent magnetization is not significant.

The second major assumption of the method is that the geology can be represented by vertical prisms of infinite depth extent. At the scale of observation, and by limiting observations about the apparent susceptibility to sources greater in horizontal extent than the gridding interval (25m to 50m), it is reasonable to represent the geology as a set of vertical prisms. However, there is probably significant deviation from this assumption where the geological units are not sub-vertical especially in the D_3 fold hinge areas. The depth extent in these areas is also probably less than can be considered infinite, in terms of magnetic responses. Also, the depth extent of the eastern part of the Loken Lake pluton is probably less than 'magnetically infinite'. As a result, the apparent susceptibility is in error, contaminated by the magnetic response of underlying higher susceptibility material.

In practice, the calculation of the apparent susceptibility is a combination of the reduction to the pole filter, a downward continuation to the ground surface with a 100m low pass filter to avoid ringing and division of the grid values by $2\pi * 59489.0$ (the local Earth's magnetic field intensity). Furthermore, the grid values were divided by 12.57 (4π) to convert from cgs-emu susceptibility to SI susceptibility.

The apparent magnetic susceptibility grid was calibrated to known measured susceptibilities (E. Zaleski, pers.comm., see Appendix 1). A first attempt to calibrate the grid involved

comparing measured susceptibilities with apparent susceptibility values interpolated from the grid at each of the known locations. Figure 4.11 is a graph of the measured values versus the difference with apparent susceptibilities. Although the differences appear increase consistently with increasing measured susceptibility, this effect is due to the predominance of lower susceptibilities in the grid and the inability of the airborne survey to completely sample the field. Very similar results could be expected if the apparent susceptibility grid had a constant value around zero. In light of this relationship, the calibration was achieved by finding the grid values over a large area known to be of very low susceptibility and comparing to measured values for that rock type. The metasediments in the southern limb of the Manitouwadge synform have very low susceptiblities while average values in the grid are about -14.5 SI x 10^{-3}. This value was added to the apparent susceptibility grid.

The apparent susceptibility grid is used in this study to provide a background for edge determination techniques such as analytic signal and the horizontal gradient of the pseudo-gravity. Characterizing geological units by their susceptibility and known contacts allows using the combined apparent susceptibility and body edge locations to extend the contacts to areas of poor exposure or sparse geological mapping. The apparent magnetic susceptibility map of the study area is presented as a 1:50 000 scale colour plot attached to this thesis (Map 2).

4.2.2. ANALYTIC SIGNAL

The analytic signal method of magnetic interpretation is a filtering procedure that produces a signal from the orthogonal derivatives of the magnetic field that is dependent on the position of magnetization contrasts and the depth to that contrast. The only assumptions made are that

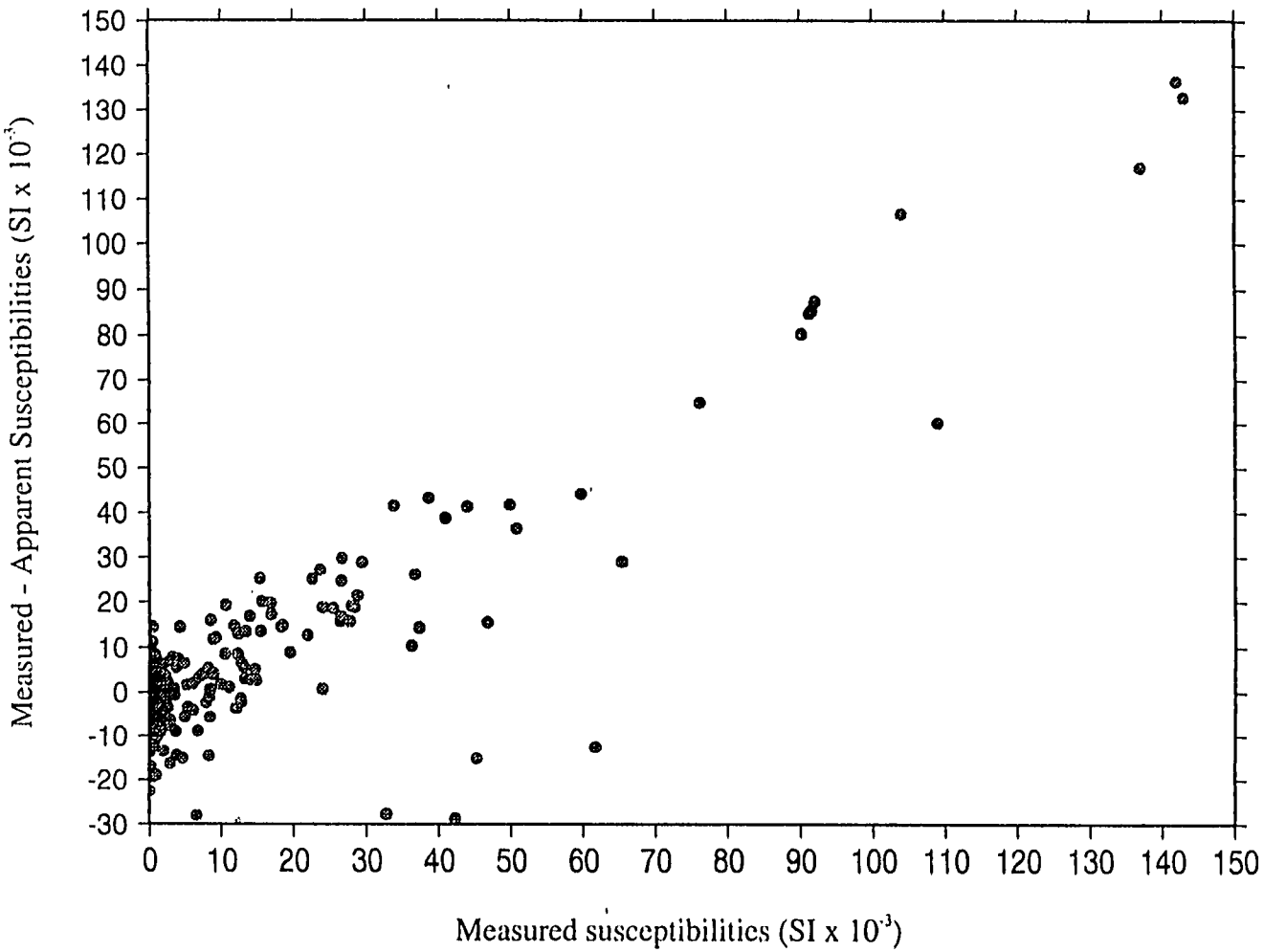

Fig. 4.11. Measured magnetic susceptibilities versus the difference between measured and apparent susceptibilities.

the source bodies have uniform magnetization and that the bodies can be represented in cross-section by a polygon.

Nabighian (1972) describes the derivation of the analytic signal or function of 2D magnetic data and the properties of that function. The analytic function of an anomaly, ΔM, due to a magnetization contrast is given by;

$$A(x) = T(x) - iT_1(x) \tag{24}$$

where

$$T(x) = \frac{\partial(\Delta M)}{\partial x}, \quad T_1(x) = \frac{\partial(\Delta M)}{\partial y}, \tag{25}$$

and $i = \sqrt{-1}$

The required condition for a complex function to behave as an analytic signal is that the real and imaginary parts form a Hilbert transform pair. Nabighian (1972) shows this relationship exists in the frequency domain by demonstrating that the horizontal derivative ($T(x)$, the real part) can be used to determine the vertical derivative ($T_1(x)$, the imaginary part). If $F(w)$ is the Fourier transform of $T(x)$ and $F_1(w)$ is the Fourier transform of $T_1(x)$ then,

$$F_1(w) = i\, sgn(w)\, F(w) \tag{26}$$

where

$$\begin{aligned} sgn(w) &= 1 \text{ for } w>0 \\ sgn(w) &= 0 \text{ for } w=0 \\ sgn(w) &= -1 \text{ for } w<0 \end{aligned} \tag{27}$$

The amplitude of the analytic signal, $a(x)$ is given by;

$$a(x) = |A(z)|^2 = T^2(x) + T_1^2(x) \tag{28}$$

For a polygonal-shaped body, this takes the form;

$$\frac{\alpha^2}{h^2 + x} \tag{29}$$

where α is a term containing information on the geometry of the source body, the magnetic susceptibility of the source body and the Earth's magnetic field and z is the complex variable ($z = x + iy$). The amplitude function has a bell shape (Fig.4.12) and displays a maximum directly over a magnetization contrast (or over the corners of a polygon-shaped body in cross section). The half-width is equal to the depth to source, h. Nabighian (1972) continues the derivation to illustrate the possibility of determining other source parameters, once h is calculated. Figure 4.13 shows the magnetic anomaly due to a vertical contact between two differently magnetized bodies and the amplitude of the analytic signal.

Roest et al.,(1992) develop the analytic signal for the 3D case in the frequency domain. The Fourier transform, $g(kx,ky)$ of the function, $f(x,y)$, is defined, using their variables, as:

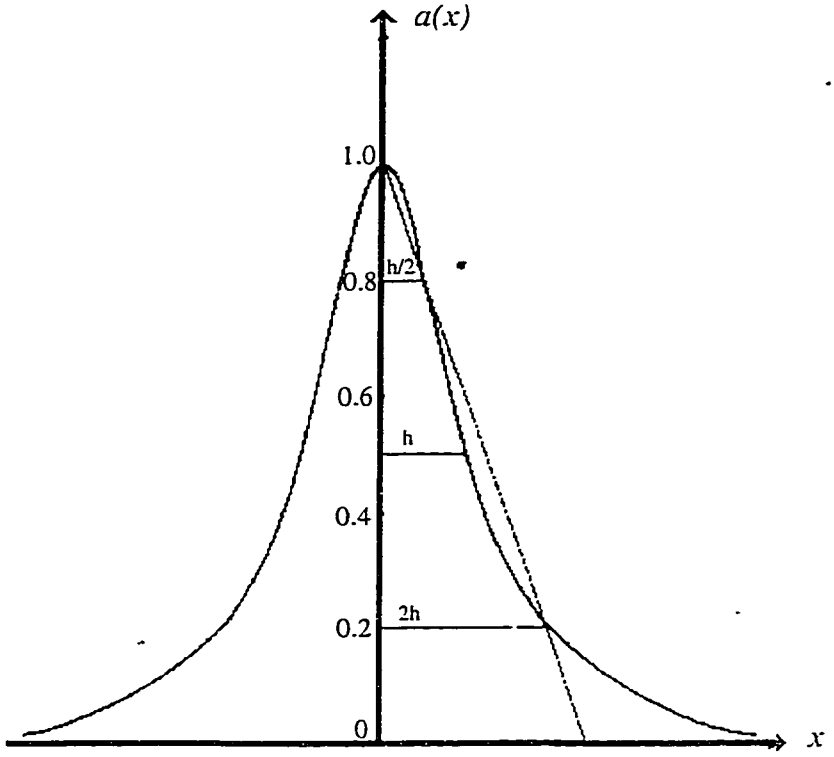

Fig 4.12. The amplitude of the analytic signal. The value h is the distance to the magnetic source. (After Nabighian, 1972).

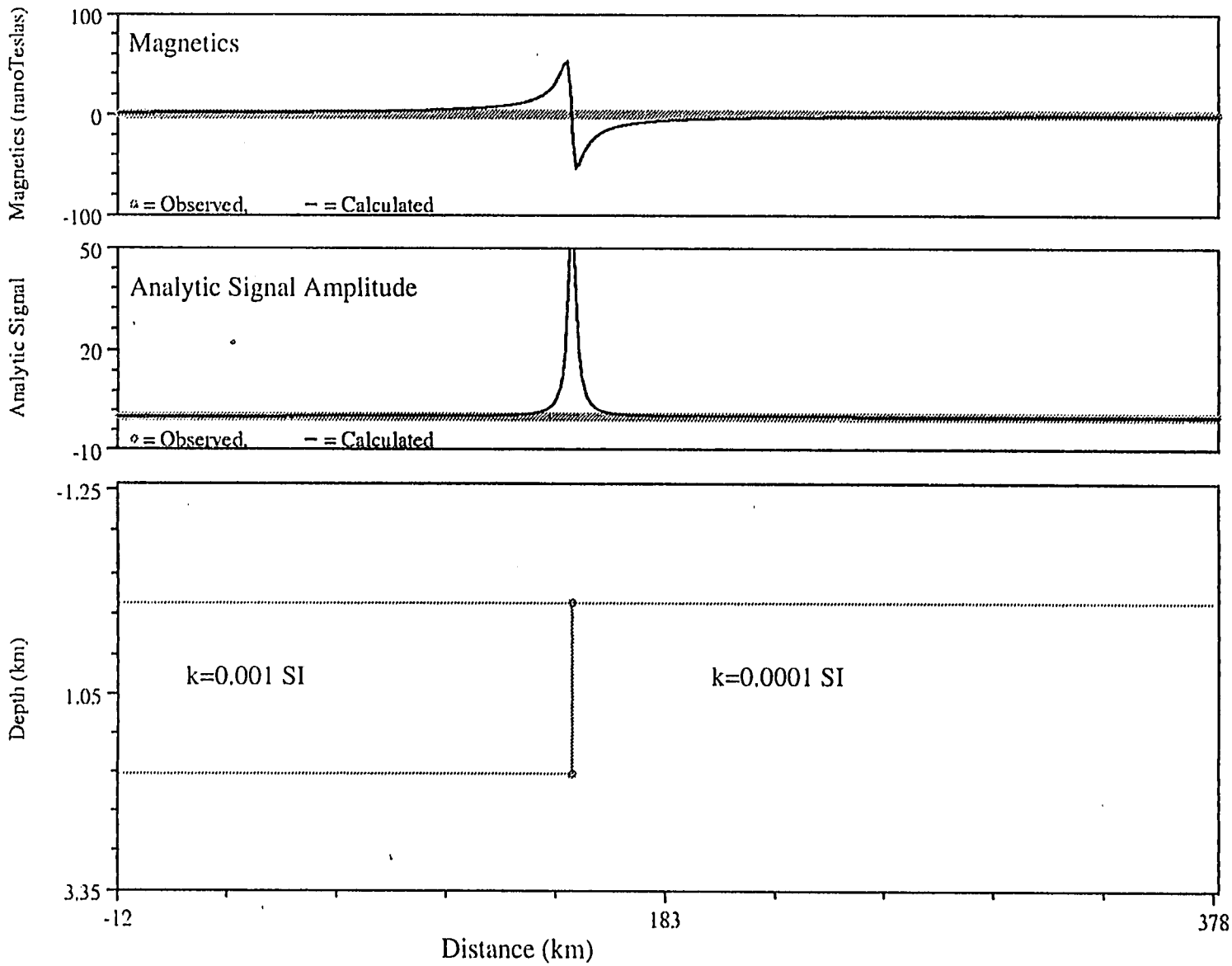

Fig. 4.13. The magnetic anomaly and its analytic signal amplitude due to a vertical contact between two differently magnetized bodies.

$$g(k_x,k_y) = \int_{-\infty}^{\infty}\int_{-\infty}^{\infty} f(x,y)\, e^{-i(k_x x + k_y y)}\, dx\, dy \qquad (30)$$

where k_x and k_y are the wavenumbers in the x and y directions. The inverse Fourier transform is given by;

$$f(x,y) = \frac{1}{4\pi^2}\int_{-\infty}^{\infty}\int_{-\infty}^{\infty} g(k_x k_y)\, e^{i(k_x x + k_y y)}\, dk_x\, dk_y \qquad (31)$$

The 3D analytic signal of a magnetic field, M, is given by;

$$A(x,y) = \left(\frac{\partial M}{\partial x}\right)\boldsymbol{x} + \left(\frac{\partial M}{\partial y}\right)\boldsymbol{y} + \left(\frac{\partial M}{\partial z}\right)\boldsymbol{z} \qquad (32)$$

where $\boldsymbol{x}$, $\boldsymbol{y}$ and $\boldsymbol{z}$ are unit vectors in the directions of x, y and z, respectively. In order to satisfy the basic requirement of the analytic signal, it must be shown that the real and imaginary parts of Eqn. 32 form a Hilbert transform pair. Transforming Eqn. 32 into the frequency domain in terms of the gradient of the Fourier transform;

$$\boldsymbol{t}\cdot F[A(x,y)] = \boldsymbol{h}\cdot\nabla F[M] + i\boldsymbol{z}\cdot\nabla F[M] \qquad (33)$$

where ∇ is the gradient operator in the frequency domain $(ik_x\boldsymbol{x} + ik_y\boldsymbol{y} + |\boldsymbol{k}|\boldsymbol{z})$, $\boldsymbol{t} = \boldsymbol{x} + \boldsymbol{y} + \boldsymbol{z}$ and $\boldsymbol{h} = \boldsymbol{x} + \boldsymbol{y}$. Breaking Eqn. 33 into its real (horizontal derivative) and imaginary (vertical derivative) parts and applying the relation between horizontal and vertical derivatives of

potential fields of Pedersen (1989) we see that;

$$\begin{aligned} \boldsymbol{h}\cdot\nabla F[M] &= i\boldsymbol{h}\cdot\boldsymbol{k}F[M] = i\frac{(\boldsymbol{h}\cdot\boldsymbol{k})}{|\boldsymbol{k}|}|\boldsymbol{k}|\,F[M] \\ &= i\frac{(\boldsymbol{h}\cdot\boldsymbol{k})}{|\boldsymbol{k}|}z\cdot\nabla F[m] \end{aligned} \tag{34}$$

indicating that the horizontal derivative (real part) is related to the vertical derivative (imaginary part) by $i(\boldsymbol{h}\cdot\boldsymbol{k})/|\boldsymbol{k}|$, which is the 3D Hilbert transform operator. This allows for the extension of Nabighian's definition of the analytic signal to the 3D case. From this point it is straightforward to define the amplitude of the analytic signal as;

$$|A(x,y)| = \sqrt{(\frac{\partial M}{\partial x})^2 + (\frac{\partial M}{\partial y})^2 + (\frac{\partial M}{\partial z})^2} \tag{35}$$

The important properties of the amplitude of the analytic signal are that it achieves a maximum directly over magnetization contrasts and that this maximum's location is independent of the orientation of the Earth's magnetic field and of the orientation of the magnetization of the bodies. The benefit of these properties is that no assumptions about the nature of the magnetization of the sources are required. For the simpler 2D case, it can be shown that the shape of the absolute value of the analytic signal has this independence. The Fourier transform of the 2D analytic signal is given by;

$$
\begin{aligned}
F[A(x)] &= (1+\frac{|k_x|}{k_x})\, F[\frac{\partial M(x)}{\partial x}] \\
&= i(k_x+|k_x|)F[M(x)] \\
&= 2ik_xF[M(x)]
\end{aligned}
\tag{36}
$$

when $k_x > 0$. The inverse Fourier transform of this equation yields the analytic signal of a given anomaly (M_{pole}) at the magnetic pole (inclination = 90°);

$$
A_{pole}(x) = \frac{2i}{2\pi}\int_0^{\infty} k_x F[M_{pole}(x)]e^{ik_x x}dk_x \tag{37}
$$

A similar expression for the analytic signal of an anomaly not observed at the magnetic pole can be derived from the above equation and the reduction to the pole operator;

$$
\begin{aligned}
F[M_{pole}(x,y) &= M_{pole}(k_x,k_y) \\
&= [\frac{|k|^2}{(G\cdot B_0)(G\cdot M_0)}]M(k_x,k_y)
\end{aligned}
\tag{38}
$$

where $G = (ik_x, ik_y, k)$ and $B_0 = (\alpha_x, \alpha_y, \alpha_z)$ and $M_0 = (l_x, l_y, l_z)$. B_0 and M_0 are the cosines of the Earth's magnetic field and the source body magnetization, respectively. Dropping the k_y term in the reduction to the pole operator for the 2D case and substituting into the previous equation;

$$A(x) = \frac{2i}{2\pi}\int_0^{\infty} k_x \frac{(\boldsymbol{G}\cdot\boldsymbol{B}_0)(\boldsymbol{G}\cdot\boldsymbol{M}_0)}{k^2_x} M_{pole}(k_x)e^{ik_x x}dk_x$$
$$= (i\alpha_x - \alpha_z)(il_x - l_x)A_{pole}(x) \qquad (39)$$

Assuming the Earth's magnetic field and the magnetization have constant directions, their directional cosines for a 2D body are given by;

$$\alpha_x = \left(\frac{\sin I_r}{\sin I'_r}\right)\cos I_r \qquad \alpha_z = \left(\frac{\sin I_r}{\sin I'_r}\right)\sin I_r$$
$$\beta_x = \left(\frac{\sin I_r}{\sin I'_p}\right)\cos I_p \qquad \beta_z = \left(\frac{\sin I_r}{\sin I'_p}\right)\sin I_p \qquad (40)$$

where I'_p and I'_r are the Earth's magnetic field and the source's magnetization inclinations, respectively, projected perpendicular to the strike, α, of the body. The absolute value of the analytic signal for an anomaly not observed at the pole becomes;

$$|A(x)| = \left(\frac{\sin I_p}{\sin I'_p}\right)\left(\frac{\sin I_r}{\sin I'_r}\right)|A_{pole}(x)| = C_p\,|A_{pole}(x)| \qquad (41)$$

This shows that the shape of the absolute value of the analytic signal is independent of both the Earth's magnetic field orientation and the direction of magnetization of the source. The amplitude, however, is not independent of these orientations.

In practice, the amplitude of the analytic signal is computed by first computing, in the frequency domain, the three components, namely, the first vertical derivative, the horizontal

derivative in the X direction and the horizontal derivative in the Y direction, squaring each of the derivatives, adding them together and then finding the square root. The resulting grid of the amplitude of the analytic signal can be inspected for local maxima.

The use of local maxima, for either horizontal gradient or analytic signal methods, requires a method of identifying these maxima. Blakely and Simpson (1986) developed a method that locates and provides a measure of the quality of the maxima. Their automated method of locating maxima from a data grid involves comparing each grid cell to its eight nearest neighbours (Fig.4.14) and determining if the central grid cell value is a local maximum in each of the four directions. The grid cell is assigned a value (N) between 0 and 4, one point for each direction in which the cell is a local maximum. An N value of 0 indicates that the point is not a local maximum in any direction. N values of 4 are isolated maxima, which are of minimal geological interest and probably represent noise when based on a single grid cell. N values of 2 and 3 represent local maxima that have lateral continuity and tend to define boundaries or linear features.

As the grid represents a continuous surface at discrete points, the actual maxima may not fall on grid cells. The position of the maxima is calculated from the grid cell and the eight nearest neighbours by;

$$x_{max} = -\frac{bd}{2a} \qquad (42)$$

where

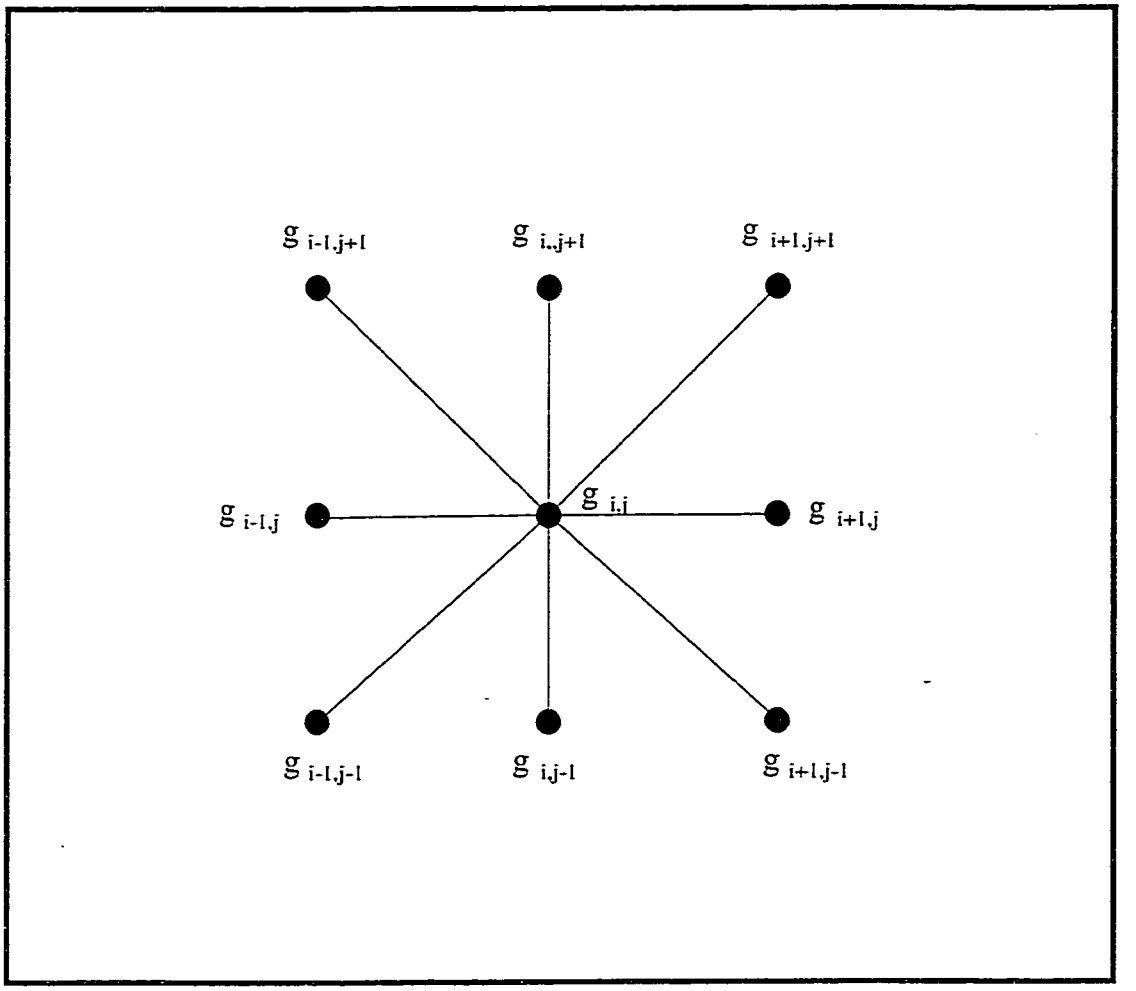

Fig. 4.14. Eight nearest grid cell neighours to $g_{i,j}$ and the four directions in which local maxima are tested. (after Blakely and Simpson, 1986).

$$a = \frac{1}{2}(g_{i-1,j} - 2g_{i,j} + g_{i-1,j})$$
$$b = \frac{1}{2}(g_{i-1,j} - g_{i-1,j}) \quad (43)$$

and d is the grid cell size. The value of the analytic signal at this point can be used as an acceptance criterion and is calculated by;

$$g_{\max} = ax^2_{\max} + bx_{\max} + g_{i,j} \quad (44)$$

For each grid cell checked, the highest value of g_{max} is used as the acceptance criterion. Local maxima can be discriminated by number of directions in which the grid cell is a maximum and by the amplitude of the maximum. The analytic signal maxima for the study area are presented on Map 3 attached to this thesis.

The use of derivatives to define the analytic signal amplitude function accentuates near surface effects and noise in the data. As a result, the analytic signal maxima tend to form discontinuous trends, even along seemingly continuous total field anomalies. The high frequency bias also limits the depth to which the method can detect magnetization contrasts. Imperfections in the grid, including line-to-line levelling problems and the inability of the gridding algorithm to accurately represent the 3D magnetic field from the 2D profile data, can be accentuated by the analytic signal. These problems can be diminished by improving grid quality with trend reinforcement and micro-levelling and by upward continuing the data by a

distance equal to the grid interval, an effective low pass filter.

It was determined that the vertical derivative grid computed from a grid in the frequency domain was contributing the largest part of the noise to the final analytic signal grid. In an effort to minimize this error, the vertical derivative was computed on the 2D profile data, also in the frequency domain, then gridded. The resulting derivative grid had less obvious line-to-line levelling error and gridding artefacts. As this 2D filter assumes that the source bodies are infinite in the Y direction, theoretically this process is not correct. However, since the surveys flight line directions were selected to be perpendicular to the general strike of the geology, this concern is minimized. Furthermore, a plot of the difference between the 2D and 3D data-based vertical derivative grids (Fig.4.15) shows that the 2D method corrected line-to-line problems more than it affected real magnetic signal. Figure 4.16 shows the analytic signal maxima generated from both 2D and 3D vertical derivatives. It also shows that the noise has been diminished in the former, but not at any great expense of the maxima of true signal. The greatest divergence from the true 3D vertical derivative would be in areas where the flight lines are at an angle to the general strike of the geology, notably in the hinge zones of the major mapscale D_3 folds.

4.2.3. HORIZONTAL GRADIENT MAXIMA OF PSEUDO-GRAVITY

Pseudo-gravity is a transformation of the magnetic field to a simpler, non-dipolar representation. The technique is based on Poisson's relation, which defines the relationship between magnetic and gravitational potential fields. Transforming the magnetics to an equivalent gravity field allows us to take advantage of some simpler interpretation techniques.

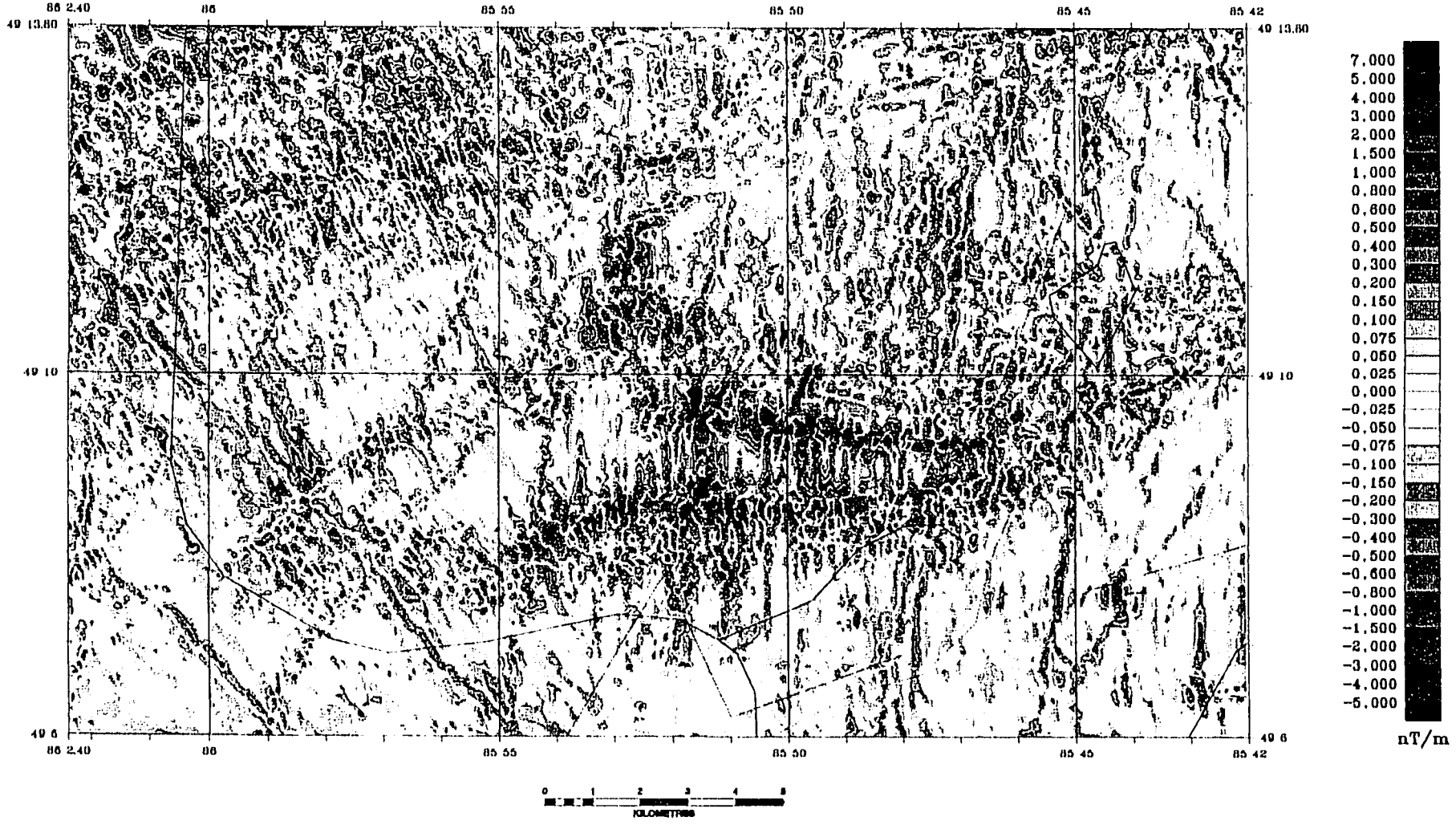

Fig. 4.15. Difference between 2D (profile) vertical derivative and 3D (grid) vertical derivative, western part of study area. Differences between the methods are concentrated along flight lines.

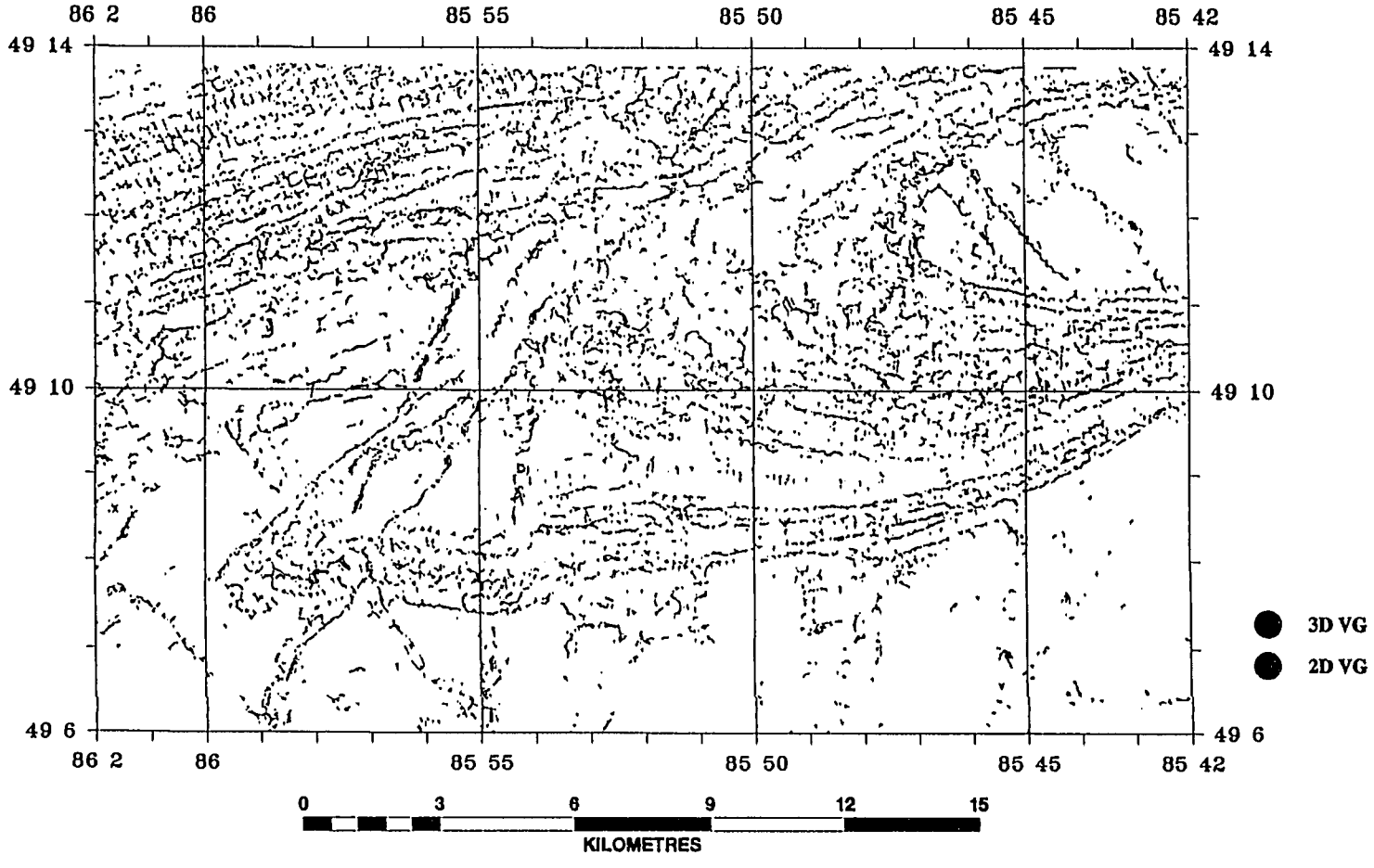

Fig. 4.16. Comparison of analytic signal maxima based on 2D vertical derivative (red dots) and 3D vertical derivative (blue dots).

One of these techniques is using the maxima of the horizontal gravity gradient to define boundaries between bodies of differing density.

Poisson's relation demonstrates that an interesting link between the magnetic and gravitational fields exists. Basically, it allows that all properties of the magnetic field due to a homogeneous body are derivable from the gravitational field and vice-versa.

Newtons's law of universal gravitation states that the mutual gravitational attraction between two particles having mass m_1 and m_2 which are separated by a distance, r, has the value;

$$\mathcal{F}(r) = G\frac{m_1 m_2}{r^2} \tag{45}$$

where G is the gravitational constant and $\mathcal{F}$ acts in the direction of r. The force per unit mass on a particle at a point, P, at a distance $\boldsymbol{r}$ from m_1 is defined as the gravitational field of the particle m_1;

$$\boldsymbol{F}(\boldsymbol{r}) = -G\frac{m_1}{r^3}\boldsymbol{r} \tag{46}$$

Such a field is conservative and is therefore derivable from a scalar potential function, $U(\boldsymbol{r})$, as follows;

$$\boldsymbol{F}(\boldsymbol{r}) = -\nabla U(\boldsymbol{r}), \quad \textit{when } U(\boldsymbol{r}) = -G\frac{m_1}{r} \tag{47}$$

and is said to be the gravitational potential of the mass m_1.

The gravitational potential due to continuous distributions of matter (particles) may be calculated at external points by integration. As described in Figure 4.17, if the mass is distributed continuously with density, $\rho(\boldsymbol{r}_0)$, throughout the volume V, the gravitational potential at an exterior point P is;

$$U_P(\boldsymbol{r}) = -\int_V \frac{Gdm}{|\boldsymbol{r}-\boldsymbol{r}_0|} = -G\int_V \frac{\rho(\boldsymbol{r}_0)d^3r_0}{|\boldsymbol{r}-\boldsymbol{r}_0|} \tag{48}$$

Similar to particles, magnetic dipoles act upon each other. a magnetic dipole of moment, $\boldsymbol{m}$, exerts a force per unit pole strength on a single magnetic pole at a distance, r, from the dipole is given by;

$$H(r) = \frac{2m\cos\hat{\theta}}{r^3}\boldsymbol{r}_1 + \frac{m\sin\hat{\theta}}{r^3}\hat{\theta}_1 \tag{49}$$

$\boldsymbol{H}$ is said to be the magnetic field intensity at P, where $\hat{\theta}$ is the angle measured from $\boldsymbol{m}$ to $\boldsymbol{r}$ and where $\boldsymbol{r}_1$ and $\hat{\theta}_1$ are unit vectors in the directions of increasing r and of increasing $\hat{\theta}$ respectively. The magnetic field intensity is, as with the gravitational field, derivable from a scalar potential function;

$$\boldsymbol{H}(\boldsymbol{r}) = -\nabla A(\boldsymbol{r}) \tag{50}$$

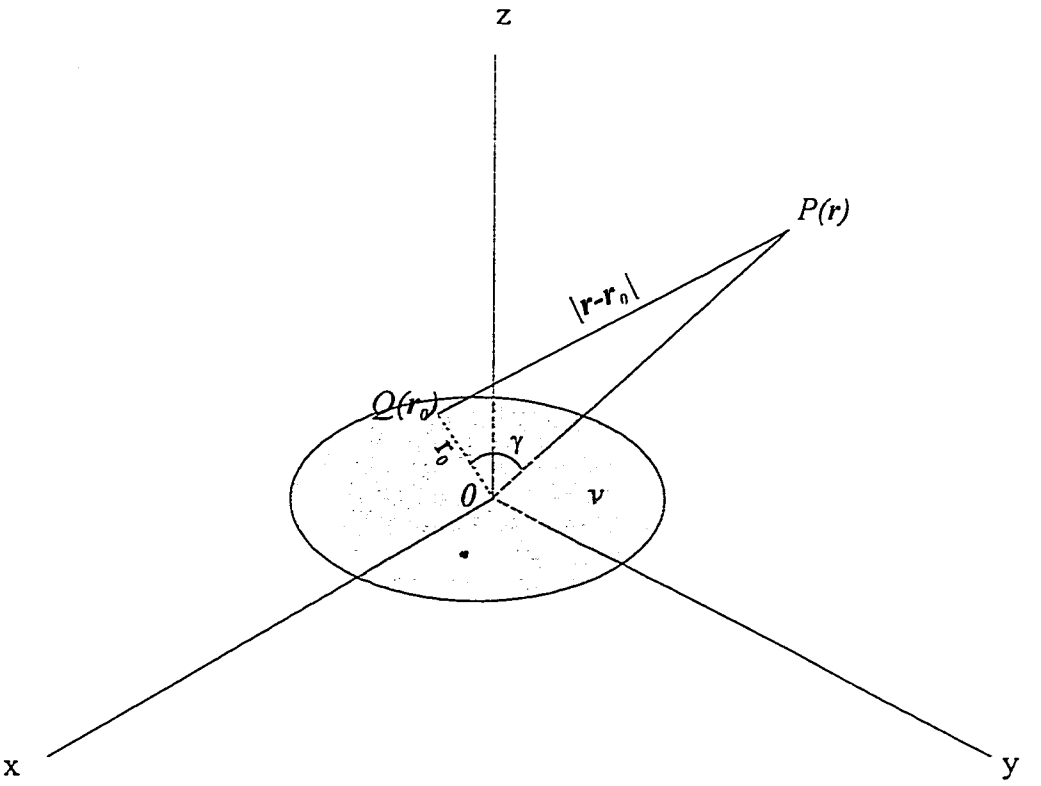

Fig. 4.17. The gravitational potential at a point, P, exterior to volume, V. (After Grant and West , 1965)

where

$$A(\boldsymbol{r}) = \frac{m\cos\vartheta}{r^2} = \boldsymbol{m}\cdot\nabla\left(\frac{1}{r}\right) \tag{51}$$

$a(\boldsymbol{r})$ is said to be the scalar magnetic potential of the dipole ($\boldsymbol{m}$). If a body of volume V has a constant magnetic susceptibility with a magnetic dipole moment per unit volume ($\boldsymbol{M}(\boldsymbol{r}_0)$), then the magnetic scalar potential at a point P outside V is given by:

$$A(\boldsymbol{r}) = -\int_V \boldsymbol{M}(\boldsymbol{r}_0)\cdot\nabla\frac{1}{|\boldsymbol{r}-\boldsymbol{r}_0|}d^3r_0 \tag{52}$$

As the total magnetic field intensity at P is $\boldsymbol{H}(\boldsymbol{r})$ and this is equal to $-\nabla a(\boldsymbol{r})$, then by substituting this relationship into Eqn. 52;

$$\boldsymbol{H}(\boldsymbol{r}) = \nabla\int_V (\boldsymbol{M}\cdot\nabla)\frac{1}{|\boldsymbol{r}-\boldsymbol{r}_0|}d^3r_0 \tag{53}$$

The expression for $\boldsymbol{H}$ can be made very similar to that of $U_P(\boldsymbol{r})$ by assuming that the direction of magnetization is also constant throughout the volume V. With the direction denoted as α, then

$$\boldsymbol{M}\cdot\nabla = M\left(\frac{\partial}{\partial\alpha}\right) \tag{54}$$

and substituting this relation into Eqn. 53 we get;

$$H(r) = \nabla \frac{\partial}{\partial \alpha} \int_V M(r_0) \frac{1}{|r - r_0|} d^3 r_0 \qquad (55)$$

Assuming M in Eqn. 55 and ρ in Eqn. 48 are constant, then Poisson's relation is;

$$H(r) = \frac{M}{G\rho} \frac{\partial}{\partial \alpha} F(r) \qquad (56)$$

This relation allows that, given that the magnetization of a body is constant, in one direction and equal to the density of the body (times some constant, k), then a pseudo-gravity field may be calculated from the magnetic field by integration.

The pseudo-gravity transformation is a two step process. Magnetic data are reduced to the pole and then integrated. As this is performed in the frequency domain, the order of the operations is of no consequence. Both filters are described in the section on filtering.

Cordell (1979) first used the maxima of horizontal gravity gradients to map faults that bound blocks of contrasting density. Figure 4.18 shows the magnetic and gravity profiles over the contact between two differently magnetized and different density blocks. Also shown is the horizontal gradient of the gravity field. Consider the geometry of a semi-infinite horizontal slab (Fig. 4.19). The gravity effect of this model is given by:

$$\begin{aligned} g = {} & 2G\rho [\sin^2\alpha (x - d\cot\alpha) \log \frac{r_2}{r_1} + \\ & (x - d\cot\alpha) \sin\alpha \cos\alpha (\theta_2 - \theta_1) + \\ & D(\frac{\pi}{2} + \theta_2) - (d(\frac{\pi}{2} + \theta_1)] \end{aligned} \qquad (57)$$

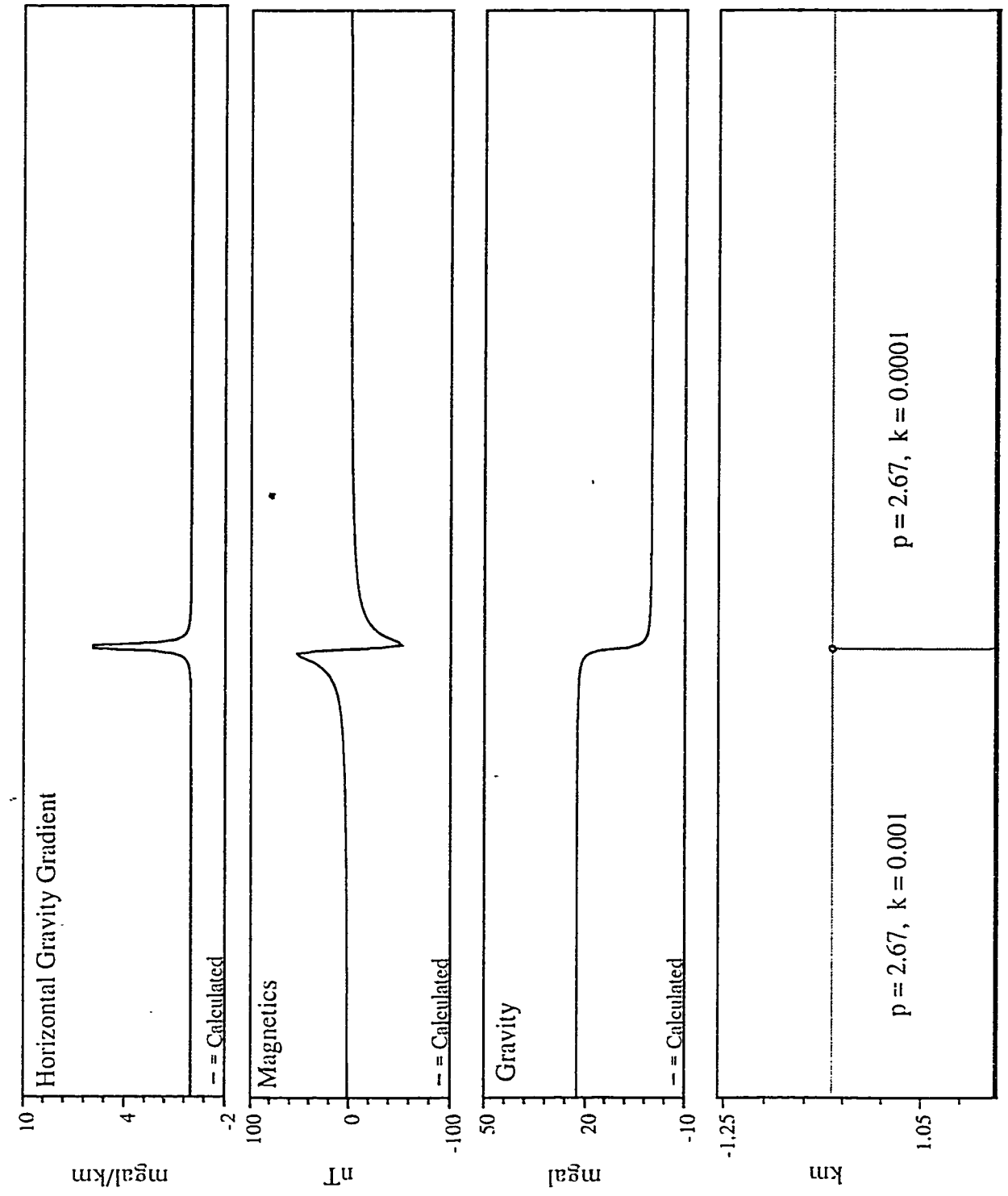

Fig. 4.18. Gravity, magnetic and horizontal gravity gradient profiles over a vertical contact between two different density and differently magnetized blocks.

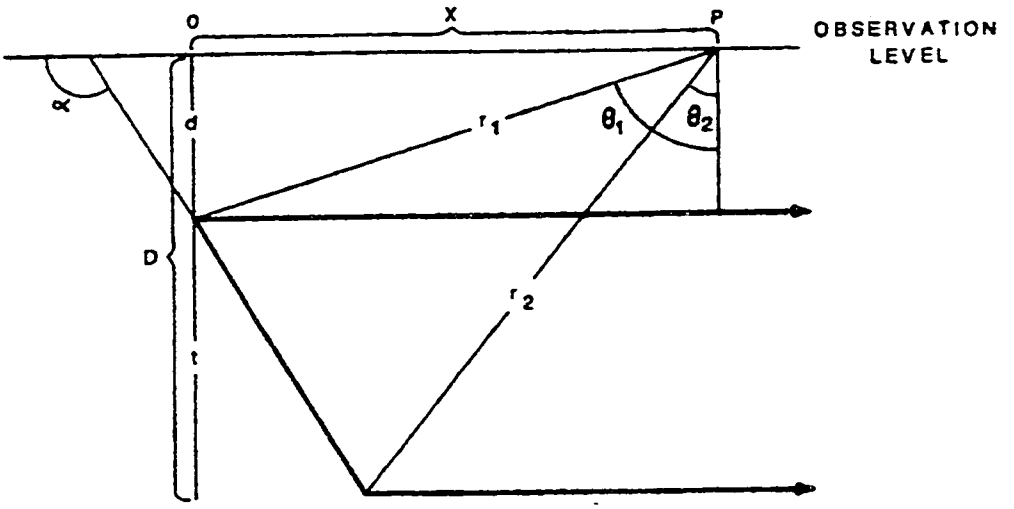

Fig. 4.19. Gravity effect of a semi-infinite horizontal slab. The variables shown here are those used in Eqn. 13. (From Grauch and Cordell, 1987).

where

ρ = *density*
G = *Gravitational constant*
$r_1 = \sqrt{x^2 + d^2}$
$r_2 = \sqrt{[x + (D-d)\cot\alpha]^2 + D^2}$
$\theta_1 = \tan^{-1}\frac{x}{a}$
$\theta_2 = \tan^{-1}\frac{x-(D-d)\cot\alpha}{D}$

and the horizontal gradient (or derivative) of this effect is given by;

$$\nabla g = \frac{\partial g}{\partial x}\boldsymbol{x} = 2G\rho\sin\alpha[\sin\alpha\log\frac{r_2}{r_1} + \cos\alpha(\theta_2 - \theta_1)]\boldsymbol{x} \qquad \textbf{(59)}$$

where $\boldsymbol{x}$ is the unit vector in the x direction. The requirement is to find where the magnitude of ∇g is a maximum, or, where $(\partial g/\partial x)^2$ is a maximum. To find x_0, solve for x when,

$$\frac{\partial g}{\partial x}(\frac{d^2 g}{dx^2}) = 0 \qquad \textbf{(60)}$$

Setting $d^2g/dx^2 = 0$ and $t = D\text{-}d$ and solving for x_0 we find;

$$x_0 = \frac{-dt\cot\alpha}{2d + t} \qquad \textbf{(61)}$$

Allowing t to approach infinity we find;

$$x_0 = -d\ \cot\ \alpha \qquad \textbf{(62)}$$

The gradient offset is down dip from the top edge of the contact. For α=90°, x_0=0 so that there is no offset of the horizontal gradient magnitude over such vertical boundaries. If α=45°, then for a depth of 30m, x_0 has 30m of down dip offset. So it is shown that, for contacts between blocks of rock with sufficient density contrast, the horizontal gradient maxima will be offset downdip from the actual contact. As the cotangent varies between 0 and 1 for dips of between 90° to 45°, the offset should not be more than the depth to source. For thin dykes, the offset is given by;

$$x_0 = -d \cot \alpha \pm d \operatorname{cosec} \alpha \qquad \textbf{(63)}$$

If $\alpha = 90°$, gradient maxima occur at two locations, hence the ± operator. So the offset can be greater than the depth, depending on the geometry of the bodies. It is also important to keep in mind that the depth to source is not necessarily the surface/sensor separation.

The method of finding local maxima described for analytic signal (AS maxima) can be used to determine the local maxima of the of the magnitude of the horizontal gradient of pseudo-gravity (HGPG maxima). The maxima can be plotted and the maxima form linear patterns describing magnetization contrast boundaries. a 1:50 000 scale plot of both maxima is attached to this thesis as Map 3.

As previously discussed, AS maxima can be used to locate the boundaries or contacts between two bodies with sufficiently contrasting magnetization, regardless of the dip of that contact. HGPG maxima will also mark similar boundaries, but only where the dip of the contact is vertical, the position of the maxima being offset in the down dip direction for inclined

contacts. The AS maxima tend to be more discontinuous than the HGPG maxima.

Hansen et al. (1987) suggest combining the AS and HGPG maxima on one plot. The first benefit of this scheme is that the more continuous linear arrangements of HGPG maxima will be subparallel to those of the more accurately located AS maxima and aid in their interpretation. Secondly, since the HGPG maxima are offset in the down dip direction from a contact, they should give an indication of the dip direction when compared to the AS maxima. For the present study, AS maxima were plotted as red dots and the HGPG maxima as blue dots (Map 3).

4.2.4. POTENTIAL FIELD TILT

The potential field tilt is an interpretation technique applied to magnetic data. As the technique combines the three orthogonal first derivatives of the field, it enhances near surface anomalies. The method is based on the analytic signal derivation.

The potential field tilt developed by Miller and Singh (1994) is the arctangent of the ratio of the vertical component and the horizontal component of the gradient given by;

$$TILT = \tan^{-1} \frac{\frac{\partial T}{\partial z}}{\sqrt{(\frac{\partial T}{\partial x})^2 + (\frac{\partial T}{\partial y})^2}}$$

and illustrated in Fig. 4.20. As with the analytic signal derivation, the relationship between the horizontal and vertical derivatives is defined by the 3D Hilbert transform operator.

The horizontal component of the gradient achieves a maximum near or over source edges and tends to zero elsewhere. The vertical component of the gradient is positive over the source, zero over or near source edges (Hood, 1965) and negative elsewhere. As a result, the tilt of the

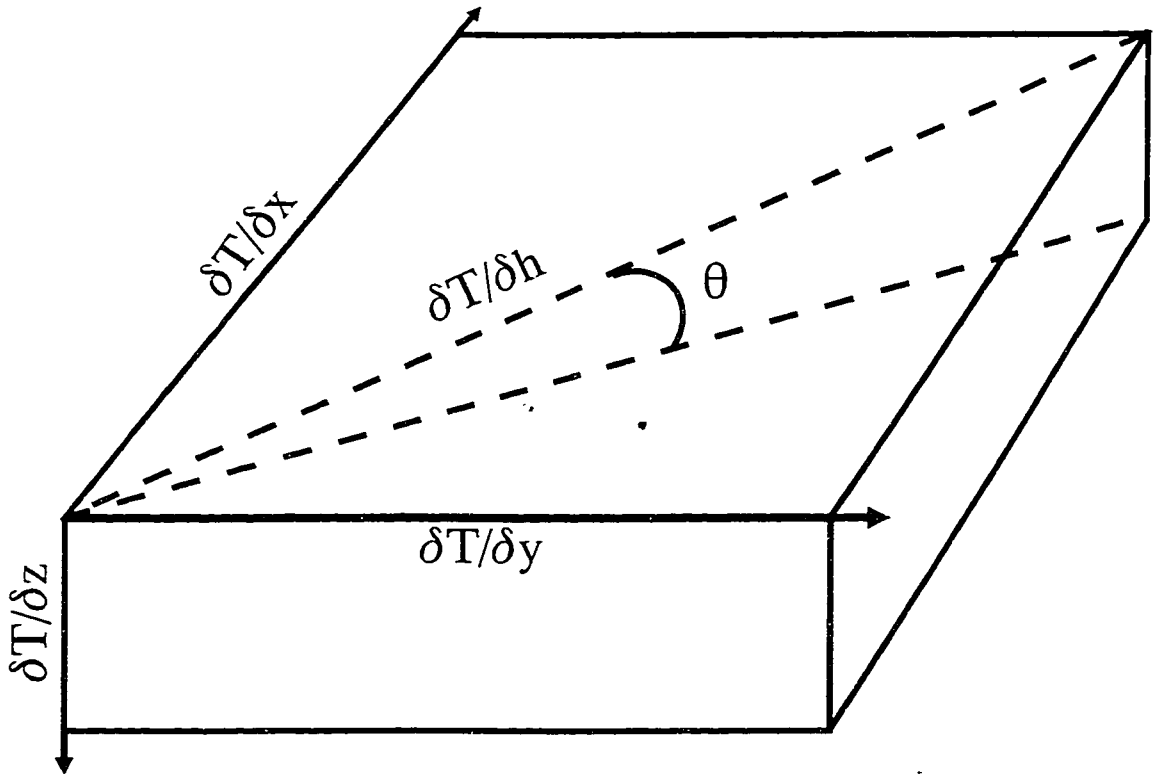

Fig. 4.20. Geometry of the potential field tilt. $\delta T/\delta h = SQRT[(\delta T/\delta x)^2 + (\delta T/\delta y)^2]$ and θ is the tilt angle. (After Miller and Singh, 1994).

magnetic field will be positive over sources, zero over source edges and negative elsewhere. The benefit of the tilt over the vertical derivative is that, being a ratio, weak sources or sources at greater depths, will be enhanced. A weak vertical component of the gradient divided by a weak horizontal component will generate the same response as a strong vertical component over a strong horizontal component. Expressing the ratio by its arctangent ensures values fall in the range of -90° to 90°.

The method is particularly useful for delineating faults that have demagnetized the rocks they fracture. The demagnetization may be due to mylonitization or to the oxidizing effects of circulating ground water. The tilt signature of such faults has a negative value. If the tilt is presented in map form with a black-to-white grey colour scheme, positive tilts will be white and negative tilts, signifying the lack of source material, will be black. The magnetic tilt map of the study area is presented as Map 4 at 1:50 000 scale and is attached to this thesis. This striking presentation makes the demagnetized fault zone (dark) and offsets of anomalies (light) across the zone obvious.

A subtle advantage to the tilt technique is that, despite combining derivatives of the data, aliasing and line-to-line levelling errors are not as apparent as those seen in the vertical derivative or the analytic signal.

4.2.5. EULER DECONVOLUTION

Euler deconvolution is an automated interpretation method for potential field data. The method uses gridded (3D) magnetic or gravity data as input to calculate the position of the top of the source of anomalies, and to differentiate between simple source body geometries.

The method was first described by Thompson (1982), who developed deconvolution of magnetic anomalies for the 2D (profile) case, but noted that 3D interpretation is also possible. The basis of the method is to consider the 3D data as a continuous function and use Euler's homogeneity equation to derive information about the source of the anomalous potential field.

Consider the field as a function, $f(x,y,z)$. This function is said to be homogeneous of degree n if;

$$f(tx,ty,tz) = t^n f(x,y,z) \tag{65}$$

Many simple point magnetic sources are of the functional form;

$$f(x,y,z) = \frac{G}{r^N} \tag{66}$$

where $r=(x^2+y^2+z^2)^{1/2}$, $N=1,2,3,...$, and G is not dependent on x, y, and z.

To test for homogeneity of degree n, substitute Eqn. 66 into Eqn. 65;

$$\frac{G}{[(tx^2+ty^2+tz^2)^{1/2}]^N} = \frac{t^n G}{[(x^2+y^2+z^2)^{1/2}]^N} \tag{67}$$

then, simplifying,

$$\frac{1}{t^N}\,\frac{G}{[(x^2+y^2+z^2)^{1/2}]^N} = \frac{t^n G}{[(x^2+y^2+z^2)^{1/2}]^N} \tag{68}$$

and,

$$\frac{1}{t^N} = t^n \tag{69}$$

If n=-N, then this function is said to be homogeneous of degree n, and therefore Euler's homogeneity equation,

$$x\left(\frac{\partial f}{\partial x}\right) + y\left(\frac{\partial f}{\partial y}\right) + z\left(\frac{\partial f}{\partial z}\right) = nf \tag{70}$$

is satisfied.

The total magnetic intensity, ΔT, caused by a point source at x, y, z, relative to the plane of measurement can be described by the function;

$$\Delta T(x,y) = f[(x-x_0),(y-y_0),z_0] \tag{71}$$

and Euler's equation is written as;

$$(x-x_0)\frac{\partial \Delta T}{\partial x} + (y-y_0)\frac{\partial \Delta T}{\partial y} + (z-z_0)\frac{\partial \Delta T}{\partial z} = -N\Delta T(x,y) \tag{72}$$

noting that n=-N and that N is the power to which the distance to the source is raised in the denominator of the functional form of a simple point magnetic source (Eqn. 66). As the value of N increases, the rate of fall of the anomaly intensity with distance from the point (x_o,y_o) increases. The value of N is referred to by Thompson as the 'structural index' (SI). The value of the structural index may be solved for in this equation, but is better understood by looking at

the rate of fall off of magnetic intensity for various source geometries (Fig. 4.21).

Thompson continues to develop the method for the 2D case, assuming that the magnetic gradient in the transverse (y) direction is 0. This assumption is not necessary for the 3D case. The final form of Euler's equation for magnetic fields is derived by the solution of two problems. First, most anomalies are located better in xy space by higher structural indices and in depth estimate by lower structural indices. This problem is alleviated by fixing the structural index in equation and solving for a series of standard indices and comparing results. Second, the absolute level of ΔT is inaccurate or unknown due to interference from the regional field or neighbouring anomalies. Thompson assumes ΔT is perturbed by a constant amount, B, in the local area. The observed intensity is:

$$T(x)=\Delta T(x)+B \tag{73}$$

Solving for ΔT we find:

$$\Delta T(x)=T(x)-B \tag{74}$$

and substituting into the Euler's equation and evaluating the derivative of $T(x)$-B;

$$(x-x_0)\frac{\partial T}{\partial x}+(y-y_0)\frac{\partial T}{\partial y}+(z_0)\frac{\partial T}{\partial z}=N(B-T) \tag{75}$$

is the result. This is the form of the Euler's equation used by Reid et al.(1990) in the first published use of the method on 3D data.

Having derived Euler's homogeneity equation for magnetic fields, we can look more closely

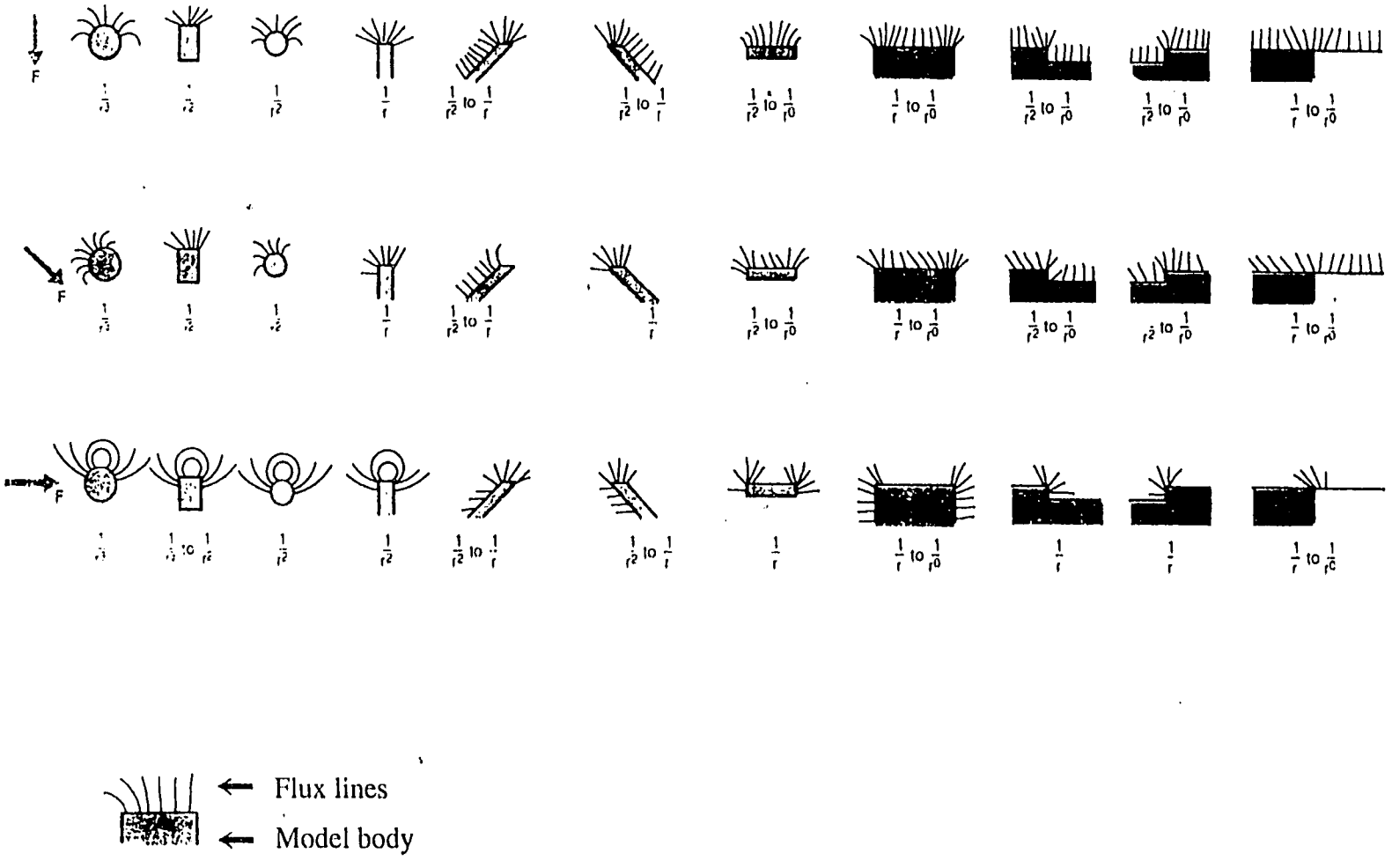

Fig. 4.21. Field lines and fall-off rates of various geologic models. Flux lines are superimposed on representative geologic models for various orientations of the inducing field (F). Anomaly amplitude is proportional to the indicated term $1/r^n$. From Breiner, 1980.

and rigorously at the structural index. The structural index is a measure of the rate of change of the field with distance from the source and this is typical of the geometry of the source (Fig. 4.21). Most simple geological situations can be approximated by an arrangement of monopoles and dipoles. The geometry of most geological structures can be described by structural indices 0, 1, 2, and 3. A structural index of 0 corresponds to a vertical contact, 1 corresponds to a dyke, 2 corresponds to a vertical pipe, and 3 to a sphere. Other geological features can be represented by these individual structures or any combination of structures.

Some structural indices are obvious from Fig. 4.21, but also can be derived theoretically. Reid et al.(1980) derive structural indices for the magnetic anomaly of a thin dyke and a sloping contact as well as the index for the gravity anomaly of a finite step. The thin dyke index is developed here as an example.

Reid et al.(1990) define, from Bosum (1968), the vertical magnetic anomaly, Z, of an infinite thin dyke (see Fig. 4.22) as:

$$Z(x,y) = \frac{AS}{r^2} \qquad (76)$$

where

$A = 2Mt \cos$ y

M = magnetization intensity

t = dyke thickness

x_o, z_o = coordinates of the dyke top

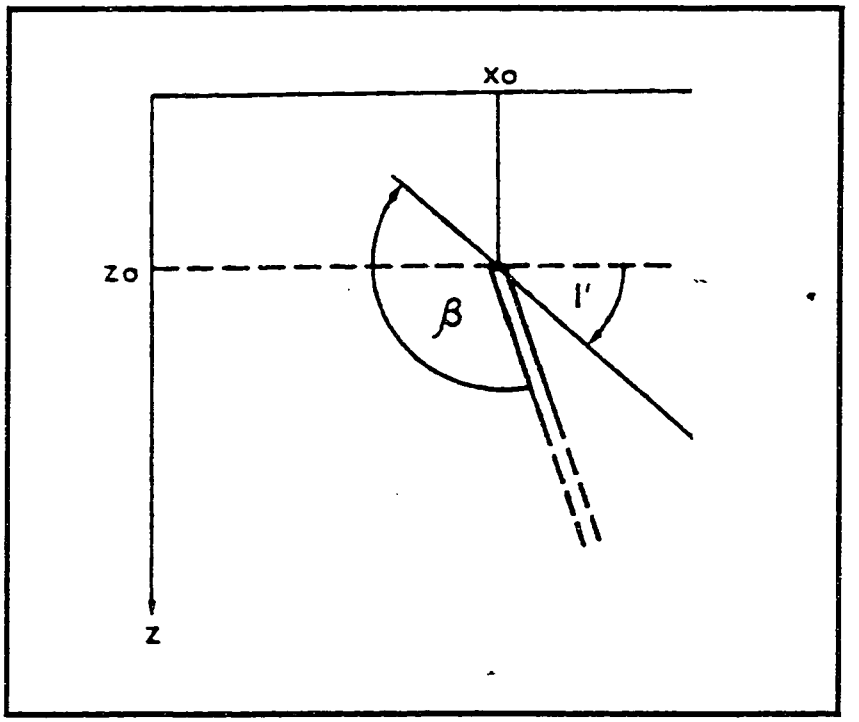

Fig. 4.22. The vertical magnetic anomaly of an infinite thin dyke, from Reid et al., 1991.

$cos\ y = [cos^2 a\ cos^2 I + sin^2 I]^{1/2}$

a = azimuth of profile w.r.t. magnetic north

I = inclination of geomagnetic field

$tan\ I' = (tan\ I)/(cos\ a)$ = reduced field inclination

$S = [-(x - x_o)\ sin\ B + (z - z_o)\ cos\ B]$

B = dip of dyke w.r.t. reduced inclination of field

$r^2 = (x - x_o)^2 + (z - z_o)^2$

Taking the derivatives with respect to x and with respect to z simplifies the expression:

$$\frac{\partial Z}{\partial x} = \frac{-A[r^2 \sin B + 2S(x-x_0)]}{r^4} \qquad (77)$$

and

$$\frac{\partial Z}{\partial z} = \frac{A[r^2 \cos B - 2S(z-z_0)]}{r^4} \qquad (78)$$

Substituting into the Euler's equation (Eqn. 75) ($\partial Z/\partial y = 0$ as this is a 2D structure);

$$\frac{A\{-(x-x_0)\sin B r^2 + (z-z_0)\cos B r^2 - 2S[(z-z_0)^2 + (x-x_0)^2]\}}{r^4} \qquad (79)$$

$$= \frac{A(Sr^2 - 2Sr^2)}{r^4} = \frac{A(-Sr^2)}{r^4} = \frac{-AS}{r^2} = -Z(x,z) \qquad \textbf{(80)}$$

Substitute into the right hand side of the Euler's equation;

$$-Z(x,z) = N(B-T) \qquad \textbf{(81)}$$

$$N = \frac{(B-T)}{-Z(x,z)} \qquad \textbf{(82)}$$

Since $Z = T - B$, then $-Z = B - T$ and substituting:

$$N = \frac{(B-T)}{(B-T)} = 1 \qquad \textbf{(83)}$$

The structural index of a thin dyke is therefore 1. Reid et al.(1990) note that, due to the absence of a term to describe the dip, this index is valid for any dyke regardless of the angle of dip and that sill edges will also have an index of 1 (a sill can be considered a dyke of zero dip). Further, this index can be used with total field data as well as the vertical component as the result is independent of declination and inclination of the geomagnetic field.

It has been shown that Euler's equation (Eqn. 75) of a function describing a total intensity magnetic field is of the form:

$$(x-x_0)\frac{\partial T}{\partial x} + (y-y_0)\frac{\partial T}{\partial y} + (z_0)\frac{\partial T}{\partial z} = N(B-T)$$

where x, y = coordinates of the sensor location (z is considered 0)

x_o, y_o, z_o = coordinates of the magnetic source top

$\partial T/\partial x$ = horizontal gradient of the total field in the x-direction

$\partial T/\partial y$ = horizontal gradient of the total field in the y-direction

$\partial T/\partial z$ = vertical gradient of the total field (in the z-direction)

N = structural index

B = regional magnetic total field intensity

T = total field magnetic intensity

The three gradients can be calculated from the total magnetic field in the frequency domain and the structural index will be assigned a value leaving an equation in four unknowns; x_o, y_o, z_o, and B. The solution strategy is to generate more equations than unknowns by creating a window of m x m grid cells to be moved systematically over the grid, creating m x m equations in four unknowns for each cell in the grid.

To solve the overdetermined case;

$$\boldsymbol{x} = A^{-1} + \boldsymbol{b} \qquad \textbf{(85)}$$

where $\boldsymbol{x}$ = the solution vector

A^{-1} = inverse of the matrix of unknowns

$\mathbf{b}$ = the constant vector

Rearranging the equation to fit the solution method;

$$(x_0)\frac{\partial T}{\partial x} + (y_0)\frac{\partial T}{\partial y} + (z_0)\frac{\partial T}{\partial z} + NB = (x)\frac{\partial T}{\partial x} + (y)\frac{\partial T}{\partial y} + NT \qquad \textbf{(86)}$$

so that,

$$x = x_0 + y_0 + z_0 + B, \qquad \textbf{(87)}$$

$$b = (x)\frac{\partial T}{\partial x} + (y)\frac{\partial T}{\partial y} + NT \qquad \textbf{(88)}$$

and the matrix of unknowns is given by;

$$A = \begin{vmatrix} \partial x_1 & \partial y_1 & \partial z_1 & N_1 \\ \partial x_2 & \partial y_2 & \partial z_2 & N_2 \\ \partial x_3 & \partial y_3 & \partial z_3 & N_3 \\ \vdots & \vdots & \vdots & \vdots \\ \partial x_n & \partial y_n & \partial z_n & N_n \end{vmatrix} \qquad \textbf{(89)}$$

where n is the number of equations. The solution strategy is then to generate A^T (the transpose of A), find the product of A^T and A (a 4 X 4 matrix), invert A^TA and then the dot product of $(A^TA)^{-1}$ and A will yield A^{-1}, the inverse of A.

The transpose of A is:

$$A^T = \begin{vmatrix} \partial x_1 & \partial x_2 & \partial x_3 & \cdots & \partial x_n \\ \partial y_1 & \partial y_2 & \partial y_3 & \cdots & \partial y_n \\ \partial z_1 & \partial z_2 & \partial z_3 & \cdots & \partial z_n \\ N_1 & N_2 & N_3 & \cdots & N_n \end{vmatrix} \tag{90}$$

and the product of the two matrices is,

$$A^t \cdot A = \begin{vmatrix} \Sigma \partial x^2 & \Sigma \partial x \partial y & \Sigma \partial x \partial z & \Sigma \partial x N \\ \Sigma \partial y \partial x & \Sigma \partial y^2 & \Sigma \partial y \partial z & \Sigma \partial y N \\ \Sigma \partial z \partial x & \Sigma \partial z \partial y & \Sigma \partial z^2 & \Sigma \partial z N \\ \Sigma N \partial x & \Sigma N \partial y & \Sigma N \partial z & \Sigma N^2 \end{vmatrix} \tag{91}$$

where $\sum$ is the sum of the expression from 1 to n. The matrix, $A^T \cdot A$, is a 4 x 4 matrix and is inverted using Cholesky decomposition (Press et al., 1986) and the dot product of this inverse and A^T yields the inverse of A. Solving the following,

$$\boldsymbol{x} = A^{-1} \cdot \boldsymbol{b}$$

yields the vector $\boldsymbol{x}$ where,

$$\boldsymbol{x}(1) = x_o$$

$$\boldsymbol{x}(2) = y_o$$

$$\boldsymbol{x}(3) = z_o$$

$$\boldsymbol{x}(4) = B$$

This method is used to solve for the unknowns because it produces an easily inverted 4x4 matrix. Also the the inverse of $A^T \cdot A$ is closely related to the standard uncertainties of the estimated

parameters *x(1), x(2), x(3),* and *x(4).* The relationship is;

$$\sigma^2[x(j)] = (A^T \cdot A)^{-1}_{jj} \quad \textbf{(92)}$$

or

$$\sigma[x(j)] = [(A^T \cdot A)^{-1}_{jj}]^{1/2} \quad \textbf{(93)}$$

so the diagonal elements of $(A^T A)^{-1}$ are the variances of the estimated source locations and the regional field.

The tolerance of an Euler deconvolution depth solution is a measure of the uncertainty of that solution. The tolerance of a solution is defined as the ratio of the standard deviation of the depth estimate to that depth estimate, usually expressed as a percentage. This measure of uncertainty is used to eliminate spurious solutions. A review of the limited literature follows and the importance of the x, y, and z tolerances and methods of choosing a reasonable tolerance level are investigated.

Thompson (1982) derives the acceptance criterion from the variances yielded by the least squares solution of the overdetermined set of equations. The tolerance should depend p. 33) He defines the tolerance of the depth estimate to be the depth divided by the product of the structural index and the standard deviation of the depth estimate ($z/N\sigma$). A solution is accepted if this value is greater than or equal 20. Where the SI equals 0.0, Thompson's tolerance measure is undefined. Thompson considers only the 2D case and does not allow an SI lower than 0.5.

Reid et al.(1990) consider that if the standard deviation of the estimated depths is less than

some percentage (15%) of the estimated depth, the solution should be retained. Generally, the choice of tolerance level is empirical. If the acceptance criterion is too strict, the calculated depths may be accurate (z) but the body will be poorly delineated in x and y due to too few solutions. If the acceptance criteria are too wide, spurious solutions may obscure both depth estimates and body definition. Reid et al. (1990) also point out that lower structural indices generate solutions with lower certainty.

The standard deviation of the x and y estimates are also products of the computation of Euler depth estimates. Generally, as the standard deviation of the depth estimate decreases, the standard deviation of the horizontal position estimates also decreases. Some interpreters of Euler solutions use the total error (the sum of the standard deviations of x, y, and z) rather than the depth error (standard deviation of z) in calculating the tolerance value. x and y tolerances will not be considered further as fundamentally different from z tolerances.

Once a set of depth solutions has been obtained, the results are displayed by a point on a map with depth indicated by either a circle with radius proportional to the depth, by a symbol or by a colour. Where many solutions are present, a dot at the X and Y location on the map with a colour based on the estimated depth (blue shallowing to red) provides relative depth information without the cluttering of overlapping circles. This is the presentation method used in this study and is illustrated at 1:50 000 scale as Map 5 attached to this thesis.

The Euler deconvolution method can accurately and quickly define the boundary between two bodies of sufficient magnetization contrast as well as provide relative depth to source information.

The method's insensitivity to body dip helps locate contacts at the expense of providing any information about the dip. One of the great advantages of using this method is its insensitivity to the inclination of the core field. This is not of great importance at very high magnetic latitudes, but can be significant depending on the scale of observation. The input data does not require reduction to the pole. Similarly, the Euler solutions are unaffected by remanent magnetization effects.

Any structural index can produce solutions that will delineate the source in X and Y. Only an appropriate choice of structural index for a given source body will generate accurate depth information. As source body geometry is usually unknown, there depth estimates are best to be viewed as relative rather than absolute.

Tolerance levels are critical to the interpretation of Euler depth solutions. Spurious solutions abound. A tolerance level should be high enough to delineate major anomaly source bodies , but low enough that spurious solutions do not obscure the boundary trends. As the choice of suitable tolerance is empirical, a trial and error method is generally used to find the most useful tolerance.

Window size is also a critical parameter. The maximum depth solution is about twice the window size (Reid et al., 1990). Increasing the window size increases the sensitivity of the method. Limiting window size to allow only one anomaly per window is desired, but may lead to limiting the depth extent of the method.

As the method employs the three orthogonal derivatives, the input grids must optimized to reduce noise and inspected to ensure that no ringing (Gibb's phenomenon) has been introduced. These problems can be minimized with low pass filtering, trend reinforcement, micro-levelling

and by limiting the window size. Smaller grid intervals will improve the method's detection of high frequency anomalies, but the window size may have to be adjusted to detect deeper sources.

It is important to note that the method computes the location of source bodies using their derivatives. If the gradient or derivative field is flat (non-anomalous) no real solutions can be expected.

4.2.6. 2.5D MODELLING

In addition to the previously described 3D interpretation techniques, profile modelling was used to support the interpretations. The three dimensional shape of causative bodies can be constrained by magnetic profile forward and inverse modelling. The basis of this technique is to calculate the magnetic anomaly of a proposed model and compare the calculated profile to the observed profile. Profile matching does not indicate that the model is a geological reality but rather indicates it as a geophysical possibility. Confidence in the model is enhanced by its simplicity, consistency across several profiles, consistency with other geophysical models, and its geological probability. The method is used here to support the interpretations based on 3D techniques.

Magnetic profiles were modelled using the 2.5 dimensional modelling package GM-SYS (Northwest Geophysical Associates, Inc., 1995). Profile line locations are shown on Figure 5.9.3. Magnetic profiles can be modelled anywhere in the study area due to the uniform coverage by aeromagnetic survey methods. The use of 2.5 dimensional models limits the location of profiles to geological contacts where the strike extent either side of the profile is roughly equal. Limited magnetic susceptibility sampling places loose constraints on the

geophysical properties of the rock units modelled. These factors limit modelling results to general bulk trends.

The models are constrained by known geological contacts and by the measured magnetic susceptibilities of the lithologies. Geological contacts are taken from the map by Zaleski et al.(1995). The lack of continuous exposure has resulted in many extrapolated contacts on the geological map. Similarly, the paucity and variability of measured susceptibilities casts some uncertainty on the results of the modelling.

5.0. INTERPRETATION

The interpretation of the high resolution aeromagnetic data over the Manitouwadge greenstone belt is largely limited to the study area, defined by the map area of Zaleski et al. (1995). The magnetic data and the tools described in the previous chapter on data enhancement will be used to interpret faults, dykes, magnetic and lithological units, dips of magnetic units and folding. The resulting interpretations will be extrapolated outside the study area to the surrounding Black Pic batholith and neighbouring greenstone belts.

In order to illustrate the interpretation, figures are presented as related sets, eg. 5.9.1, 5.9.2,and 5.9.3. The figures cover limited areas pertinent to the interpretation and are of the same size and scale. The magnetic data, interpretive tools and the interpretation should be viewed as a set; the interpretation figure should be used to help locate magnetic features. The original interpretation was performed using 1:25 000 scale maps. 1:50 000 scale maps are attached as Maps 1 through 6. The 1:50 000 maps are included to provide more regional context to the magnetic features.

An infinite number of possible bodies can generate a given magnetic anomaly (Breiner, 1980). As there is no unique solution, interpretations must be constrained as much as possible and make geological sense. All magnetic interpretations, including those presented here, suffer from this uncertainty.

5.1 FAULTS, DYKES AND CULTURAL EFFECTS

The interpretation of geology from aeromagnetic data is complicated by faulting, dyke emplacement and cultural features. The latter provide no useful information, but fault geometry and fault displacements does have a bearing on structural interpretations. As a first step, the

positions and interpreted displacement on the faults, the positions and attitudes of dykes as well as known cultural effects were defined.

5.1.1. FAULTS

Faults are interpreted largely based on the TILT map. The TILT technique produces positive (white) values over sources and negative (black) values elsewhere. Offset of linear positive features at a high angle to the negative TILT anomalies representing faults, indicates the strike-slip or horizontal component of displacement and the sense of relative motion.

The interpreted faults trend, generally, to the NW or to the NNE (Fig. 5.1). The NW trending faults tend to have little identifiable strike-slip component, while the NNE trending faults usually have some component of strike-slip, up to about 500m. The faults are magnetic lows due to the demagnetization of the rocks in the vicinity of the fault, probably to due to the oxidation of magnetite by circulating ground water. The NW trending faults are largely interpreted from long linear TILT lows, identified from series of TILT lows. These lows are disrupting east-west trending linear highs (Fig. 5.2, fault marked by arrow). This makes tracing the fault through areas of low magnetic gradients more difficult. The fault traces were also defined by truncations of linear arrangements of maxima of the horizontal gradient of the pseudo-gravity.

The NW trending faults are often sub-parallel and adjacent to the NW trending Matachewan dykes. The faults were recognized when linear magnetic lows extending north of the Manitouwadge synform were investigated. Offsets in a Matachewan dyke within the western Loken Lake pluton led to the recognition of the sub-parallel faults (Fig. 5.5, arrow marks dyke offset). The faults appear to be extensions of the Matachewan dykes to the north west, but have a negative TILT anomaly. The faults may predate the emplacement of the dykes, but appear to

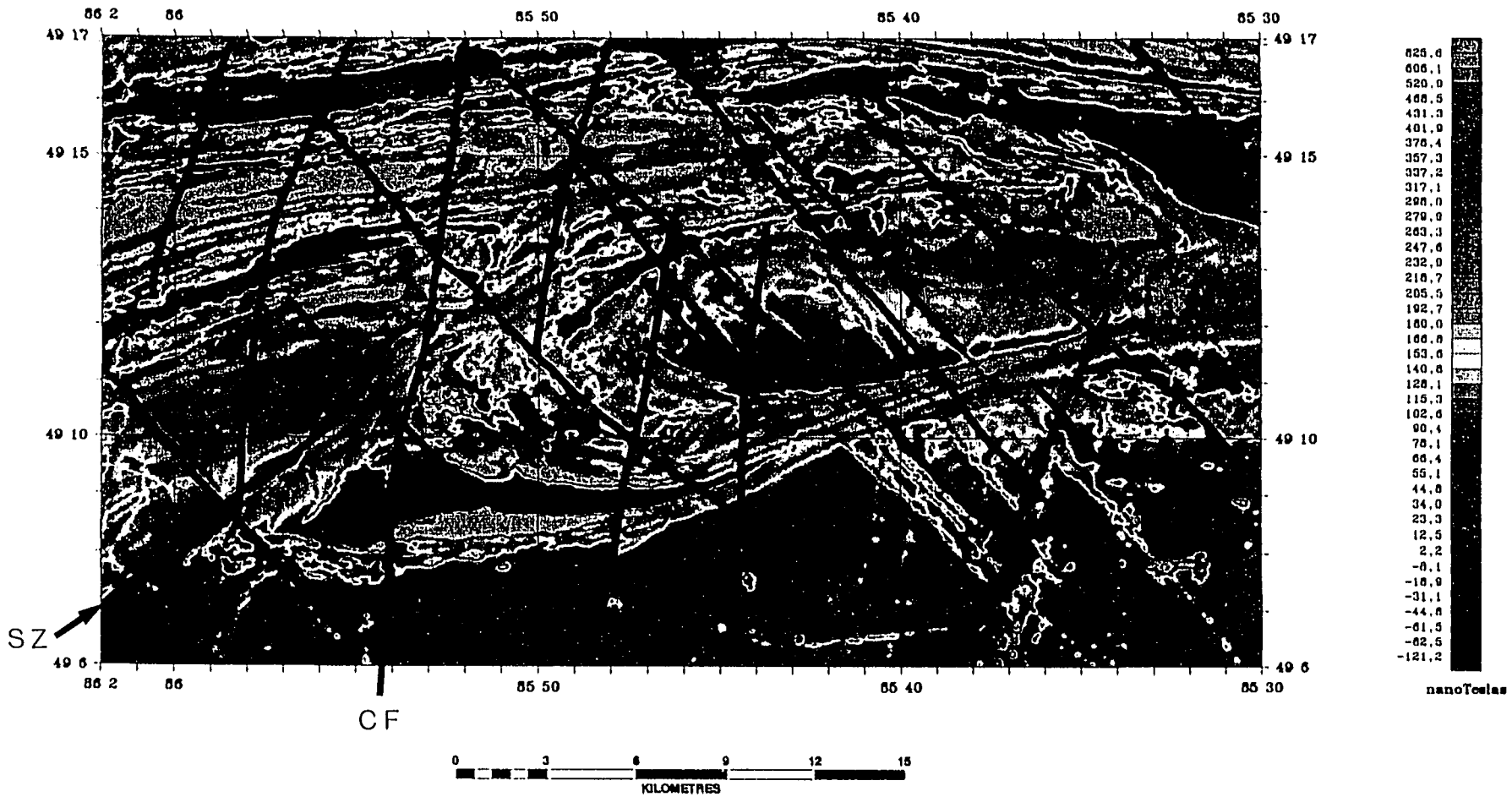

Fig. 5.1. Faults interpreted from TILT map of magnetics. Black lines represent interpreted faults.

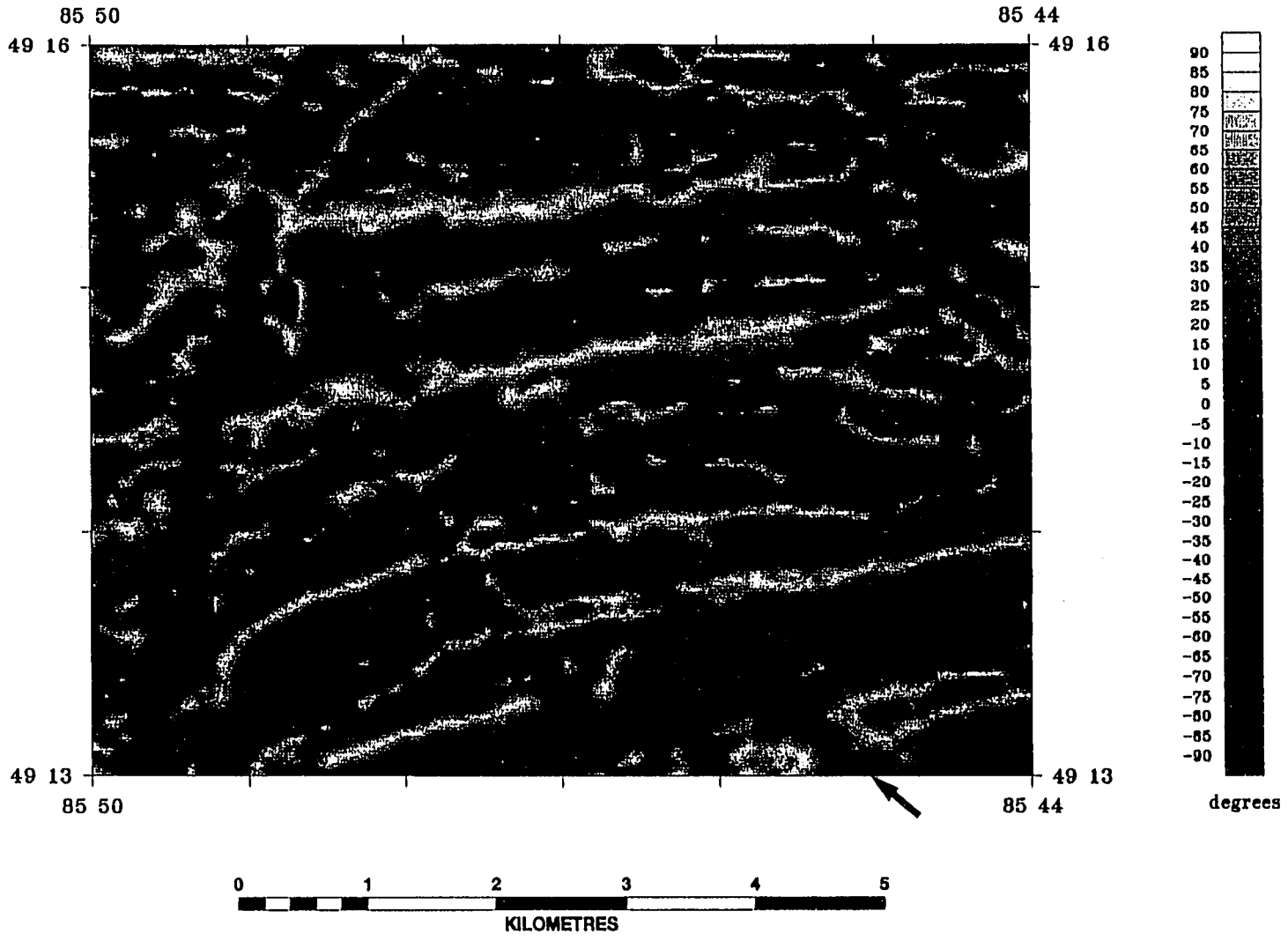

Fig. 5.2. TILT showing fault related lows. TILT lows in east-west trending linear highs align along a north-west trending fault (diagonal line across centre of image).

have been active or reactivated following emplacement by their disruption of dyke anomalies.

The Loken Lake pluton is cross-cut by six Matachewan dykes, at least five of which can be interpreted to have associated sub-parallel faults. From west to east across the NW trending faults, the intensity of the magnetic field is seen to increase in a step-like fashion (Fig. 5.3). As the Loken Lake pluton has a very low magnetic susceptibility (less than 1.0 X 10^{-3} SI) the increase in intensity is interpreted as a decrease in the depth to the magnetic sources that underlie the pluton. This implies a thinning to the east and, when coupled with the interpreted fault bounded steps in intensity, indicate that these faults have significant vertical displacement. A 2.5D magnetic model across the east-west long axis of the Loken Lake pluton (Fig. 5.4), suggests that there is a stepping of the intensity of the magnetic field to the east, with steps defined by the positions of the NW trending dykes (and their sub-parallel faults). This model suggests that there is significant vertical offset across the NW trending faults, cumulatively representing as much as a kilometre within the Loken Lake Pluton.

The NNE trending faults were interpreted in the same way as the NW trending faults, however, there is usually a component of strike-slip recognizable along the NNE trending faults. The sense of motion along the faults is sinistral. The Cadawaja fault cuts through the outer hinge zone of the Manitouwadge synform, creating a 500m offset in the southern limb of the fold (Fig. 5.1, arrow 'CF' marks the Cadawaja fault). The southern limb to the east of the fault has significantly higher magnetic intensity and a more continuous anomaly pattern, suggesting that there may also be some vertical displacement along this fault. The strike slip component on other NNE trending faults is relatively minor.

A NE trending fault is interpreted along the northern limb of the western end of the

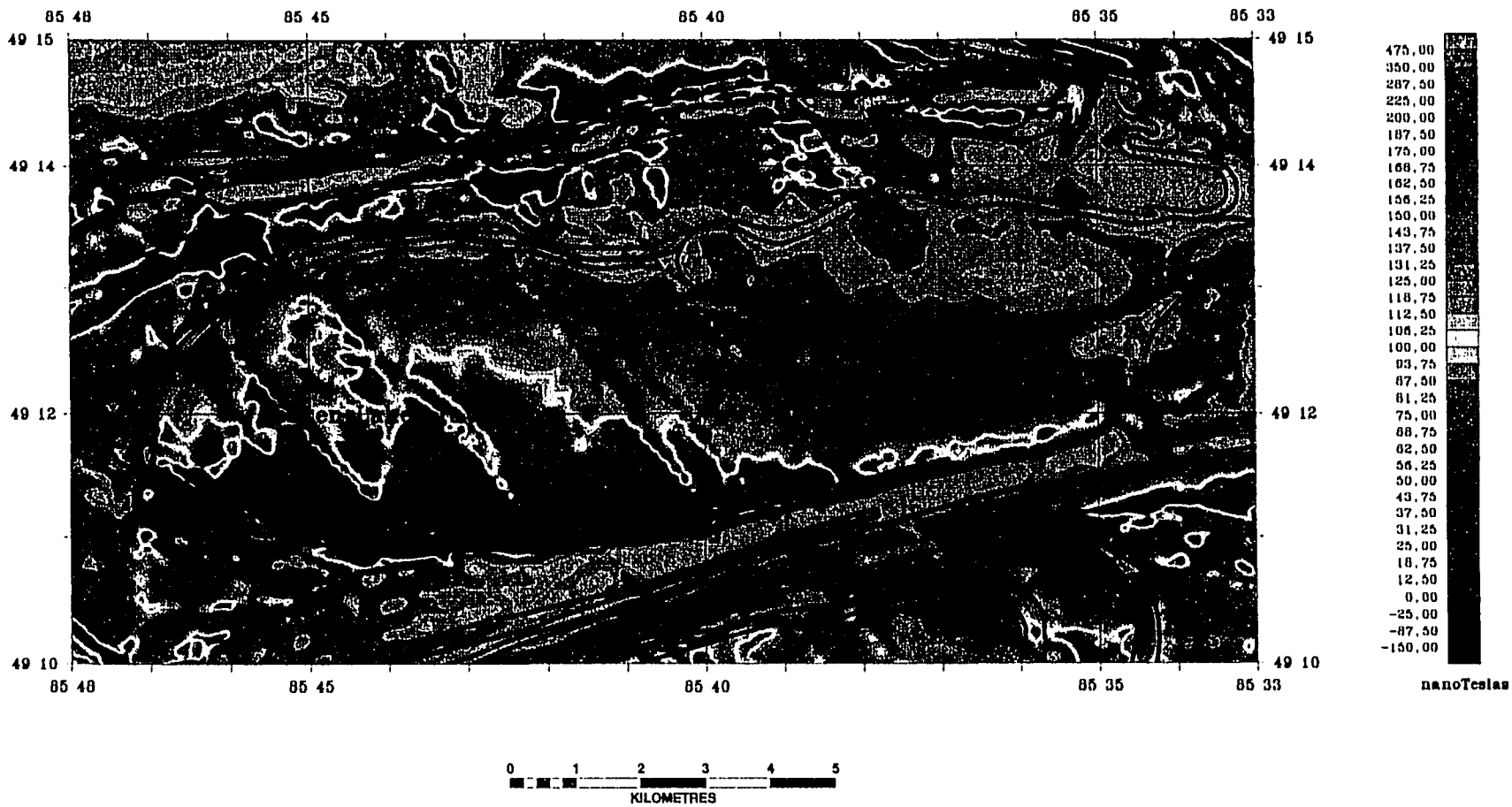

5.3. Residual total field magnetics over the Loken Lake pluton. There is a step-wise increase in intensity to the east across the NW trending dykes.

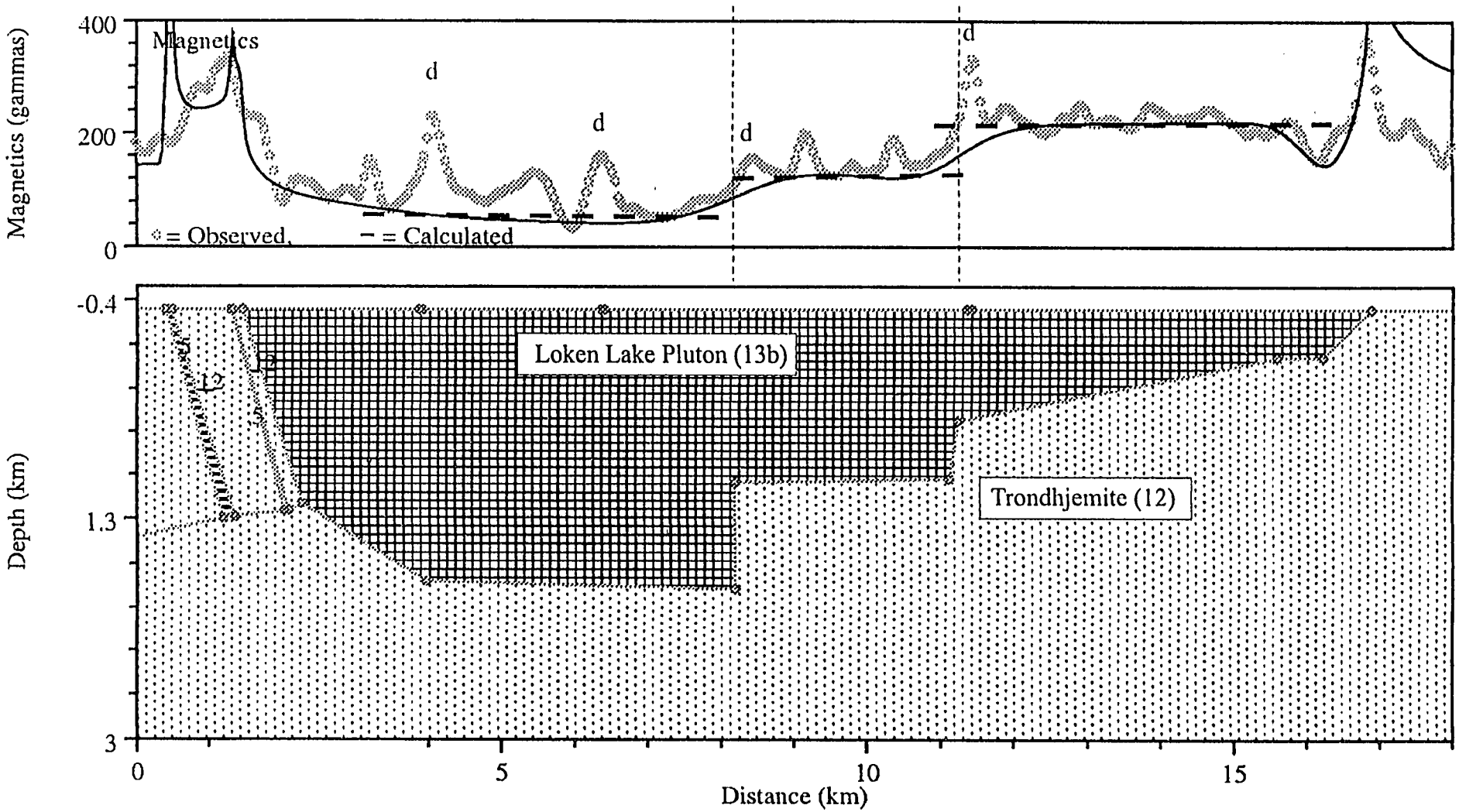

Fig. 5.4. 2.5D modelling of magnetic profile across the east-west long axis of the Loken Lake pluton. 'd' labels indicate the magnetic anomalies due to Matachewan dykes and the vertical dashed lines mark the position of faults sub-parallel to the dykes. Horizontal dashed lines represent the steps in magnetic intensity caused by the vertical offset along the faults.

Manitouwadge synform (Fig. 5.1, arrow marked 'SZ'). The fault is interpreted from the truncations of linear magnetic anomalies to the west of the fault along the northern limb of the fold. Zaleski et al. (1995) have interpreted this shear zone as indicating sinistral deformation.

All the interpreted faults have been presented with their minimum extent. The faults are extremely straight and may continue for great distances along their strike. The faults are difficult to trace when they are sub-parallel to a dyke and when they traverse an area of low magnetic gradient or lacking in features that could show offset or truncation. This is especially true for the Black Pic batholith south of the Manitouwadge synform.

5.1.2. DYKES

Three generations of major diabase dykes, the Matachewan, Biscotasing and Marathon, can be mapped from the magnetic data quite readily (Fig. 5.5). The first vertical derivative highlights the dyke positions rather well. The dykes can be recognized by their thin, straight, linear pattern, usually striking a high angle to the east-west regional geological strike. The dyke's magnetic signature may be segmented and/or gently curving, but are usually not anastomosing. These characteristics can be used to distinguish dykes from sub-parallel striking Archean rocks.

The Matachewan dykes are the oldest of the three main swarms emplaced within the greenstone belt, as discussed in chapter 1. The dykes are obvious on the first vertical derivative map as six NW trending linear red anomalies within the Loken Lake pluton (Fig. 5.5) and extending to the southeast into the Black Pic batholith. They are difficult to trace north of the Manitouwadge synform and may, in fact, not have propagated at the deeper crustal levels exposed in the area.

The coincidence of maxima of the horizontal gradient of the pseudo-gravity (HGPG) and the

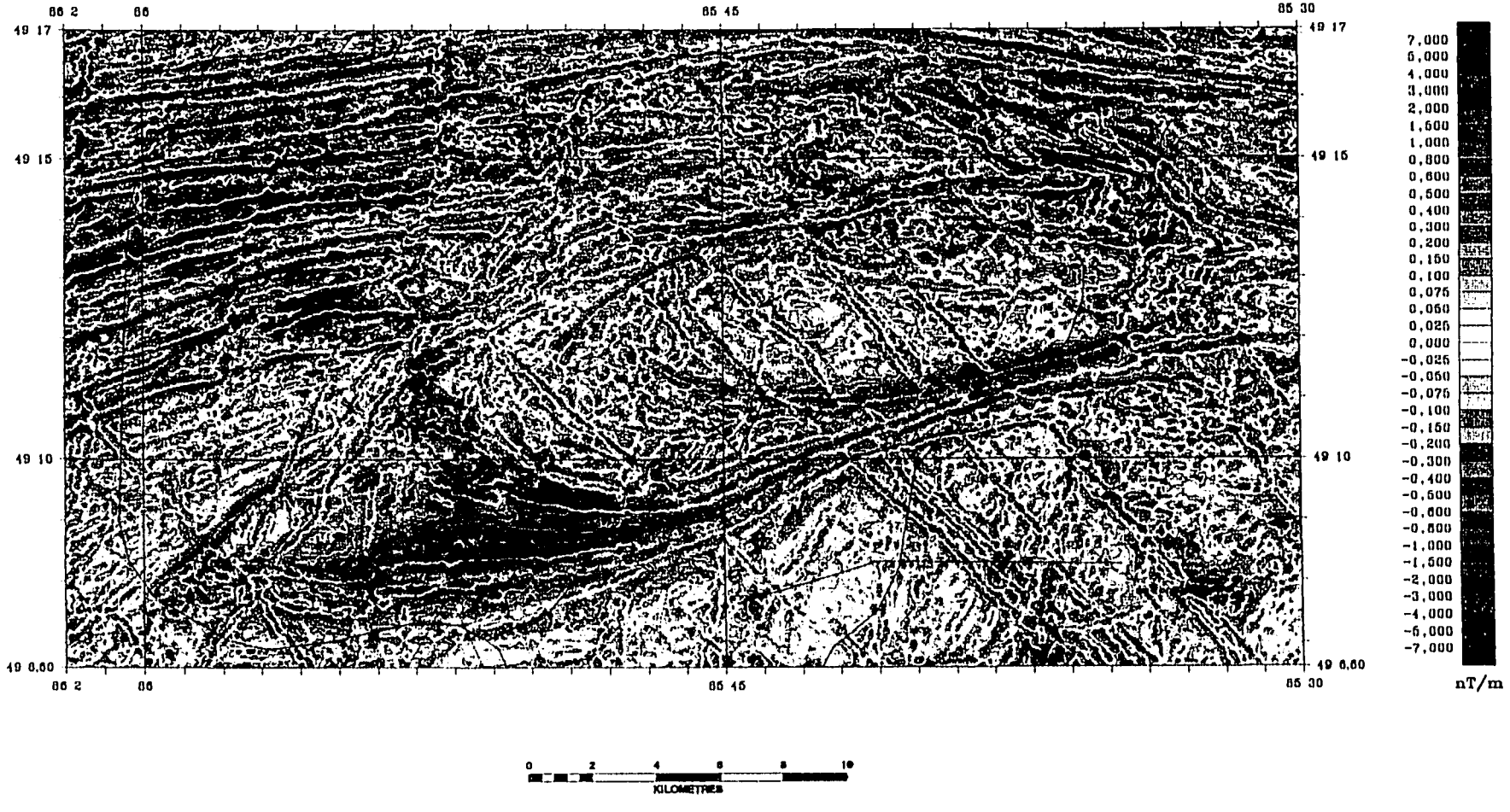

Fig. 5.5. First vertical derivative showing dykes.

maxima of the analytic signal (AS) (Fig. 5.6), indicates the dykes are sub-vertical. The Matachewan dyke near the western end of the Loken Lake pluton (Fig. 5.6, arrow 'A') illustrates this relationship. Towards the east, the AS maxima pattern over a Matachewan dyke (Fig is a globular distribution aligned along the strike of the dyke, while the HGPG maxima represents the dyke as in the west. As the AS is the product of derivatives of the magnetic field, it is more sensitive than the HGPG and detects maxima on both sides of the linear anomalies representing the dykes.

The other two generations of dykes are not imaged as well by the vertical derivative because they intersect the flight lines at lower angles and, as a result were not as well trend-reinforced as the Matachewan dykes. Furthermore and for the same reason, these anomalies suffer more from the 'string-of-pearls' effect of minimum curvature gridding. This combination of effects gives them a weak, segmented signature. The Biscotasing dykes trend to the NE and the Marathon dykes trend about 5° east of due north. The latter dykes are very poorly sampled by the north-south oriented survey flight lines.

5.1.3. CULTURE

The known cultural effects in the magnetic data include the town of Manitouwadge and two tailings ponds. The magnetic field over the town appears muted due to post-acquisition low pass filtering to reduce the magnetic signal due to cultural effects, eg. buildings, automobiles, iron pipes etc. The tailings ponds of the Geco and Willecho mines appear as anomalous highs. Their positions are noted on Figure 5.7. In addition, there is a prominent magnetic low on the northern limb of the Manitouwadge synform around the Rabbitskin Lake area. The area is covered by the lake and a great amount of swamp. The magnetic low is probably in part attributable to the

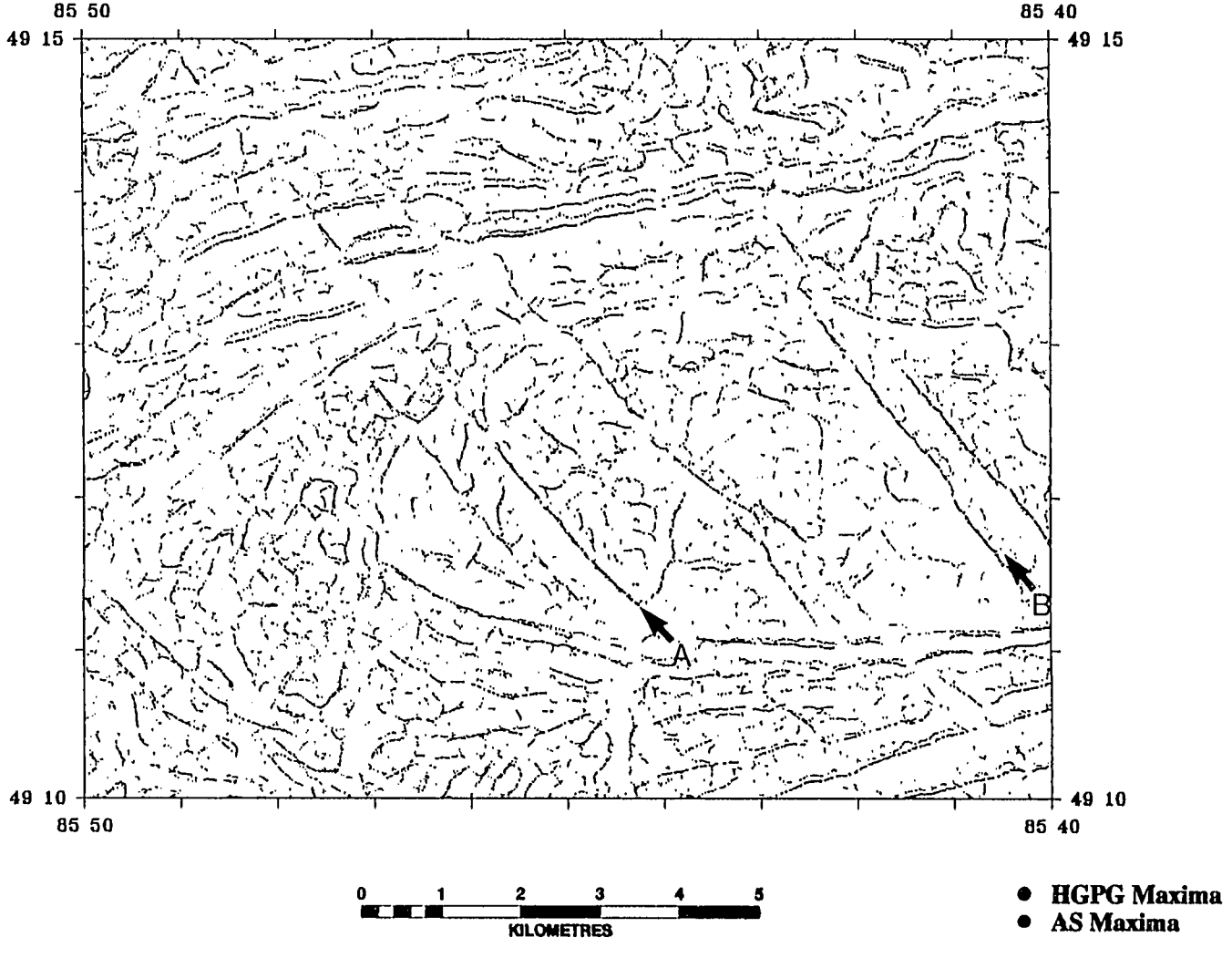

Fig. 5.6. AS and HGPG maxima over dykes within Loken Lake pluton.

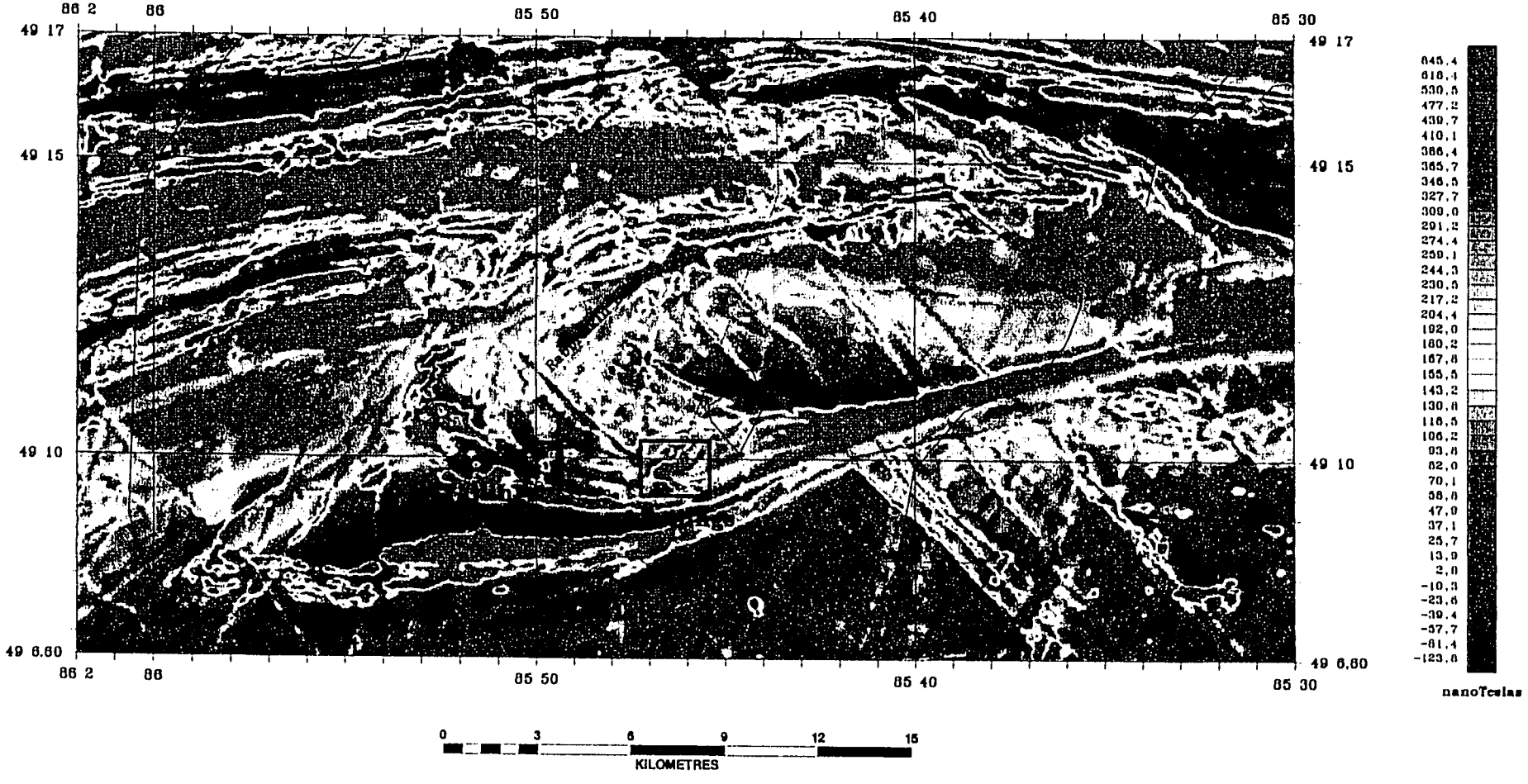

Fig. 5.7. Cultural magnetic features. Dashed red lines are railroads, blue lines are highways.

increase in the distance to magnetic sources caused by the lake. However, the location of the lake may be controlled by local faulting. The low modifies the magnetic signature of the Manitouwadge synform significantly and may be important to structural interpretations.

5.2 MAGNETIC AND LITHOLOGICAL UNITS OF THE STUDY AREA

The apparent magnetic susceptibility grid combined with AS maxima, HGPG maxima and Euler deconvolution solutions can be used to define units of similar magnetization characteristics (magnetic units). The apparent magnetic susceptibility relates the magnetic field to a physical property of the source lithologies and the AS and HGPG maxima define the contacts between bodies of sufficient magnetic susceptibility contrast.

It is unrealistic to assign a single magnetic susceptibility to a geological unit. Mappable geological units are rarely based on their bulk volume of magnetite and a small increase in magnetite content can increase the magnetization significantly. Mappable units are not necessarily homogeneous geochemically, mineralogically or petrologically. It is more useful to interpret the magnetic data in terms of magnetic units with the understanding that there is some general relationship between certain geological and magnetic units. For example, some magnetite-bearing iron formations can be characterized by their extremely high intensity magnetic signature and certain homogeneous felsic intrusions can be characterized by a constant low magnetic intensity.

The magnetite content of rocks can be greatly modified by regional metamorphism. The effects of metamorphism on the magnetic susceptibility of rocks varies both with rock type and chemistry, but also varies with metamorphic grade. Unmetamorphosed mafic volcanics have moderate to high magnetic susceptibilities. Regional metamorphism to amphibolite facies will

tend to reduce the susceptibilities of mafic volcanics whereas coarser grained gabbros tend to maintain their susceptibility (Clark, 1997). Generally in volcanic rocks, amphibolite grade metamorphism will produce bimodal magnetic susceptibility with chlorite and /or biotite amphibolites tending to be weakly magnetic and hornblende amphibolites tending to higher susceptibility (Clark, 1977). Granulite facies metamorphism of mafic rocks tends to increase susceptibility by the generation of secondary magnetite, although magnetite is consumed at pressures greater than 10 kbar (Clark, 1997). Secondary magnetite may be produced in amphibolite grade rocks that have undergone retrograde metamorphism.

Metamorphic effects on the magnetic susceptibility of sedimentary rock reflect the generation of secondary magnetite which is controlled by the ferric iron content of the sediments and the grade of metamorphism. Granulite facies metamorphism develops more magnetite in pelitic layers than in psammitic layers (McIntyre, 1980). Iron formations tend to be self-buffering and maintain their susceptibility throughout the range of metamorphism seen locally.

The metamorphic grade increases from greenschist in the Hemlo-Schrieber greenstone belt to upper amphibolite in the Manitouwadge greenstone belt to granulite near the Wawa-Quetico subprovince boundary. This is reflected in the obvious regional magnetic gradient, high in the north and low in the south. The effect of metamorphism on magnetic susceptibility must be kept in mind when attempting to extrapolate contacts and units from areas of known geology to unmapped areas.

5.2.1 IRON FORMATION (UNIT 9)

Within granite-greenstone belts, magnetite-bearing iron formation is readily recognised by its extremely high intensity magnetic signature. Such iron formations (Units 9a and 9b, Zaleski

et al., 1995) tend to have magnetic susceptibilities one or two orders of magnitude greater than other rocks usually present in this geological setting. They were originally precipitated in horizontal strata and tend to form linear anomalies, although they may be folded. Magnetic iron formation can have complicated magnetic properties including high Koenigsberger ratios (high remanent magnetization), anisotropy of magnetization and complications due to its own disturbance of the local geomagnetic field (Clark, 1997). However, the bulk magnetic susceptibility of the iron formation will usually be at least an order of magnitude higher than that of any other rock found in the greenstone belt, with the exception of serpentinized ultramafic rocks and gabbros. As AS maxima and Euler deconvolution solutions are unaffected by source body remanent magnetization, an interpretation of the iron formation contacts and depths should be possible without detailed knowledge of the magnetic properties of the rocks. However, 2.5D modelling of such iron formations may be unreliable as these properties must be defined to calculate model anomalies accurately.

Measured susceptibilities for the magnetic iron formations are limited but indicate that the values will range from about 100 x 10^{-3} SI to more than 250 x 10^{-3} SI (see Appendix 1). Magnetic iron formation mapped by Zaleski et al. (1995) as units 9a and 9b, is exposed in the inner volcanic belt and is structurally repeated by the D_2 Manitouwadge syncline, all within the hinge zone of the Manitouwadge synform. Thin mappable units of this iron formation outcrop on the southern limb of the Blackman Lake antiform near the nose of the fold and within the Black Pic tonalite south and west of Kern Lake (see Map 1). The iron formation attains greatest apparent thickness within the Manitouwadge synform. Over these thicker iron formations south of the Manitouwadge synform axial trace, the apparent magnetic susceptibility has values greater

than 150 x10^{-3} SI (orange to pink areas, Fig. 5.8.1), while north of the axial trace the values are lower. This difference may be due to the reduced magnetic intensity caused by the more shallow dip of the northern units. As well, the northern units outcrop pattern and strike is to the north, parallel the magnetic survey flight lines, while the southern units strike more perpendicularly to the flight lines and as such are better sampled by the magnetic survey. The northern iron formations have less apparent thickness and are probably not as well sampled by the survey as those south of the Manitouwadge synform's axial trace.

A combined plot of AS and HGPG maxima define contacts around the iron formations (Fig. 5.8.1) that correspond to contacts mapped by Zaleski et al. (1995) in a general way. In the area of these iron formations, the exposure is good and detailed mapping has been carried out by several authors (Pye (1957), Milne (1974) and Zaleski et al. (1995)). The resolution of the geological mapping is higher than that of the magnetic survey in this area. On the southern limb of the outer volcanic belt, the structurally repeated iron formation is in contact with high susceptibility mafic metavolcanics and metagabbros and differentiation of signal from these sources is difficult. Figure 5.8.1 provides a lower resolution approximation to the mapped geology. Euler deconvolution depth solutions for the same area (Fig. 5.8.2) correlate well to the AS and HGPG maxima, although they are more diffuse. The depth information is shown by the hot-to-cold (shallow-to-deep) colour of the solutions and indicates that the contacts defined by the AS and HGPG maxima lie near the surface. In the circled area on Figure 5.8.2, iron formation is overlain by tonalite and metasediments. The apparent susceptibility indicates the iron formation continues underneath these lower susceptibility units. While the AS and HGPG maxima end abruptly at the mapped contact, the Euler solutions indicate a magnetization contrast

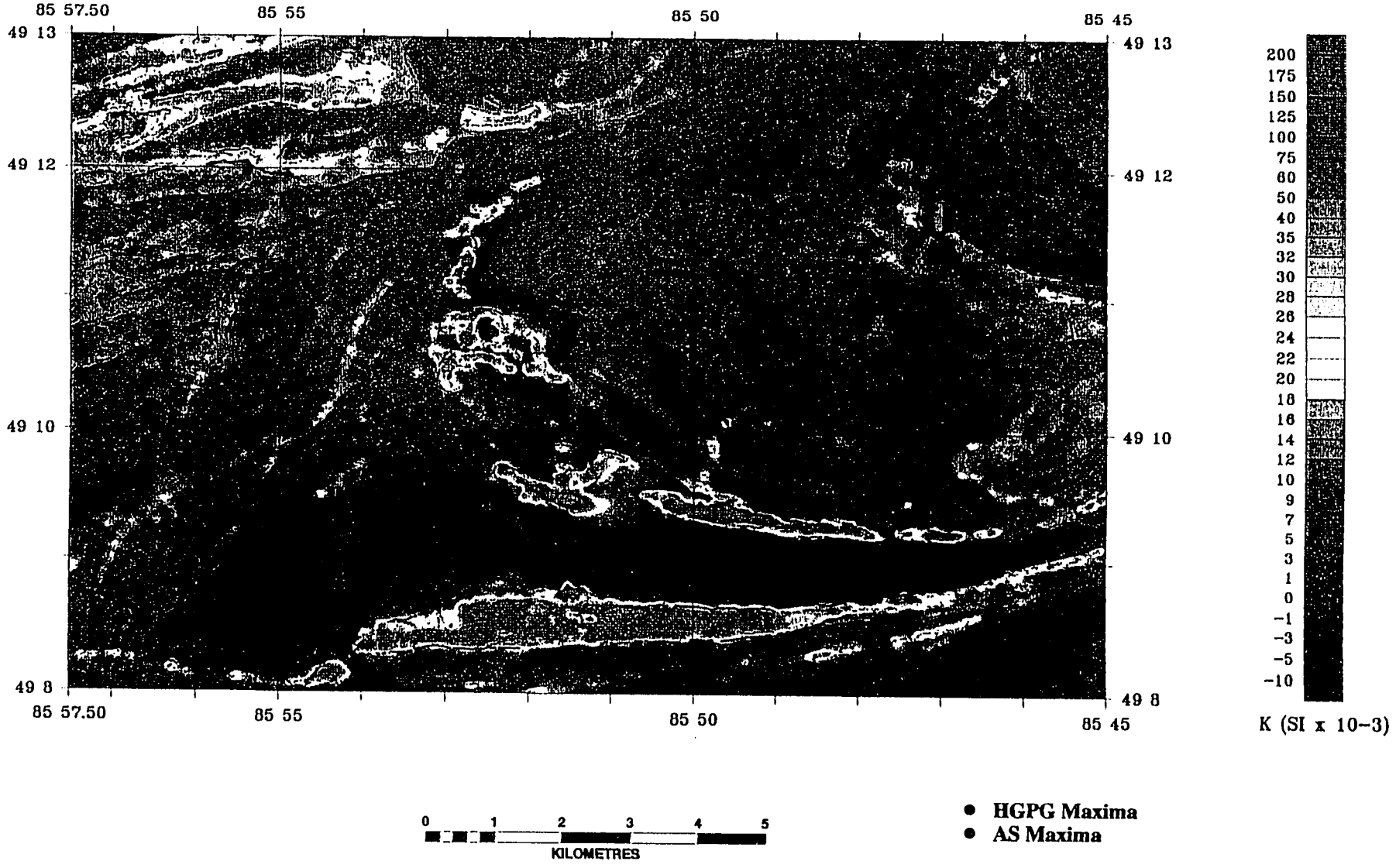

Fig. 5.8.1. Magnetic iron formation as indicated by apparent susceptibility, with AS and HGPG Maxima. The highest apparent susceptibility values are interpreted to represent areas underlain by magnetic iron formation.

Produced by PLOTSYS 5.15, created by Regional Geophysics/CGD/GSC/NRCan

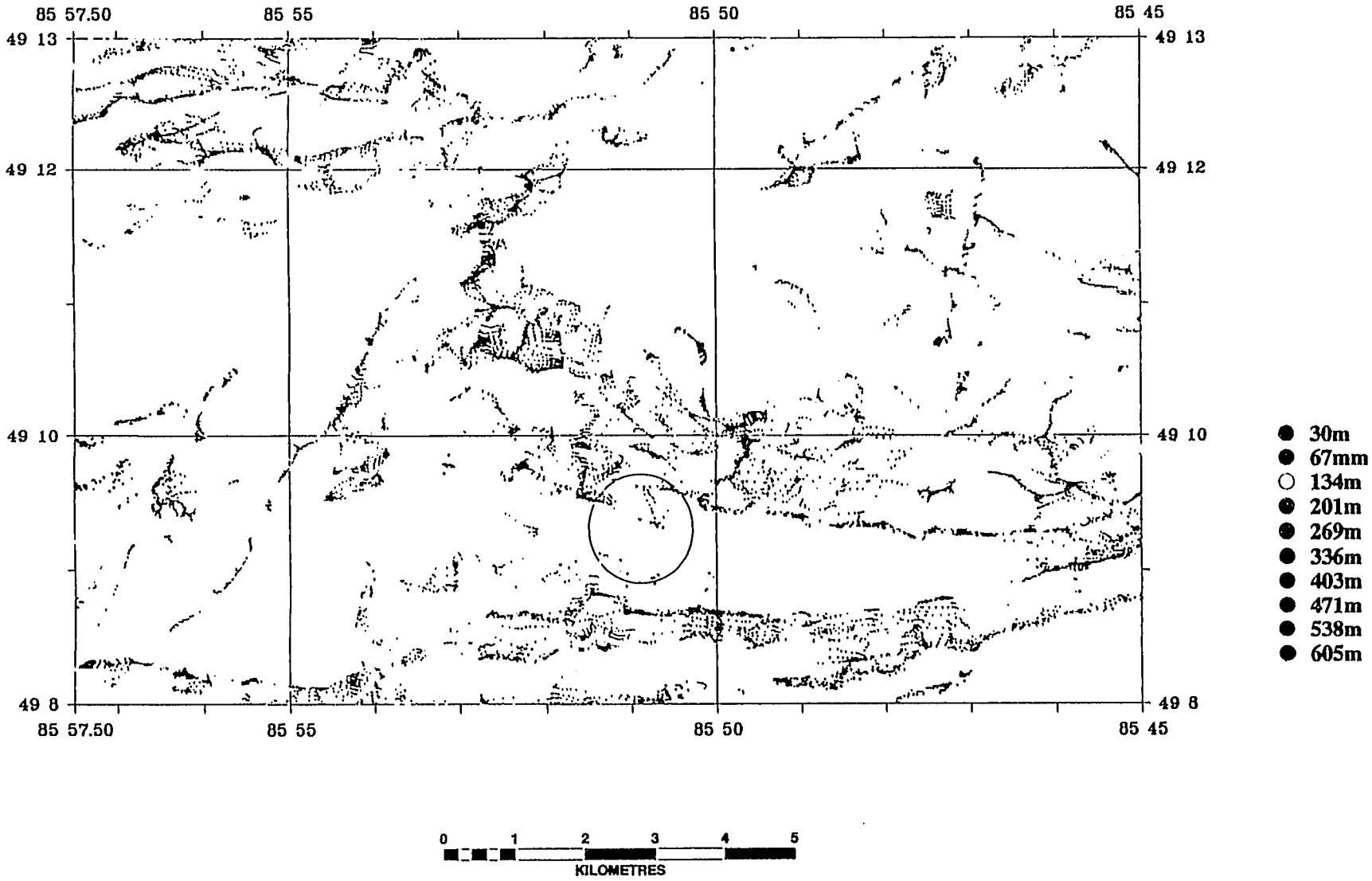

Fig. 5.8.2. Euler depth solutions colour keyed to estimated depths.

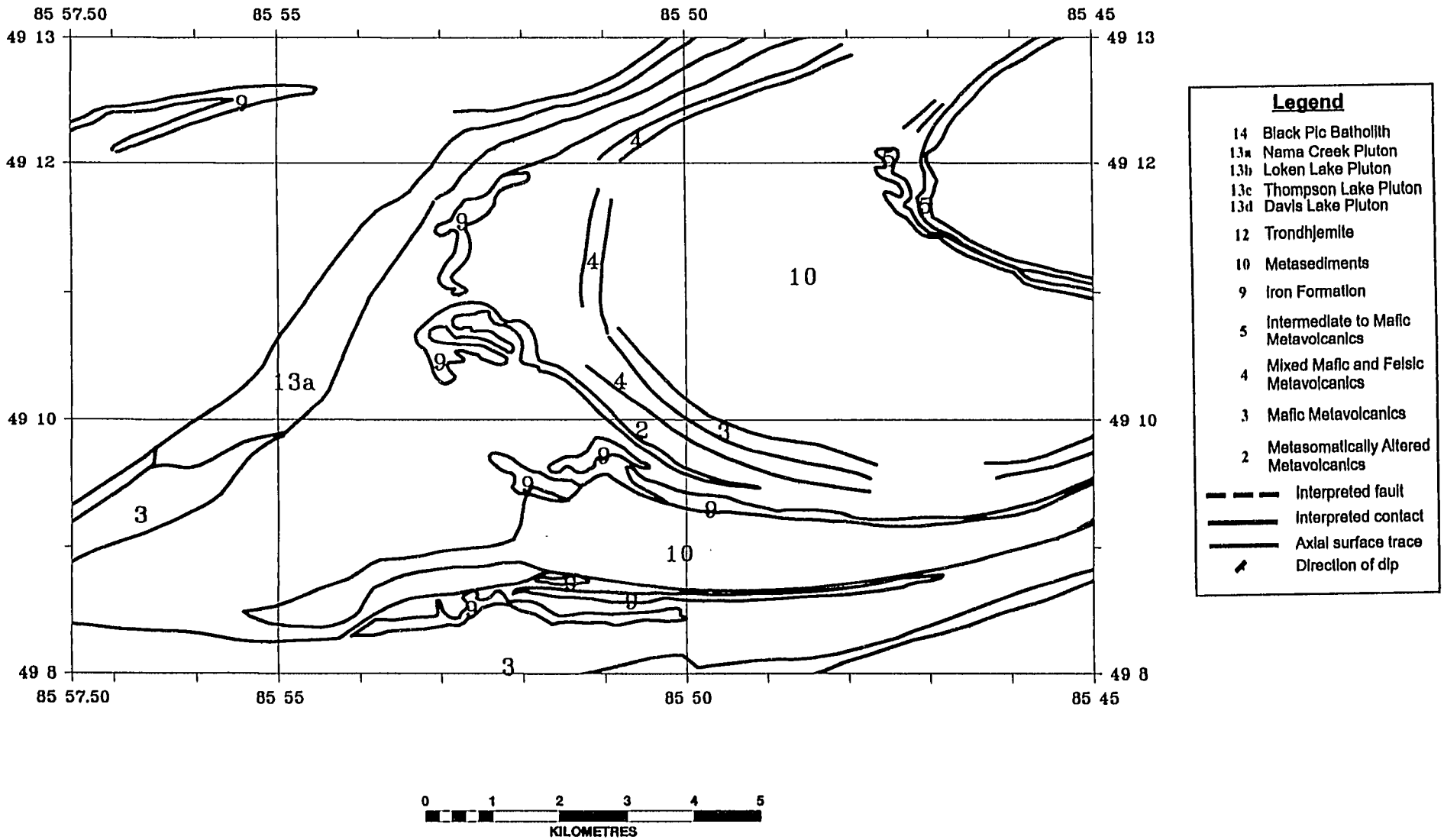

Fig. 5.8.3. Magnetic Interpretation. Unit numbers (in red) following Zaleski et al. (1995).

at depth. The contacts of the iron formation, interpreted from the above discussion, are presented in Figure 5.8.3.

The iron formation of the inner volcanic belt appear discontinuous yet folded by the D_3 Manitouwadge synform. The discontinuous, curving patterns suggest a complex pre-D_3 deformational history.

5.2.2 FELSIC METAVOLCANICS (UNITS 6, 7 AND 8)

The felsic metavolcanic units as mapped by Zaleski et al. (1995), units 6, 7 and 8, are limited to the hinge zone of the Manitouwadge synform (see Map 1). Their low susceptibility make them difficult to distinguish magnetically from local metasediments, mafic metavolcanics and the Nama Creek pluton. The lack of high magnetic gradients between these units obviates the use of AS and HGPG maxima to define their contacts. The measured susceptibilities available for these rocks are in the same range as the metasedimentary rocks of the hinge zone. The apparent susceptibility map (Fig. 5.8.1) does indicate they occupy an area with slightly higher susceptibility values than the metasediments, but the differences are gradational, not sharp. As a result, contacts of the felsic volcanics were not interpreted. The extent of felsic to intermediate volcanics (unit 6) as mapped by Zaleski et al. (1995) corresponds to an area of apparent susceptibility higher than metasediments to the southeast and lower apparent susceptibiltiy than the Nama Creek pluton to the west and northwest (Figs. 5.8.1 and 5.8.2). Where the felsic metavolcanics enclose magnetic iron formation, the apparent susceptibility is quite low and is an artifact of the extreme magnetic intensity of the iron formation.

5.2.3 METASOMATICALLY ALTERED METAVOLCANICS (UNIT 2)

Orthoamphibole-garnet ± cordierite gneiss is strongly associated with the known VMS deposits and is interpreted by Zaleski et al. (1995) to represent felsic and mafic volcanics metasomatically altered by the synvolcanic trondhjemite. Outcrops of this unit are mapped within the inner volcanic belt of the Manitouwadge synform and within trondhjemite east of the Loken Lake pluton (see Map 1).

The measured susceptibility of the unit from three samples within the inner volcanic belt are 0.4, 2.4 and 12.5 x 10^{-3} SI. The unit has an apparent susceptibility ranging from 5.0 to 10.0 x 10^{-3} SI on the northern limb of the Manitouwadge synform, where it is in contact with felsic metavolcanics, to -3.0 to -5.0 x 10^{-3} SI on the southern limb where it is close to magnetic iron formation (Figs. 5.8.1 and 5.8.3). The lower values may be the result of superposition of a negative part of the magnetic anomaly due to the intense magnetic high of the iron formation. The unit occupies a nondescript magnetic low between linear magnetic highs defining the iron formation and mixed mafic and felsic metavolcanics folded about the synform (Fig. 5.8.1 and Fig. 5.8.3). The magnetic low associated with the metasomatically altered unit pinches out on the southern limb at Wowun Lake. Zaleski et al. (1995) map the unit as thinning and continuing on to the eastern edge of the map sheet. If this is so, and only one outcrop near Wowun Lake suggests this continuation, the magnetic susceptibility of the altered rock increases dramatically at that point. A linear magnetic high does generally follow the geologically mapped unit.

East of the Loken Lake pluton, within the trondhjemite, units of the altered rock correspond to second vertical derivative highs, although the units are hard to trace due to their limited apparent thickness and that parts of the folded unit are parallel to local magnetic survey flight

lines. Two measured susceptibilities for the unit in this area are only 2.9 and 4.5 x 10^{-3} SI, although apparent susceptibilities range to 20 x 10^{-3} SI, although it is quite variable.

5.2.4 LOKEN LAKE, NAMA CREEK AND OTHER RELATED GRANITOIDS (UNIT 13)

Granitoids within a granite-greenstone terrain can be differentiated from other lithologies by their relatively low magnetic signature and lack of primary internal aeromagnetic anomalies (Jaques et al, 1997). The generalization of granitoids as having low magnetic susceptibility is subject to modification depending on the nature of the intrusions. Magnetite-series or I-type granites can have a high magnetic susceptibility. While volcanic rocks may have similar low magnetic susceptibility, they tend to contain linear anomalies parallel to their contacts representing units of highly magnetized mafic and ultramafic rock and iron formation. Anomalies within granitoids tend to represent post-emplacement dykes and faults as well as included country rock and xenoliths..

The Loken Lake pluton (Fig. 5.9.3, unit 13b) is bisected by the axial trace of the Manitouwadge synform and extends from Dead Lake in the west to Banana Lake in the east (see Map 1). As most of the pluton is poorly exposed, the contacts of the pluton, as mapped by Zaleski (1995), were largely inferred from a preliminary interpretation of the total magnetic field.

Measured magnetic susceptibilities of the Loken Lake pluton are limited to eight samples, but show a consistently low value, averaging 0.8 x 10^{-3} SI. These samples are concentrated in the western end of the pluton, but one sample taken at the eastern end, south of Thompson Lake, has a measured susceptibility of 0.025 x 10^{-3} SI. The apparent susceptibility of the pluton averages about 2 x 10^{-3} SI, with lower values in the west and south and higher values to the east (Fig.

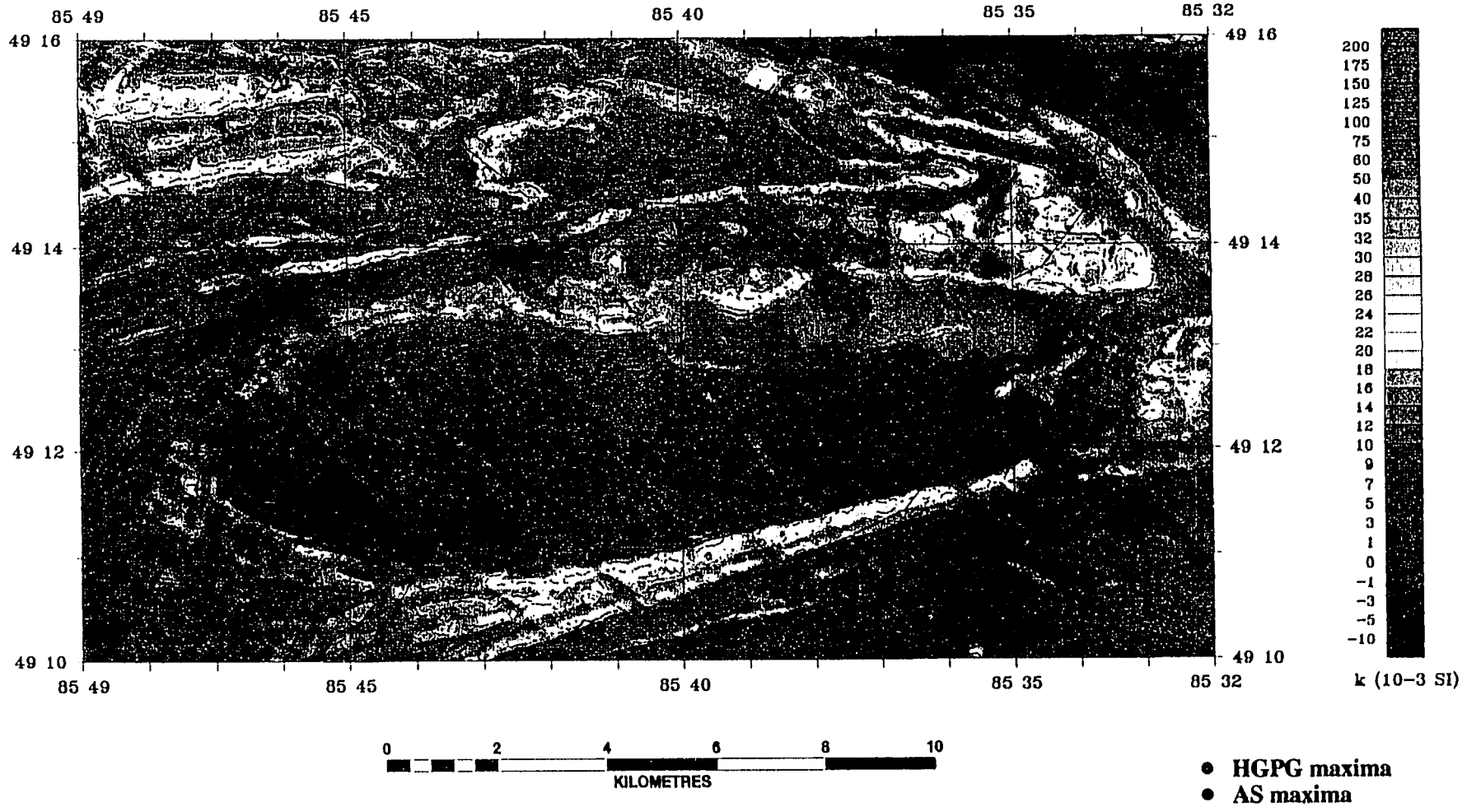

Fig. 5.9.1. Apparent susceptibility and AS and HGPG maxima over granitoids.

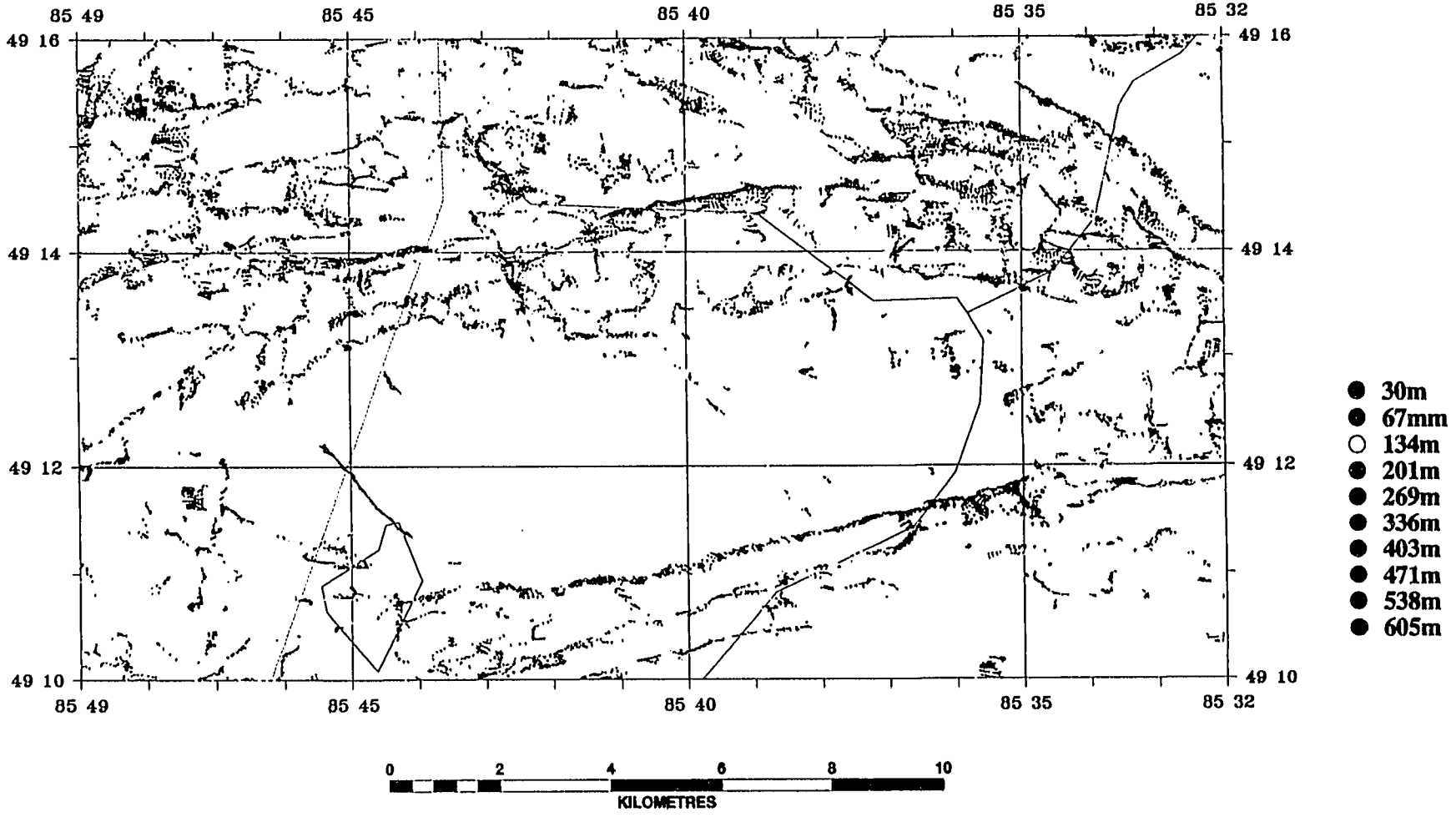

Fig. 5.9.2. Euler depth solutions colour keyed to estimated depths.

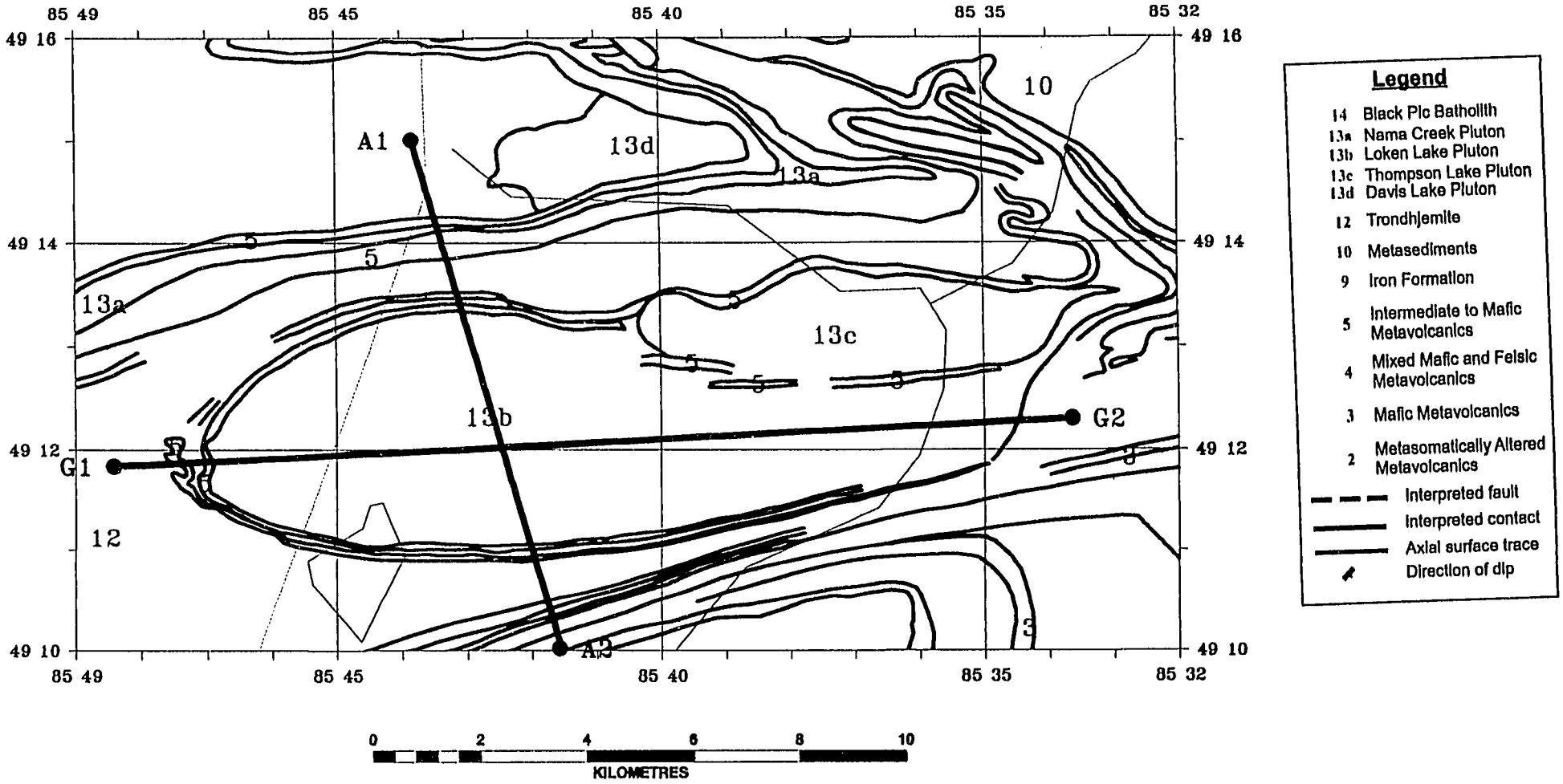

Fig. 5.9.3. Magnetic Interpretation. Unit numbers (in red) following Zaleski et al. (1995). Blue lines represent model profiles.

5.9.1). This difference represents the variations in the intensity of the magnetic field over the pluton due to variations in its thickness as modelled in a previous section on interpreted faults. The higher values represent the additional contribution to the signal by underlying trondhjemite and Dead Lake suite metavolcanics. The apparent susceptibility map shows eastward step-wise increases across the faults more clearly than the residual total field map (Fig. 5.9.1).

The combined AS and HGPG maxima map outlines sharp, northwest trending linear anomalies corresponding to Matachewan dykes and less well defined northeast trending anomalies corresponding to Biscotasing and possible Marathon dykes (see arrow, Fig. 5.9.1). An east-west trending anomaly (an apparent susceptibility local high) represents a mapped unit of mafic volcanics. The remaining features are short, randomly oriented anomalies within the pluton and may represent anomalies within the underlying rock. The western and southern contacts of the pluton are well defined but the eastern and northeastern contacts, as mapped by Zaleski (1995) are problematic. The pluton is mapped as surrounded by trondhjemite, however, there is an elliptical area northeast of the pluton that appears to have a significantly different magnetic signature. This area has an average apparent susceptibility similar to the trondhjemite, but a much smoother appearance (Fig. 5.9.1). The AS and HGPG maxima define fewer magnetization contrasts over this area than over a similar sized area of the trondhjemite. The limit of the Loken Lake pluton must be redrawn to reflect this interpretation. This area is interpreted to represent another granitoid intrusion (tentatively named the Thompson Lake pluton, Figure 5.9.3., Unit 13c). The northern limit of the Loken Lake pluton has been placed by Zaleski (1995) to coincide with the east-west trending metavolcanic unit. A 2.5D model profile trending to the northwest (profile A, Fig. 5.10, see Figure 5.9.3 for profile location)

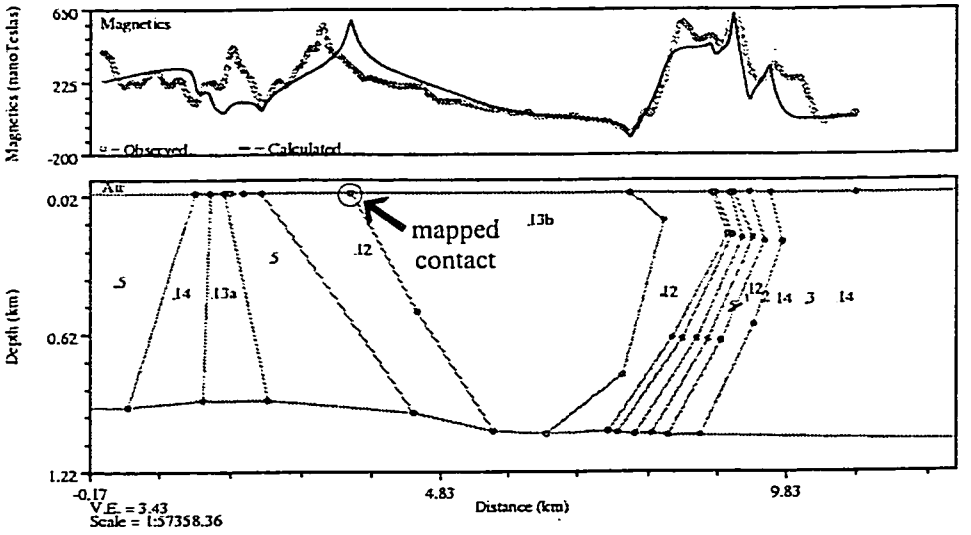

(a)

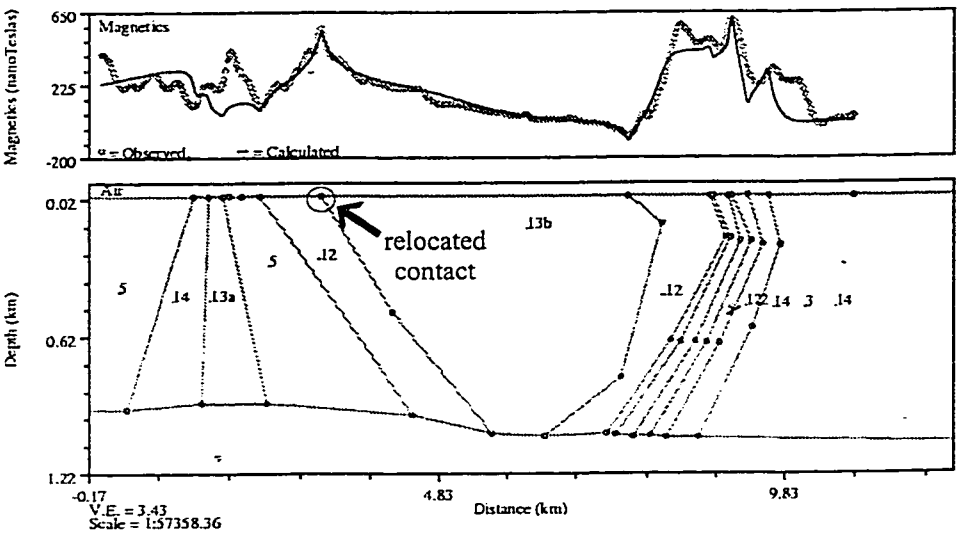

(b)

Fig. 5.10. Magnetic profile A bearing southeast across the western end of the Loken Lake pluton. a) Contacts as mapped by Zaleski et al. (1995), b) with relocated northern contact between Loken Lake pluton and trondhjemite unit.

indicates the contact with the trondhjemite unit should be 400m to the northwest. Euler deconvolution depth solutions within the Loken Lake pluton (Fig. 5.9.2) are limited to a series of near surface, northwest trending lines of solutions representing the Matachewan dykes. The lack of other solutions is due to low magnetic gradients and the fact that the method cannot resolve depths greater than twice the window size (maximum depth of the solutions presented is 800m). The contact with the trondhjemite unit is well defined by depth solution locations. The contact with the Thompson Lake pluton is not similarly defined by depth solution locations, but the two plutons can be differentiated on the basis of the presence of solutions within the Thompson Lake pluton.

The Thompson Lake pluton (unit 13c) is not exposed. The apparent susceptibility over the pluton ranges from less than 10 x 10^{-3} SI at its western end to greater than 16 x 10^{-3} SI toward its eastern extent (Fig. 5.9.1). This is similar to the increasing apparent susceptibility trend within the Loken Lake pluton, although without obvious stepping of values across faults. It may represent a thinning of the pluton to the east.

The Thompson Lake pluton can be differentiated from the Loken Lake pluton based on its higher magnetic intensity, higher apparent susceptibility, density of AS and HGPG maxima (Fig. 5.9.1), and the presence of Euler depth solutions (Fig. 5.9.2), although the latter may be due to differences in pluton thickness and the limited effective depth resolution of the method. The contact between the two plutons can be defined by the linear arrangement of AS and HGPG maxima subparallel to the mapped unit of mafic volcanics used by Zaleski (1995) to mark the contact between the northeastern end of the Loken Lake pluton and the trondhjemite. The contact at the western end of the Thompson Lake pluton may be structurally controlled by a fault

subparallel to a Matachewan dyke (Fig. 5.9.3).

The Thompson Lake pluton can be differentiated from the trondhjemite unit by its smoother total field magnetic intensity anomaly pattern, smoother apparent susceptibility, the absence of Euler depth solutions less than 200m (Fig. 5.9.2) and its lower density of AS and HGPG maxima (Fig. 5.9.1). The contact between the two units is defined by curvilinear arrangement of near surface Euler depth solutions coincident with continuous curvilinear arrangements of AG and HGPG maxima (Fig. 5.9.3).

South of Davis Lake, east of Fox Lake and bisected by the axial trace of the Blackman Lake antiform is an area with a magnetic signature similar to the Loken Lake pluton (Fig. 5.9.3, unit 13d). The area is roughly elliptical in outline and has a low, flat magnetic field, relative to surrounding areas. The magnetic intensity of the unit is higher in the north and lower in the south. Its flat signature is in contrast to the signature of the Black Pic batholith north of the Manitouwadge synform's axial trace, which is dominated by east-west trending magnetic lineaments. No measured susceptibilities are available. The apparent susceptibility is low and very similar in magnitude and map pattern to the Loken Lake pluton's apparent susceptibility (Fig. 5.9.1). The AS and HGPG maxima (Fig. 5.9.1) show a fairly strong east-west trending magnetization contrast following the axial trace. Euler depth solutions within the area are generally greater than 300m, while surrounding areas and contacts have depth solutions on generally shallower than 200m (Fig. 5.9.2). If this area is interpreted as a granitoid intrusion, the presence of the AS and HGPG maxima defined contrast may be explained as a feature in underlying rock or included mafic supracrustal material. Given the limited size of the area, the interpretation is far from conclusive. However, the area is also similar to the Loken Lake pluton

in that it is surrounded by a high susceptibility, highly variable intensity material (possibly trondhjemite). Both plutons are bisected by a D_3 axial trace, are sub-elliptical and pinch to the east. To the west of the suspected pluton is the nose of a fold that is contrary to the Blackman Lake antiform. This has local and regional structural implications, as well as presenting a possible exploration target. Within the Manitouwadge synform, west of the Loken Lake pluton, the trondhjemite unit is considered by Zaleski et al.(1995) to be the heat engine for VMS deposits.

For the sake of easier reference, the possible pluton is very tentatively named the Davis Lake pluton (unit 13d). It is defined by fairly continuous AS and HGPG maxima and its low apparent susceptibility. The western end of the 'pluton' appears folded and also coincides with a northwest trending fault. The eastern end pinches into the nose of the Blackman Lake antiform and may also coincide with a northwest trending fault (Fig. 5.9.3).

The Nama Creek pluton is similar in composition to the Loken Lake pluton, but more melanocratic with up to 35% hornblende and biotite. Zaleski et al. (1995) mapped the unit as a long sinuous body between the Black Pic batholith and the supracrustal rocks of the northern limb of the Manitouwadge synform, folded about the Blackman Lake antiform and present on the southern limb of the Jim Lake antiform. West of the Cadawaja fault, the mapped unit coincides with a fairly flat, low magnetic field with the southeastern contact marked by a sharp linear high (representing a wide Biscotasing dyke) and the northwestern contact on the northwestern side of a linear magnetic high. This relationship is best seen in the first vertical derivative of the field (Fig. 5.11.1). East of the Cadawaja fault, the mapped unit coincides again with a magnetic low and the contacts are defined both north and south of unit by linear magnetic

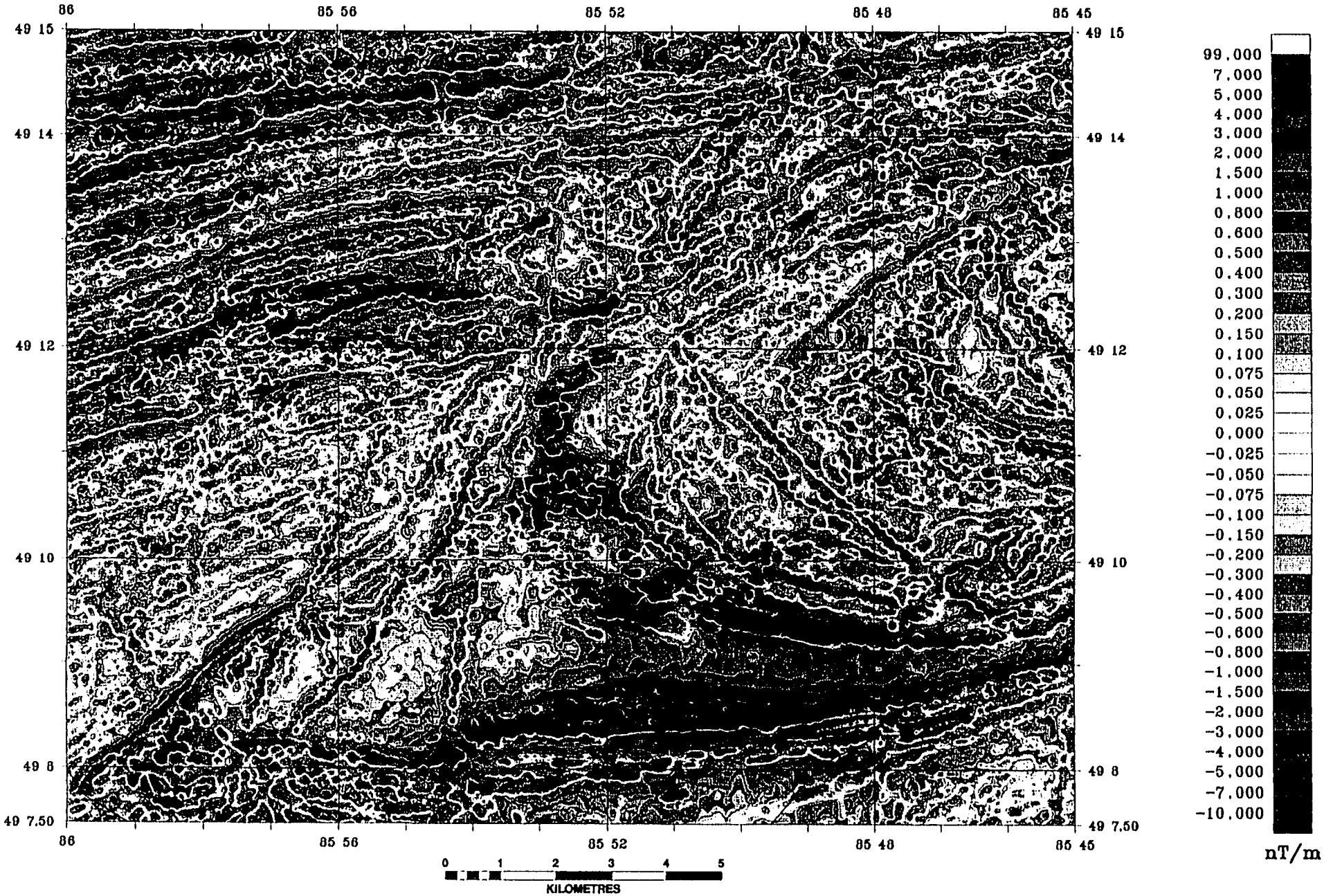

Fig. 5.11.1. First vertical derivative, western Nama Creek pluton.

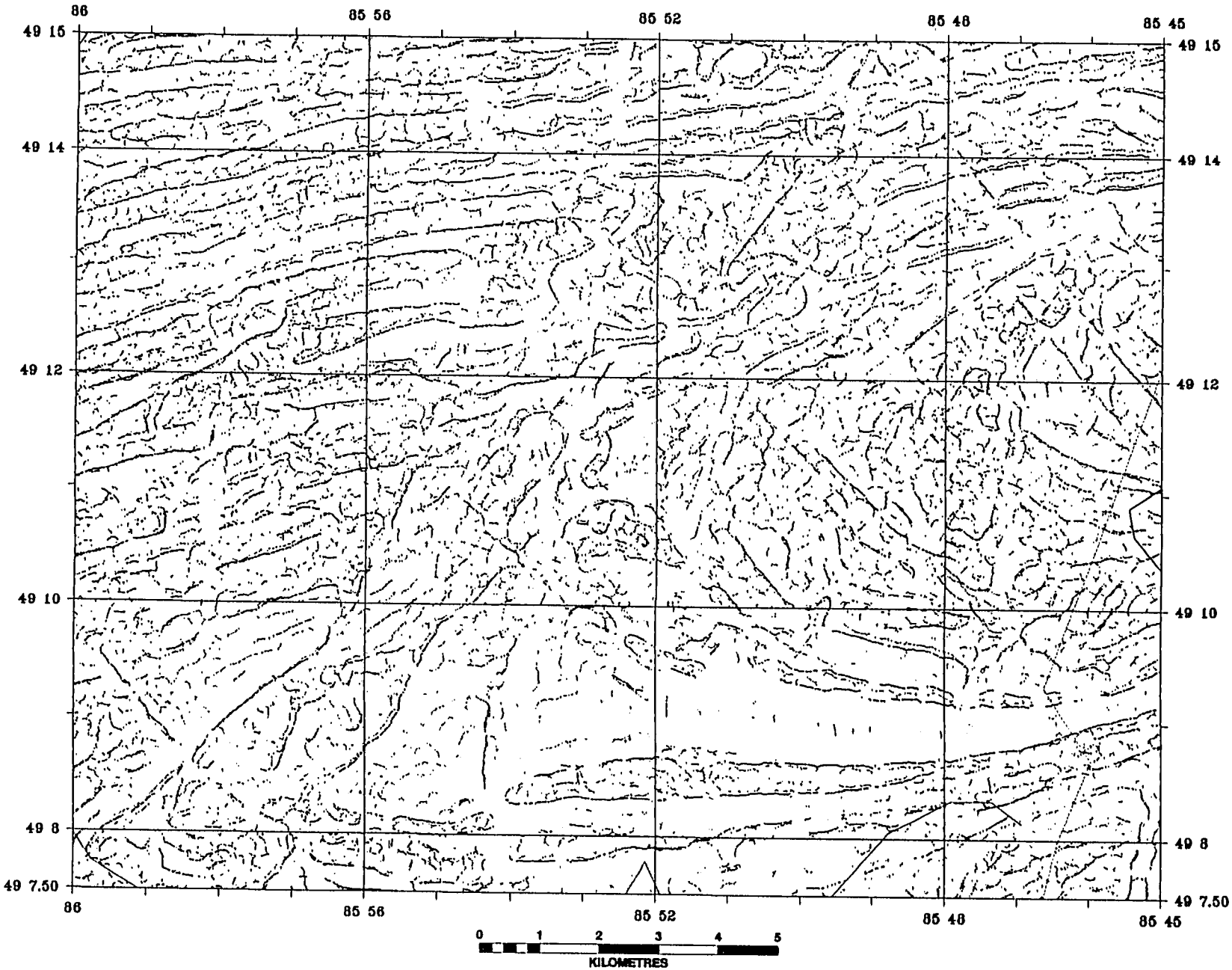

Fig. 5.11.2. AS and HGPG Maxima, western Nama Creek pluton.

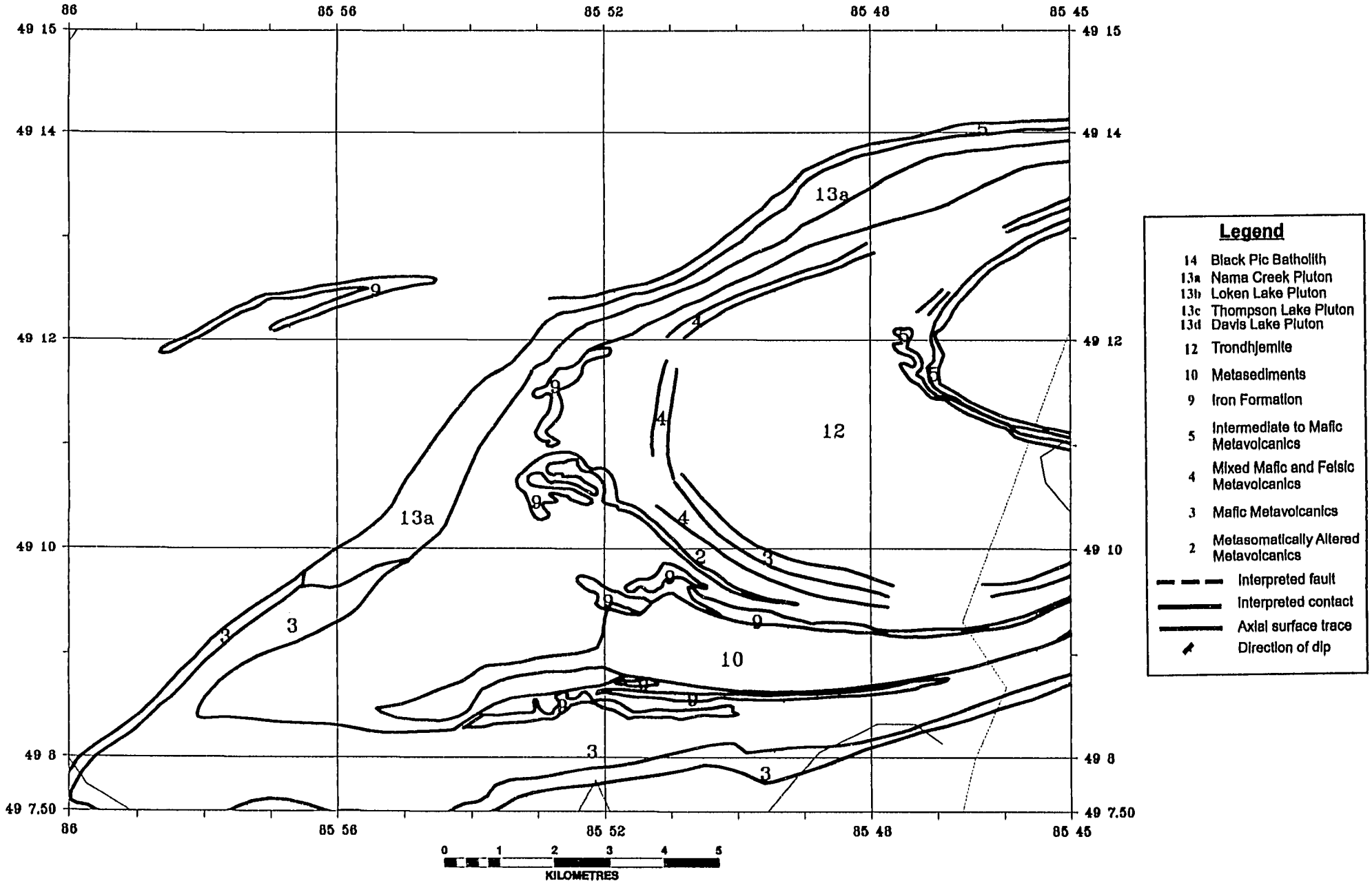

Fig. 5.11.3. Magnetic interpretation, western Nama Creek pluton.

highs.

Measured susceptibilities are again limited. Four values from samples taken within the outer volcanic zone, west of the Cadawaja fault average about 2.9 x 10^{-3} SI. Only one sample east of the Cadawaja fault is available. It is due south of Larry Lake (see Map 1) and has a measured susceptibility of 9.8 x 10^{-3} SI. This may be an anomalously high value, as hornblende and biotite are variable in abundance in this pluton. The apparent susceptibility is generally low and somewhat variable, ranging from 0.0 to 7.0 x 10^{-3} SI, with the exception of the area of the linear magnetic high southeast of the unit's contact with the Black Pic batholith west of the Cadawaja fault (Fig. 5.11.3 and Fig. 5.11.1).

The Nama Creek pluton can be mapped as a magnetic low sandwiched between two linear magnetic highs. Certainly the measured susceptibilities correspond to the magnetic lows and the source of the linear highs would appear to be due to other units, except west of the Cadawaja fault where the northwestern high appears within the mapped unit. A mafic metavolcanic unit outcrops along the northern boundary of the Nama Creek pluton east and west of Fox Lake (see arrow 'A', Fig. 5.12.1). This unit coincides with a vertical derivative high where it is not cut by northwest trending faults or under Fox Lake. This unit may be more extensive than originally mapped or only locally a geologically mappable unit.

Using the AS and HGPG maxima (Fig. 5.11.2) and vertical derivative map (Fig. 5.11.1) to mark the contacts of the apparent susceptibility low, the Nama Creek pluton can be mapped magnetically in agreement with the mapped geology (Fig. 5.11.3). West of the Cadawaja fault, a magnetic low between two linear highs, similar to the Nama Creek pluton signature, appears to be a sinistrally offset continuation of the pluton. However, the vertical derivative map (Fig.

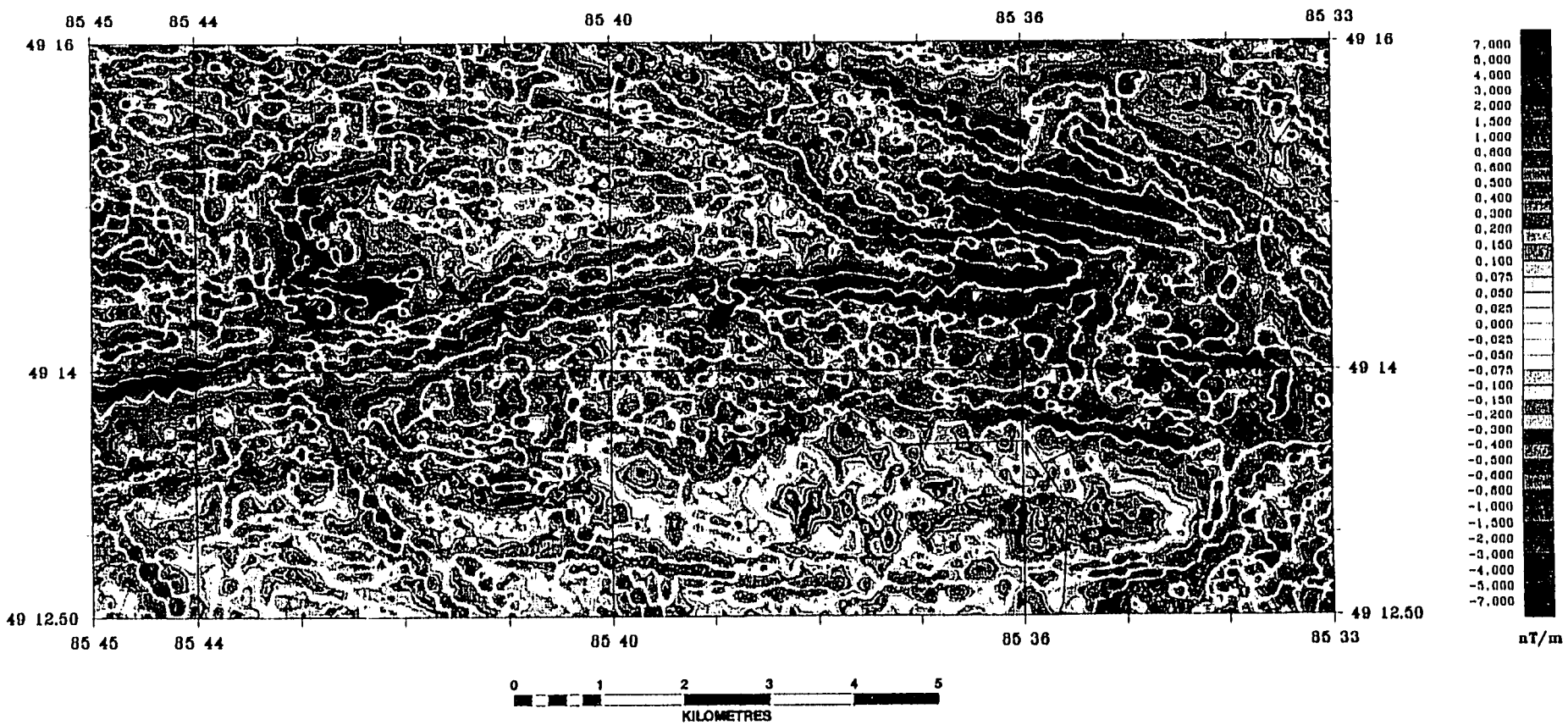

Fig. 5.12.1. First vertical derivative, eastern Nama Creek pluton.

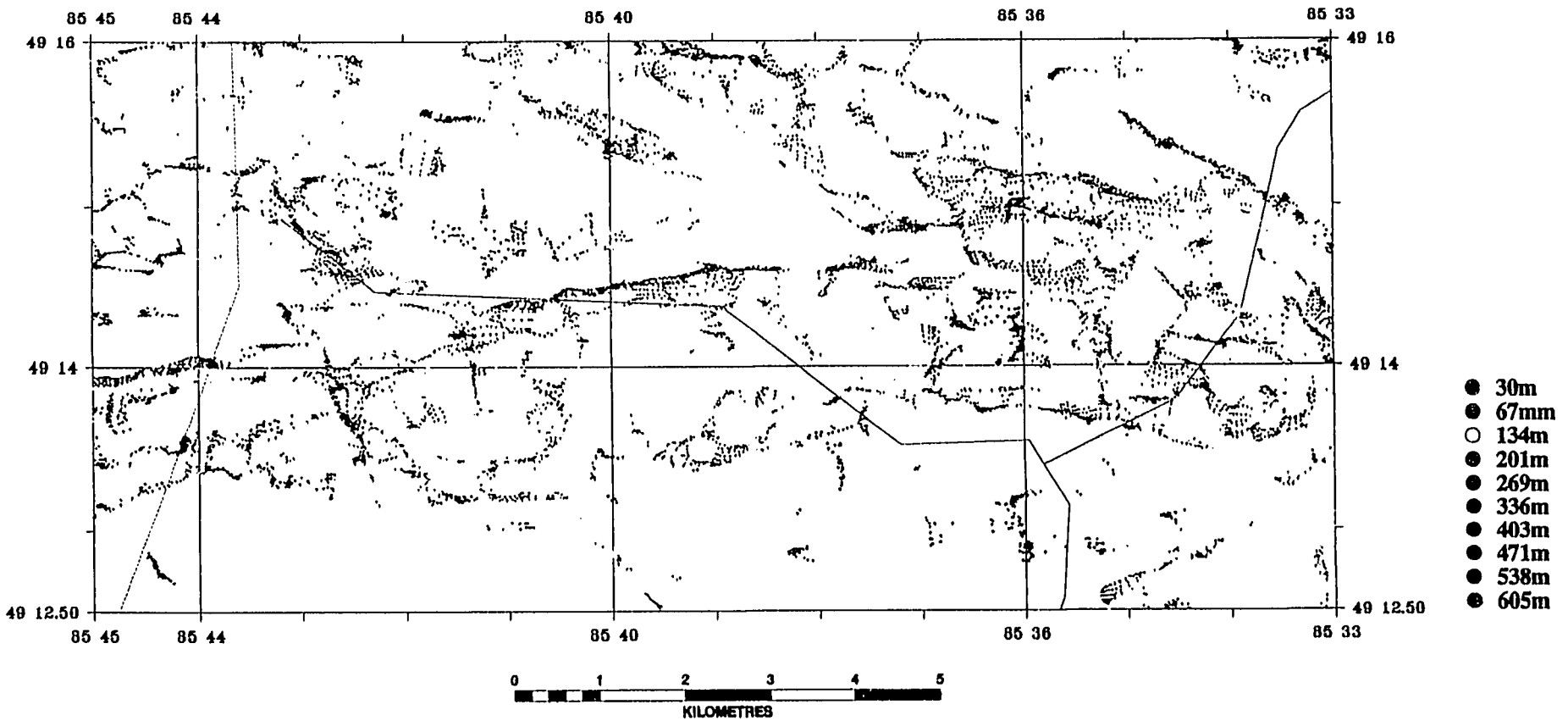

Fig. 5.12.2. Euler depth solutions colour keyed to estimated depth, eastern Nama Creek pluton.

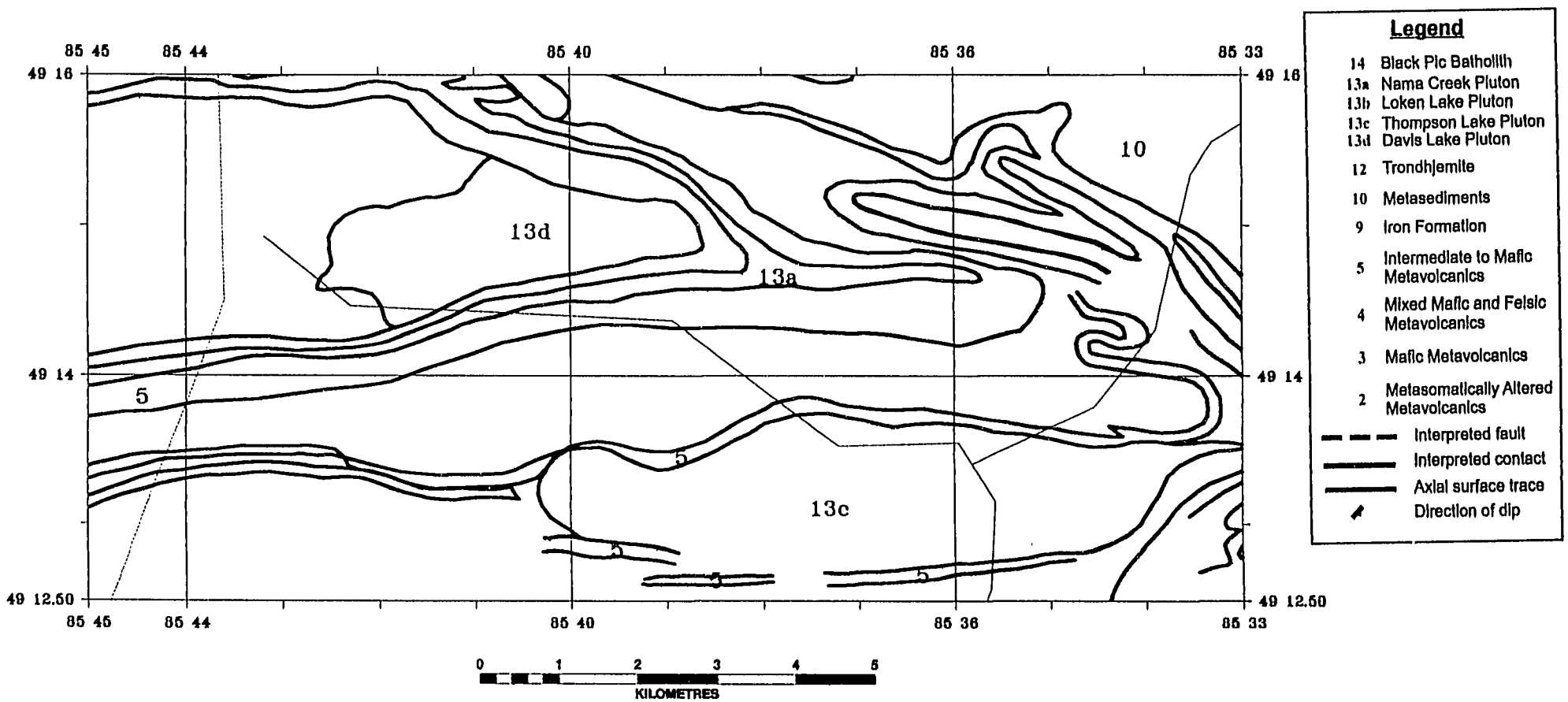

Fig. 5.12.3. Magnetic interpretation, eastern Nama Creek pluton.

5.11.1) shows the low (arrow 'A', Fig. 5.11.1) to have a more continuous, smoother pattern than the pluton (arrow 'B', Fig. 5.11.1). To the east, south of Larry Lake, the unit is intercepted by an interpreted northwest trending fault. Here the magnetic signature (arrow 'B', Fig.5.12.1 and Fig. 5.12.3) is at odds with the mapped geology. Across the fault, the northern bounding linear high disappears and the mapped Nama Creek pluton is drawn over a magnetic linear high traversing the nose of the Blackman Lake antiform. Although the detailed geometry of the fold is beyond the resolution of the data and the strike of the rock is rotating to parallel the flight lines, it seems incongruous that the linear high is not folded like the mapped contacts. The linear high cannot be an included unit within the pluton and is either a later feature (Proterozoic dyke?) or an alternate explanation must be found. Any resolution to this problem must take into account the limited resolution of the data, the attenuation of magnetic intensity over the local lakes and the vertical displacement across the northwest trending faults.

The linear highs that bound the magnetic low associated with the Nama Creek pluton are well represented by near surface Euler depth solutions (Fig. 5.12.2). There are very few solutions within the magnetic low itself. Conversely, the area mapped by Zaleski et al. (1995) in the nose of the Blackman Lake antiform south of the axial trace (discussed as a problematic area previously) is peppered with evenly spaced, near surface solutions.

5.2.5 METASEDIMENTARY ROCKS (UNIT 10)

The metasedimentary rocks of the Manitouwadge greenstone belt are mapped by Zaleski et al. (1995) as monotonous metagreywackes and biotite schists and are considered equivalent to Quetico subprovince metasediments, with the exception that the latter have been metamorphosed to a higher metamorphic grade and have undergone migmatization.

The metasediments of the Manitouwadge greenstone belt are mapped in the hinge of the D_2 Manitouwadge syncline along the southern limb of the D_3 Manitouwadge synform. They are bounded to the north by inner volcanic belt rocks, to the south by outer volcanic belt rocks, to the west by a late tonalitic intrusion and the east by a similar intrusion. The contacts are interpreted by Zaleski et al. (1995) as faults or unconformities.

The magnetic intensity over these metasediments is extremely low and flat, indicating they attain considerable thickness. Five measured susceptibilities average less than 0.4×10^{-3} SI. The apparent susceptibility (Fig. 5.13.1) is extremely low (averaging -8.0×10^{-3} SI) and flat, without any internal linear highs. The apparent susceptibility increases gradually to the east. As the measured susceptibilities of samples of the tonalite to the west and east are as low or lower than those of the metasediments, the tonalite may not be homogeneous and/or the thickness of the tonalite is less than the metasediments. The gradual increase in apparent susceptibility may indicate the metasediments shallow to the east.

The combination of AS and HGPG maxima (Fig. 5.13.1), Euler depth solutions and the apparent susceptibility map allow an interpretation of the contacts (Fig. 5.13.3) and varying thickness of the metasediments. First, however, it must be noted that there are AS maxima within the metasediments aligned in a north-south orientation. These are artefacts in the data due to levelling errors or gridding effects. They are parallel to the local flight line direction and should be discounted. The metasediments can be differentiated from the outer volcanic belt and inner volcanic belt units to the south and north, respectively, by their much lower apparent susceptibility and the contact can be defined by the east-west continuous alignment of AS and HGPG maxima. Euler depth solutions indicate that the cause of the diffuse apparent

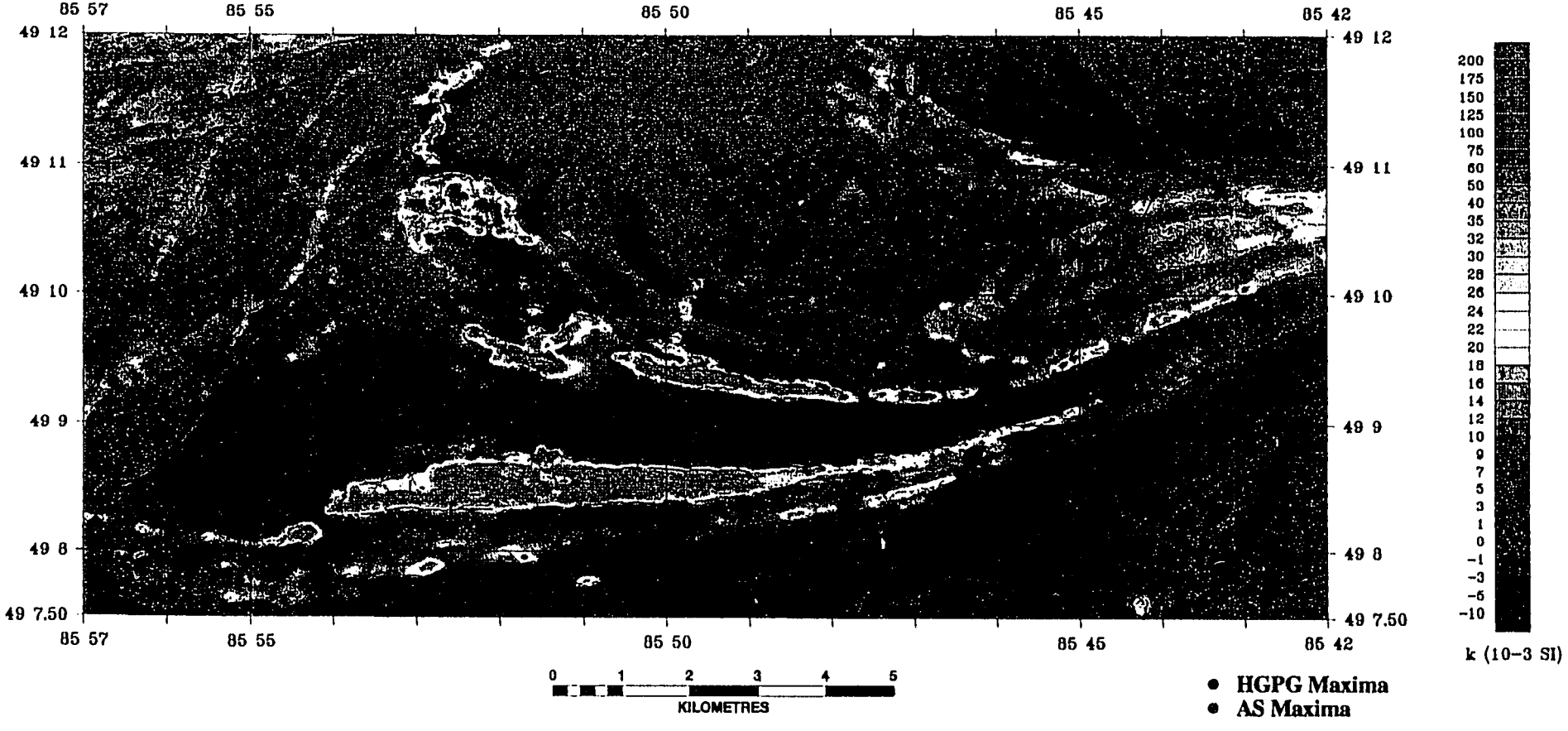

Fig. 5.13.1. Apparent susceptibility with AS and HGPG Maxima, Metasediments.

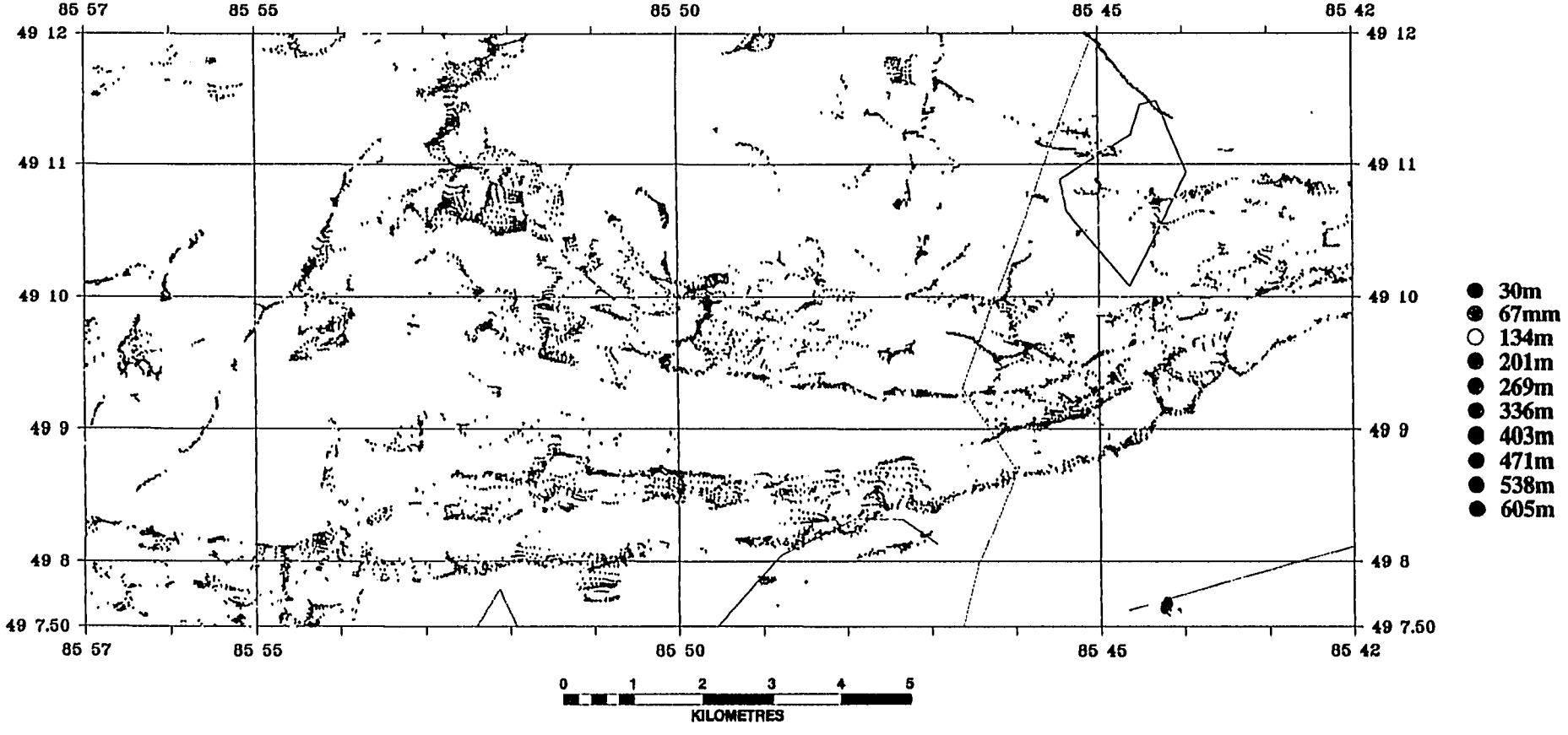

Fig. 5.13.2. Euler depth solutions colour keyed to estimated depths, Metasediments.

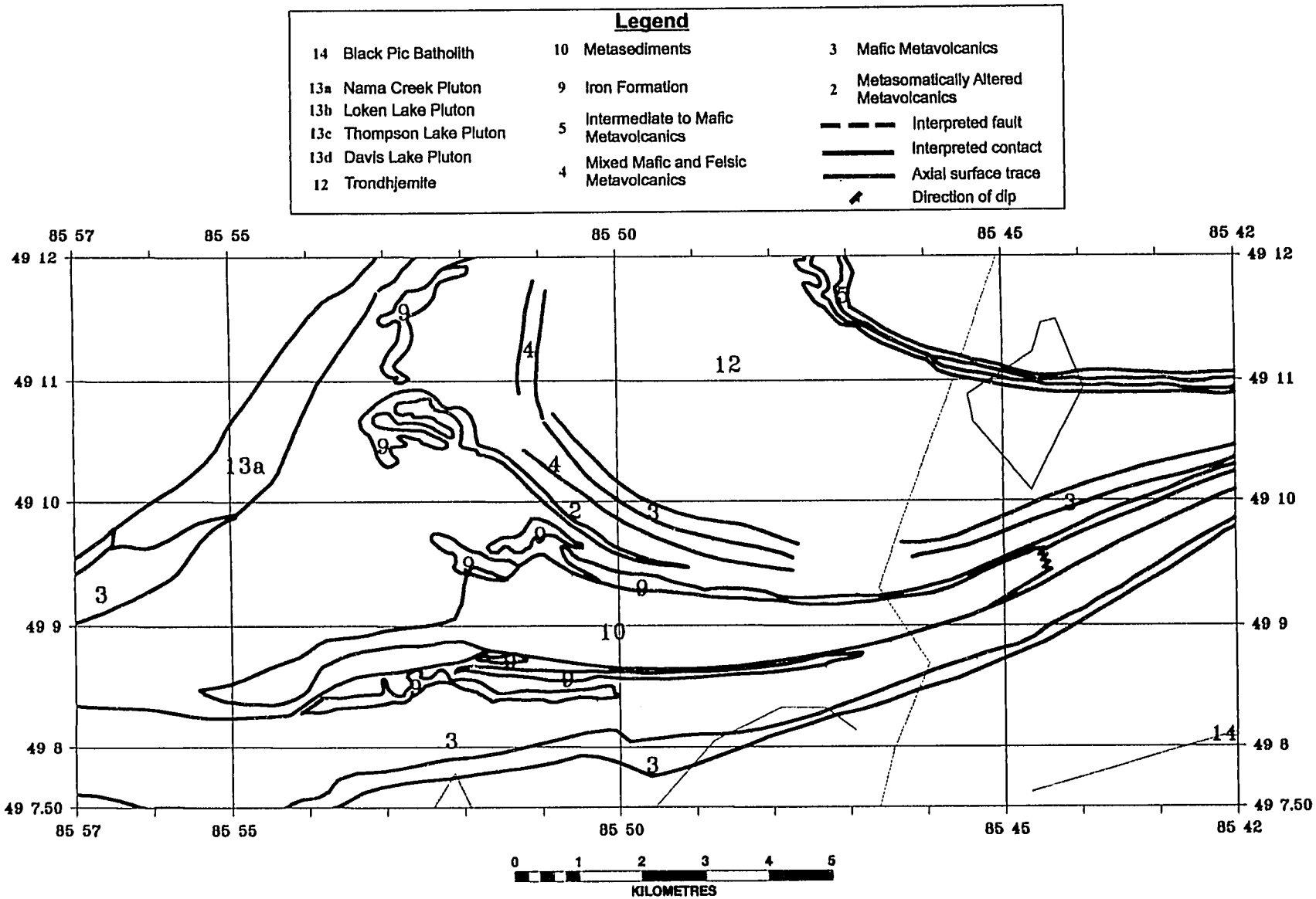

Fig. 5.13.3. Magnetic Interpretation, Metasediments.

susceptibility high 1 km north of Agam Lake is due to magnetic iron formation at depth under the metasediments and the AS and HGPG maxima's abrupt truncations indicate the near surface contact between the metasediments and inner volcanic belt rocks. The appearance of clusters of Euler solutions within the west-bounding tonalite indicates the limit of the metasediments. Due to the lack of sharp magnetic gradients between the metasediments and tonalite, there are no AS and HGPG maxima to mark the contact. However, the metasediments have no real AS maxima while the tonalite has a pattern of short, curvilinear segments of aligned maxima. Near the Mose Lake fault, east of the railroad (dashed red line, Fig.5.13.2), the thinning of the metasediments is signalled by the appearance of Euler solutions. A small, crescentic shaped metasedimentary unit is mapped 1 km east of Cadawaja Lake(see Map 1) and has no discernable magnetic signature. It is elongate parallel the local flight line direction and may have been poorly sampled by the survey. If it has limited depth extent, it may not have a measurable magnetic response.

5.2.6 MIGMATIZED QUETICO METASEDIMENTS WITHIN THE WAWA SUBPROVINCE

The Quetico metasediments are interpreted by Zaleski et al. (1995) to be infolded with Manitouwadge greenstone belt supracrustal rocks south of the Wawa-Quetico subprovince boundary by the D_3 Jim Lake synform. In this area the metasediments are migmatitic biotite schists. The rocks are in a metamorphic transition zone from upper amphibolite to granulite facies.

Seven measured susceptibilities average 0.35 x 10^{-3} SI for the infolded Quetico metasediments. The apparent susceptibility (Fig. 5.14.1) is also low, ranging from -2.0 to -5.0 x 10^{-3} SI.

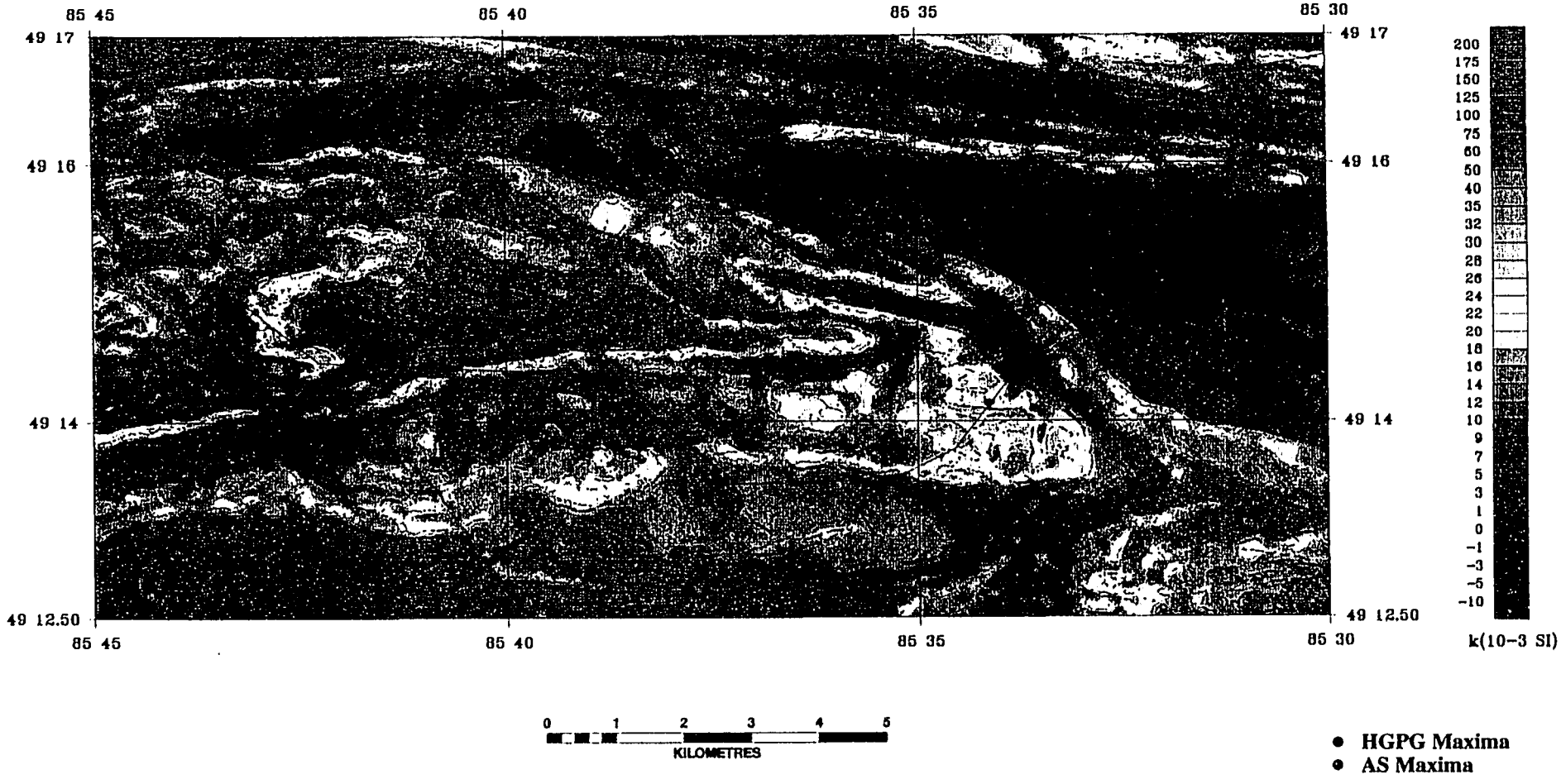

Fig. 5.14.1. Apparent susceptibility with AS and HGPG maxima, Quetico metasediments.

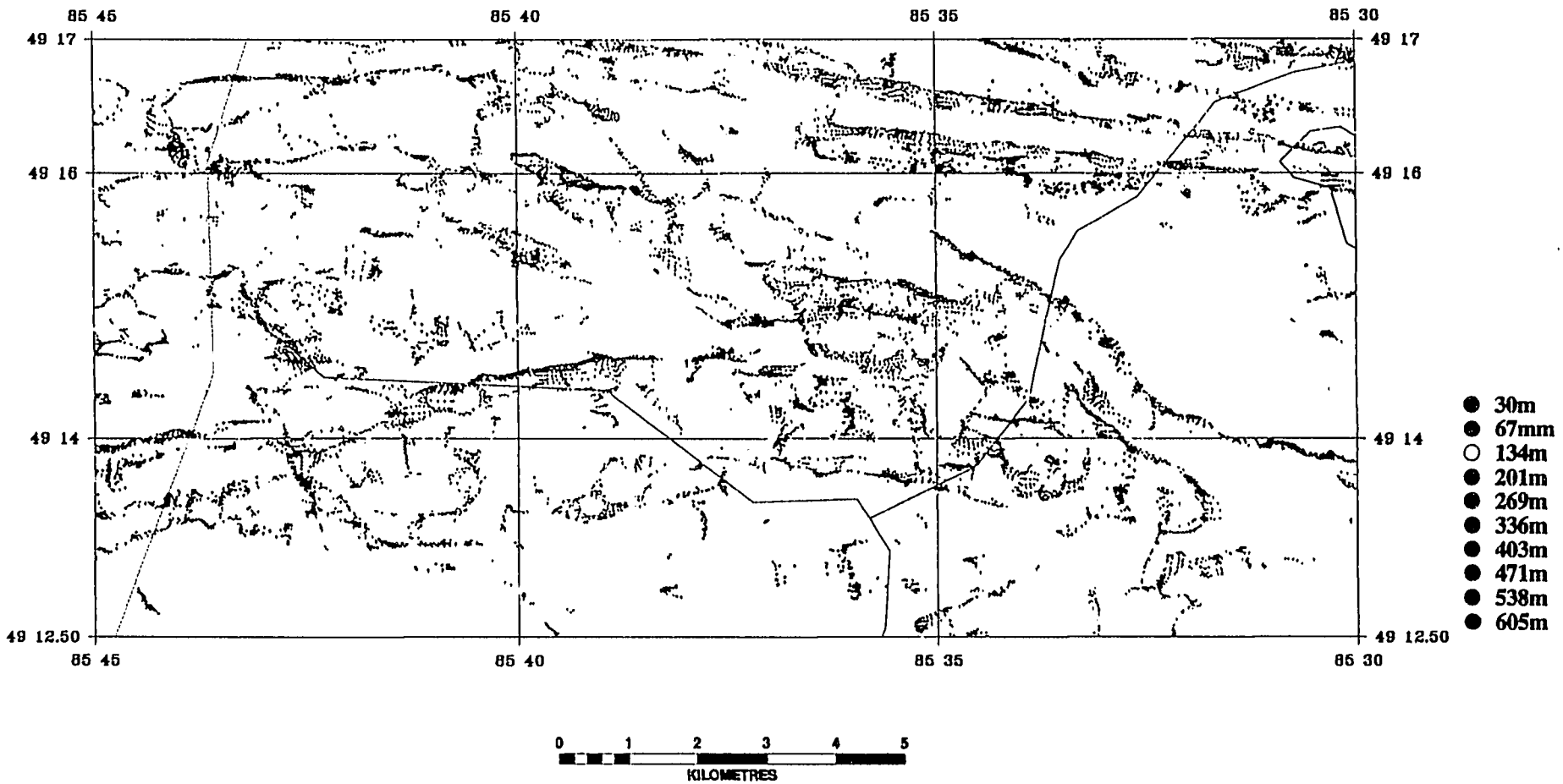

Fig. 5.14.2. Euler depth solutions colour keyed to estimated depth, Quetico metasediments.

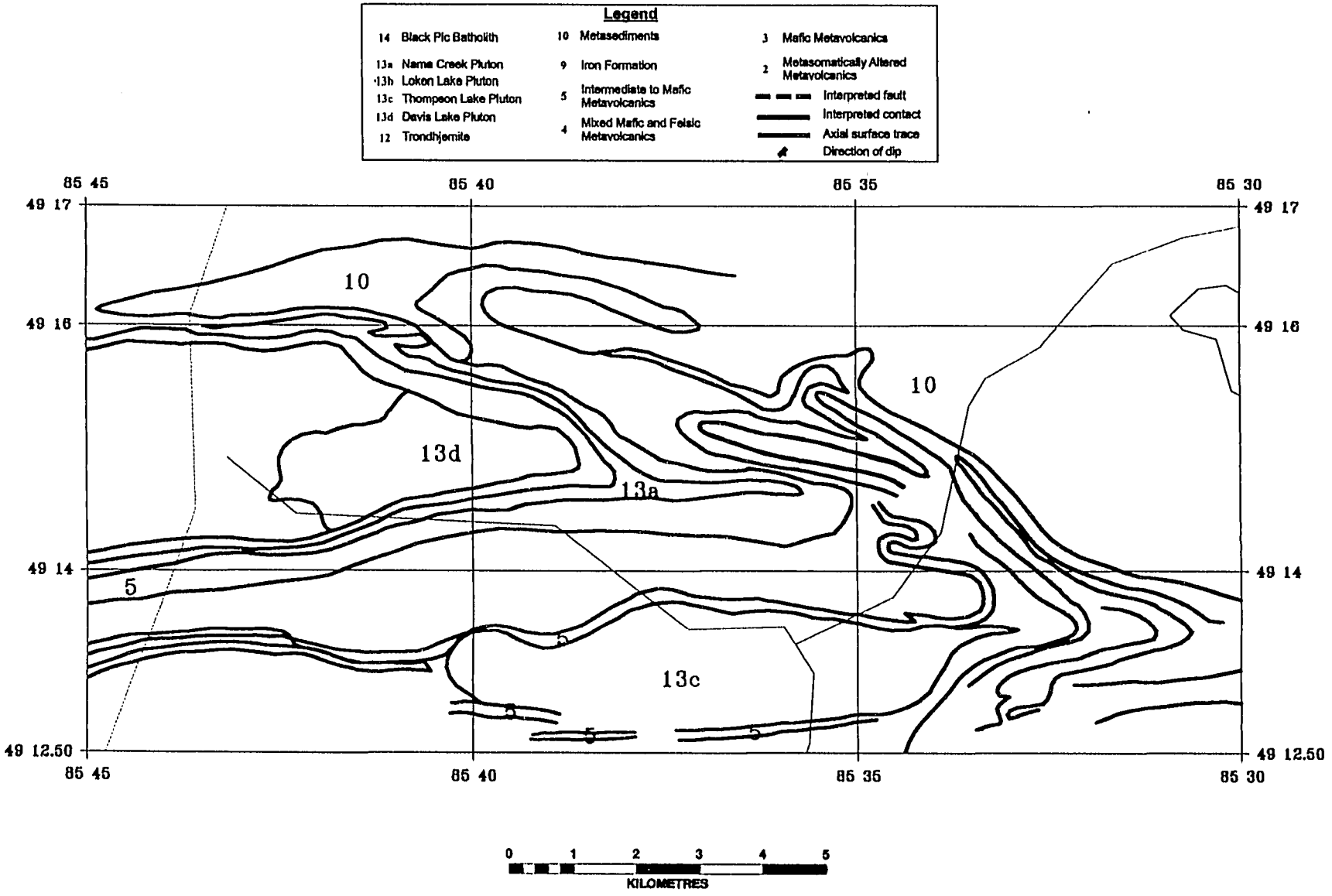

Fig. 5.14.3. Magnetic interpretation, Quetico metasediments.

The mapped areas of metasedimentary rocks are largely free of Euler depth solutions (Fig. 5.14.2). West of W85°35', the mapped area contains only sparse AS and HGPG maxima that may correspond to levelling errors. East of W85°35', the mapped area has short, linear arrangements of both maxima, some corresponding to dykes and some possibly due to inclusions of supracrustal rock. The contacts with mixed mafic and intermediate volcanics and trondhjemite are well delineated by continuous, linear arrangements of both maxima (Fig. 5.14.1).

5.2.7 QUETICO METASEDIMENTARY UNITS NORTH OF WAWA-QUETICO BOUNDARY

The most northern unit mapped by Zaleski et al. (1995) are monotonous, migmatized greywackes and biotite schists within the Quetico subprovince. Zaleski et al. (1995) describe these rocks as metamorphic equivalents to the metasediments within the Manitouwadge greenstone belt. West of Appelle Lake (see Map 1), gabbroic-dioritic sheeted intrusions (Everest Lake pluton) are interlayered with the metasediments.

The metasediments of the Quetico subprovince have measured magnetic susceptibilities ranging from 0.02 x 10^{-3} SI to 38.6 x 10^{-3} SI. For the purpose of this study the magnetic susceptibility of an area of outcrop of interlayered sheeted diorite and Quetico metasediments 1 km north of the western end of Appelle Lake was measured (arrow 'A', Fig. 5.16.1). 48 measurements were taken along a north trending profile of approximately 50m of continuous outcrop of the Quetico metasediments (Fig. 5.15). The measured susceptibility ranges from south to north along the profile from 0.18 x 10^{-3} SI to 28.8 x 10^{-3} SI, with the higher values occurring together along an approximately 10 to 15m segment of the profile. The magnetic

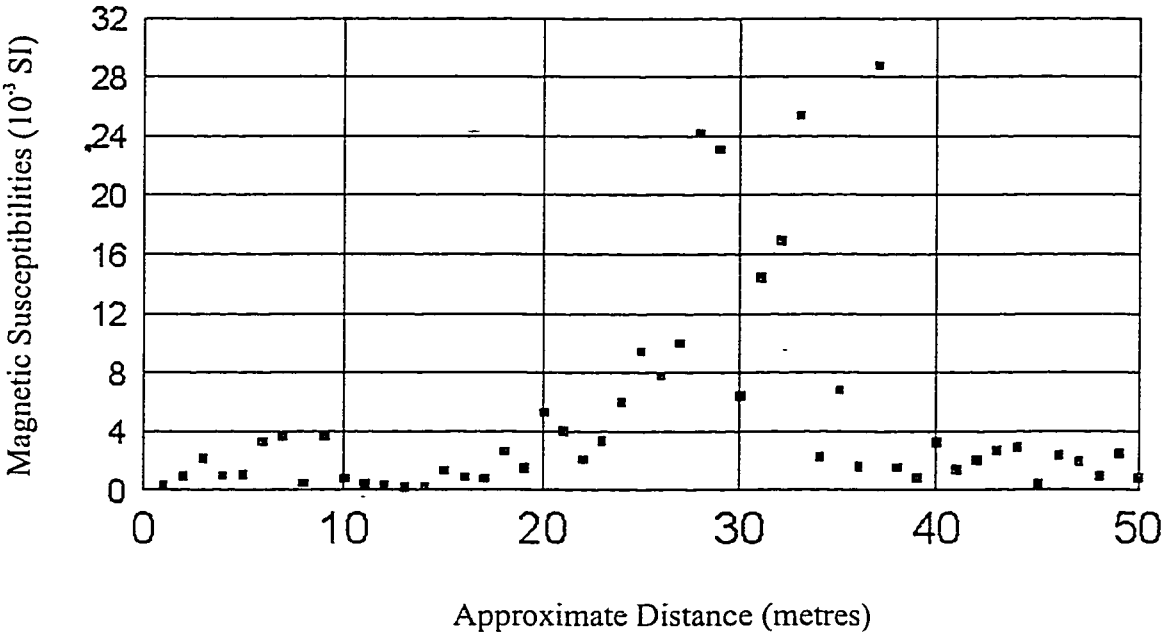

Fig. 5.15.. Measured magnetic susceptibilities across 50m of Quetico metasedimentary rock outcrop, 1km north of the west end of Appelle Lake.

susceptibility of the diorite ranged from 3.94 x 10^{-3} SI to 16.4 x 10^{-3} SI. By way of illustration, the Matchewan dykes that trend northwest across the mapped area have a measured magnetic susceptibility of about 20 x 10^{-3} SI. It would be difficult to distinguish magnetically between the sheets of diorite and the more highly susceptible units of Quetico metasediments. Using the empirical formula for estimating the volume percent of magnetite from magnetic susceptibility, a unit with a susceptibility of 0.5 x 10^{-3} SI has 0.023% magnetite and a unit with a susceptibility of 25.0 x 10^{-3} SI has 0.788 % magnetite. Given that this magnetite may be highly disseminated throughout the unit, the highly susceptible metasediments are not geologically mappable as separate units.

Magnetite development in metasediments is controlled by the bulk composition of the original sediments and the oxidation state of the original sediments given by $Fe^{3+}/Fe^{3+}+Fe^{2+}$ (McIntyre, 1980) and is favoured by higher total iron content (Clark, 1997). As the less metamorphosed equivalents of the Quetico metasediments within the D_2 Manitouwadge syncline show little variation in magnetic susceptibility, the observed variations in the Quetico are due to variations of the oxidation state inherited from the original sediment. As the Quetico metasediments dip steeply in the mapped area, an observed magnetic pattern due to the metasediments would reflect the depositional environment of the original sedimentary sequence. The higher susceptibility units may represent more pelitic layers due to their higher total iron content.

The apparent susceptibility map (Fig. 5.16.1) over the Quetico metasediments west of Appelle Lake shows a generally E to ENE trending linear pattern of alternating highs (8.0 to 12.0 x 10^{-3} SI) and lows (-3.0 to -5.0 x 10^{-3} SI). The AS maxima are very noisy in this area due to levelling problems and gridding artefacts stemming from the ratio of the local flight line spacing to the

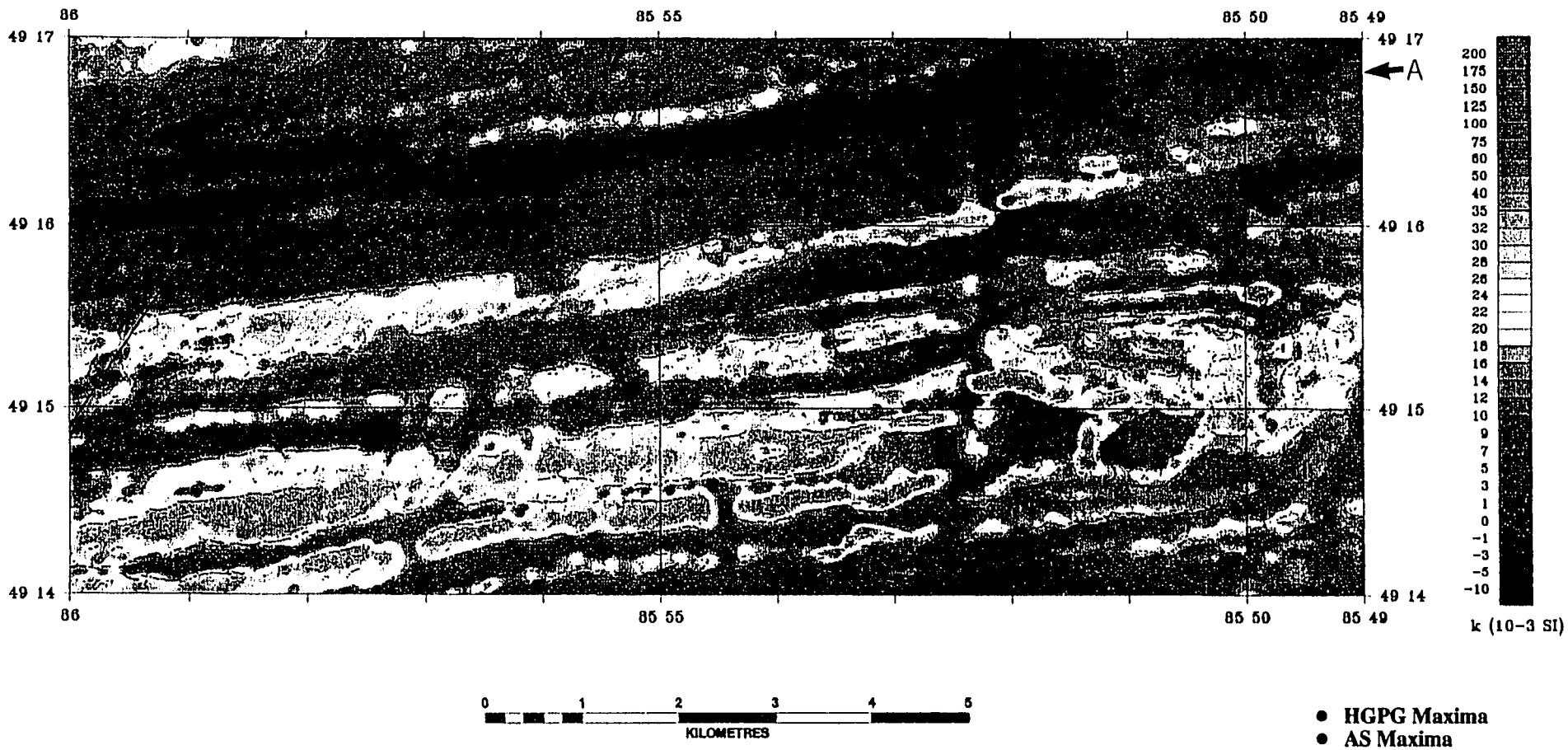

Fig. 5.16.1. Apparent susceptibility with AS and HGPG Maxima, northern Quetico metasediments

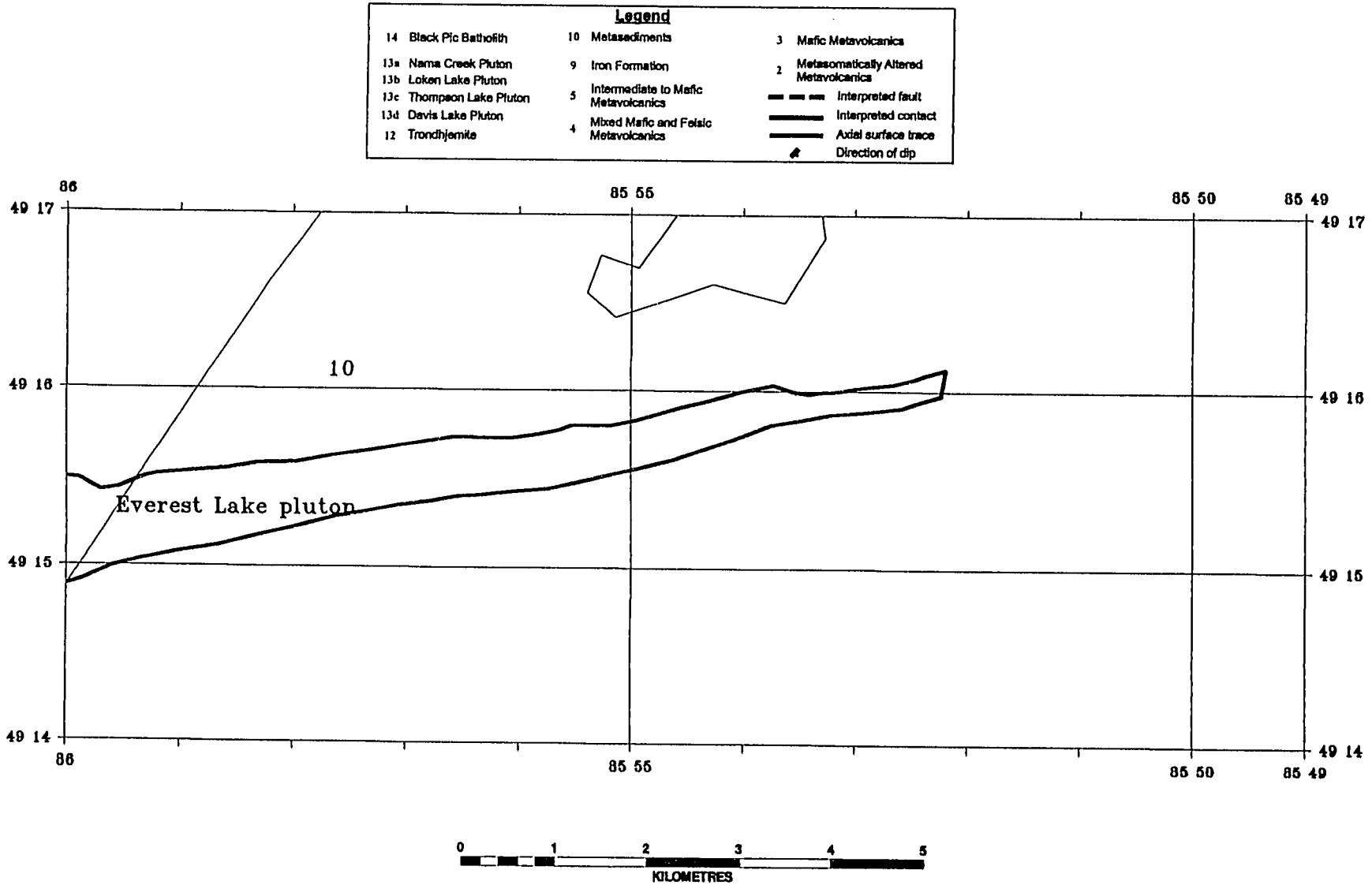

Fig. 5.16.2. Magnetic interpretation, northern Quetico metasediments

flight altitude and to the gridding interval. The HGPG maxima are less sensitive to these problems and strongly outline the steeply dipping units. The combined maxima and apparent susceptibility (Fig. 5.16.1), as well as the colour shaded relief of the residual total field, indicate a pinching of units to the west between Everest Lake (arrow 'B') and Slingshot Lake (arrow 'C'), indicating possible tight, isoclinal folding of the units represented by the linear magnetic anomalies. The large susceptibility high to the immediate south of this area may correspond to a more dominantly dioritic area (Everest Lake pluton) (Fig. 5.16.2), due to its less obvious internal linear patterns, higher apparent susceptibility and its trend transgressing the trends of the metasediment's magnetic pattern. Interleaved units of the Everest Lake pluton probably occur discontinously to the NNE towards arrow 'A' in Figure 5.16.1.

The apparent susceptibility and patterns of AS and HGPG maxima (Fig. 5.14.1) over Quetico metasediments east of Jim Lake change dramatically across N49°16' (Fig. 5.14.3). To the south are the previous described Quetico metasediments involved in the Jim Lake synform. The the north of this line, the magnetic signature is similar to that over Quetico metasediments west of Appelle Lake. This line may mark a metamorphic transition from upper amphibolite to granulite facies. From regional magnetic data, Pan et al. (1994) noted a correlation between the granulite zone they defined from an orthopyroxene-in isograd and an increase in magnetic intensity over this part of the Quetico subprovince. The higher resolution data used in this study resolves the regional high into the observed alternating high and low east-west trending magnetic features.

5.2.8 INTERMEDIATE AND MAFIC VOLCANICS (UNIT 5) AND SYNVOLCANIC TRONDHJEMITE (UNIT 12)

Intermediate and mafic volcanics and the synvolcanic trondhjemite are in contact along the northern limb of the Manitouwadge synform, around the Blackman Lake antiform and the Jim Lake synform. They are considered here together as their contact is not sharp, but lies somewhere in a magnetic low between the linear magnetic high interpreted as the contact of the metavolcanics with the Nama Creek pluton and the variable, hummocky magnetic pattern of the trondhjemite. Also, high susceptibility variants of the metavolcanics, the Dead Lake suite, are included within the trondhjemite and are marked by the occurrence of linear magnetic highs within that unit.

The AS and HGPG maxima become confusing as the units they map become thin. As seen with the Matachewan dykes, the AS maxima may image both edges of a thin dyke, one edge or only the centre of the dyke, depending on the thickness. To interpret the thin folded units and sub-units of the mixed intermediate and mafic volcanics, the second vertical derivative map (Fig. 5.17.1) was used.

The contact of the mixed metavolcanic unit with the Nama Creek pluton along the north limb of the Manitouwadge synform (Fig. 5.17.2) is relatively clear from the magnetic signature, a long linear high bordered by a linear low to the north. East of Larry Lake, around the Blackman Lake antiform and west to the Jim Lake antiform, the magnetic signature is not so clear. The area is cut by northeast and northwest trending faults and dykes. Due south of Larry Lake along the mixed volcanic unit, the unit is intercepted by a northwest trending fault. Within the metavolcanics, a unit of iron formation develops, complicating the pattern. The iron formation-bearing unit can be traced on the second vertical derivative map east to One Otter Lake. The magnetic interpretation is in conflict with the mapped geology of Zaleski et al. (1995). The

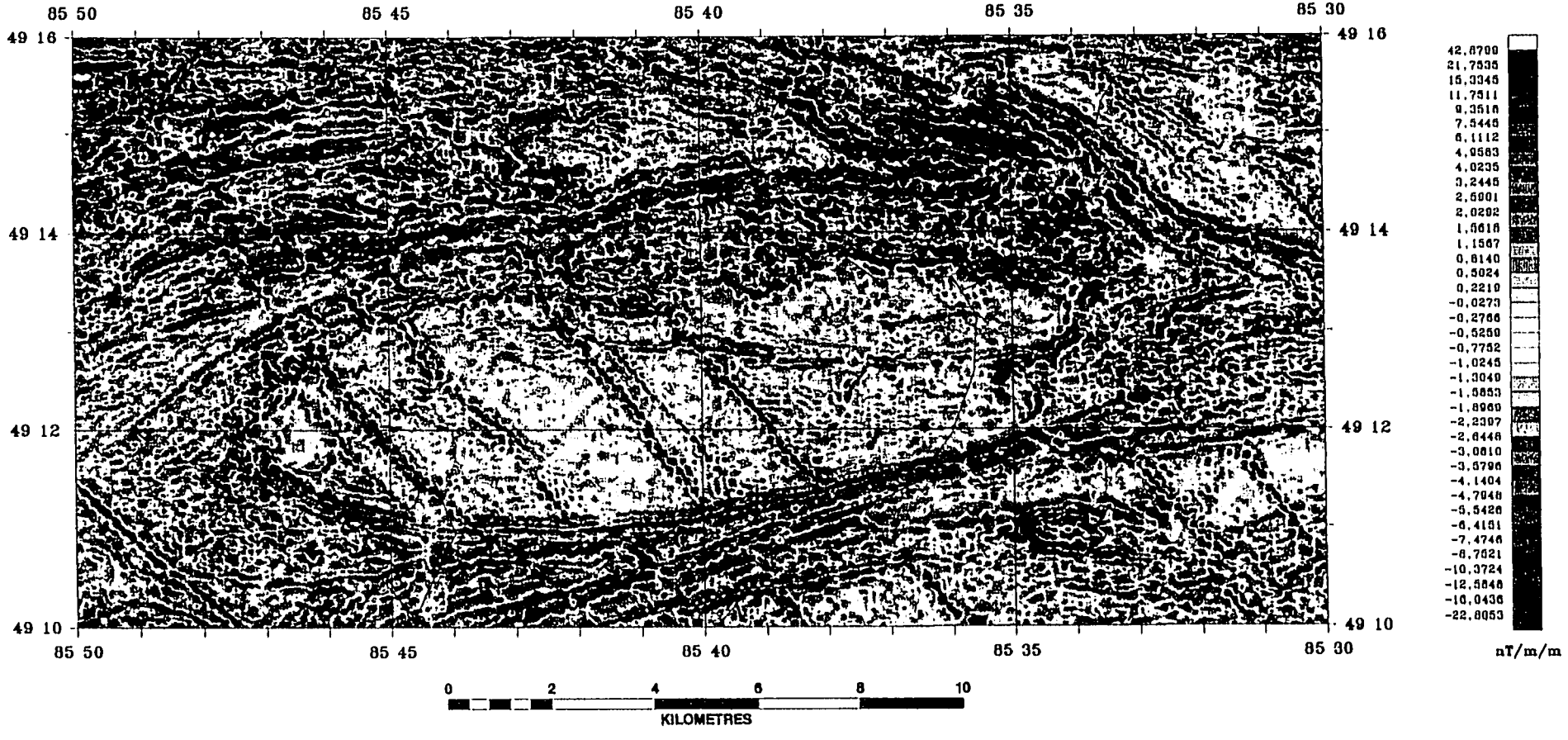

Fig. 5.17.1. Second vertical derivative, units 5 and 12.

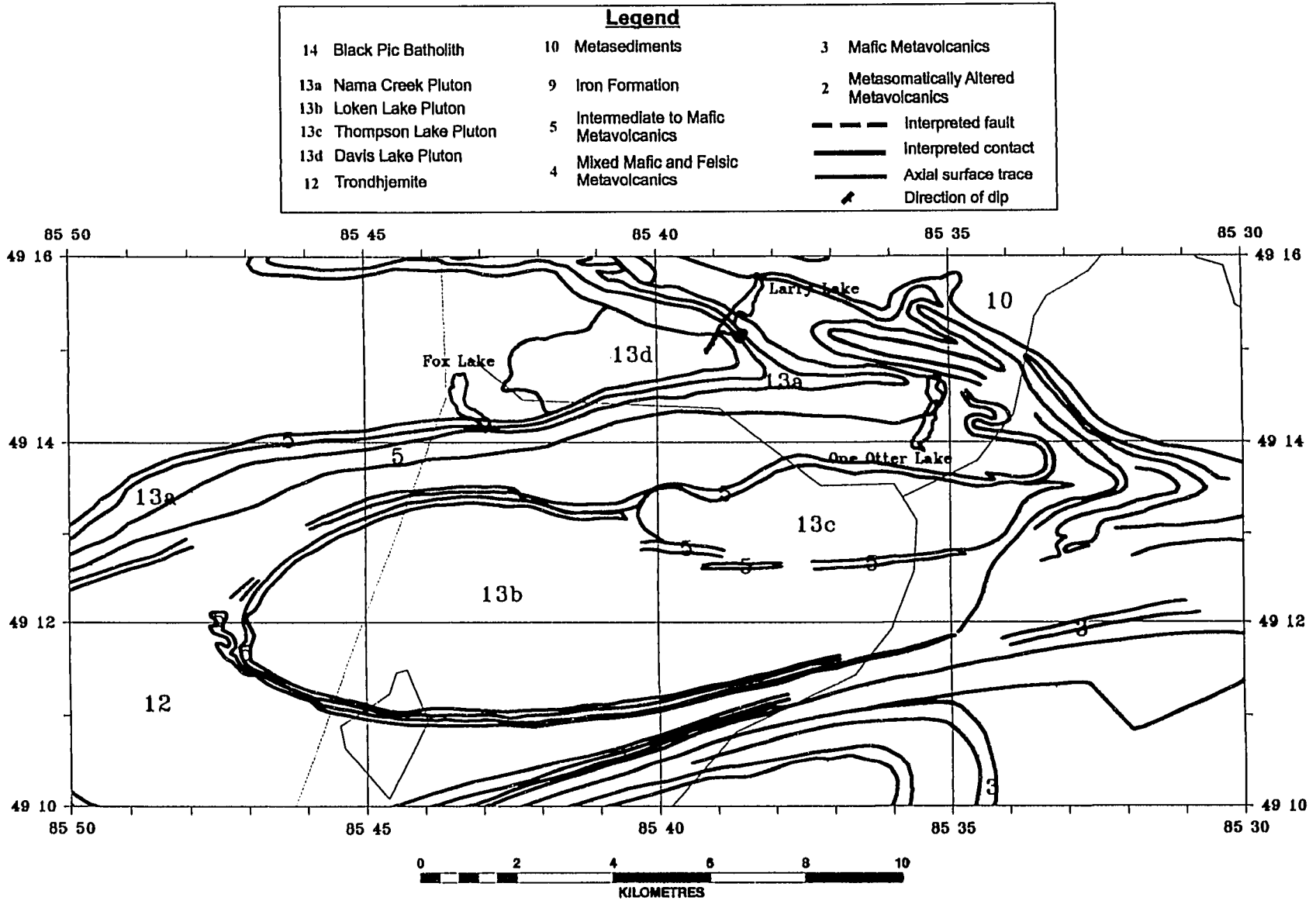

Fig. 5.17.2. Magnetic interpretation, units 5 and 12.

geologically mapped Nama Creek pluton is extended to include an outcrop of the pluton 500m south of the Blackman Lake antiform axial trace about 1km west of One Otter Lake. The mapped Nama Creek pluton in this area contains the east-west trending magnetic high interpreted here to represent iron formation. If this is actually a primary inclusion in the pluton, it too should be folded. The outcrop of Nama Creek Pluton in this area is problematic and will be disregarded in the magnetic interpretation. The isolated outcrop of plutonic material may represent local intrusion of the metavolcanics by the Nama Creek pluton or a thin, covering sheet. The magnetic signature suggests the area is underlain most significantly by metavolcanics rather than plutonic rock.

The contact of the mixed metavolcanic unit and the trondhjemite is interpreted as being within the magnetic low that separates the linear high along the southern edge of the Nama Creek pluton and the hummocky second vertical derivative magnetic pattern of the trondhjemite. East of the intercepting northwest trending fault south of Larry Lake, the contact here is in the magnetic low between the linear highs attributed above to the appearance of iron formation within the volcanics and the hummocky pattern of the trondhjemite. The contact is folded around the Blackman Lake antiform on the eastern side of the northern end of One Otter Lake, continues northwest in the second vertical derivative linear low and is folded by the Jim Lake antiform.

A unit of intermediate and mafic volcanics is mapped east and west of Fox Lake along the northern contact with the Nama Creek pluton. It is associated with a linear second vertical derivative high that is continuous across the northern limb of the Manitouwadge synform, except where it is cut by faults or covered by Fox Lake. This mapped unit is interpreted to continue east

and west along the high and is folded by the Blackman Lake antiform.

The Dead Lake suites have much higher measured magnetic susceptibilities than the associated intermediate and mafic metavolcanics sampled outside the synvolcanic trondhjemite. The linear second vertical derivative high that marks the limit of the northern, western and southern parts of the Loken Lake pluton is interpreted by Zaleski et al. (1995) as representing a unit of the Dead Lake suite. The mafic volcanic unit that separates the Loken Lake and the Thompson Lake plutons may also be of the Dead Lake suite. Two long, locally undulating second vertical derivative highs wrapping around the Loken Lake pluton are interpreted as units of the Dead Lake suite, given their linear nature and high magnetic signature. The unit in contact with the Loken Lake pluton and a sub-parallel unit are interpreted to extend from the southeast side of the pluton along its southern edge, folded by the Manitouwadge synform and continue east toward the Blackman Lake antiform. 1.5km south of Fox Lake, the unit closest to the pluton appears to be faulted and/or folded to the south. The unit continues to the east, including the zone mapped by Zaleski et al. (1995), producing a linear second vertical derivative high that separates the Loken Lake and Thompson Lake plutons. The unit becomes difficult to trace east of the eastern end of the Loken Lake pluton. The unit further away from the Loken Lake pluton continues east of the point where the closer unit veers south. It forms the undulating linear magnetic high that defines the northern contact of the Thompson Lake pluton. At the eastern end of the Thompson Lake pluton, the unit is tightly folded by the Blackman Lake antiform. This fold links the unit to a WNW trending, strong linear magnetic high. Although beyond the resolution of the magnetic survey, the unit is interpreted to be folded again to include strong curvilinear magnetic highs and to connect to another strong linear magnetic high north of One

Otter Lake. This interpretation of more complex folding is more reasonable magnetically than the geologically mapped intermediate and mafic volcanics east of One Otter Lake. The mapped fold is traversed by a strong linear magnetic feature that is clearly not folded in the manner suggested by the geologically mapped contacts and the fold pattern interpreted from the magnetics is largely consistent with local strike information.

5.2.9 MAFIC METAVOLCANICS (UNIT 3)

Mafic metavolcanics are found in both the outer and inner volcanic belts, but in much greater volume and diversity in the outer belt. In the outer belt, the unit has two magnetic signatures; 1) intense, strongly linear anomalies toward the inside of the Manitouwadge synform and 2) low, flat anomalies with sparse linear highs toward the outer part of the fold. Parts of the unit with the second signature are in sheeted contact (Zaleski et al. 1995) with the Black Pic batholith along the southern limb to the Manitouwadge synform and can be differentiated on the presence or absence of linear magnetic subparallel to the synform and the vertical derivative pattern where the mafic metavolcanics are flat and low and the Black Pic batholith is irregular.

Measured susceptibilities reflect the two signatures of the mafic metavolcanics. Of the 20 measured samples, 14 have values less than 2.0 x 10^{-3} SI and 4 are greater than 27.0 x 10^{-3} SI. One of the high susceptibility values is from a metagabbro. Apparent susceptibility (Fig. 5.18.1) of the outer, magnetically low, flat area is -2.0 to -5.0 x 10^{-3} SI, while linear apparent susceptibility highs in the inner part reach 150 to 175 x 10^{-3} SI. The more intense inner mafic metavolcanics of the outer volcanic belt may represent metagabbros or Dead Lake suite-type metavolcanics, however the greater volume of mapped iron formation on the north side of the D_2 Manitouwadge syncline suggests that there may be more iron formation than is currently

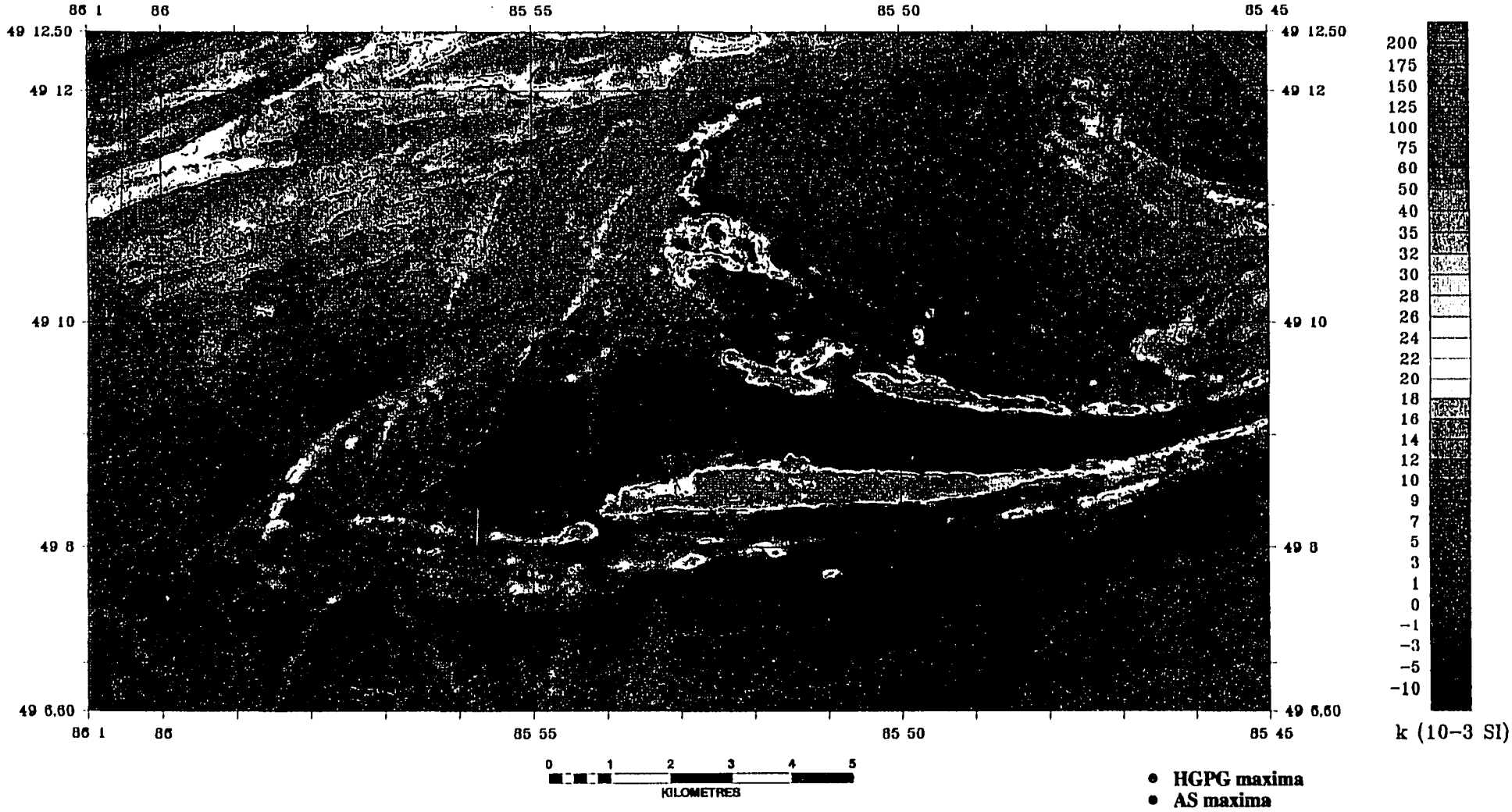

Fig. 5.18.1. Apparent susceptibility with AS and HGPG maxima, mafic metavolcanics.

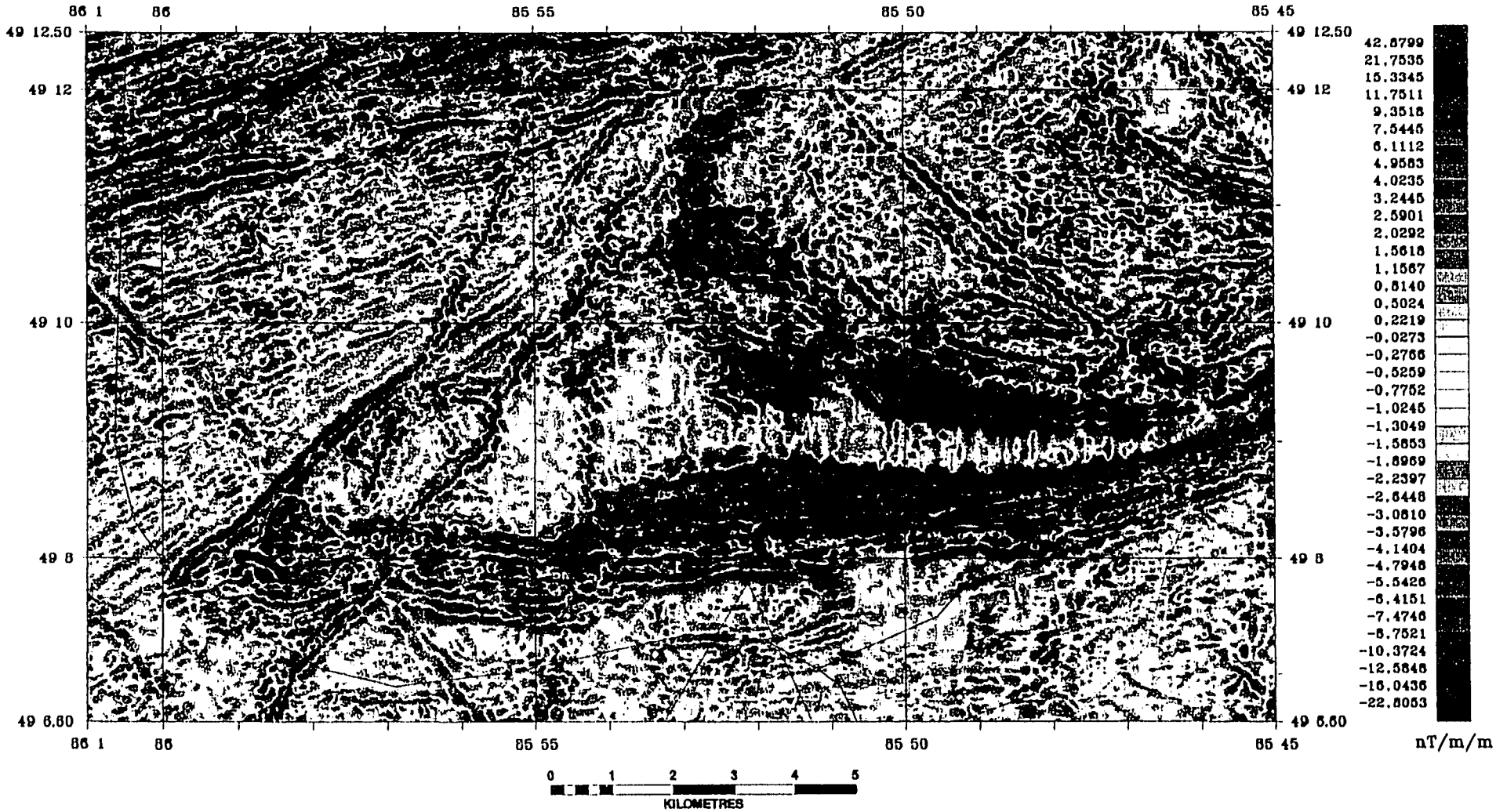

Fig. 5.18.2. Second vertical derivative, mafic metavolcanics.

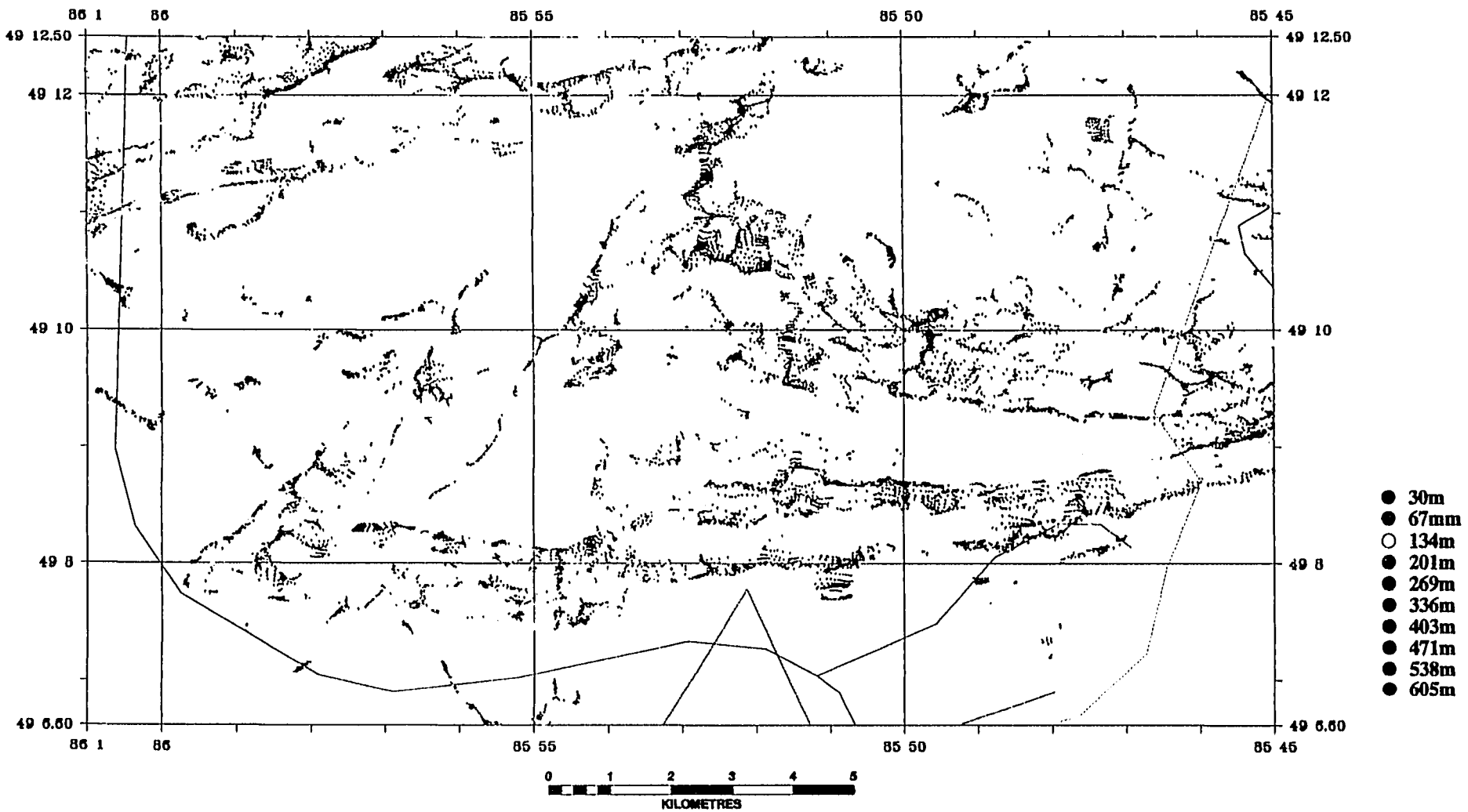

Fig. 5.18.3. Euler depth solutions with colour keyed estimated depths, mafic metavolcanics.

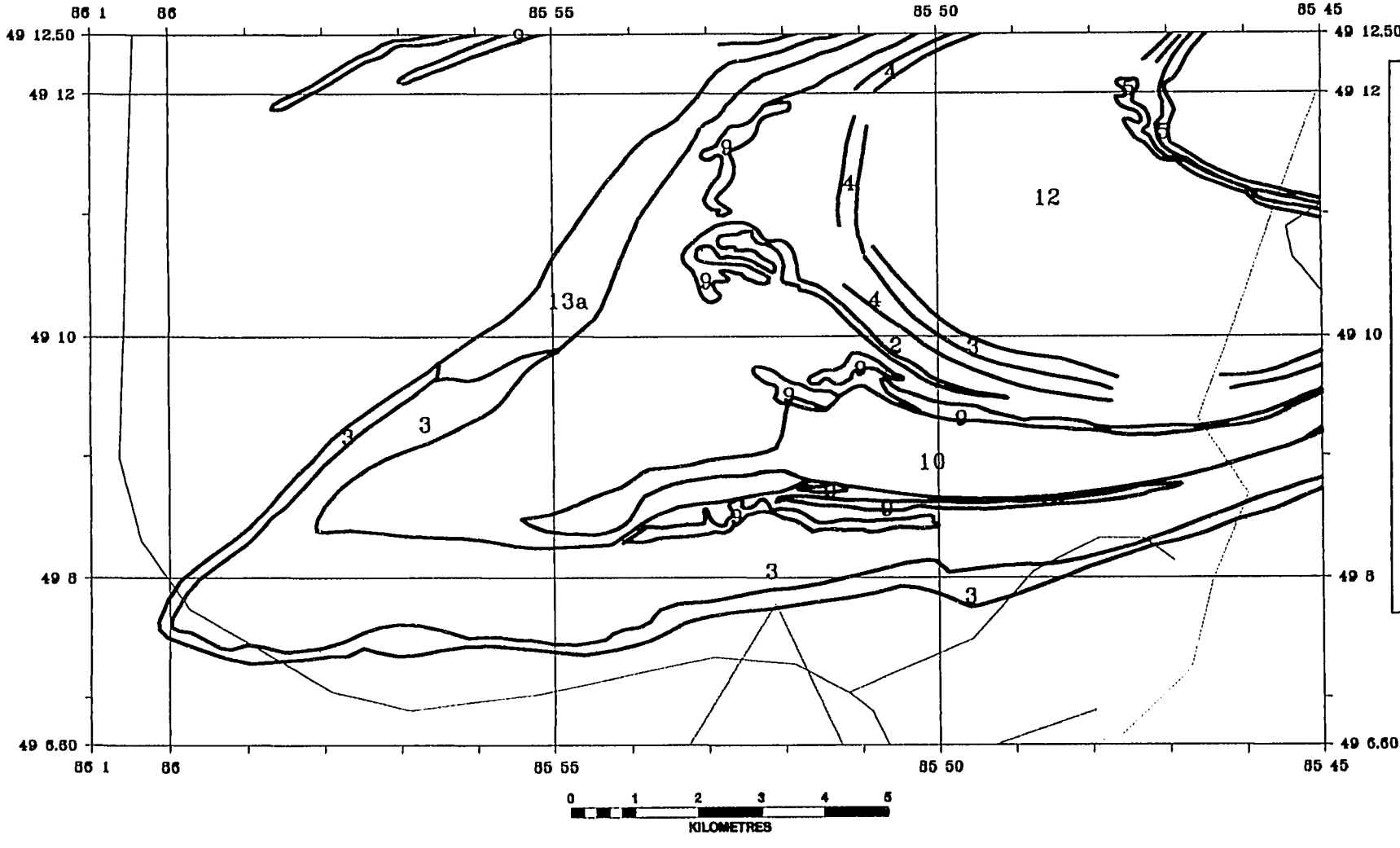

Fig. 5.18.4. Magnetic interpretation, mafic metavolcanics.

mapped on the southern side of that fold.

As the outer, lower intensity mafic metavolcanics are difficult to differentiate magnetically from the neighbouring tonalite, a contact drawn within the unit (Fig. 5.18.4) separating the two magnetic signatures will indicate the general pattern of the unit and the outer contact with the tonalite should be roughly parallel to this magnetic contact. A strong linear magnetic feature clearly defined on the AS and HGPG maxima (Fig. 5.18.1) and second vertical derivative (Fig. 5.18.2) maps illustrates a change from high to low susceptibility mafic metavolcanics. The outer contact with the tonalite is here defined subparallel to this linear feature and where the second vertical derivative changes from a monotonously flat pattern to a more random pattern of isolated and linear anomalies. The linear anomalies within the Black Pic batholith subparallel to the the Manitouwadge synform are interpreted as supracrustal units included in the tonalite.

The mafic metavolcanics in the outer volcanic belt can be traced along the outside of the Manitouwadge synform from the contact with the Nama Creek pluton on the northern limb, folded around the Manitouwadge synform, offset by various faults, and continuing east to the Banana Lake antiform where the outer volcanic belt appears to be folded to the south (Fig. 5.19.2), towards the Faries Lake greenstone belt. The metavolcanics start to diverge southward and are juxtaposed against WNW trending linear magnetic features by a NW trending fault.

On the northern limb of the Manitouwadge synform within the mafic metavolcanics, shallow Euler depth solutions (Fig. 5.18.3) are associated with high intensity linear magnetic features. The linear features appear to continue across the contact with the Nama Creek pluton but the depth solutions do not. The lack of solutions and the presence of less sharp linear features within the Nama Creek pluton may indicate the mafic metavolcanics continue along the northern limb

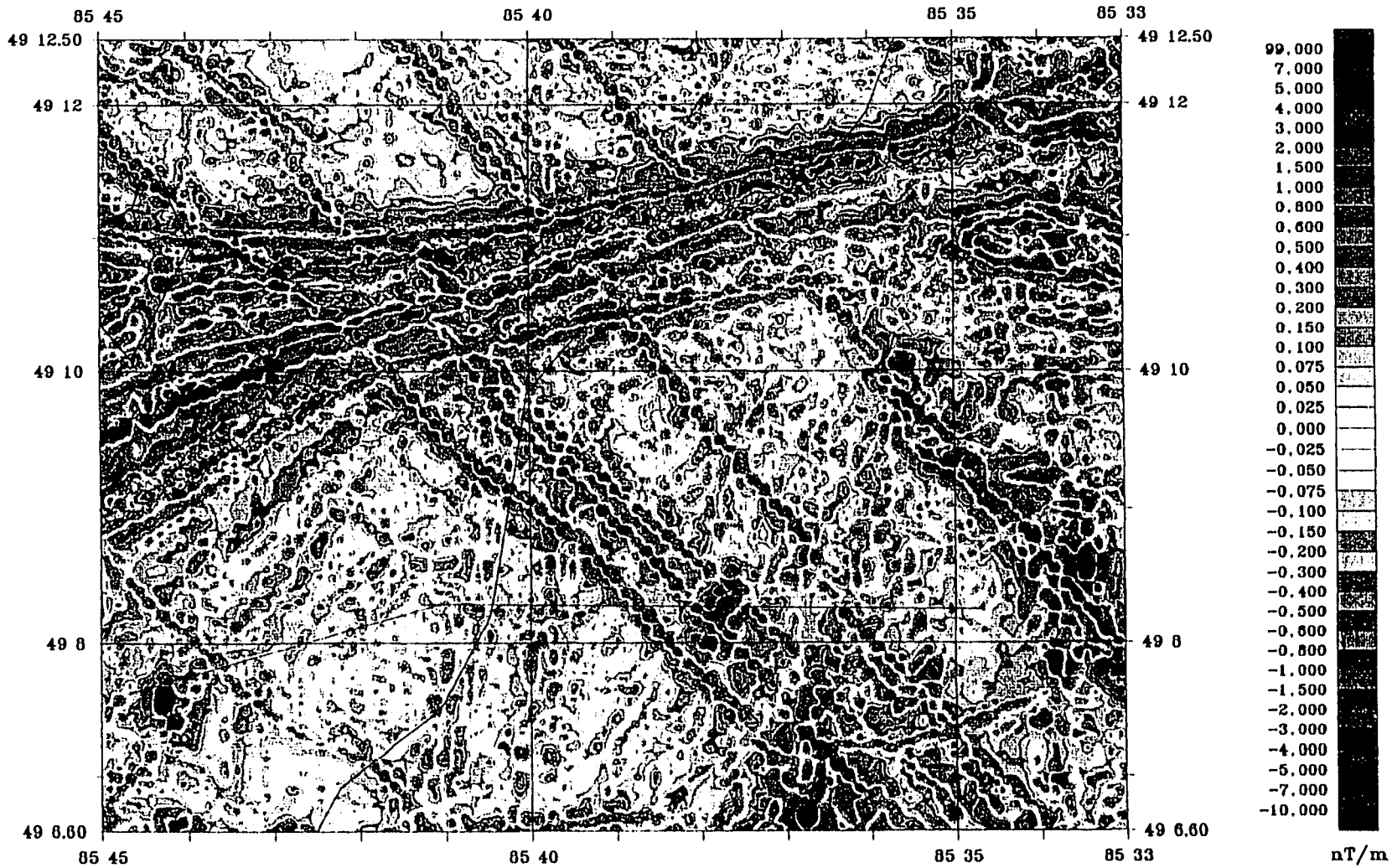

Fig. 5.19.1. Vertical derivative, mafic metavolcanics.

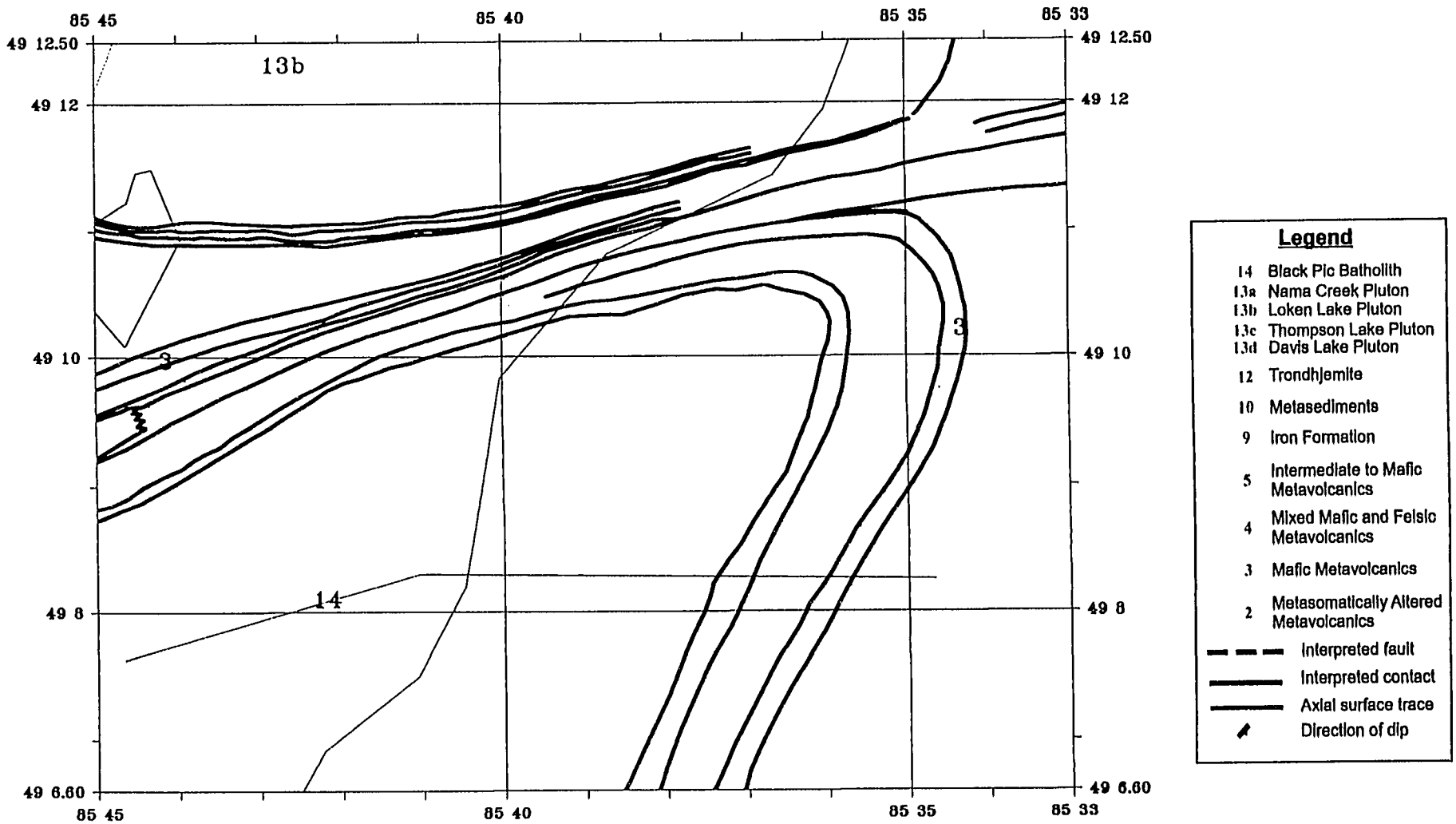

Fig. 5.19.2. Magnetic interpretation, mafic metavolcanics.

Produced by PLOTSYS 5.15, created by Regional Geophysics/CGD/GSC/NRCan

of the synform overlain by the pluton.

In the inner volcanic belt one unit of mafic metavolcanics is mapped within the trondhjemite. The measured susceptibility of a sample from this unit is 0.6 x 10^{-3} SI and the apparent susceptibility (Fig. 5.18.1) is about -3.0 x 10^{-3} SI. The apparent susceptibility map and the AS and HGPG maxima suggest a sharp contact of a low susceptibility unit extending to the northwest, folded by the Manitouwadge synform and also extending to the the east along the fold's southern limb. Also traceable on these maps and the vertical derivative map is a higher susceptibility unit in contact with the mafic metavolcanics and towards the outer part of the fold. This magnetic unit coincides generally with Zaleski's Unit 4, mixed mafic and felsic metavolcanics. Three measured susceptibilities of the this geological unit are 2.3 x 10^{-3} SI (mafic), 4.1 x 10^{-3} SI (felsic) and 29.3 x 10^{-3} SI (felsic), and the apparent susceptibilities range from 5.0 to 10.0 x 10^{-3} SI. The magnetic signature of the more felsic unit is more quickly attenuated along both north and south limbs of the Manitouwadge synform. Both units 3 and 4 display complicated discontinuous patterns near the synform's axial trace, perhaps indicating local folding (M-folding?) not well resolved by the magnetic survey due to line spacing and orientation.

5.2.10 BLACK PIC BATHOLITH (UNIT 14)

The Black Pic batholith is a multiphase tonolitic to monzodioritic intrusion that is the youngest of the major rock types within the Manitouwadge greenstone belt. Zaleski et al. (1995) have not differentiated the known phases on their map, but recognize the Everest Lake pluton, and the Banana Lake monzodiorite as such phases. The batholith on their geology map

encompasses everything south of the Quetico metasediments and outside the Manitouwadge greenstone belt. The presence of inclusions of supracrustal rocks within the Black Pic batholith is noted as largely discontinuous, non-mappable units. The batholith has not been mapped in as much detail as the supracrustal units of the greenstone belt.

The residual total magnetic field map (Fig. 5.20.1) shows that the magnetic signature of the area mapped as Black Pic tonalite (Fig. 5.20.3) is highly varied, with variations consistent from north to south. The northern area is dominated by alternating linear magnetic highs and lows subparallel to the contact with Quetico metasediments. Toward the south, the linear features curve more to the southwest, decrease in number and decrease in intensity.

Measured susceptibilities of samples of the Black Pic tonalite range between about 1.0×10^{-3} SI and about 5.0×10^{-3} SI, with values of 21.8×10^{-3} SI and 12.2×10^{-3} SI in samples with accessory magnetite. Only two samples, with values of 2.5×10^{-3} SI and 2.7×10^{-3} SI, are from north of N49°11' and none is available north of N49°12'. The apparent susceptibility (Fig. 5.20.2) also indicates highly variable, but linearly continuous, bands of alternating high and low apparent susceptibility values.

In a previous discussion on mixed intermediate and mafic volcanics, a second vertical derivative linear anomaly (Fig. 5.17.1 and 5.17.2) north of the Nama Creek pluton within the mapped Black Pic batholith was interpreted to represent extensions to the east and west of a metavolcanic unit mapped to the east and west of southern Fox Lake. By extension, subparallel linear magnetic features adjacent to the north are interpreted to represent supracrustal rocks invaded and possibly somewhat digested by the late tonalite. Similarly, linear magnetic highs are seen within the Black Pic tonalite trending subparallel to mapped mafic metavolcanics of the

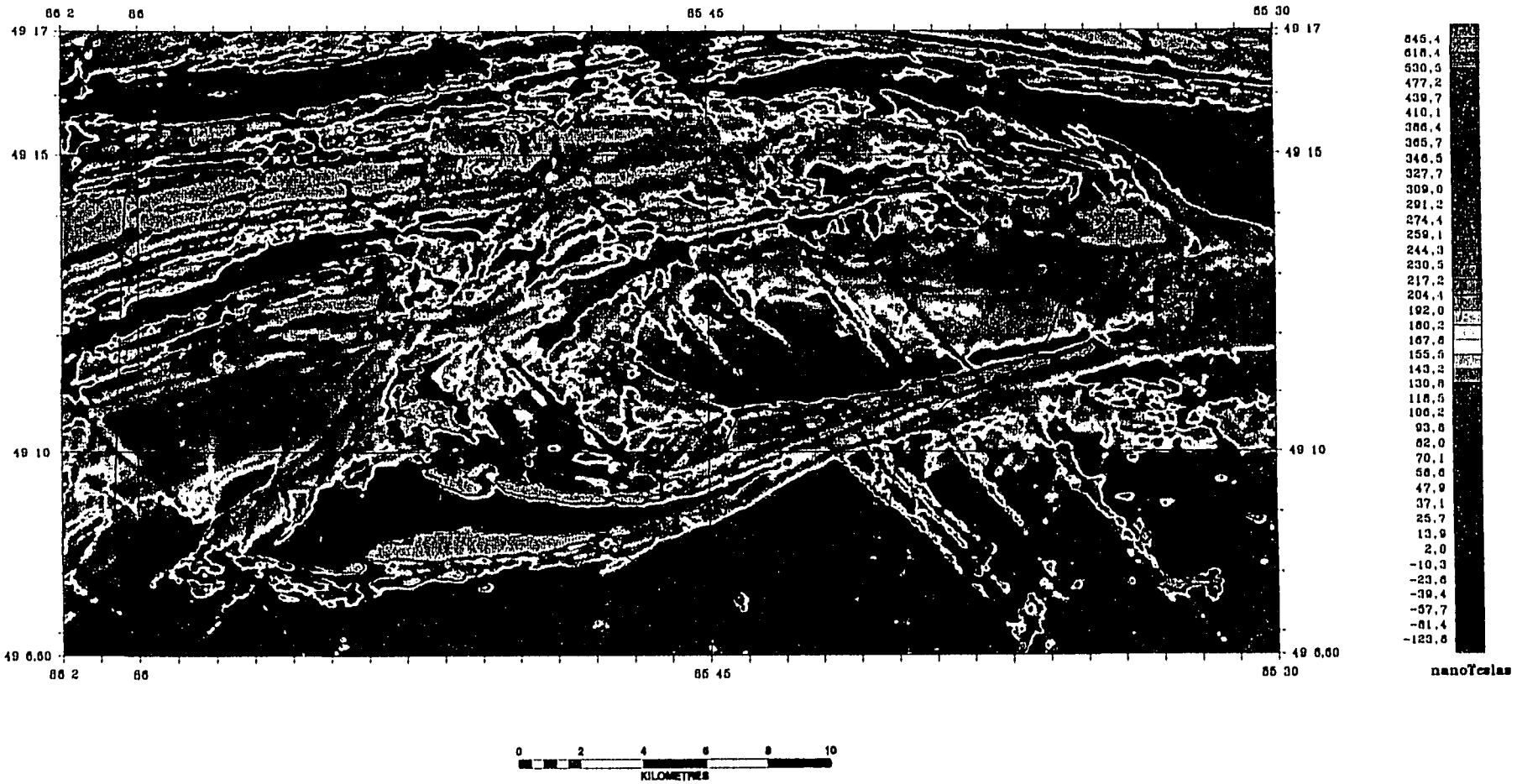

Fig. 5.20.1. Residual total field magnetics, Black Pic batholith (unit 14).

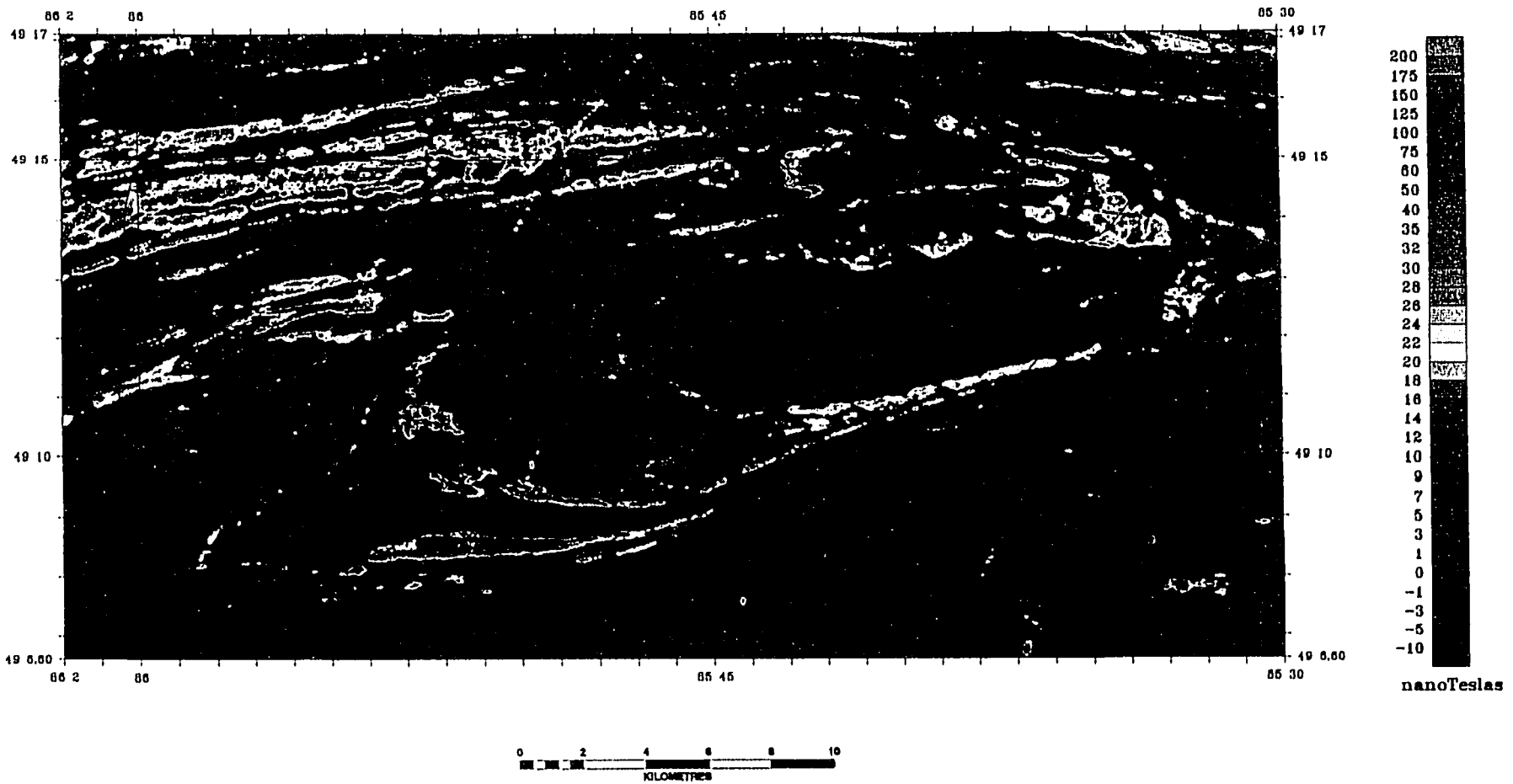

Fig. 5.20.2. Apparent susceptibility, Black Pic batholith (unit 14).

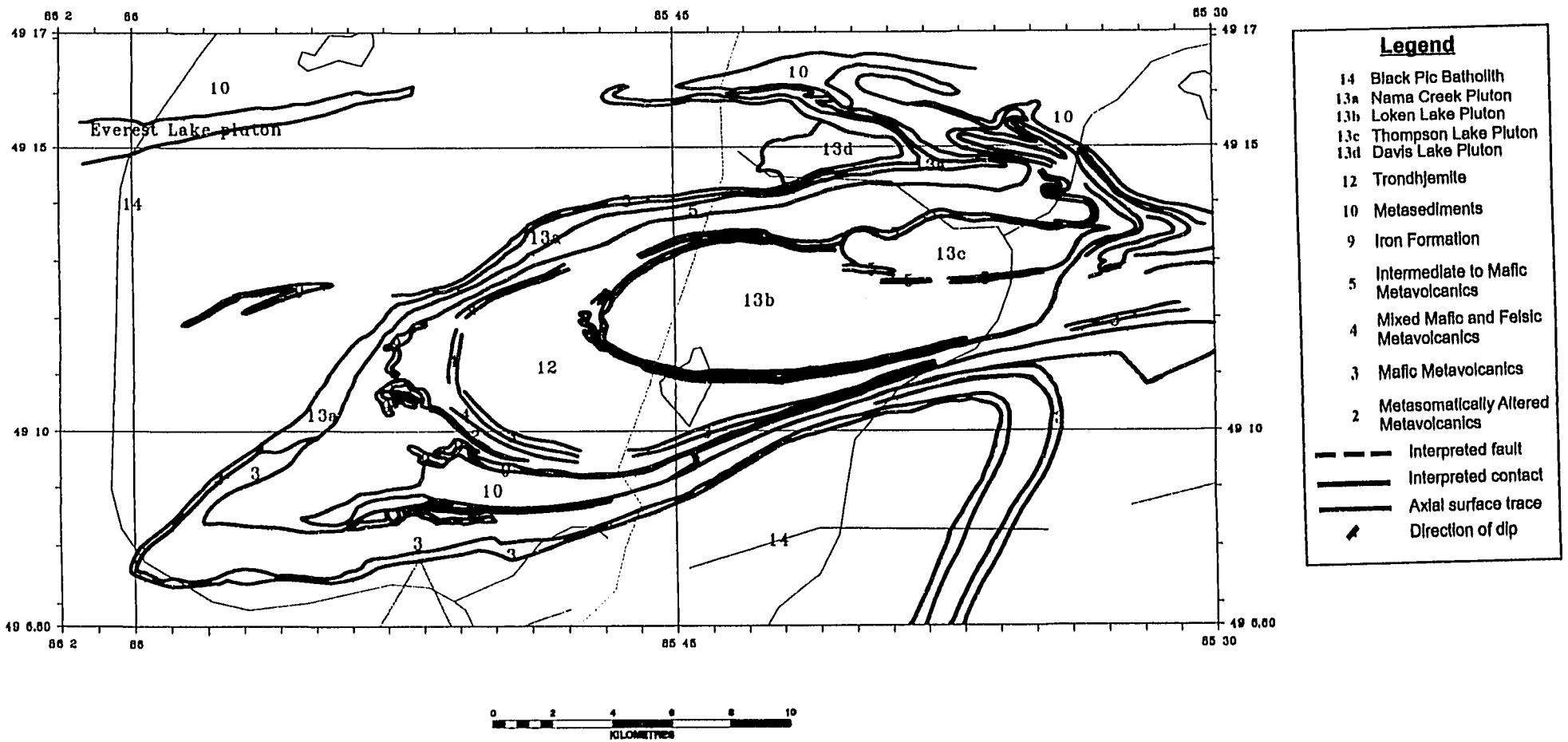

Fig. 5.20.3. Magnetic interpretation, Black Pic batholith (unit 14).

southern limb of the Manitouwadge synform. The source of the magnetic striping within the tonalite is attributed to the presence of included supracrustal rock. The variation in intensity of the striping from the north to south reflects the development of secondary metamorphic magnetite, which is controlled largely by the amount of total iron and the metamorphic grade. Across the map sheet from north to south, the overall decrease in magnetic intensity within the Black Pic tonalite is interpreted to reflect the decrease in metamorphic grade from near granulite facies in migmatized tonalite near the Wawa-Quetico boundary to mid-amphibolite facies south of the Manitouwadge synform. Locally, variations causing the alternating high and low magnetic stripes reflect the availability of iron for the development of magnetite, generally controlled by the presence or absence of included supracrustal rock.

5.3 DIP DIRECTION DETERMINATION

Following the method of Hansen et al. (1987), the dip directions of magnetization contrasts defined by AS and HGPG maxima were investigated. Figure 5.21 contains eighty-three interpreted dip direction indicators. Near vertical dips, defined by coincident AS and HGPG maxima, are marked as such, but all other dip indicators have no estimate of the dip angle.

The method of dip direction determination requires that the source of the AS maxima be the same as the source of the HGPG maxima. This is not always straightforward to interpret. Thin steeply dipping layers and thin dykes may be imaged by the AS maxima on either edge, the centre of the unit or any combination of the three, while HGPG maxima may only image the edge with the greatest horizontal gradient. As a result, an apparent offset between the two types of maxima may be an artifact of the method. Care must be taken to interpret maxima only from sufficiently thick and homogeneous bodies.

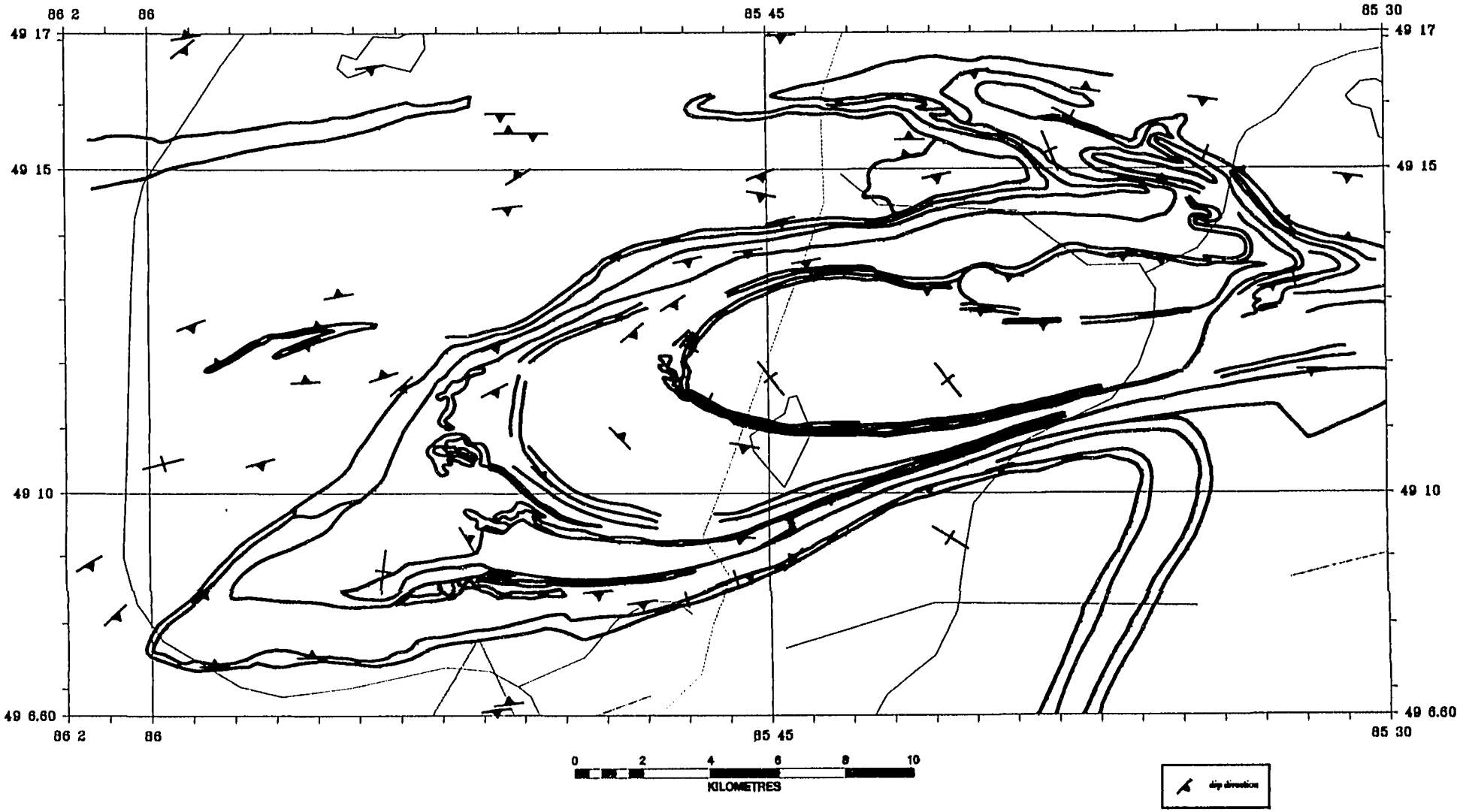

Fig. 5.21. Interpreted dip directions with interpreted contacts.

As with most magnetic interpretation methods, the interpretation of the dip direction is greatly enhanced by comparison with known dips, allowing extrapolation to areas of sparser geological sampling. Where known dips are shallow and the geologic strike is subparallel to the magnetic survey flight lines, suitable AS and HGPG maxima for dip direction determination are rare. Higher gradients provide more maxima of both types and thereby allow more opportunities for interpretation. For example, the contact of the Loken Lake pluton with the Dead Lake suite has a high gradient and dip direction determinations were possible, however, the Black Pic batholith south of the Manitouwadge synform has high gradients only where cut by Proterozoic dykes and dips of Archean inclusions were difficult to determine.

For more accurate and reliable dip direction determinations, the usual increases in grid and data fidelity apply to reduce noise. Dips of units perpendicular to the survey flight lines will be more reliable, as will be the interpreted dips of bodies with greater apparent thickness and homogeneity. However, Figure 5.21 shows a reasonable indication of the dip direction is possible with finer grid intervals, from thin units and where the geologic strike is at a low angle to the flight line direction.

5.4 FOLDS

The style and form of folding within the study area have been well described by Zaleski et al. (1995) and much, but not all, of her information can be confirmed from the magnetic data (Fig. 5.22).

The mapped D_2 Manitouwadge syncline is not easily interpreted from the magnetics. Although magnetic units are repeated on both limbs of this fold, their distribution and apparent thickness are different. The lack of sufficient magnetization contrast of the metasediments in

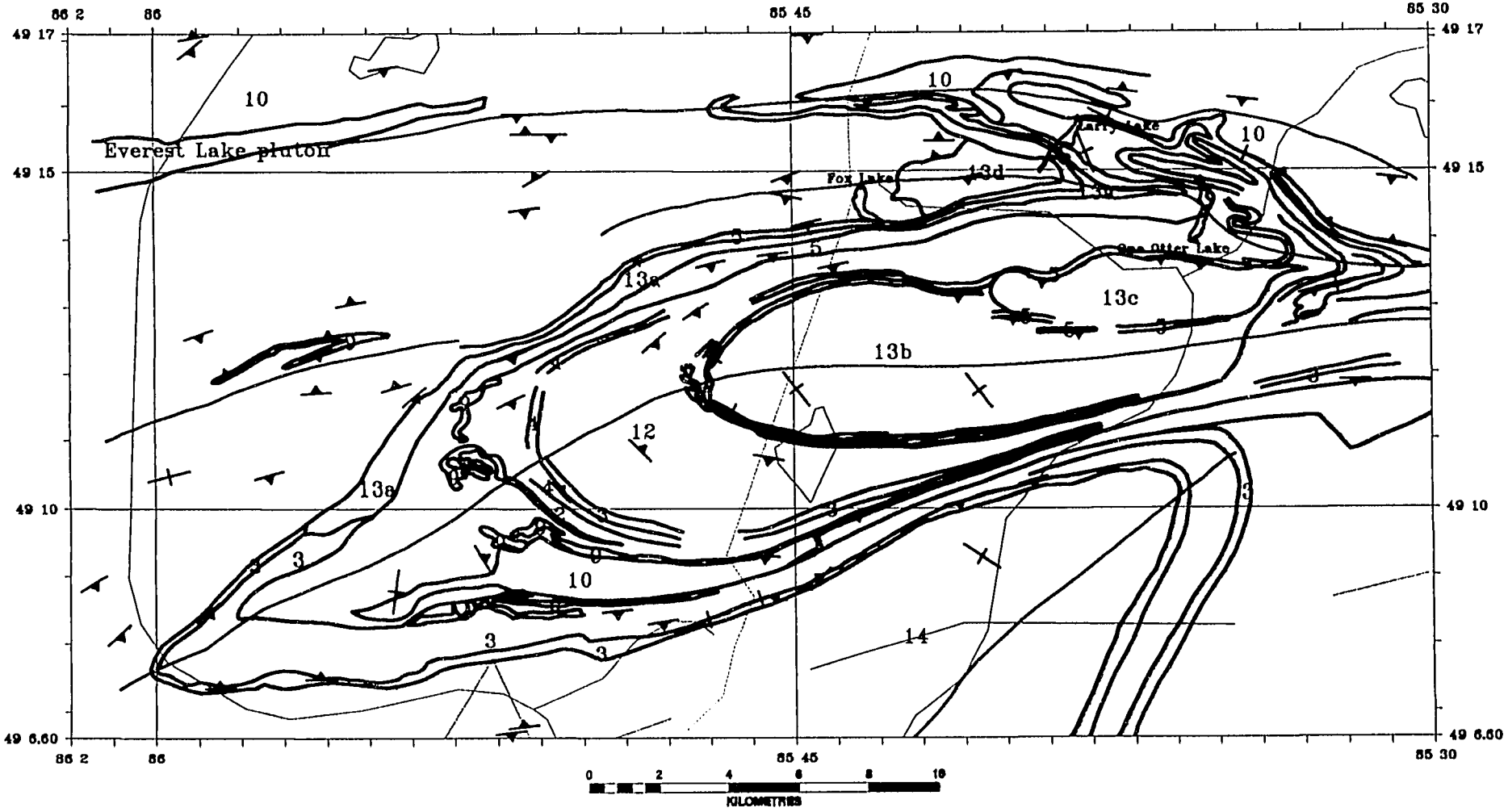

Fig. 5.22. Interpreted folds, Manitouwadge study area. Major D3 folds are, from south to north, Banana Lake antiform, Manitouwadge synform, Blackman Lake antiform, and Jim Lake synform.

the hinge zone with the felsic metavolcanics within the area make magnetic interpretations locally difficult.

The synformal character of the Manitouwadge synform is borne out by the folding of interpreted units and the AS and HGPG maxima-derived dip directions. The north and south limbs dip to the south and within the hinge zone along the axial surface trace the units dip to the northeast, defining a concave-up, synformal shape. Assuming from the series of roughly east west axial surface traces of the Banana, Manitouwadge, Blackman Lake and Jim Lake folds that they define a fold train, and from less definitive, yet consistent, dip directions, the folds can be assigned synformal or antiformal character consistent with the mapping of Zaleski et al. (1995) from their magnetic signatures alone.

Along the axial surface trace of the Manitouwadge synform at the west end of the Loken Lake pluton, the Dead Lake Suite interpreted contact undulates. This may be an artifact of the magnetic survey as the flight lines are parallel the strike of the unit or it may represent a second order M-fold.

D_3 folds generally have sharp closures except about the Manitouwadge synform between the western end of the Loken Lake pluton and the outer volcanic belt. The rocks in this area are dominated by synvolcanic trondhjemite and felsic volcanics which are more competent than the more mafic volcanics seen elsewhere. This area includes the D_2 Manitouwadge syncline. The presence of felsic volcanics and VMS deposits indicates the proximity to a volcanic centre. The coincidence of the D_2 and D_3 fold hinges and the volcanic centre indicate the more competent centre may provide a focus for folding with in the volcanic sequence.

The Blackman Lake antiform hinge area east and north of One Otter Lake is much more

complicated than originally mapped by Zaleski et al. (1995) as indicated by mapped folded units traversed by non-dyke related magnetic lineaments. The area is cut by northeast and northwest trending dykes and faults, complicating the magnetic signature. As well, One Otter Lake overlies a magnetic low that terminates magnetic lineaments. The interpretation of a Z-fold defined by a unit of the Dead Lake suite due east of One Otter Lake is an attempt to account for the presence of a discontinuous, segmented second vertical derivative lineament, but the relationship to the folded magnetic lineament due north of the Z-fold and S-fold slightly farther north is unclear. The Z and S folds may be parasitic, higher order folds related to the Jim Lake synform, the Blackman Lake antiform or another fold between these two not yet defined.

The interpreted eastern extent of the Jim Lake synform based on the folding of reasonably continuous supracrustal units is limited to Appelle Lake. Folded magnetic lineaments, however, can be used to extend the fold to at least another 4km to the west.

5.5 MAGNETIC FEATURES WITHIN THE BLACK PIC BATHOLITH OUTSIDE THE STUDY AREA

From the first vertical derivative magnetic map of the entire surveyed area (Fig. 5.23), east-west trending magnetic lineaments or stripes are obvious over the northern mapped areas of the Black Pic tonolitic-dioritic batholith. Zaleski et al. (1995) interpret the striping as due to inclusions of supracrustal rocks, as well as the sheeted Everest Lake pluton. Sparse and isolated units of mafic to intermediate metavolcanics and iron formation are mapped within the northern Black Pic tonalite by Zaleski et al. Williams et al. (1991) describe the supracrustal inclusions as abundant and link them to strong linear magnetic anomalies. The intensity of the magnetic field over this area is significantly higher than that seen over the supracrustal rocks of the

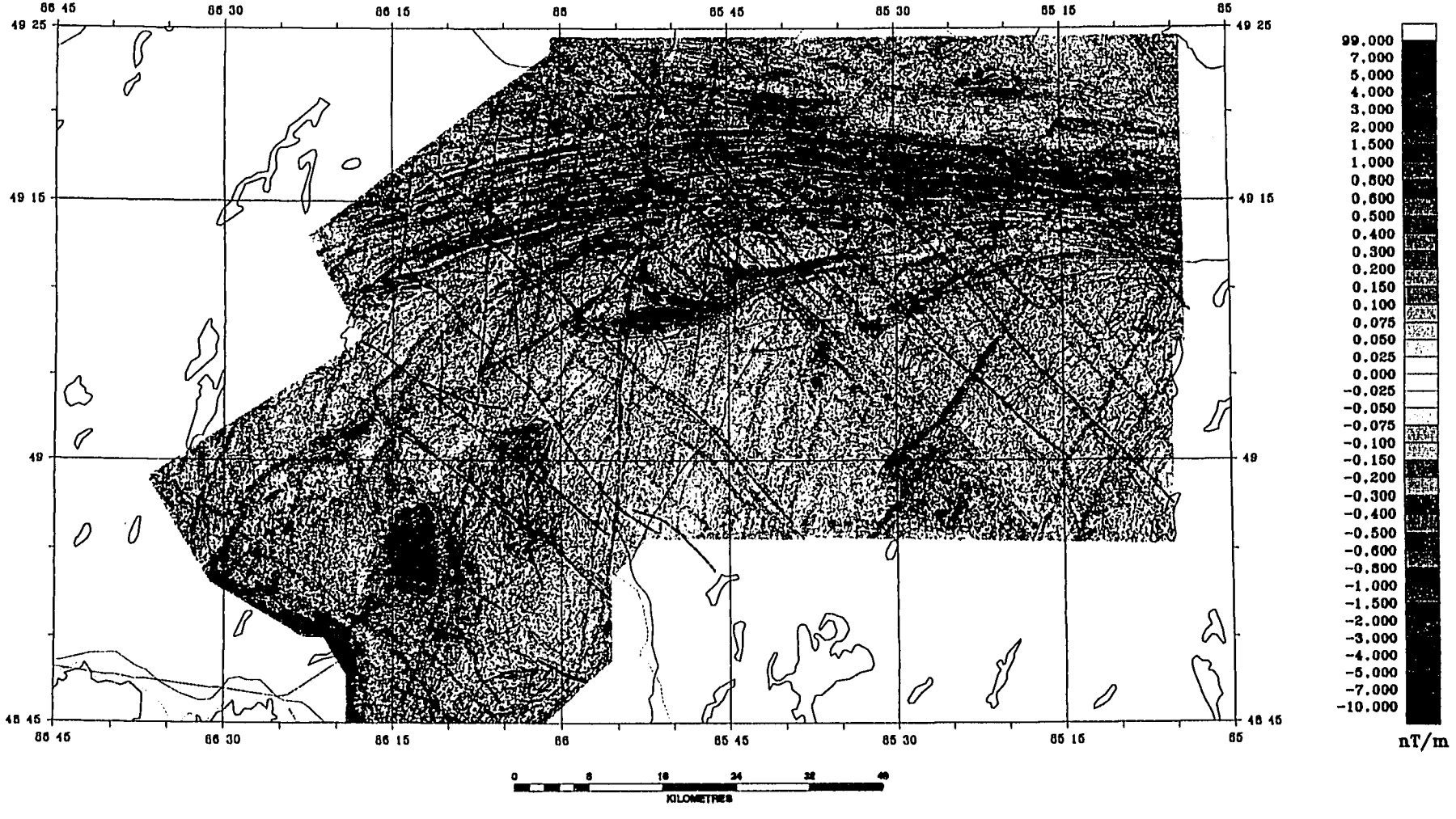

Fig. 5.23. First vertical derivative with interpreted faults (dashed lines).

Manitouwadge greenstone belt, excepting iron formation.

Mapping by Coates (OGS Map 2192, 1970) identifies outcrop of biotite-hornblende migmatite within biotite granite gneiss northeast of Vein Lake (Fig. 5.24) . To the north about 4.5 km, Coates maps biotite-hornblende migmatite as a unit separate from the granitic gneisses. Williams et al. (1991) in their compilation interpreted this more northern unit as migmatized supracrustal rocks and extend the unit to the southeast about 9km, to include the area mapped by Coates as granitic gneiss and two northeast trending units of mafic to intermediate metavolcanics, also mapped by Coates. The magnetic signature of the biotite-hornblende migmatite unit mapped by Coates can be traced to the western end of the eastern part of the Blackman Lake antiform. To the west, the unit is faulted by a north trending fault with about 600m of sinistral strike-slip offset and then isoclinally folded with a rounded closure. Coates also mapped metavolcanic rocks of the northeastern Schreiber-Hemlo greenstone belt that are represented by linear magnetic highs that can be traced semi-continuously to the magnetic feature near Janet Lake, previously interpreted as iron formation, based on its high apparent susceptibility. The mafic metavolcanic sub-units that are the source of this linear magnetic high have a high magnetic susceptibility and may be analogous to the high susceptibility mafic metavolcanics of the outer volcanic belt or the Dead Lake suite. The tracing of the first vertical derivative linear anomalies representing units of mapped metavolcanics in the Hemlo-Schreiber greenstone belt to the Janet Lake area confirms the interpretation of Williams et al. (1991) that the Manitouwadge greenstone belt may have been continuous with the supracrustal rocks of northern edge of the Schreiber-Hemlo greenstone belt.

The northern Black Pic batholith has a high percentage of included supracrustal rocks.

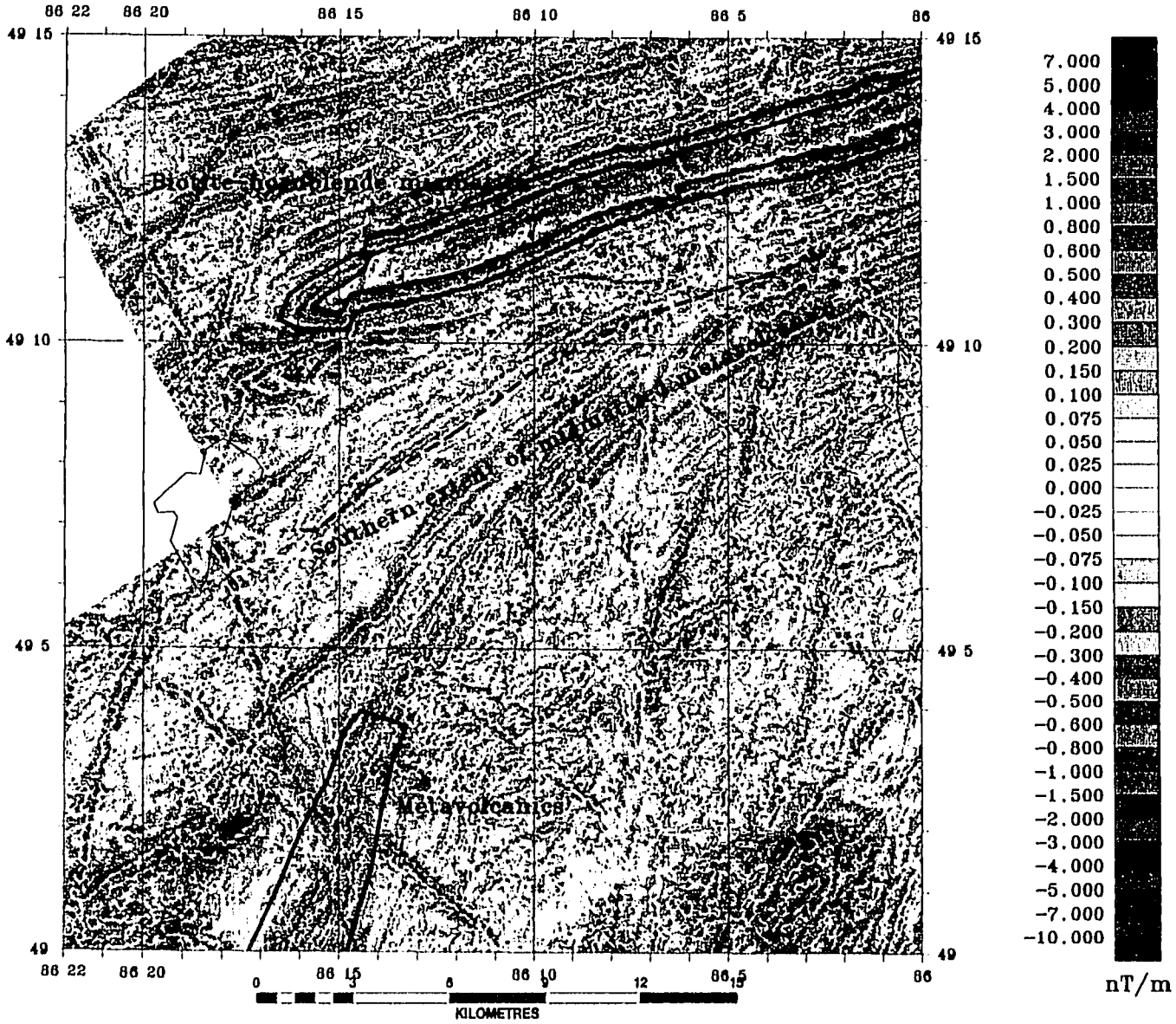

Fig. 5.24. Mapped metavolcanics within northern and western Black Pic Batholith. Base is first vertical derivative of magnetics.

Progressively lower amounts of supracrustal inclusions are seen to the south, with more open folding and more tonolitic intrusion. The northern metavolcanics/migmatites have significantly more secondary magnetite developed by higher grades of metamorphism than similar inclusions to the south.

South of the Manitouwadge synform, the sheeted contact of Black Pic tonalite with mafic metavolcanics produces curvilinear magnetic lineations within the tonalite due to the inclusions of metavolcanics. Tracing the supracrustals through the tonalite by their magnetic signature is difficult as there is little or no secondary magnetite developed due to the lower metamorphic grade. Furthermore, there are numerous dykes and faults, generally trending both northeast and northwest, and line-to-line levelling errors and gridding effects complicating the magnetic signal. However, the mafic metavolcanics of the outer part of the southern limb of the Manitouwadge synform have very low measured magnetic susceptibilities, generally less than 1.0×10^3 SI, while the Black Pic tonalite has higher measured susceptibilities, generally between 1.0 and 4.0×10^3 SI. Giguerre (OGS Map 2219, 1972) maps a NNE trending quartz-plagioclase-hornblende schist (Fig. 5.25.2), interpreted by Giguerre as a metavolcanic rock, on the southeast limb of the magnetically interpreted Banana Lake antiform. The unit coincides with a linear magnetic low (Fig. 5.25.1). The low is interrupted by a local broad magnetic high, but appears to continue to the southeast as wispy first vertical derivative curvilinear features, eventually abutting at an elliptical magnetic high.

Supracrustal units from the Moshkinabi greenstone belt east and south of the Manitouwadge greenstone belt, are strongly represented in the first vertical derivative of magnetics trending WSW in the eastern central portion of the map (Fig. 5.25.1). These features become less intense

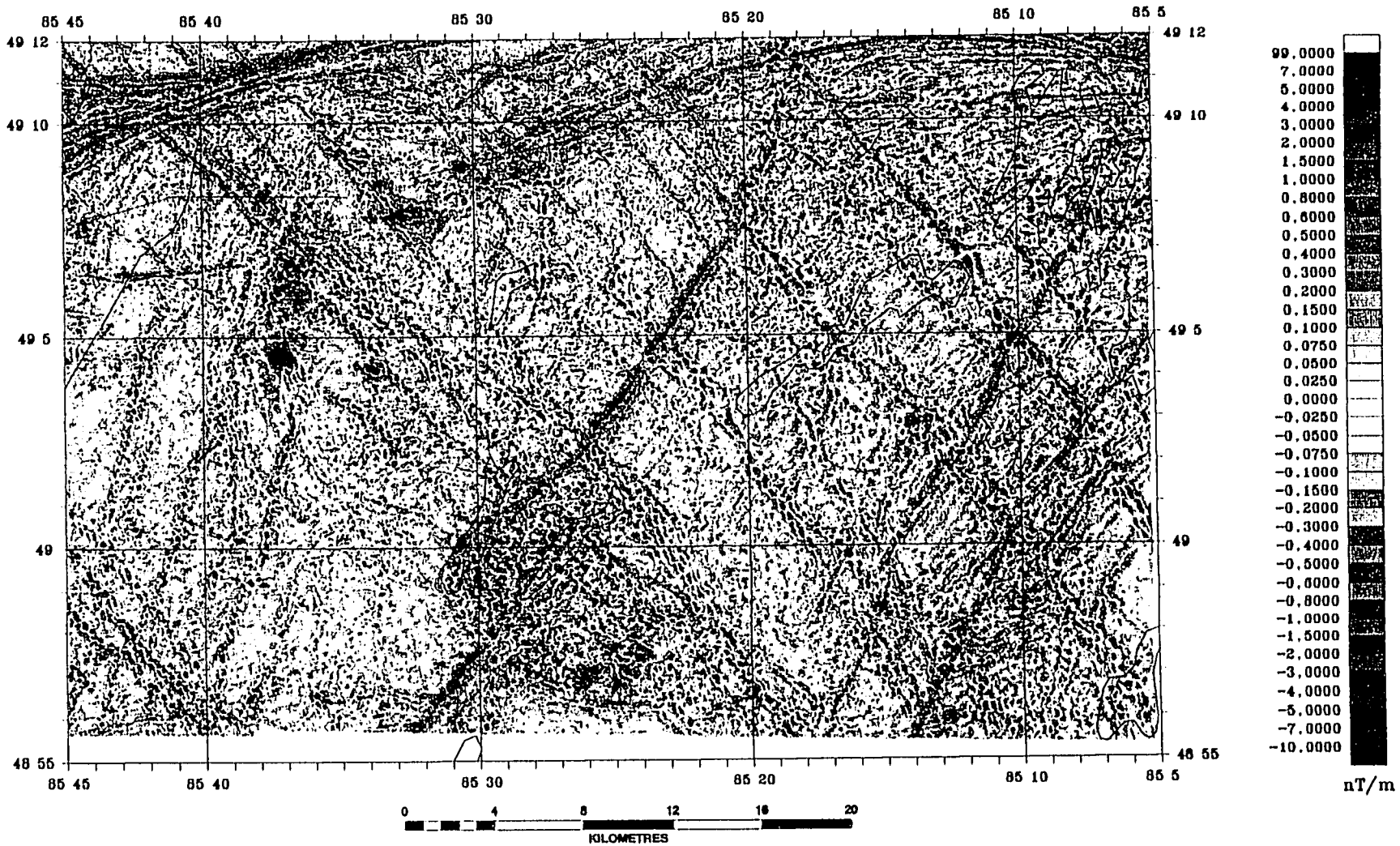

Fig. 5.25.1. First vertical derivative, Banana Lake antiform within the Black Pic batholith.

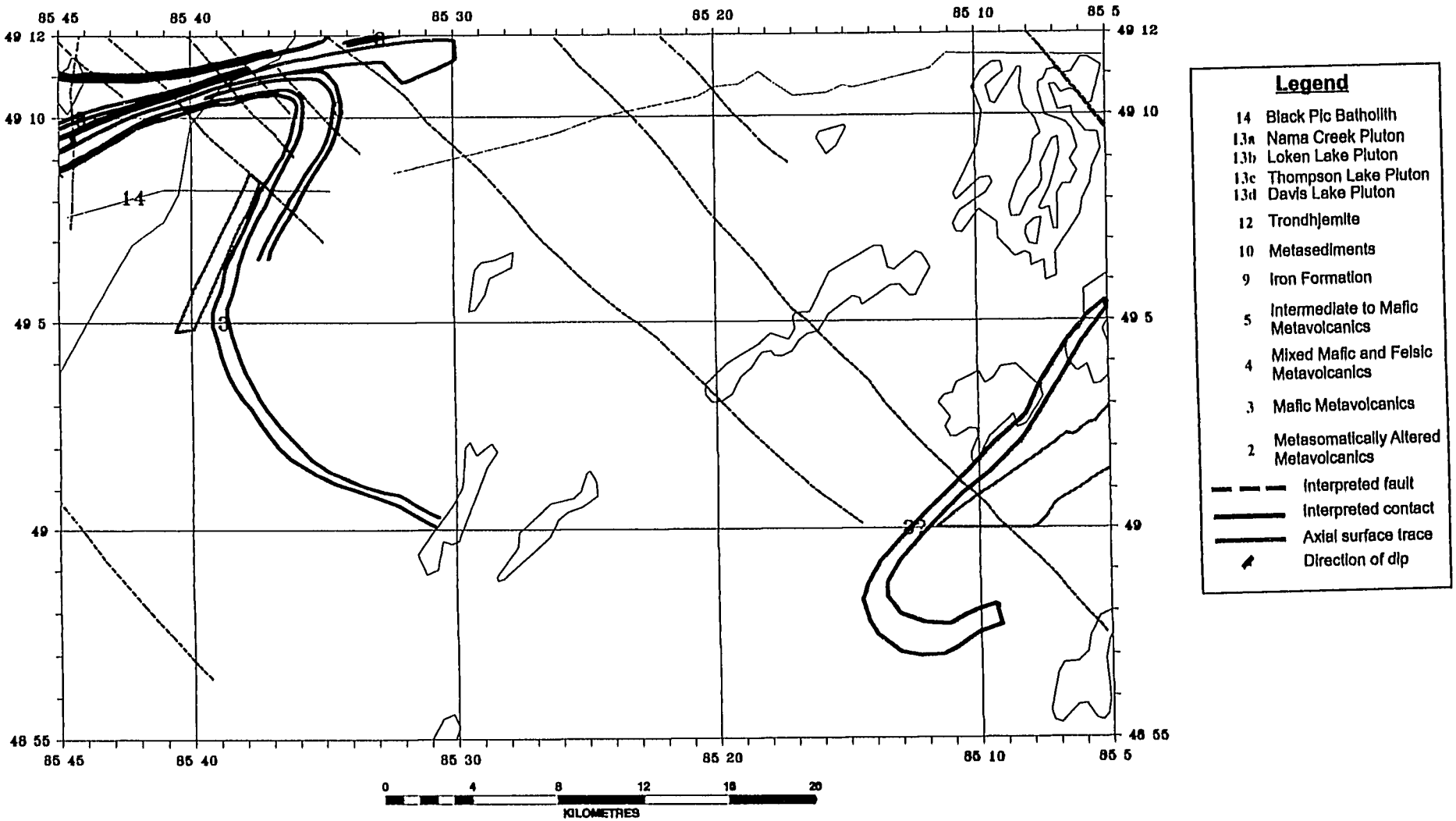

Fig. 5.25.2. Metavolcanics (in green, mapped by Giguerre, 1972) and interpreted magnetics, near the Banana Lake antiform within the Black Pic batholith. Dashed lines are interpreted faults.

and trend more to the south towards the southwest. Here the units are traceable as curvilinear segments of magnetic lows often subparallel to Biscotasing dykes. These magnetic features are seen to be folded southeast of N49° W85°15'. Giguerre (1972) mapped metavolcanics striking parallel to the low magnetic features just northeast of the interpreted fold hinge area (Fig. 5.25.1). The linear vertical gradient highs and lows, interpreted as representing supracrustal rock included in the Black Pic batholith, are segmented and reoriented between the northwest trending Matachewan dykes and their subparallel faults. The apparent reorientation of these magnetic features is interpreted to reflect the effect of vertical offset of the faults.

The fine wispy magnetic anomalies, interpreted to represent supracrustal inclusions with the Black Pic batholith, define broad open folding patterns continuous with the D_3 folds of the Manitouwadge greenstone belt. The axial surface traces of the folds within the southern Black Pic batholith trend to the northeast. Toward the north, the axial surface traces of the D_3 fold train rotate to an orientation roughly parallel the Wawa-Quetico boundary. Within a transpressive regime folds will form at right angles to the maximum principle stress direction and, as they are in an oblique zone, the folds are *en echelon* structures (Fig. 5.26). With progressive closing of the zone, the axes of the folds rotate to more parallel to the oblique zone (Harland, 1971). Coupled with the Z asymmetry of the folds (as noted by Zaleski et al., 1995), the rotation implies that a dextral transpression regime at the boundary drove the deformation.

The residual total field magnetic map (Fig. 5.27) has a series of lobate magnetic anomalies with northeast trending axes, repeated *en echelon* across the centre of the sheet. A broad, lower intensity anomaly occurs trending to the northeast south of the Manitouwadge synform within the Black Pic tonalite and mimics the lobate pattern. It is truncated to the southwest by the large,

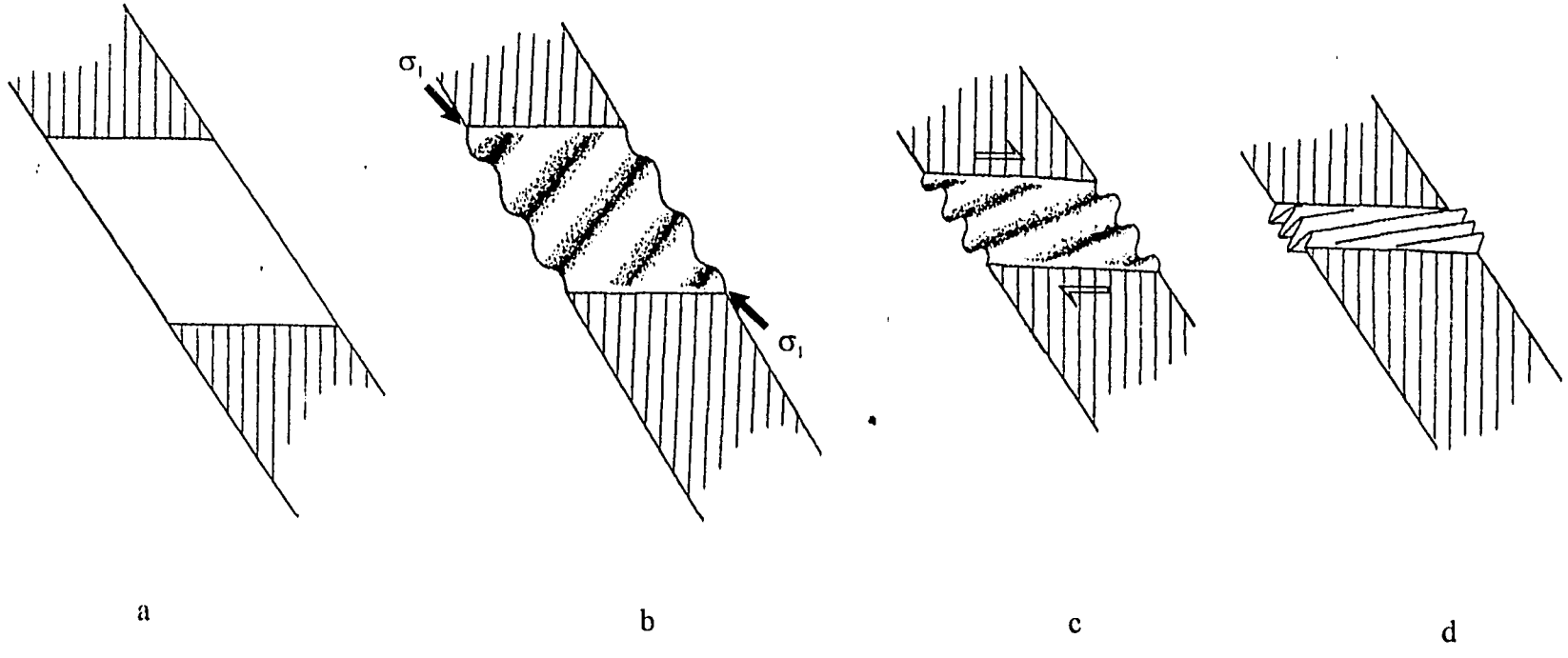

Fig. 5.26. Diagram of two plates closing in a dextral transpressive regime. a) intiation of closure, b) formation of *en echelon* folds perpendicular to the maximum principal stress (σ_1), c) and d) rotation of fold trends towards the orientation of the plate boundary. (After Harland, 1971).

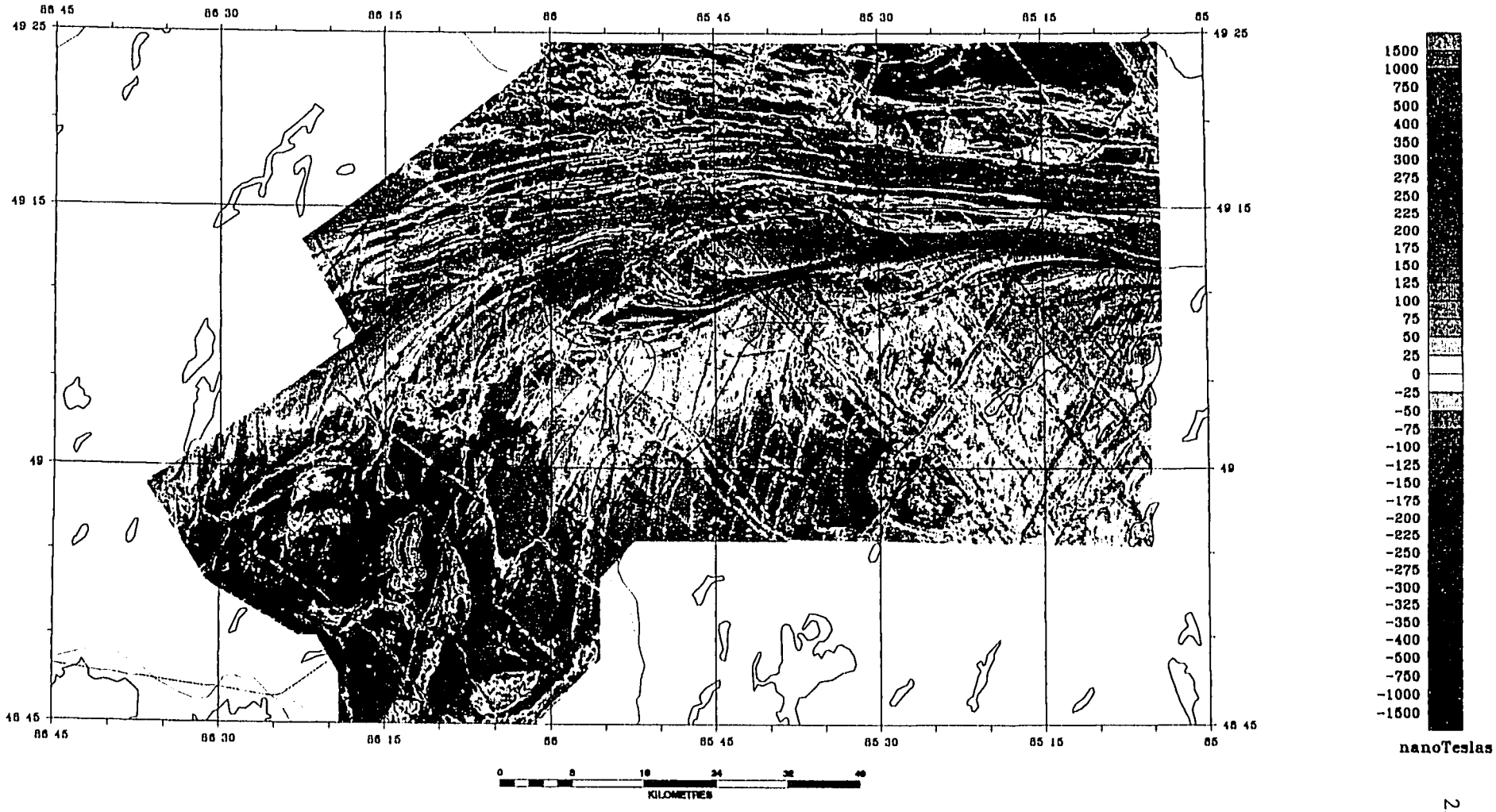

Fig. 5.27. Residual total field magnetics.

roughly rectangular, late Fourbay intrusion (arrow Fig. 5.27). The linear magnetic features within the northeastern part of the anomaly can largely be attributed to dykes and faults. The area appears to have limited amounts of included supracrustal rock. The anomaly may represent a higher susceptibility phase of the Black Pic batholith or perhaps a folded greenstone belt, similar to the Manitouwadge synform, but underlying the batholith, with the high frequency, folded magnetic signature of folded greenstones attenuated due to the depth of burial. No measured susceptibilities of the tonalite in this area are available to attribute the anomaly to either possibility.

6.0. SUMMARY AND CONCLUSIONS

The purpose of this study is to investigate and improve advanced processing and interpretation techniques for aeromagnetic data and to apply them to high resolution, detailed surveys over the Manitouwadge greenstone belt. The aim is to optimize the data quality and maximize the utility of the interpretation techniques. The Manitouwadge area is an excellent region for such a case study because of the availability of high resolution, detailed aeromagnetic data as well as recently published detailed geological mapping. The ultimate goal is to extend geological interpretation from areas of detailed mapping to areas where the geology is not as well known, due to limited outcrop and/or lower mapping priority.

In this study, it is assumed that data acquisition and primary data processing effects on the magnetic field sampling have been reconciled. The next greatest source of error in magnetic interpretation is derived from gridding. The process of interpolating 2D high resolution magnetic data to a 3D representation introduces lower magnetic gradients to the grid where it is not supported by actual data. Furthermore, the 2D data will usually have more high frequency information than can be reasonably interpolated into a grid. If the ratio of flight line spacing to flying height above the magnetic source is too great, upward continuation must be applied to the gridded data in order to reduce aliasing to an acceptable level. The gridding interval must be chosen judiciously to maximize the frequency content of the grid and minimize the relaxed gradients generated by the gridding algorithm. As noted by Reid (1980), the problems introduced by gridding can be reduced by flying surveys at higher altitudes and gridding at wider intervals, but this improvement comes at an intolerable loss of high frequency information.

Any line-to-line levelling errors will be evident in derivative-filtered grids of the data. Micro-

levelling is generally an important step in improving the quality of the data and is specifically useful when the quality of the line-to-line levelling is low. It has been clearly shown that the method reduces effects that are parallel to the flight lines and represent some error in the levelling process. The method is flexible enough to remove longer wavelength errors in the case of very poorly levelled data. Micro-levelling may not be warranted on data that has been properly levelled line-to-line and when there has been limited short term variation in the Earth's magnetic field.

Survey-to-survey levelling was performed to produce a seamless grid. The vertical derivative of the master grid of all eleven surveys displays no edge effects at the boundaries of the sub-surveys. The method as developed here is simple, effective and powerful. The high frequency corrections must be limited to a zone no wider than the flight line spacing to avoid introducing errors to the data.

The trend reinforcement used in this study improves the gridding by reinforcing all trends (outside the exclusion angle), but cannot reinforce linear features striking at low angles to the flight lines. In addition, this method only reinforces maxima and minima. Away from the reinforcement points, the gridding algorithm will still produce relaxed gradients. The method could be improved by extending trend reinforcement to include inflection points of anomalies associated with reinforced maxima and minima, to better define the reinforced anomalies. As trend reinforcement methods improve, the grid interval can be reduced producing grids which contain more of the high frequency information available in the flight line data.

Filtering gridded data enhances different frequency components, which can facilitate interpretation, and is the basis of many 3D interpretation techniques. Careful attention must be

paid to the choice of filters and filter parameters to avoid introducing error generated by Gibb's phenomenon to the filter products. Gibb's phenomenon, also caused by sharp gradients or discontinuities in the input data, can be reduced by using well-levelled input grids, low pass filtering (or upward continuation) and adequate padding or tapering of the data.

3D interpretation techniques have become popular over the last ten years. Euler deconvolution and analytic signal are becoming widely available tools for the interpreter. As these methods are based on derivatives of the magnetic field, high quality gridding is essential to their utility. As a result, examples of the methods (Reid et al. 1990, for example) are usually presented using gridded data with small ratios of line spacing to grid interval. However, it has been shown here that geologically significant interpretations of magnetic data using these techniques can be made even when the input gridded data has a high ratio of line spacing to grid interval. This allows for significantly higher resolution interpretation. However, a critical limit was reached where this ratio was greater than about 6:1 and flight line related features became unacceptable.

The features enhanced by the interpretation techniques used in this study are commonly visible in the total magnetic field. The techniques serve to break the magnetic field down to components or characteristics of the field that may not be obvious, especially to non-experienced interpreters and to quantify or define features. These techniques focus the interpreter on the feature of the magnetic field required for the interpretation at hand.

The apparent susceptibility reduces the magnetic intensity to a measurable rock property that can be characterized for a given lithological unit.

The analytic signal maxima provide a semi-quantitative indication of the boundary between

domains of sufficiently contrasting magnetization. This derivative-based method accentuates noise as well as the high frequency signal. This results in a discontinuous alignment of AS maxima along seemingly continuous magnetic features. The method is very sensitive to aliasing effects in the grid and significant noise reduction was achieved by using a 2D filter to generate the vertical derivative used in calculating the analytic signal. This approach is reasonable for anomalies that trend perpendicular to the flight line direction and appears to provide acceptable results throughout the study area.

The horizontal gradient of pseudo-gravity is the derivative of the integral of the magnetic field and is, as a result, a lower order representation of the magnetic field than the analytic signal. It is less noisy than the analytic signal and has more continuous maxima. The HGPG maxima act as a guide for the theoretically more accurate AS maxima.

The combination of the analytic signal maxima and the horizontal gradient of the pseudo-gravity maxima provide information on the dip of the boundary defined by the analytic signal. Determining dips of magnetic units in this manner is complicated by the different sensitivities of the two maxima. It is of prime importance to ensure that the AS and HGPG maxima are responding to the same source.

The potential field tilt map, although based on the same orthogonal derivatives, appears less noisy than the analytic signal. It is excellent for marking faults where the faults are demagnetized linear features.

Euler deconvolution has limited application when the depth to magnetic source in the area of interest is relatively constant. The depth solutions in that case are too sparse, discontinuous and unfocused to be useful for marking magnetic boundaries near the surface. They can be used

to investigate contacts at depth not imaged by AS or HGPG maxima.

Conventionally, inadequacies in gridded data are acknowledged and accounted for by experienced interpreters. The high frequency information contained in the original flight line data were maintained by performing the interpretation techniques on 2D data and allowing the interpreter to decide how to continue trends across lines, rather than using a minimum curvature surface to dictate the interpolation. Both Euler deconvolution and the analytic signal methods were originally derived for the 2D case. As most surveys are designed to have flight lines perpendicular to the local geologic strike, the 2D case would be sufficient for most features. Generally, a 2D interpretation would maximize the use of the frequency content of the data and 3D interpretation interpolates the magnetic features best where the across line component is constant. This means that a 3D interpretation is most reliable where a 2D interpretation is defined. Still, it remains to the interpreter whether it is more useful to have all the available frequencies or to have a 3D image of the aliased field.

Using known geology to calibrate the interpretation of the high resolution magnetics within the study area offers insights into areas of limited outcrop or mapping. To make a reasonable extrapolation from the known to the unknown based on magnetics requires information on the magnetic petrology of the area and the geological controls on the magnetization of the rocks, as well as an understanding of the limitations of the interpretation methods.

To interpret the map pattern and extent of geological units from magnetics with the aid of limited areas of well-mapped geology, one must characterize the magnetic signature of the known and project extensions of the units into areas with possibly different signatures due to metamorphic effects, variable depth to source and geological/environmental conditions. The

magnetic intensity differences between Quetico metagreywackes and those found in the D_2 Manitouwadge syncline are an example of metamorphic conditions altering the magnetic signature. Attenuation of signal over lakes and swamps can lead to truncation of magnetic linear features, as seen in the mixed mafic and intermediate metavolcanics under Fox Lake. Demagnetization of highly magnetized units due to circulating ground water along faults can complicate interpretation if the faults are not recognized.

Extrapolation of the known geology, largely limited to the supracrustal rocks of the Manitouwadge greenstone belt, to the less well known areas, principally poorly exposed areas of the greenstone belt and the Black Pic batholith, allows targeting of areas of interest for further study. The magnetically interpreted Z-fold east of One Otter Lake is such an area, where resolving the geological and magnetic interpretation may have local and regional deformation implications. Interpreting the location of significant, previously unrecognized volumes of iron formation, given its association in the inner volcanic belt with VMS deposits, provides useful exploration targets. Extrapolating supracrustal rocks into the Black Pic batholith provides an opportunity to look at the D_3 tectonic regime.

The magnetic interpretation map (Map 6) compares favourably with the mapped geology of Zaleski et al. (1995). Certainly the interpretation was affected and biased by the *a priori* information on the geology map and large portions of the geology map were interpreted from the preliminary magnetic data. In areas of good exposure where the geology has been mapped in detail, the 150m line spacing aeromagnetic survey data interpretation only roughly approximates the resolution of the geological mapping. Conversely, in areas of poor exposure and more complex deformation, the magnetic interpretation offers an improvement on the mapped

geology. The interpretations are documented as being based on the components of the magnetic signature as accentuated by the various interpretation techniques.

The magnetic interpretation, together with *in situ* magnetic susceptibility measurements, indicate the magnetic striping of the Quetico metasediments is locally explained by the preferential development of secondary, metamorphic magnetite in certain strata of those rocks. This could be extended to all east-west oriented linear magnetic features within the Quetico metasediments, however, with the high degree of infolding of the Quetico subprovince with the Wawa subprovince, the presence of Manitouwadge greenstone belt supracrustal inclusions is highly probable.

Curvilinear magnetic lineaments within the northern Black Pic batholith clearly represent inclusions of supracrustal rock, highly metamorphosed, with variably developed secondary magnetite. These linear features offer the opportunity to interpret the variable deformation of the greater Black Pic batholith and it's relationship to regional tectonic evolution. Future work based on the recognition of included supracrustal material within the Black Pic batholith from the magnetic data has bearing on regional deformation and the relationship between the local greenstone belts. The relationship between the Schreiber-Hemlo and Moshkinabi greenstone belts with the Manitouwadge greenstone belt is not as simple as the latter's relationship with the Faries Lake greenstone belt. Complex deformation, both brittle and ductile, complicate the relationships.

The folding of the Nama Creek pluton, mixed mafic to intermediate metavolcanics, and the synvolcanic trondhjemite about the Blackman Lake antiform are more complicated than can be mapped geologically. The geological interpretation indicates folding that contradicts the

magnetic pattern and the magnetic interpretation of the map extent of these units contradicts the geological evidence. A reasonable explanation must resolve the two opposing views of the same rocks. The geological mapping appears to extend the Nama Creek pluton to the east and south to include a single outcrop. If there is only one isolated outcrop, it may represent a local intrusion of the Nama Creek pluton into the metavolcanics, a glacially transported boulder or a misidentified local intrusion related to the Thompson Lake or Loken Lake plutons or the Black Pic batholith. Location errors in the magnetic data seem unlikely given the electronic positioning used for horizontal control. A sudden change in the magnetic character of the Nama Creek pluton also seems unlikely given its relatively homogeneous pattern seen elsewhere. As the magnetics sample the rock to some depth, a thin sheet of the Nama Creek pluton overlying the metavolcanics may be undetected in a magnetic interpretation. If there is sufficient interest in this area, it would be a good example of using magnetic data to target followup geological mapping.

The proposed Thompson Lake pluton is well supported by the magnetic interpretation. The very different magnetic signature of the Thompson and Loken Lake plutons and the presence of rather well defined contacts with each other and surrounding units support the interpretation. On the other hand, the proposed Davis Lake pluton is at the limit of plausibility.

The utility of the 3D interpretation techniques presented in this study will improve as the quality of the input data improves. Aeromagnetic survey quality has improved greatly as a result of GPS horizontal and vertical control, modern processing techniques and an increased awareness of the importance of quality control, including smaller tie line to traverse line ratios. The quality of older data will continue to be improved by the application of new techniques such

as decorrugation (a longer wavelength version of micro-levelling) and trend reinforcement. The 3D interpretation techniques will become more important and useful as gridded data approaches an accurate representation of the magnetic field.

REFERENCES

Berger, B.R., 1985. Hearst-Kapuscasing area, district of Cochrane. Ontario Geological Survey, Miscellaneous Paper 126, 95-98.

Breiner, S., 1980. Applications for portable magnetometers. In Practical Geophysics. Northwest Mining Association, Spokane, WA.

Blakely, R.J., and Simpson, R.W., 1986. Approximating edges of source bodies from magnetic or gravity anomalies. Geophysics, **51**, No. 7, 1494-1498.

Briggs, I., 1974. Machine contouring using minimum curvature: Geophysics, **39**, 39-48.

Brigham, E.O., 1974. The Fast Fourier Transform. Prentice-Hall, Inc. New Jersey.

Buchan, K., Mortensen, J.K., and Card, K.D., 1993. Northeast-trending Early Proterozoic dykes of the southern Superior Province: multiple episodes of emplacement recognized from integrated paleomagnetism and U-Pb geochronology. Canadian Journal of Earth Sciences, **30**, 1286-1296.

Burch, J.L., 1974. Observations of interactions between interplanetary and geomagnetic fields. Reviews of Geophysics and Space Physics, **13**, No. 3, 363-376.

Card, K., 1990. A review of the Superior Province of the Canadian Shield, a product of Archean accretion. Precambrian Research **48**, 99-156

Clark, D.A., 1983. Comments on magnetic petrophysics. Bulletin of the Australian Society of Exploration Geophysicists, **14**, 49-62.

Clark, D.A., 1997. Magnetic petrophysics and magnetic petrology: aids to geological interpretation of magnetic surveys. Airborne magnetic and radiometric surveys: AGSO Journal of Australian Geology and Geophysics, **17**, No. 2, 83-104.

Coates, M.E., 1970. Vein Lake Sheet, Thunder Bay District. Map 2192. Ontario Department of Mines.

Cooley, J.W. and Tukey, J.W., 1965. An algorithm for machine calculation of complex Fourier series. Math. Computation. **19**, 297-301.

Cordell, L., 1979. Gravimetric expression of graben faulting in Santa Fe Country and the Espanola Basin, New Mexico. New Mexico Geol. Soc. Guidebook, 30th Field Conference, 59-64.

Cordell, L. and Grauch, V.J.S., 1987. Limitations of determining density or magnetic boundaries from the horizontal gradient of gravity or pseudogravity data. Geophysics, **52**, No. 1, 118-121.

Corfu, F. and Muir, T.L., 1989. The Hemlo-Heron Bay greenstone belt and Hemlo Au-Mo deposit, Superior province, Ontario, Canada 1. Sequence of igneous activity determined by zircon U-Pb geochronology. Chemical Geology (Isotope Geology Section), **79**.

Davis, D.W., Schandl, E.S., and Wasteneys, H.A., 1994, U-Pb dating of minerals in alteration halos of Superior Province massive sulphide deposits: syngenesis vs. metamorphism. Contributions to Mineralogy and Petrology, 115, 427-437.

Davis, J.C., 1973. Statisitics and Data Analysis in Geology. John Wiley & Sons Inc.

Dods, S.D., Teskey, D.J., and Hood, P.J., 1985. The new series of 1:1 000 000-scale magnetic anomaly maps of the Geological Survey of Canada: Compilation techniques and interpretation. The Utility of Regional Gravity and Magnetic Anomaly Maps. Society of Exploration Geophysicists. Tulsa, Oklahoma.

Fahrig, W.F., and West, T.D., 1986. Diabase dike swarms of the Canadian Shield. Geological Survey of Canada, map 1627A.

Giguere, J.F., 1972. Granitehill Lake area, Thunder Bay and Algoma Districts. Map 2219. Ontario Department of Mines and Northern Affairs.

Grant, F.S., and West, G.F., 1965. Interpretation Theory in Applied Geophysics. McGraw-Hill, New York.

Gunn, P.J., 1997. Enhancement and presentation of airborne geophysical data. Airborne magnetic and radiometric surveys: AGSO Journal of Australian Geology and Geophysics, **17**, No. 2, 63-76.

Hansen, R.O., Pawlowski, R.S., and Wang, X., 1987. Joint use of analytic signal and amplitude of horizontal gradient maxima for three-dimensional gravity data interpretation. 57th Ann. Internat. Mtg., Soc. Expl. Geophys. Expanded Abstracts, 100-102.

Harland, W.B., 1971. Tectonic transpression in Caledonian Spitsbergen. Geol. Mag. 108, 27-42.

Heamon, L.M., 1988. A precise U-Pb zircon age for a Hearst dyke. Geological Association of Canada, Program with Abstracts. **13**, A53.

Hood, P.J., 1965. Gradient measurements in aeromagnetic surveying. Geophysics, **30**, 891-902.

Jensen, L.S., 1976. A new cation plot for classifying subalkalic volcanic rocks. Ontario Division of Mines, Miscellaneous Paper 66.

Keating, P. 1997. Automated trend reinforcement of aeromagnetic data: Geophysical Prospecting, **45**, 521-534.

Luyendyk, A.P.J. 1997, Processing of airborne magnetic data: In Airborne magnetic and radiometric surveys: AGSO Journal of Australian Geology and Geophysics, **17**, No. 2, 31-38.

Mah, D., 1995. Geological and Structural Models of the Manitouwadge Greenstone Belt Based on Total Field Aeromagnetic Data. Unpublished B.Sc. Thesis.

McGrath, P., 1996. Terrestrial magnetism, its terminology and manifestations from an interpreter's point of view. Interpretation of gravity and magnetic anomalies for non-specialists. Canadian Geophysical Union Short Course Notes.

McIntyre, J.I., 1980. Geological Significance of Magnetic Patterns related to Magnetite in Sediments and Metasediments - A Review. Bull. Aust. Soc. Explor. Geophys. **11**, No. 1/2.

Miller, H. and Singh, V., 1994. Potential field tilt - a new concept for location of potential field sources. Journal of Applied Geophysics, **32**, 213-217.

Milne, V.G., 1974. Mapledoram-Gemmell, Thunder Bay District. Map 2280, Ontario Division of Mines.

Nabighian, M.N., 1972. The analytic signal of two-dimensional magnetic bodies with polygonal cross-section: its properties and use for automated anomaly interpretation. Geophysics, **37**, No. 3, 507-517.

Pan, Y., and Fleet, M.E., 1994. Granulite-facies metamorphism in the Quetico Subprovince, north of Manitouwadge, Ontario. Canadian Journal of Earth Sciences, **31**, 1427-1439.

Pedersen, L.B., 1989. Relations between horizontal and vertical gradients of potential fields. Geophysics, **54**, 662-663.

Percival, J., 1989. A regional perspective of the Quetico metasedimentary belt, Superior

Province, Canada. Canadian Journal of Earth Sciences, **26**, 677-693.

Press, W.H., Flannery, B.P., Teukolsky, S.A., and Vetterling, W.T., 1986. Numerical Recipes: The art of scientific computing. Cambridge University Press, New York.

Pye, E.G., 1957. Geology of the Manitouwadge area. Ontario Department of Mines, Annual Report 66.

Reford, S. et al. 1990. Ontario master aeromagnetic grid; a blueprint for detailed compilation of magnetic data on a regional scale. Society of Explartaion Geolphysicists, Sixtieth annual international meeting and exposition; Expanded Abstracts, 617-620.

Reid, A.B., 1980. Aeromagnetic survey design. Geophysics, **45**, 973-976.

Reid, A.B., Allsop, J.M., Granser, H., Millett, A.J., and Somerton, I.W. 1990. Magnetic interpretation in three dimensions using Euler deconvolution. Geophysics, **55**, 80-91.

Roest, W., Verhoef, J., and Pilkington, M., 1992. Magnetic interpretation using the 3-D analytic signal. Geophysics, **57**, No. 1, 116-125.

Sharma, P.V., 1976. Geophysical methods in geology. Elsevier North-Holland Inc. New York.

Spector, A. and Grant, F.S., 1970. Statistical models for interpreting aeromagnetic data. Geophysics, **35**, 293-302.

Swain, C.J. 1976. A FORTRAN IV program for interpolating irregularly spaced data using the difference equations for minimum curvature: Computers & Geosciences, **1**, 231-240.

Telford, W.M., Geldart, L.P. and Sheriff, R.E., 1990. Applied Geophysics. Cambridge University Press. New York.

Teskey, D.J. and Hood, P.J., 1991. The Canadian aeromagnetic database; evolution and applications to the definition of major crustal boundaries. Tectonophysics. **192**, No. 1-2, 41-56.

Teskey, D.J., and Irvine, J., 1996. Aeromagnetic survey design. Interpretation of gravity and magnetic anomalies for non-specialists. Canadian Geophysical Union Short Course Notes.

Thompson, D.T. 1982. EULDPH: A new technique for making computer assisted depth estimates from magnetic data. Geophysics, **47**, No. 1, 31-37.

Williams, H.R., Stott, G.M., Heather, K.B., Muir, T.L., and Sage, R.P., 1991. Wawa Subprovince. Geology of Ontario, Special Volume 4, Part 1.

Yunsheng, S., Strangway, D.W., and Urquhart, W.E.S., 1985. Geologic interpretation of a high-resolution aeromagnetic survey in the Amos-Barraute area of Quebec. The Utility of Regional Gravity and Magnetic Anomaly Maps. Society of Exploration Geophysicists. Tulsa, Oklahoma.

Zaleski, E. and Peterson, V.L., 1995. Geology of the Manitouwadge greenstone belt overlain on shaded relief of total field magnetics. Geological Survey of Canada Open File 3034.

Zaleski, E., Peterson, V.L., Lockwood, H., and van Breeman, O., 1995. Geology, structure and age relationships of the Manitouwadge greenstone belt and the Wawa-Quetico subprovince boundary, northwestern Ontario, Field guidebook. Geological Survey of Canada Contribution 13995.

APPENDIX 1 - MEASURED MAGNETIC SUSCEPTIBILITIES

This appendix contains measured magnetic susceptibilities of rock samples from the study area provided by Dr. Eva Zaleski, Geological Survey of Canada. The measurements are grouped by units as defined by Zaleski et al. (1995) for the rocks of the Manitouwadge greenstone belt. The 'code' field describes features of the sample and a list of code terms follows the list of measurements. Each group is summarized by the minimum, maximum, average and standard deviation. These statistics must be interpreted with the clear understanding that the populations are undersampled and may be biased toward non-typical members of the unit.

UNIT	CODE	k(10-3 si)	LATITUDE	LONGITUDE
2	AL	2.410	49 9 23	-85 48 38
2	AL	2.890	49 12 25	-85 32 52
2	AL	27.900	49 14 22	-85 37 30
2	AL	4.550	49 12 34	-85 32 58
2	AL ly	2.200	49 14 22	-85 37 30
2	AL ly	5.280	49 14 22	-85 37 30
2	ALFLcm	12.500	49 10 23	-85 41 23
2	ALFLsu	0.790	49 14 22	-85 37 30
2	FL AL	0.400	49 10 26	-85 41 21

Minimum = 0.400000
Maximum = 27.9000
Average = 6.54667
Average deviation = 6.06815
Standard deviation = 8.78419

UNIT	CODE	k(10-3 si)	LATITUDE	LONGITUDE
3	GB	0.394	49 8 39	-85 51 54
3	GB	2.031	49 8 9	-85 57 16
3	GB	45.213	49 8 34	-85 49 34
3	GBF	0.752	49 8 35	-85 47 36
3	IV	0.837	49 8 25	-85 53 51
3	MF	0.387	49 7 52	-85 59 44
3	MF	0.504	49 8 42	-85 51 54
3	MF	0.643	49 9 36	-85 47 55
3	MF	0.710	49 10 33	-85 41 16
3	MF	0.755	49 7 53	-85 57 20
3	MF	0.776	49 7 52	-85 57 40
3	MF	1.029	49 8 8	-85 58 39
3	MF	1.046	49 8 36	-85 49 36
3	MF	1.880	49 9 10	-85 57 0
3	MF	2.200	49 8 7	-85 57 13
3	MF	27.676	49 8 39	-85 47 36
3	MF	32.700	49 8 34	-85 49 34

UNIT	CODE	k(10-3 si)	LATITUDE	LONGITUDE
3	MF	76.125	49 8 8	-85 58 39
3	MF lm	0.623	49 10 21	-85 39 18
3	MFpw	0.685	49 8 35	-85 47 36

Minimum =	0.387000
Maximum =	76.1250
Average =	9.84830
Average deviation =	14.2321
Standard deviation =	20.2018

UNIT	CODE	k(10-3 si)	LATITUDE	LONGITUDE
4	FL	29.300	49 9 48	-85 49 55
4	FLq	4.159	49 9 55	-85 49 31
4	MF	2.329	49 9 44	-85 49 53

Minimum =	2.32900
Maximum =	29.3000
Average =	11.9293
Average deviation =	11.5804
Standard deviation =	15.0712

UNIT	CODE	k(10-3 si)	LATITUDE	LONGITUDE
5	Bts	10.400	49 14 1	-85 42 54
5	CS	0.650	49 14 22	-85 37 30
5	MF	0.790	49 12 4	-85 33 34
5	MF	0.960	49 12 53	-85 33 20
5	MF	1.010	49 11 43	-85 59 49
5	MF	12.980	49 14 3	-85 43 1
5	MF	26.300	49 14 6	-85 43 7
5	MF	3.600	49 15 56	-85 40 49
5	MF	49.800	49 14 34	-85 39 18
5	Mf	1.230	49 14 3	-85 43 1

Minimum =	0.650000
Maximum =	49.8000
Average =	10.7720
Average deviation =	11.3528
Standard deviation =	16.0051

UNIT	CODE	k(10-3 si)	LATITUDE	LONGITUDE
6	Cb,cs	0.182	49 9 25	-85 52 41
6	FL	10.552	49 9 47	-85 51 21
6	FL qcs	0.183	49 9 45	-85 52 17
6	FLQ	0.276	49 9 26	-85 52 52
6	IV	0.199	49 8 13	-85 58 13

UNIT	CODE	k(10-3 si)	LATITUDE	LONGITUDE
6	IV	0.273	49 8 16	-85 58 19
6	IVtf	1.070	49 8 21	-85 57 9
6	TN	0.120	49 8 21	-85 57 9

Minimum =	0.120000
Maximum =	10.55200
Average =	1.60687
Average deviation =	2.23628
Standard deviation =	3.62737

UNIT	CODE	k(10-3 si)	LATITUDE	LONGITUDE
7	FL	0.104	49 7 55	-85 57 27
7	FL	0.140	49 7 56	-85 56 53
7	FL	0.593	49 7 52	-85 57 40
7	FLb	8.112	49 8 43	-85 51 33
7?	FLq	0.265	49 8 50	-85 47 1

Minimum =	1.04000E-01
Maximum =	8.11200
Average =	1.84280
Average deviation =	2.50768
Standard deviation =	3.50989

UNIT	CODE	k(10-3 si)	LATITUDE	LONGITUDE
8	FLq	0.113	49 9 37	-85 49 58
8	FLq	0.248	49 9 28	-85 49 20
8	FLq	2.840	49 9 24	-85 49 38

Minimum =	0.113000
Maximum =	2.84000
Average =	1.06700
Average deviation =	1.18200
Standard deviation =	1.53695

UNIT	CODE	k(10-3 si)	LATITUDE	LONGITUDE
9	IF	91.967	49 13 24	-85 31 40
9a	IF	108.960	49 9 27	-85 50 21
9a	IF	42.221	49 9 42	-85 51 11
9b	IF	287.890	49 8 42	-85 51 33
9b	IFs	244.333	49 8 44	-85 51 53

Minimum =	42.2210
Maximum =	287.890
Average =	155.074
Average deviation =	88.8298
Standard deviation =	105.418

UNIT	CODE	k(10-3 si)	LATITUDE	LONGITUDE
14	TN	4.870	49 14 6	-85 43 7
14c	TN	0.043	49 8 55	-85 53 21
14c	TN	0.148	49 9 12	-85 52 33
14c	TN	5.990	49 12 29	-85 46 58
14c	TNf	0.160	49 9 26	-85 50 22
14c	TNf	0.280	49 8 39	-85 47 36
14c?	TN	0.120	49 11 26	-85 47 30
14c?	TN	11.900	49 11 44	-85 47 20
14c?	TN	13.900	49 12 2	-85 47 10

Minimum = 4.30000E-02
Maximum = 13.9000
Average = 4.15678
Average deviation = 4.45175
Standard deviation = 5.46637

UNIT	CODE	k(10-3 si)	LATITUDE	LONGITUDE
BP-14	FL	0.108	49 7 52	-86 1 0
BP-14	GTf	2.790	49 16 29	-85 46 31
BP-14	TN g	0.170	49 9 16	-85 59 14
BP-14	TN g	1.230	49 9 20	-85 59 18
BP-14	TN g	2.750	49 9 17	-85 59 8
BP-14	TN g	3.310	49 9 12	-85 59 2
BP-14	TN g	3.840	49 8 47	-85 59 11
BP-14	TN ly	4.760	49 8 43	-85 59 8
BP-14	TNf ly	1.830	49 16 19	-85 46 20
BP-14	TNf ly	2.030	49 16 26	-85 46 30
BP-14	TNgHbl	1.890	49 8 33	-85 59 5
BP-14	TNgHbl	3.650	49 8 40	-85 59 8
BP-14	TNgMag	12.200	49 9 8	-86 0 41
BP-14	TNmg	2.487	49 11 38	-85 54 43
BP-14	dt	0.383	49 7 52	-86 1 0
BP-14	pg Mag	21.800	49 16 29	-85 46 31
BP-14 or 1	TN	0.080	49 10 23	-85 41 25
BP-14d	DT	2.820	49 11 43	-85 59 49
BP?-14 or	TNf	0.000	49 14 11	-85 34 22
BP?-14 or	TNg	8.190	49 14 13	-85 34 27

Minimum = 0.
Maximum = 21.8000
Average = 3.81590
Average deviation = 3.17105
Standard deviation = 5.14960

UNIT	CODE	k(10-3 si)	LATITUDE	LONGITUDE
Dead Lk eq	FL	61.600	49 8 23	-85 53 36
Dead Lk eq	QT Mag	65.333	49 8 24	-85 50 31
Dead Lk su	DT Mag	26.400	49 11 49	-85 47 17
Dead Lk su	GB	0.940	49 11 37	-85 47 22
Dead Lk su	IV	230.667	49 12 30	-85 46 52
Dead Lk su	IV	6.660	49 11 44	-85 47 20
Dead Lk su	QT Hbl	15.300	49 14 2	-85 38 58
Dead Lk su	QT al	137.000	49 11 37	-85 47 22
Dead Lk su	QT al	142.000	49 12 30	-85 46 52
Dead Lk su	QT al	143.000	49 12 29	-85 46 58
Dead Lk su	QT al	350.000	49 11 12	-85 47 44
Dead Lk su	QTal	91.500	49 13 49	-85 38 58
Dead Lk su	QZ	1.330	49 12 36	-85 46 47
Dead Lk su	DT	37.203	49 14 13	-85 34 27
Dead Lk su	MF	0.710	49 14 0	-85 33 46
Dead Lk su	MF	16.790	49 15 58	-85 40 20
Dead Lk su	MF	270.000	49 14 11	-85 34 22
Dead Lk su	MF	3.700	49 14 11	-85 33 58
Dead Lk su	QTq/al	337.667	49 12 34	-85 32 58
Dead Lk su	QTq/al	36.650	49 13 17	-85 32 5
Dead Ll su	DT	1.230	49 11 31	-85 47 26

Minimum =	0.710000
Maximum =	350.000
Average =	94.0800
Average deviation =	90.6451
Standard deviation =	113.264

UNIT	CODE	k(10-3 si)	LATITUDE	LONGITUDE
Everest Lk	DT an	0.970	49 16 39	-85 48 48
Everest Lk	DT an	18.100	49 16 39	-85 48 48
Everest Lk	DT an	2.240	49 16 39	-85 48 48
Everest Lk	DT an	3.060	49 16 39	-85 48 48
Everest Lk	DT an	5.110	49 16 39	-85 48 48
Everest Lk	GB	43.900	49 16 54	-85 45 50
Everest Lk	GB	6.820	49 16 39	-85 48 48
Everest Lk	GB an	0.310	49 16 40	-85 46 17
Everest Lk	GB an	1.000	49 16 39	-85 48 48
Everest Lk	GB an	18.300	49 16 39	-85 48 48
Everest Lk	GB an	7.790	49 16 39	-85 48 48

Minimum =	0.310000
Maximum =	43.9000
Average =	9.78182
Average deviation =	9.26446
Standard deviation =	12.9881

UNIT	CODE	k(10-3 si)	LATITUDE	LONGITUDE
Geco trdj-	GTf	12.120	49 15 58	-85 40 10
Geco trnj-	FLQT	23.900	49 11 3	-85 39 43
Geco trnj-	FLqMag	59.700	49 11 0	-85 39 50
Geco trnj-	GT	12.600	49 11 3	-85 47 53
Geco trnj-	GT	25.400	49 13 49	-85 39 11
Geco trnj-	GT	36.100	49 13 52	-85 33 39
Geco trnj-	GT	46.650	49 13 40	-85 33 41
Geco trnj-	GT Mag	26.500	49 12 0	-85 33 36
Geco trnj-	GT Mag	28.300	49 13 47	-85 38 46
Geco trnj-	GTf	12.602	49 10 6	-85 49 40
Geco trnj-	GTf	15.260	49 10 5	-85 49 29
Geco trnj-	QT	0.051	49 9 31	-85 48 32
Geco trnj-	QT	0.130	49 12 55	-85 39 23
Geco trnj-	QT	0.250	49 12 55	-85 39 28
Geco trnj-	QT	0.760	49 12 55	-85 39 14
Geco trnj-	QT	1.300	49 11 12	-85 47 44
Geco trnj-	QT	13.100	49 12 29	-85 46 58
Geco trnj-	QT	24.000	49 14 11	-85 38 41
Geco trnj-	QT	28.744	49 9 47	-85 49 42
Geco trnj-	QT	7.370	49 14 4	-85 38 56
Geco trnj-	QT	7.770	49 11 57	-85 47 11
Geco trnj-	QT	8.360	49 11 31	-85 47 26
Geco trnj-	QT Hbl	91.200	49 13 51	-85 39 16
Geco trnj-	QT Mag	14.700	49 13 48	-85 38 33
Geco trnj-	QT Mag	50.733	49 12 24	-85 33 3
Geco trnj-	QT	0.460	49 13 13	-85 38 5
Geco trnj?	GT	8.190	49 12 4	-85 33 34
Geco trnj?	QT	0.080	49 12 30	-85 46 52
Geco trnj?	QT	0.100	49 11 29	-85 47 27

Minimum =	5.10000E-02
Maximum =	91.2000
Average =	19.1872
Average deviation =	15.8736
Standard deviation =	21.3135

UNIT	CODE	k(10-3 si)	LATITUDE	LONGITUDE
Loken Lk p	GT K	0.420	49 12 45	-85 40 0
Loken Lk p	TN K	0.140	49 11 48	-85 44 22
Loken Lk p	TN K	0.640	49 11 53	-85 44 38
Loken Lk p	TN K	1.220	49 12 5	-85 44 40
Loken Lk p	TN K	1.450	49 12 36	-85 45 44
Loken Lk p	TN K	1.600	49 12 13	-85 44 59
Loken Lk p	TN K	1.610	49 12 13	-85 45 18
Loken Lk p	TN Ka	0.025	49 12 9	-85 36 14

Minimum =	2.50000E-02
Maximum =	1.61000
Average =	0.888125
Average deviation =	0.581875
Standard deviation =	0.658906

UNIT	CODE	k(10-3 si)	LATITUDE	LONGITUDE
MBG msdm-6	SD	0.370	49 8 36	-85 57 47
MGB msdm-1	SD	0.290	49 9 15	-85 51 43
MGB msdm-1	SD	0.370	49 8 51	-85 50 9
MGB msdm-1	SD	0.573	49 8 45	-85 47 30
MGB msdm-6	Mcs	0.260	49 8 18	-85 57 18

Minimum =	0.260000
Maximum =	0.573000
Average =	0.372600
Average deviation =	8.01600E-02
Standard deviation =	0.122143

UNIT	CODE	k(10-3 si)	LATITUDE	LONGITUDE
Marathon d	db	14.500	49 12 4	-85 33 34
Marathon d	db	23.600	49 8 47	-85 59 11
Marathon?	db	19.400	49 14 6	-85 43 7
Marathon?	db	33.720	49 9 35	-85 49 31

Minimum =	14.5000
Maximum =	33.7200
Average =	22.8050
Average deviation =	5.85500
Standard deviation =	8.17183

UNIT	CODE	k(10-3 si)	LATITUDE	LONGITUDE
Matachewan	db	26.500	49 14 1	-85 42 54
Matachewan	db	8.040	49 9 12	-85 59 2
Matachewan	db	8.796	49 8 31	-85 58 11

Minimum =	8.04000
Maximum =	26.5000
Average =	14.4453
Average deviation =	8.03644
Standard deviation =	10.44649

UNIT	CODE	k(10-3 si)	LATITUDE	LONGITUDE
Nama Ck pl	GT K	2.480	49 10 9	-85 54 58
Nama Ck pl	GT K	9.830	49 14 34	-85 39 18
Nama Ck pl	GT k	1.247	49 11 36	-85 53 53
Nama Ck pl	GT k	2.056	49 10 16	-85 54 54
Nama Ck pl	GT k	5.980	49 9 49	-85 55 48

Minimum =	1.24700
Maximum =	9.83000
Average =	4.31860
Average deviation =	2.86912
Standard deviation =	3.57317

UNIT	CODE	k(10-3 si)	LATITUDE	LONGITUDE
Quetico mg	Mcs ly	0.130	49 15 53	-85 34 15
Quetico mg	Mcs ly	0.730	49 15 53	-85 34 15
Quetico mg	Mcs ly	8.400	49 15 53	-85 34 15
Quetico mg	pg	0.020	49 16 57	-85 45 42
Quetico mg	pg	0.070	49 16 57	-85 45 42
Quetico mg	pg	0.080	49 14 59	-85 31 13
Quetico mg	pg Mag	180.000	49 16 39	-85 48 48
Quetico mg	GT	7.350	49 16 39	-85 48 48

Minimum =	2.00000E-02
Maximum =	180.000
Average =	24.5975
Average deviation =	38.8506
Standard deviation =	62.8886

UNIT	CODE	k(10-3 si)	LATITUDE	LONGITUDE
Quetico ms	McsGrt	22.500	49 15 48	-85 40 7
Quetico ms	Mcs	0.251	49 14 59	-85 31 13
Quetico ms	Mcs	0.260	49 16 57	-85 45 42
Quetico ms	Mcs	0.280	49 16 57	-85 45 42
Quetico ms	Mcs	0.320	49 14 59	-85 31 13
Quetico ms	Mcs	0.340	49 16 26	-85 59 4

UNIT	CODE	k(10-3 si)	LATITUDE	LONGITUDE
Quetico ms	Mcs	0.350	49 14 59	-85 31 13
Quetico ms	Mcs	0.630	49 16 26	-85 59 4
Quetico ms	Mcs	1.640	49 15 48	-85 40 7
Quetico ms	Mcs	1.970	49 16 57	-85 45 42
Quetico ms	Mcs	11.600	49 16 26	-85 59 4
Quetico ms	Mcs	13.800	49 16 26	-85 59 4
Quetico ms	Mcs	15.500	49 16 57	-85 45 42
Quetico ms	Mcs	26.600	49 16 26	-85 59 4
Quetico ms	Mcs	3.100	49 16 57	-85 45 42
Quetico ms	Mcs	38.600	49 16 57	-85 45 42
Quetico ms	Mcs	8.750	49 16 26	-85 59 4
Quetico ms	Mcs	9.140	49 16 26	-85 59 4
Quetico ms	Mcs ly	0.240	49 16 57	-85 45 42
Quetico ms	Mcs ly	0.290	49 15 53	-85 34 15
Quetico ms	Mcs ly	0.590	49 15 53	-85 34 15
Quetico ms	Mcs ly	16.700	49 16 26	-85 59 4
Quetico ms	McsGrt	0.333	49 15 7	-85 32 12
Quetico ms	SD	0.429	49 15 15	-85 32 33
Quetico ms	SD mg	0.340	49 14 56	-85 30 28
Quetico ms	SDs	0.402	49 15 12	-85 32 45
Quetico ms	SiMcs	0.060	49 16 26	-85 59 4

Minimum =	6.00000E-02
Maximum =	38.6000
Average =	6.48204
Average deviation =	7.76679
Standard deviation =	9.98412

Codes-
al - altered
AL - orthoamphibole-garnet
an - plagioclase-rich
b - breccia
Bts - biotite schist
C - chert
Cm - cummingtonite
cs - calc-silicate
db - diabase
dt - diorite dyke
DT - diorite
f - foliated
FL - felsic volcanic
g - gneissic
GB - gabbro

Grt - garnet
GT - granite
Hbl - hornblende
IF - iron formation
Ifs - quartz-poor iron formation
IV - intermediate volcanic
K - K-feldspar
lm - laminated
ly - layered
Mag - magnetite
Mcs - mica schist
MF - mafic volcanic
mg - migmatitic
my - straight gneiss (annealed mylonite)
pg - pegmatite
pw - pillowed
q - quartz eyes
Q - quartz phenocrysts
Qmss - quartz-muscovite schist
Qt - trondhjemite
QZ - silicic or quartzose
s - schistose
SD - metagreywacke
SiAL - sillimanite-biotite+\-garnet+\-cordierite schist
su - sulphides
SY - syenite or hornblendite, appinite suite
TN - tonalite

NOTE TO USERS

Oversize maps and charts are microfilmed in sections in the following manner:

LEFT TO RIGHT, TOP TO BOTTOM, WITH SMALL OVERLAPS

The following map or chart has been microfilmed in its entirety at the end of this manuscript (not available on microfiche). A xerographic reproduction has been provided for paper copies and is inserted into the inside of the back cover.

Black and white photographic prints (17"x 23") are available for an additional charge.

UMI

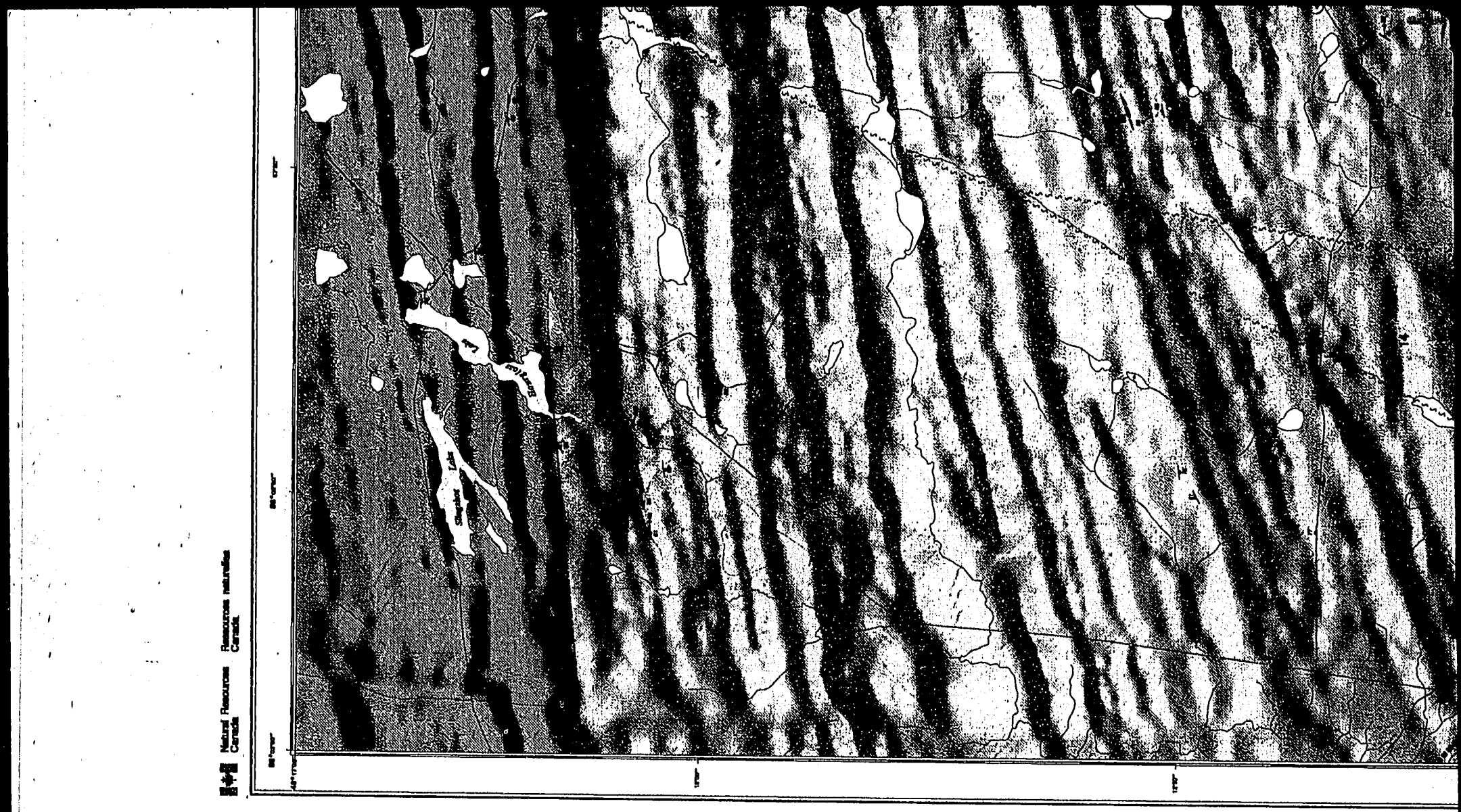

415942.vds 24/4/1998@11:16:38

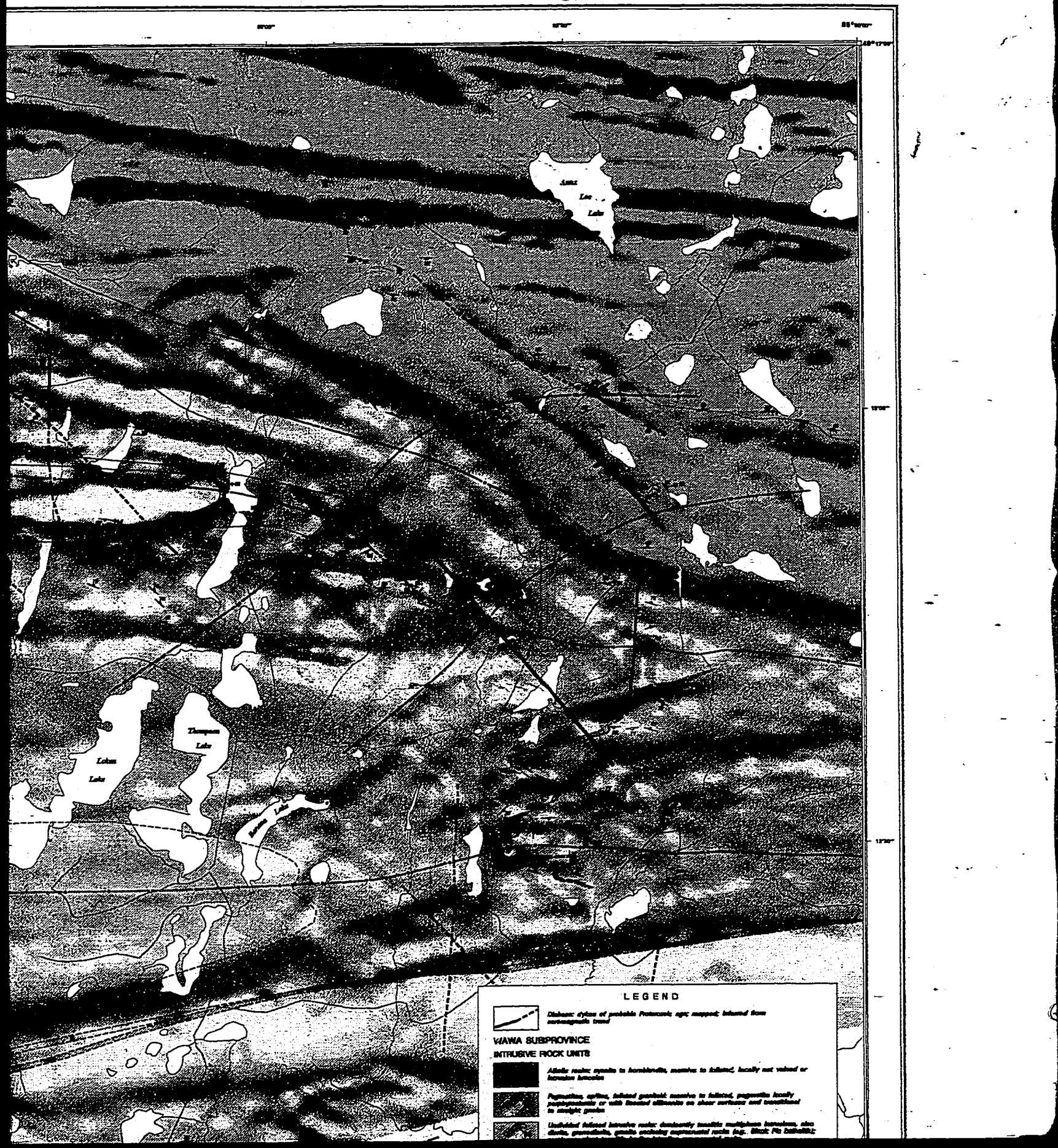
Thompson Lake
Lobstick Lake
Bantam Lake
LEGEND
Diabasic dykes of probable Proterozoic age; magnetic; inferred from aeromagnetic trend
WAWA SUBPROVINCE
INTRUSIVE ROCK UNITS
Mafic rocks; syenite to hornblendite, monzonite to foliated, locally rust colored or limonite bleached
Pegmatitic, aplitic, foliated granitoid; monzonite to foliated, pegmatite locally porphyroblastic or with flattened stilbenite on shear surfaces and transitional to aplitic granite
Undivided foliated intrusive rocks; dominantly monzonitic multiphase intrusions, also diorite, granodiorite, granite excluding supracrustal rocks (eg., Black Pic batholith)

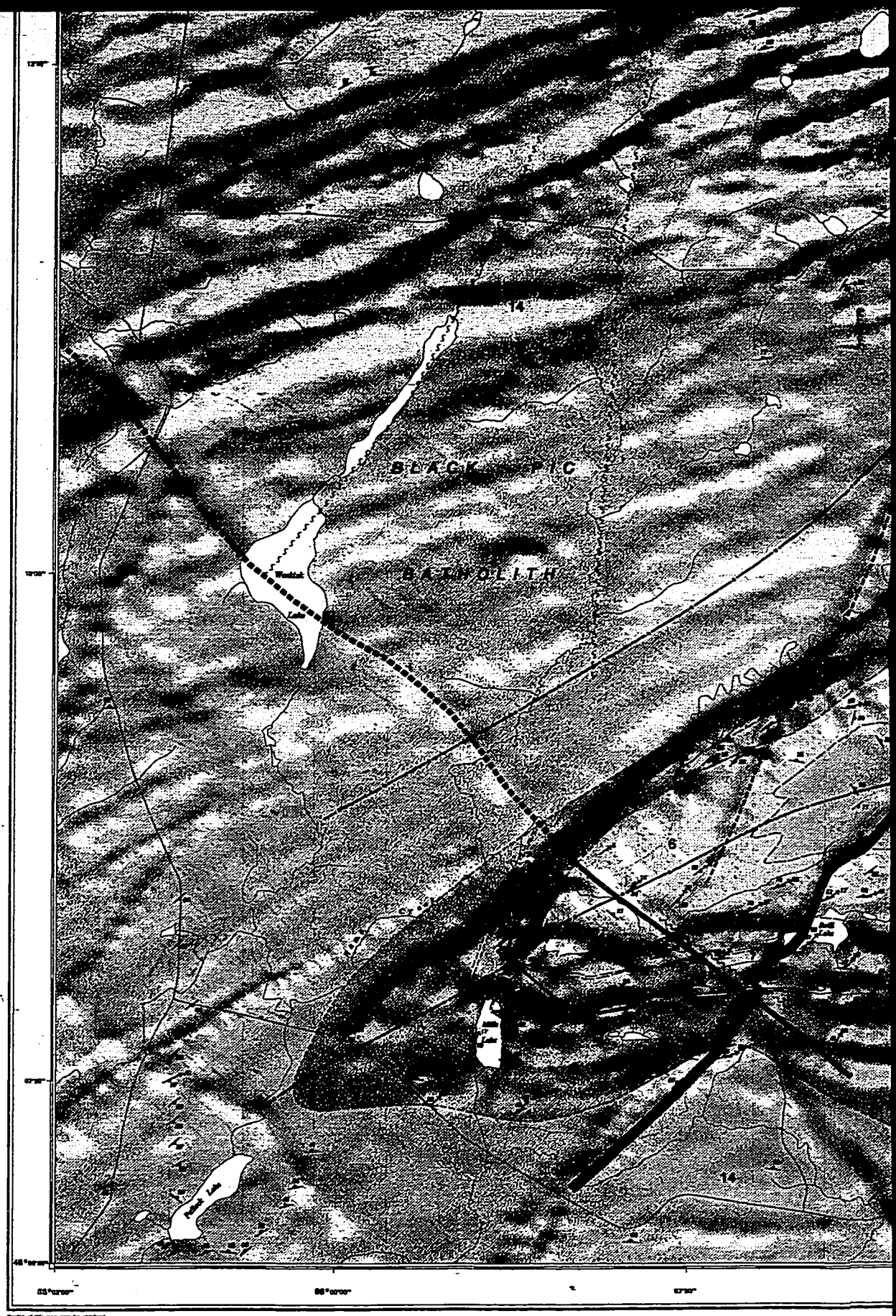

Canada

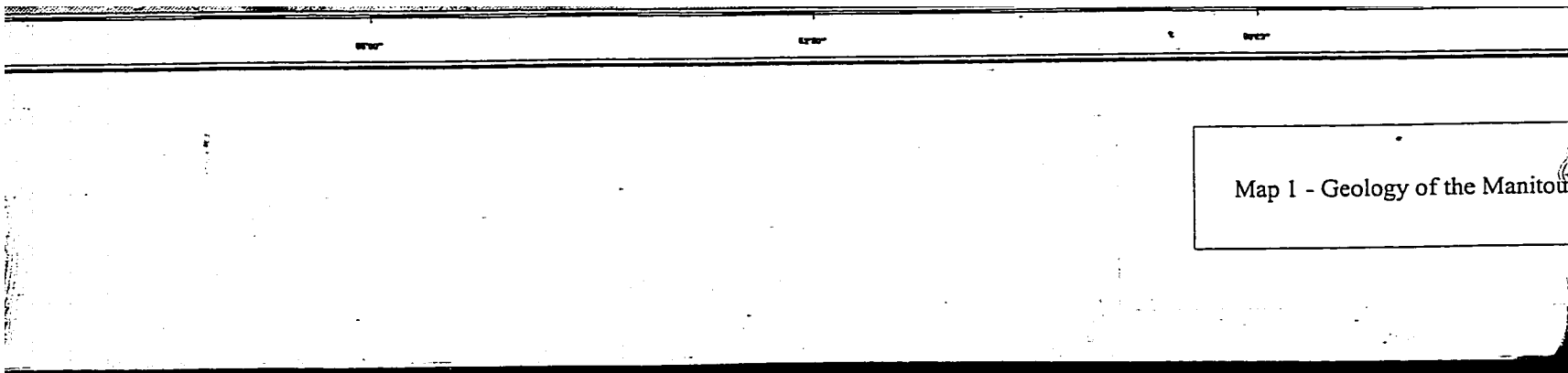

Map 1 - Geology of the Manitou

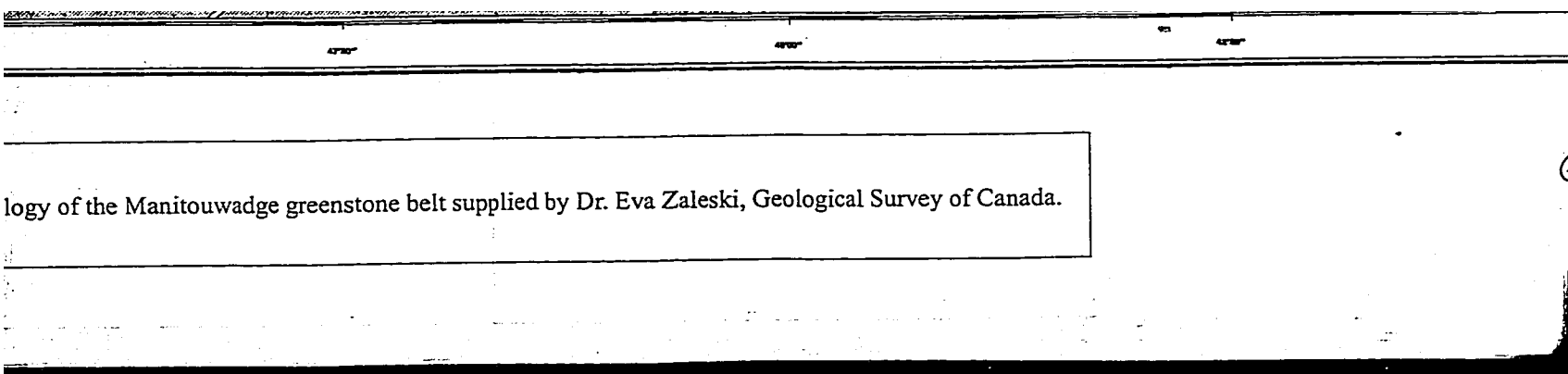

logy of the Manitouwadge greenstone belt supplied by Dr. Eva Zaleski, Geological Survey of Canada.

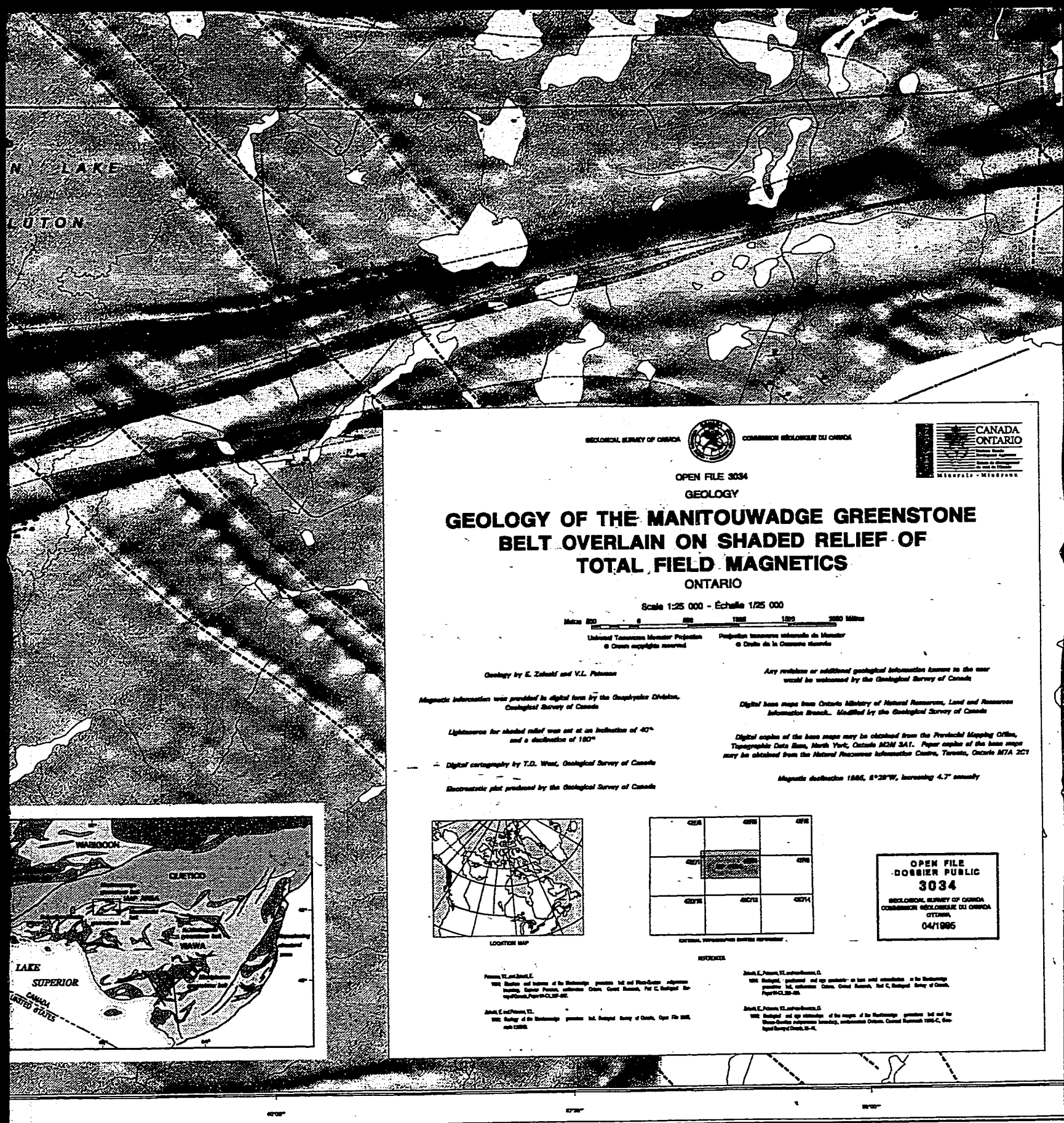

GEOLOGICAL SURVEY OF CANADA — COMMISSION GÉOLOGIQUE DU CANADA

CANADA ONTARIO

Mineral Development Agreement — Entente de développement minéral

Minerals • Minéraux

OPEN FILE 3034

GEOLOGY

GEOLOGY OF THE MANITOUWADGE GREENSTONE BELT OVERLAIN ON SHADED RELIEF OF TOTAL FIELD MAGNETICS

ONTARIO

Scale 1:25 000 - Échelle 1/25 000

Metres 800 0 800 1600 2400 3200 Miles

Universal Transverse Mercator Projection
© Crown copyrights reserved

Projection transverse universelle de Mercator
© Droits de la Couronne réservés

Geology by E. Zaleski and V.L. Peterson

Magnetic information was provided in digital form by the Geophysics Division, Geological Survey of Canada

Lightsource for shaded relief was set at an inclination of 40° and a declination of 180°

Digital cartography by T.D. West, Geological Survey of Canada

Electrostatic plot produced by the Geological Survey of Canada

Any revisions or additional geological information known to the user would be welcomed by the Geological Survey of Canada

Digital base maps from Ontario Ministry of Natural Resources, Land and Resources Information Branch. Modified by the Geological Survey of Canada

Digital copies of the base maps may be obtained from the Provincial Mapping Office, Topographic Data Base, North York, Ontario M3M 3A1. Paper copies of the base maps may be obtained from the Natural Resources Information Centre, Toronto, Ontario M7A 2C1

Magnetic declination 1985, 8°29'W, increasing 4.7' annually

LOCATION MAP

OPTIONAL TOPOGRAPHIC SHEETS REFERENCE

OPEN FILE
DOSSIER PUBLIC
3034
GEOLOGICAL SURVEY OF CANADA
COMMISSION GÉOLOGIQUE DU CANADA
OTTAWA
04/1995

REFERENCE

Peterson, V.L. and Zaleski, E.
1992: Studies and indexes of the Shebandowan greenstone belt and Wawa-Quetico subprovince boundary, Central Ontario; southwestern Ontario; Current Research, Part C; Geological Survey of Canada, Paper 91-1C, p.197-202.

Zaleski, E. and Peterson, V.L.
1992: Geology of the Shebandowan greenstone belt; Geological Survey of Canada, Open File 2600, scale 1:25000.

Zaleski, E., Peterson, V.L. and Hathaway, G.
1992: Geological, geophysical and age constraints on lava and volcaniclastic rocks in the Shebandowan greenstone belt, southwestern Ontario; Current Research, Part C; Geological Survey of Canada, Paper 91-1C, p.189-198.

Zaleski, E., Peterson, V.L. and Hathaway, G.
1992: Geological and age relationships of the margin of the Shebandowan greenstone belt and the Wawa-Quetico subprovince boundary, southwestern Ontario; Current Research 1992-C; Geological Survey of Canada, 93-98.

…VEY OF CANADA COMMISSION GÉOLOGIQUE DU CANADA

CANADA ONTARIO

Minerals - Minéraux

OPEN FILE 3034

GEOLOGY

E MANITOUWADGE GREENSTONE AIN ON SHADED RELIEF OF L FIELD MAGNETICS

ONTARIO

Scale 1:25 000 - Échelle 1/25 000

0 500 1000 1500 2000 Metres

…rse Mercator Projection
…opyrights reserved

Projection transverse universelle de Mercator
© Droits de la Couronne réservés

Any revisions or additional geological information known to the user would be welcomed by the Geological Survey of Canada

…ice Division,

Digital base maps from Ontario Ministry of Natural Resources, Land and Resources Information Branch. Modified by the Geological Survey of Canada

…' 40"

Digital copies of the base maps may be obtained from the Provincial Mapping Office, Topographic Data Base, North York, Ontario M2M 3A1. Paper copies of the base maps may be obtained from the Natural Resources Information Centre, Toronto, Ontario M7A 2C1

…anada

Magnetic declination 1995, 5°29'W, increasing 4.7' annually

…anada

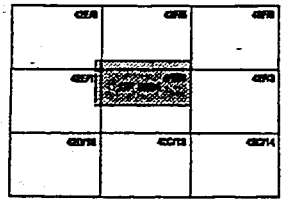

NATIONAL TOPOGRAPHIC SYSTEM REFERENCE

OPEN FILE
DOSSIER PUBLIC
3034
GEOLOGICAL SURVEY OF CANADA
COMMISSION GÉOLOGIQUE DU CANADA
OTTAWA
04/1995

REFERENCES

…-Quetico subprovince … Part C, Geological Su…

…anada, Open File 3…

Zaleski, E., Peterson, V.L. and van Breemen, O.
1995: Geological, geochronological and age constraints on base metal mineralization in the Manitouwadge greenstone belt, northwestern Ontario; Current Research, Part C, Geological Survey of Canada, Paper 94-C, [illegible].

Zaleski, E., Peterson, V.L. and van Breemen, O.
1995: Geological and age relationships of the margins of the Manitouwadge greenstone belt and the Wawa-Quetico subprovince boundary, northwestern Ontario; Current Research 1995-C, Geological Survey of Canada, [illegible].

▨ *Diabase: dykes of probable Proterozoic age; mapped, inferred from aeromagnetic trend*

WAWA SUBPROVINCE

INTRUSIVE ROCK UNITS

▨ *Alkalic rocks: syenite to hornblendite, massive to foliated, locally cut veined or intrusion breccias*

▨ *Pegmatites, aplites, foliated granitoid: massive to foliated, pegmatite locally porphyroblastic or with fibrous sillimanite on shear surfaces and transitional to straight gneiss*

▨ *Undivided foliated intrusive rocks: dominantly tonalitic multiphase intrusions, also diorite, granodiorite, granite enclosing supracrustal rocks (eg. Black Pic batholith); semiconcordant tonalitic bodies intruding supracrustal rocks*

▨ *Foliated K-feldspar porphyritic granitoid in two main bodies: a. Nama Creek pluton - long sinuous body folded by the Manitouwadge Lake antiform between Black Pic batholith and supracrustal rocks - hornblende-biotite-rich (to 25%) matrix, sparse (1-25%) 1 cm phenocrysts; b. Loken Lake pluton - in the center of Manitouwadge synform - K-feldspar megacrysts to 15 cm long*

▨ *Foliated trondhjemite to granitoid: leucocratic, medium to coarse grained, quartz-rich (30-45%), typically magnetite porphyroblastic, synvolcanic intrusion locally with garnet-orthoamphibole alteration zones; transitional more potassic variants toward synform centre*

TECTONIC ROCK UNITS

▨ *Straight gneiss: laminated annealed mylonite, mappable units of felsic composition*

SUPRACRUSTAL ROCK UNITS

▨ *Metasedimentary rocks: mainly monotonous metagreywackes and biotite schists ±garnet-sillimanite, locally with tuffaceous component (quartz and plagioclase crystal clasts), locally bedded and showing soft-sediment deformation*

▨ *Metamorphosed iron formation: three main types; a. Quartz-magnetite - alternating quartz-rich and magnetite-grunerite±hedenbergite±actinolite±garnet layers commonly folded or brecciated; b. Silicate - homogeneous intergrowth of magnetite-grunerite ±hedenbergite±actinolite±garnet; c. Sulphide - quartz-rich with disseminated pyrite -pyrrhotite, locally forming a transitional zone between quartz-magnetite iron formation and massive sulphide bodies*

▨ *Quartz-phyric felsic metavolcanic rocks: three mappable bodies varying from homogeneous to fragmental with both monolithologic and heterolithic breccias, typically some muscovite or calc-silicate minerals, patchy distribution of microcline*

▨ *Aphyric felsic metavolcanic rocks: monolithologic and heterolithic breccias, typically with abundant garnet-hornblende matrix*

▨ *Felsic to intermediate metavolcanic rocks: mainly heterogeneous and transitional breccias, schists, straight gneisses, incipient calc-silicate and sillimanite-muscovite alteration and foliated tonalites without useful marker units*

▨ *Intermediate to mafic metavolcanic rocks: heterogeneous and transitional hornblende-biotite schists, gneisses, layered rocks and foliated diorites, commonly with garnet-hornblende-rich patches*

▨ *Mixed mafic and felsic metavolcanic rocks: interlayered mafic, felsic and leucofelsic schists, transitional to garnet-orthoamphibole gneisses, epidote locally abundant, locally quartz-phyric*

▨ *Mafic metavolcanic rocks: dark laminated to schistose hornblende-rich, locally pillowed, interrelated with medium to coarse grained foliated gabbros and hornblende-augen schists, locally garnet-rich zones ±orthoamphibole*

METASOMATICALLY ALTERED ROCK UNITS

▨ *Orthoamphibole-garnet±cordierite gneiss: coarse grained, typically layered with quartz-rich layers or lenticles overgrown by orthoamphibole-garnet porphyroblasts, interrelated (on a scale of 0.5 to several metres) with sillimanite-garnet-biotite schist, also contains magnetite, biotite and staurolite mantled by cordierite, local biotite pseudomorphs of orthoamphibole*

▨ *Sillimanite-muscovite-quartz felsic gneiss/schist: includes interlayered similar or transitional rock types characterized by abundant muscovite and/or sillimanite -quartz±plagioclase-biotite-K-feldspar-garnet-cordierite-magnetite; 1) associated with Willroy and Geco mines - quartz-muscovite-sillimanite schist varies from finely interlayered quartz and muscovite to abundant sillimanite knots; 2) hinge region north of Willecho - mainly large (1-8 cm) zoned sillimanite knots dispersed in schistose quartz-plagioclase-microcline-biotite±garnet matrix, local quartz -garnet-epidote patches*

QUETICO SUBPROVINCE

▨ *Metasedimentary rocks: mainly monotonous metagreywackes and derived migmatites, biotite-garnet-sillimanite in more pelitic layers, locally with cordierite-bearing leucosome*

Geological contact (defined, approximate, assumed) . . . . ——— – – –

Fault (defined, interpreted) . . . . ∿∿∿∿ ⌣ ⌣ ⌣

Trace of fold axial surface (D3, D4) . . . . ——•——

Dominant foliation (D2) . . . . / 82

Mineral/stretching lineation (D2/D3) . . . . ↗ 14

Massive sulphide deposit . . . . ⚒

Geco (G), Willroy (orebodies 1 to 6), Nama Creek (N), Willecho (orebodies W1 to W3)

Road washout . . . . /

Published 1995

Recommended citation:
Zaleski, E. and Peterson, V.L.
1995: Geology of the Manitouwadge greenstone belt overlain on shaded relief of total field magnetics, Ontario; Geological Survey of Canada, Open File 3034, scale 1:25 000

NOTE TO USERS

Oversize maps and charts are microfilmed in sections in the following manner:

LEFT TO RIGHT, TOP TO BOTTOM, WITH SMALL OVERLAPS

The following map or chart has been microfilmed in its entirety at the end of this manuscript (not available on microfiche). A xerographic reproduction has been provided for paper copies and is inserted into the inside of the back cover.

Black and white photographic prints (17"x 23") are available for an additional charge.

UMI

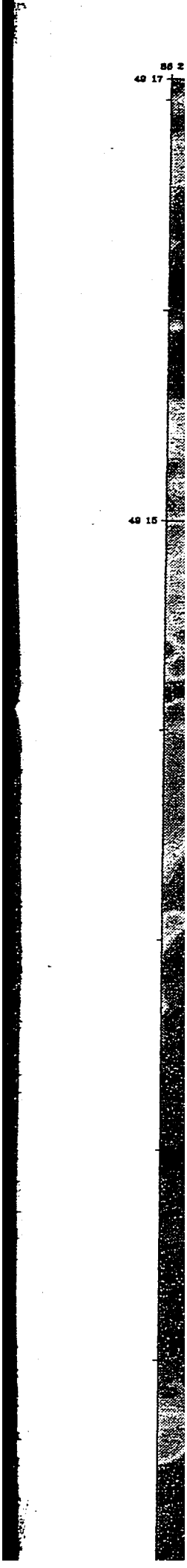
56 2
49 17
49 15

49 1

49 5.5

85 60

Map 2

Map 2 – Apparent Susceptibility, Manitouwadge study area.

200
175
150
100
75
60
50
40
35
32
28
24
20
16
14
12
10
7
5
4
3
2
1
0
-0
-2
-3
-5
-10
k(x10-3 SI)
49 10
49 8.50
30
wmiles@gdcws7 map_appsus_Ø174Ø5.vds 24/4/1998@9:52:55

NOTE TO USERS

Oversize maps and charts are microfilmed in sections in the following manner:

LEFT TO RIGHT, TOP TO BOTTOM, WITH SMALL OVERLAPS

The following map or chart has been microfilmed in its entirety at the end of this manuscript (not available on microfiche). A xerographic reproduction has been provided for paper copies and is inserted into the inside of the back cover.

Black and white photographic prints (17"x 23") are available for an additional charge.

UMI

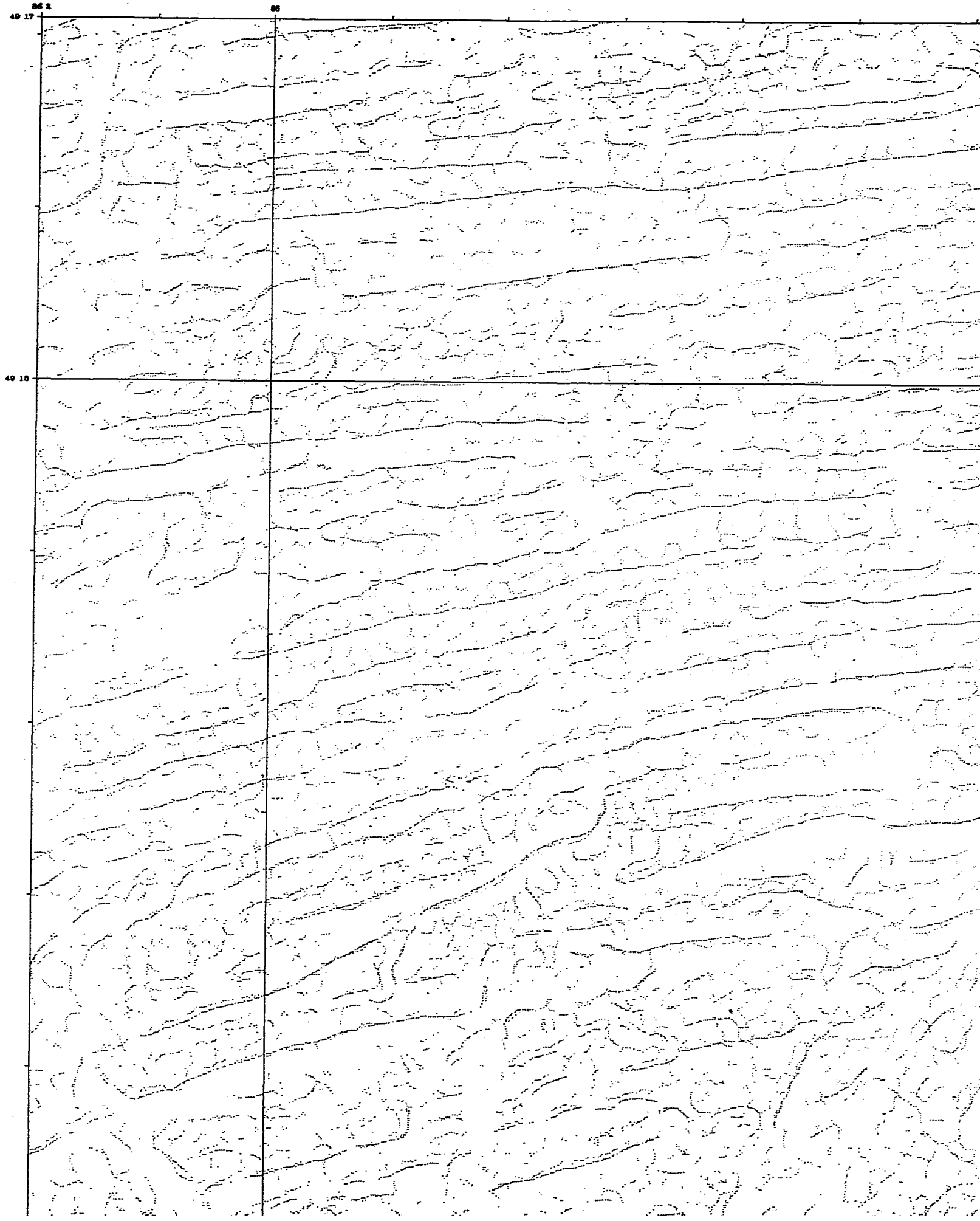
86 2
86
49 17
49 15

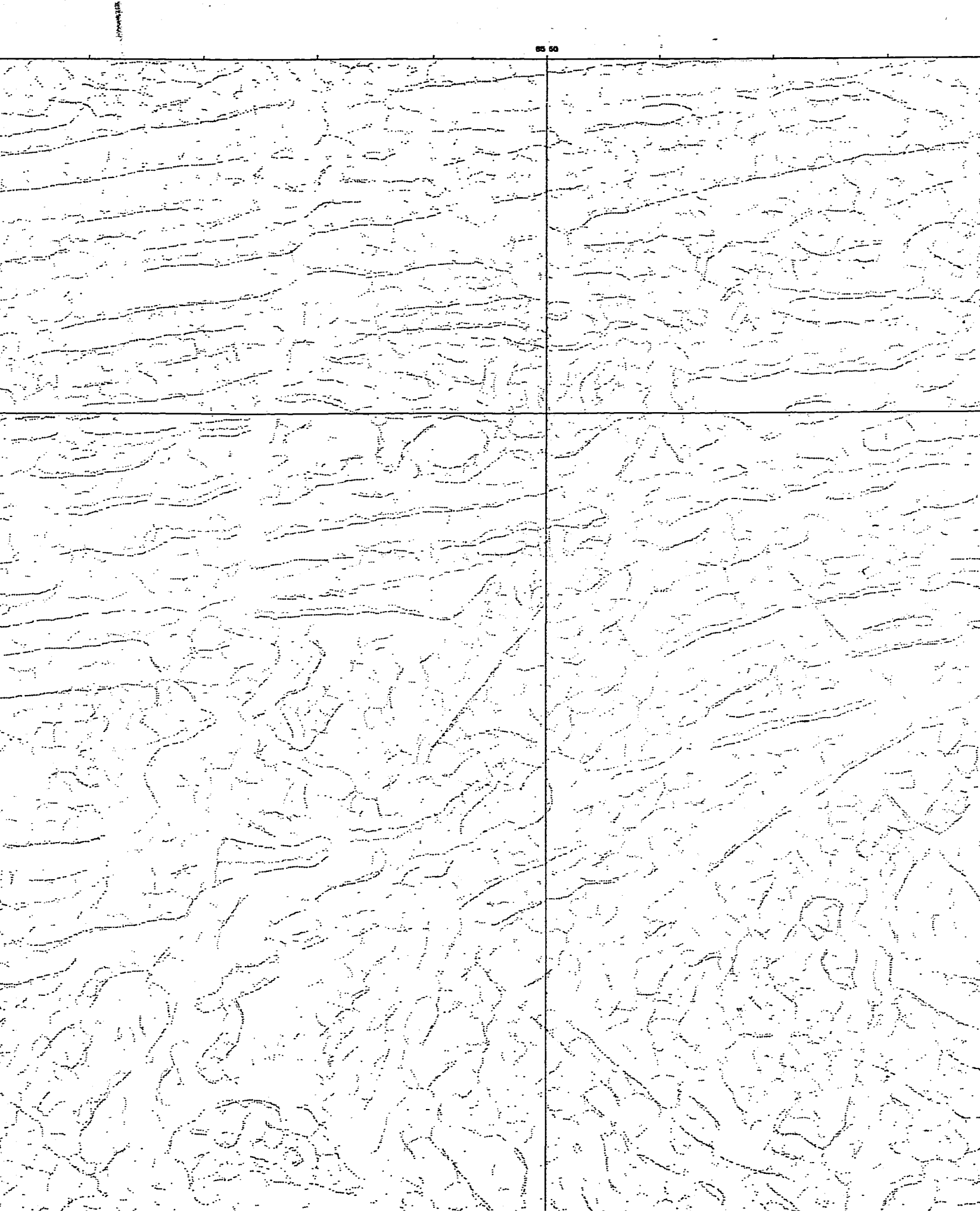
85 50

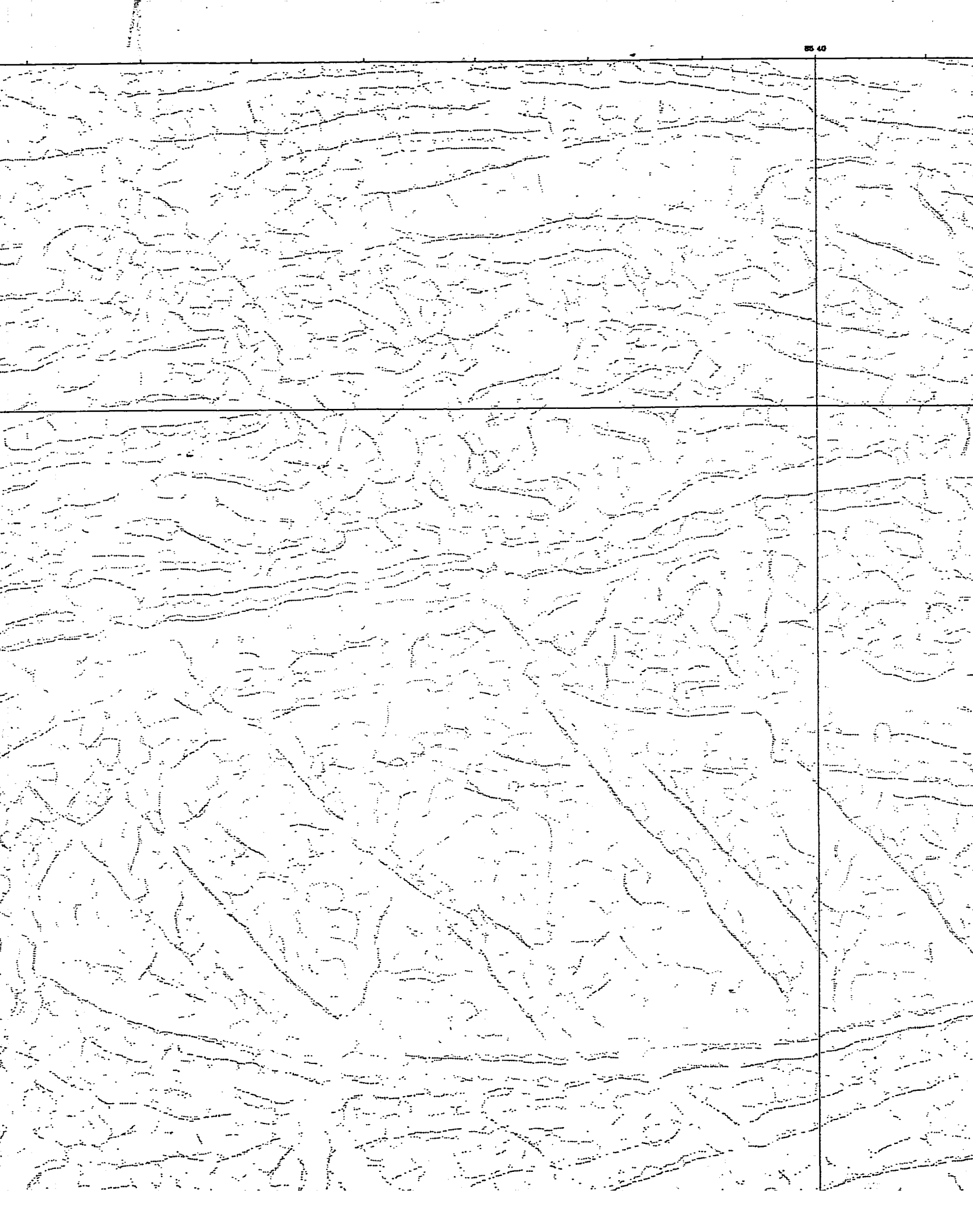
85 40

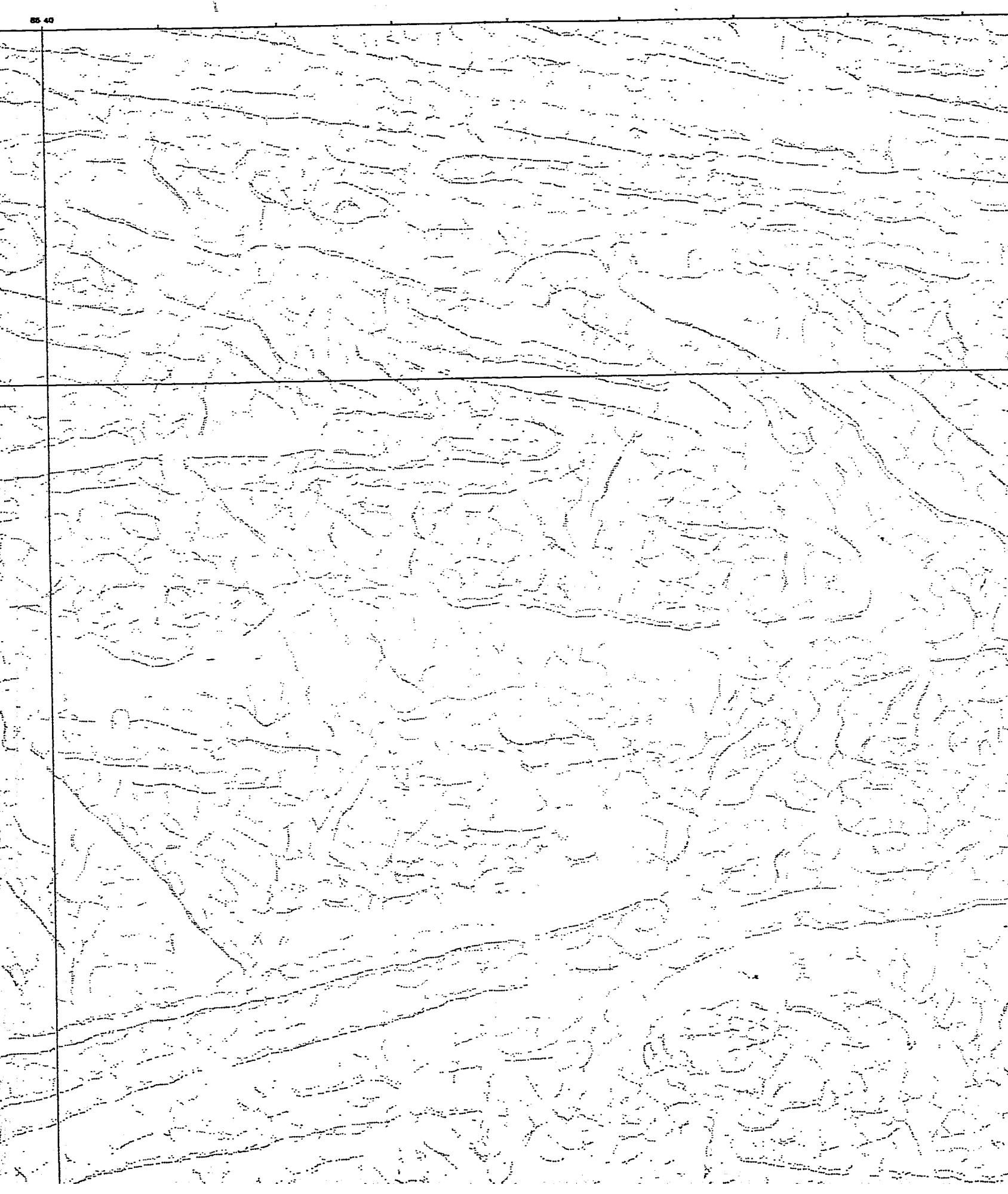
85 40

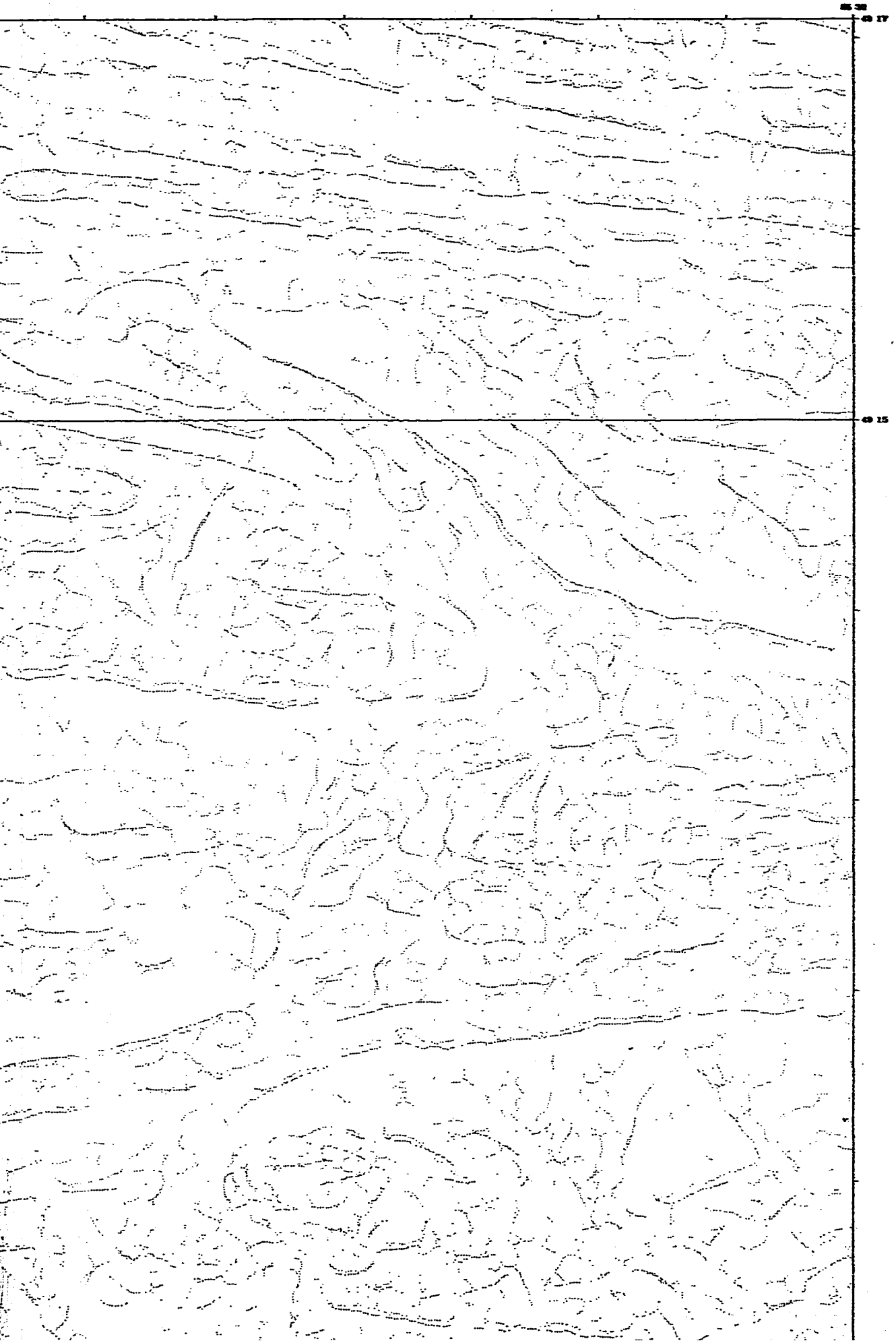

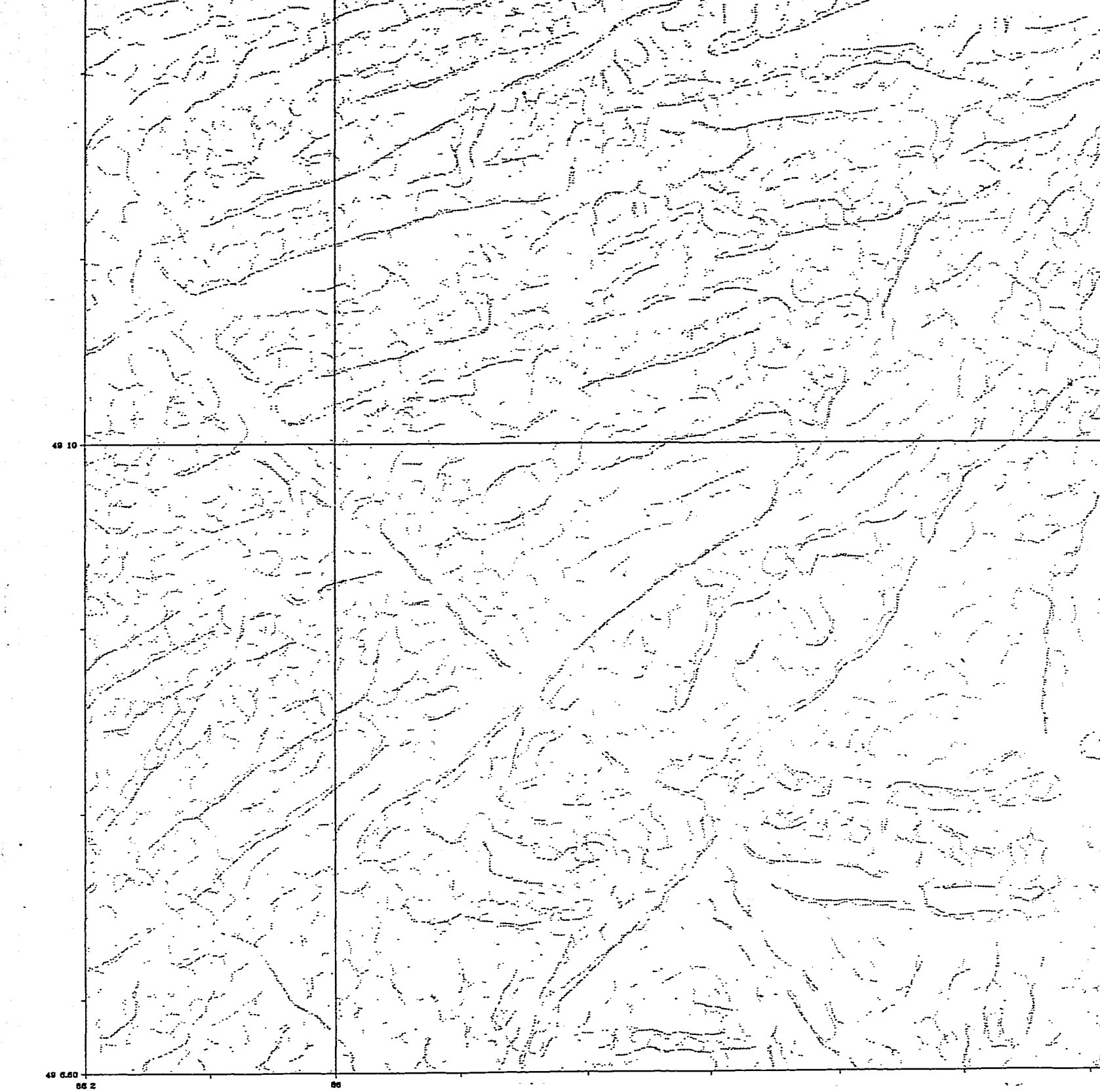

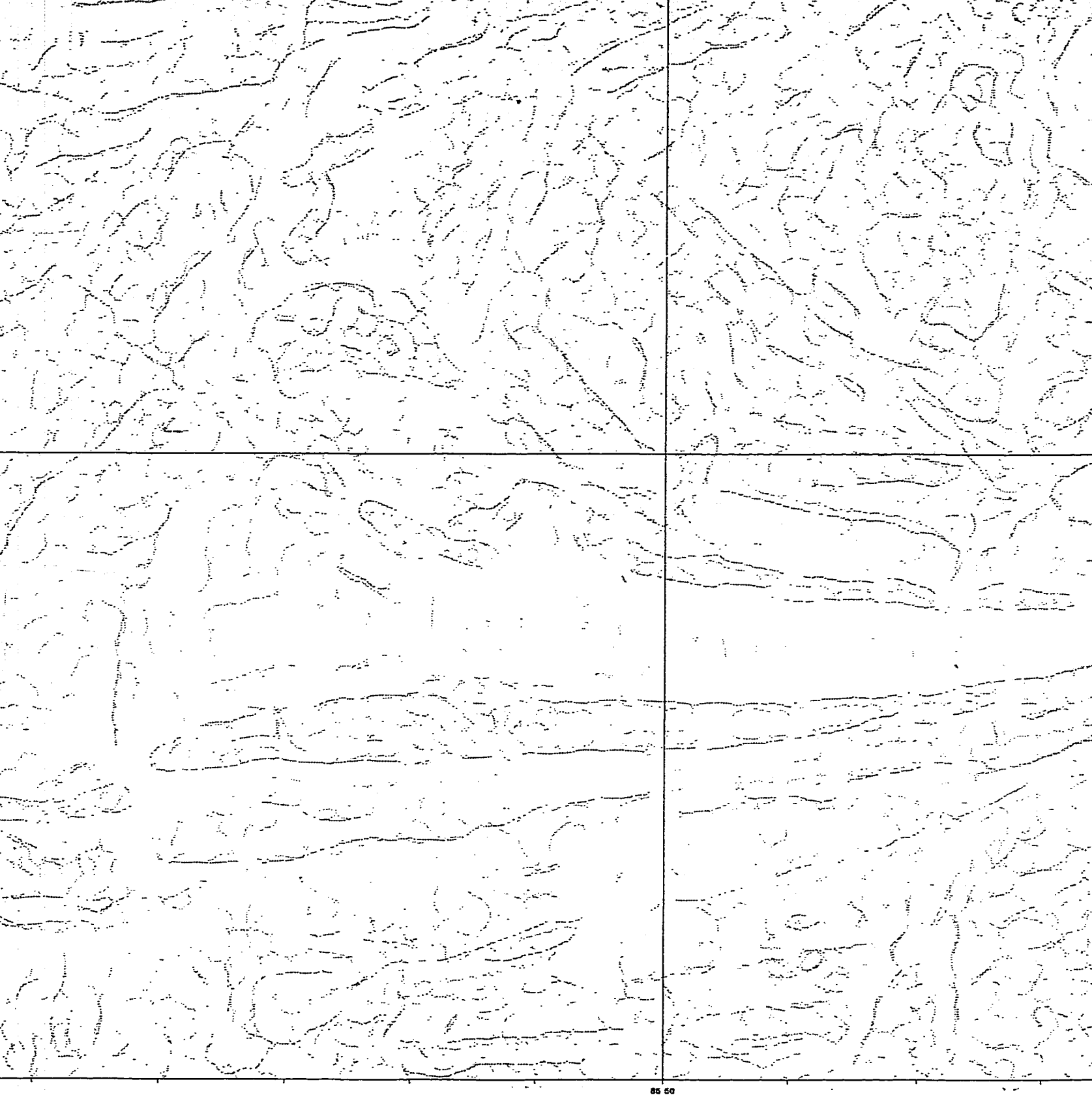

85 50

Map 3 - Analytic Signal

Map 3 - Analytic Signal and Pseudo-Gravity HGMAG Maxima (min=0)
Manitouwadge study area

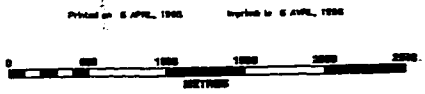

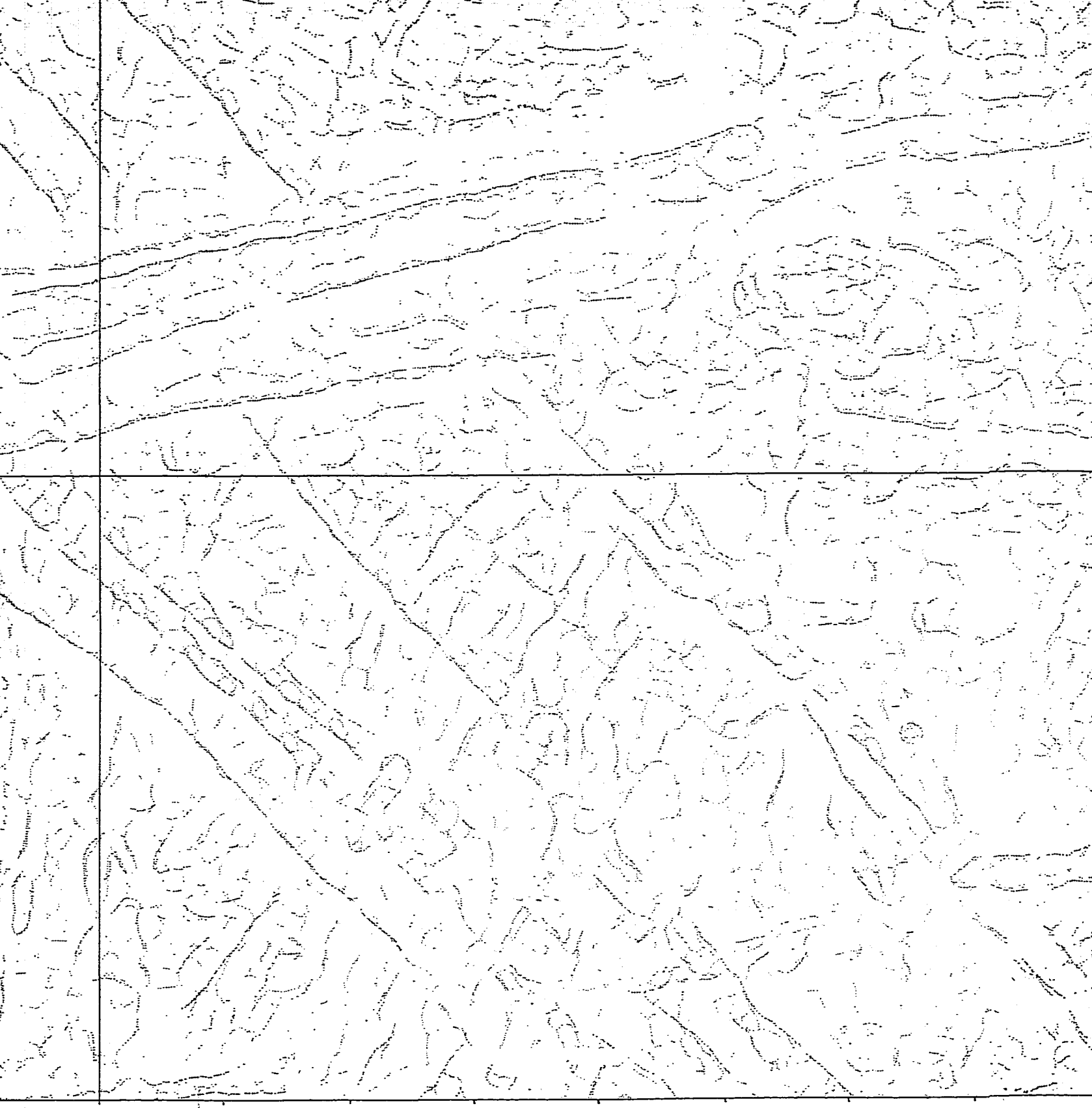

● Pseudo-gravity HGMAG Max
● Analytic Signal Maximum

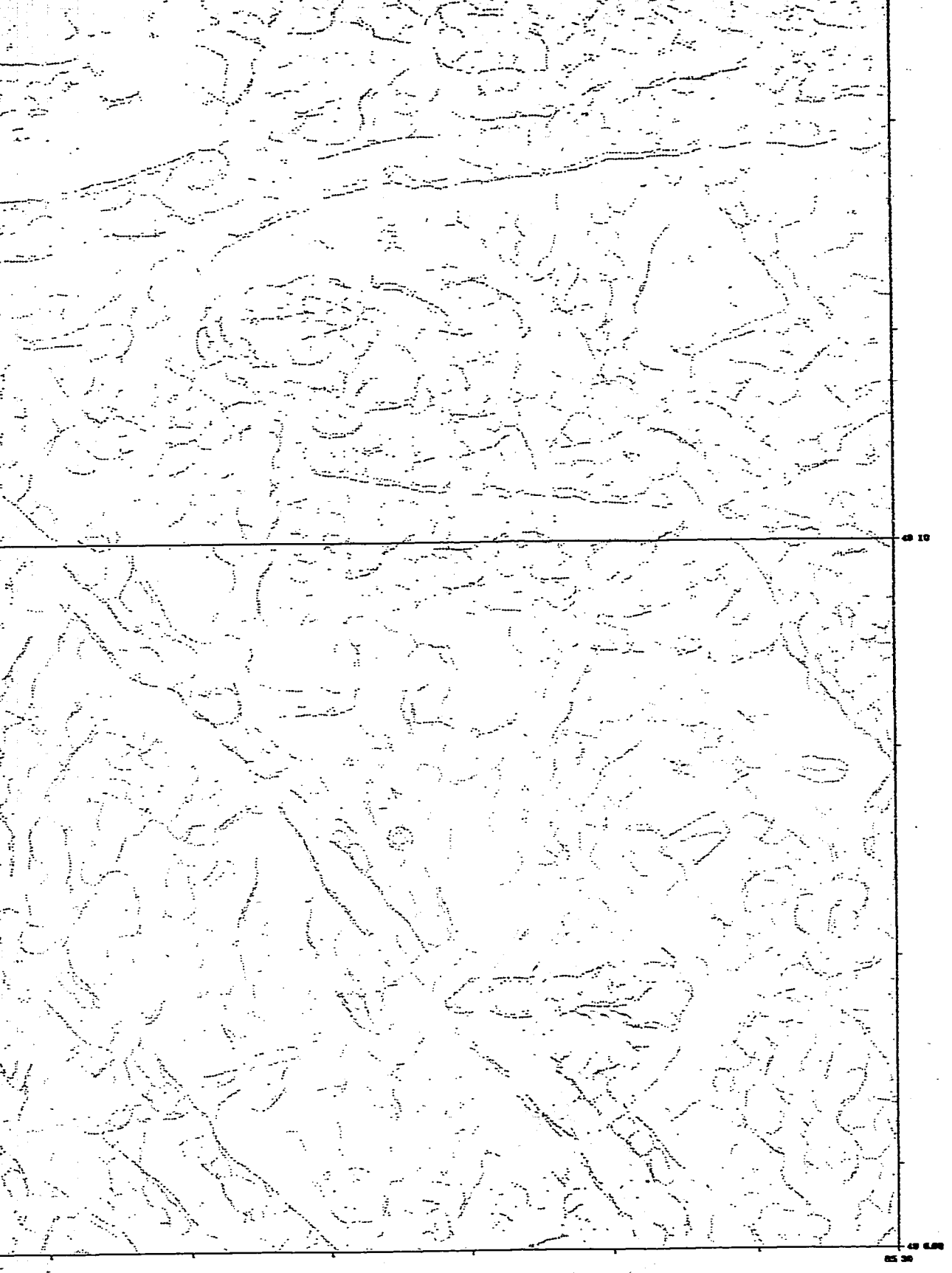

● Pseudo-gravity HGMAG Maximum
● Analytic Signal Maximum

NOTE TO USERS

Oversize maps and charts are microfilmed in sections in the following manner:

LEFT TO RIGHT, TOP TO BOTTOM, WITH SMALL OVERLAPS

The following map or chart has been microfilmed in its entirety at the end of this manuscript (not available on microfiche). A xerographic reproduction has been provided for paper copies and is inserted into the inside of the back cover.

Black and white photographic prints (17"x 23") are available for an additional charge.

UMI

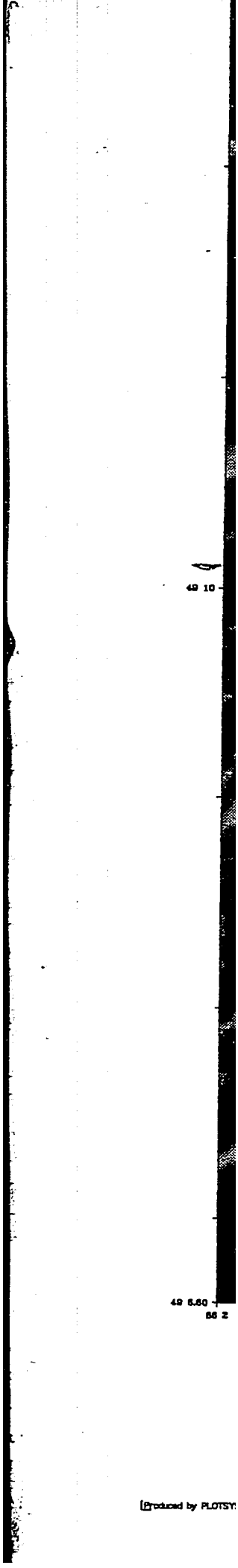
49 10
49 5.60
56 2
Produced by PLOTSY

Map 4 – Magne

Map 4 – Magnetic TILT, Manitouwadge study area.

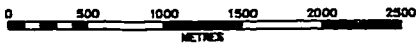

85 40

wmiles@gdcws7 map

NOTE TO USERS

Oversize maps and charts are microfilmed in sections in the following manner:

LEFT TO RIGHT, TOP TO BOTTOM, WITH SMALL OVERLAPS

The following map or chart has been microfilmed in its entirety at the end of this manuscript (not available on microfiche). A xerographic reproduction has been provided for paper copies and is inserted into the inside of the back cover.

Black and white photographic prints (17"x 23") are available for an additional charge.

UMI

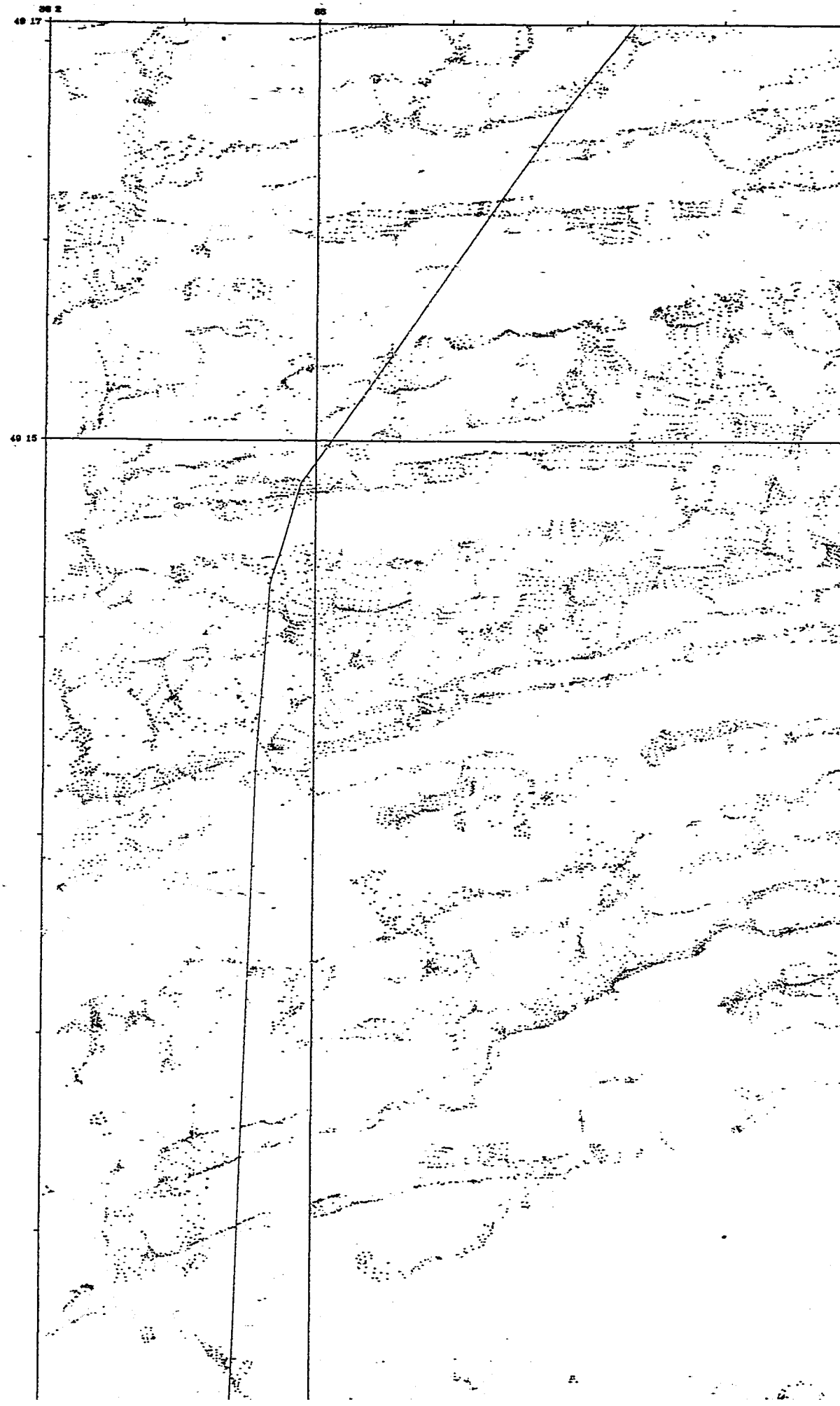

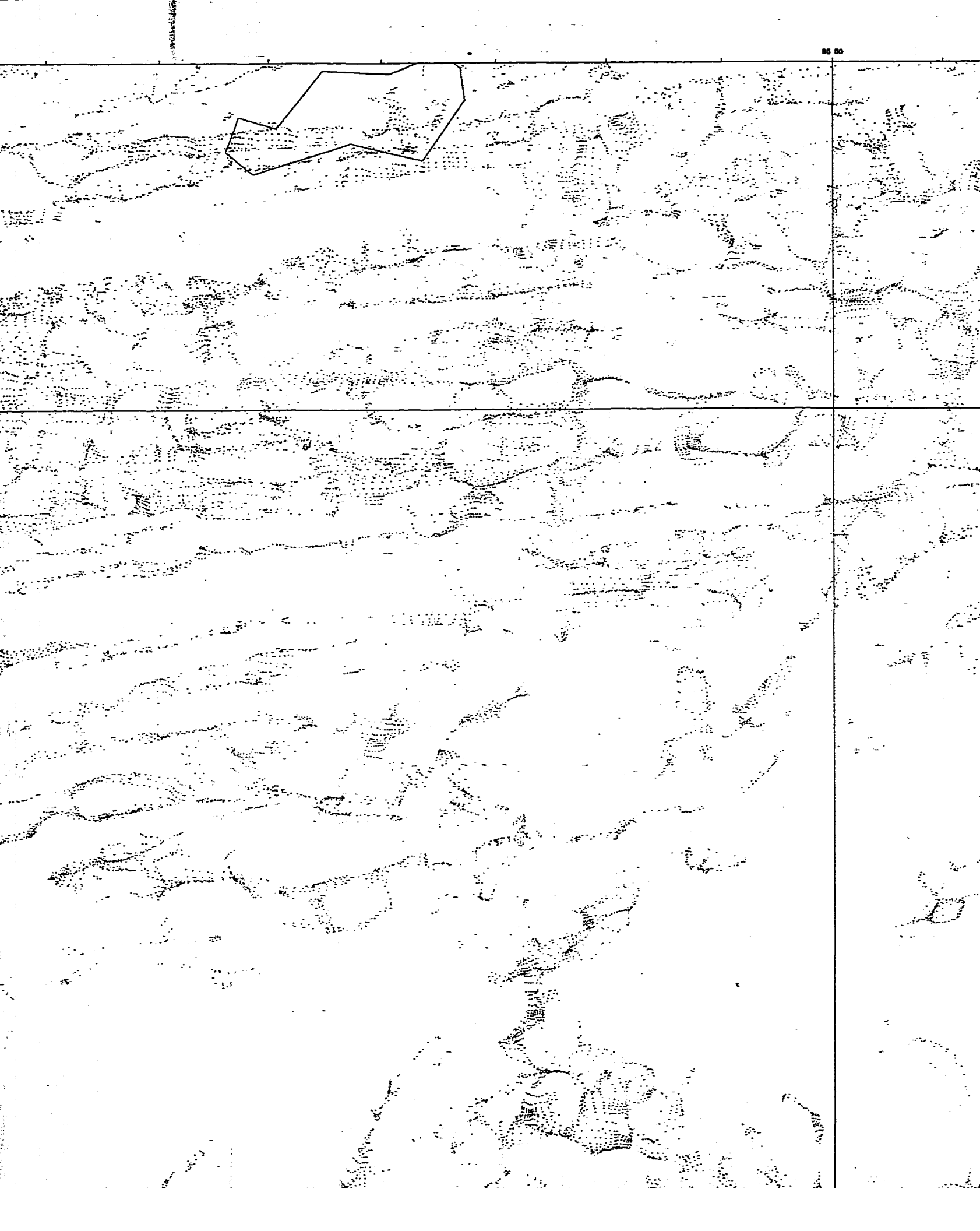
85 50

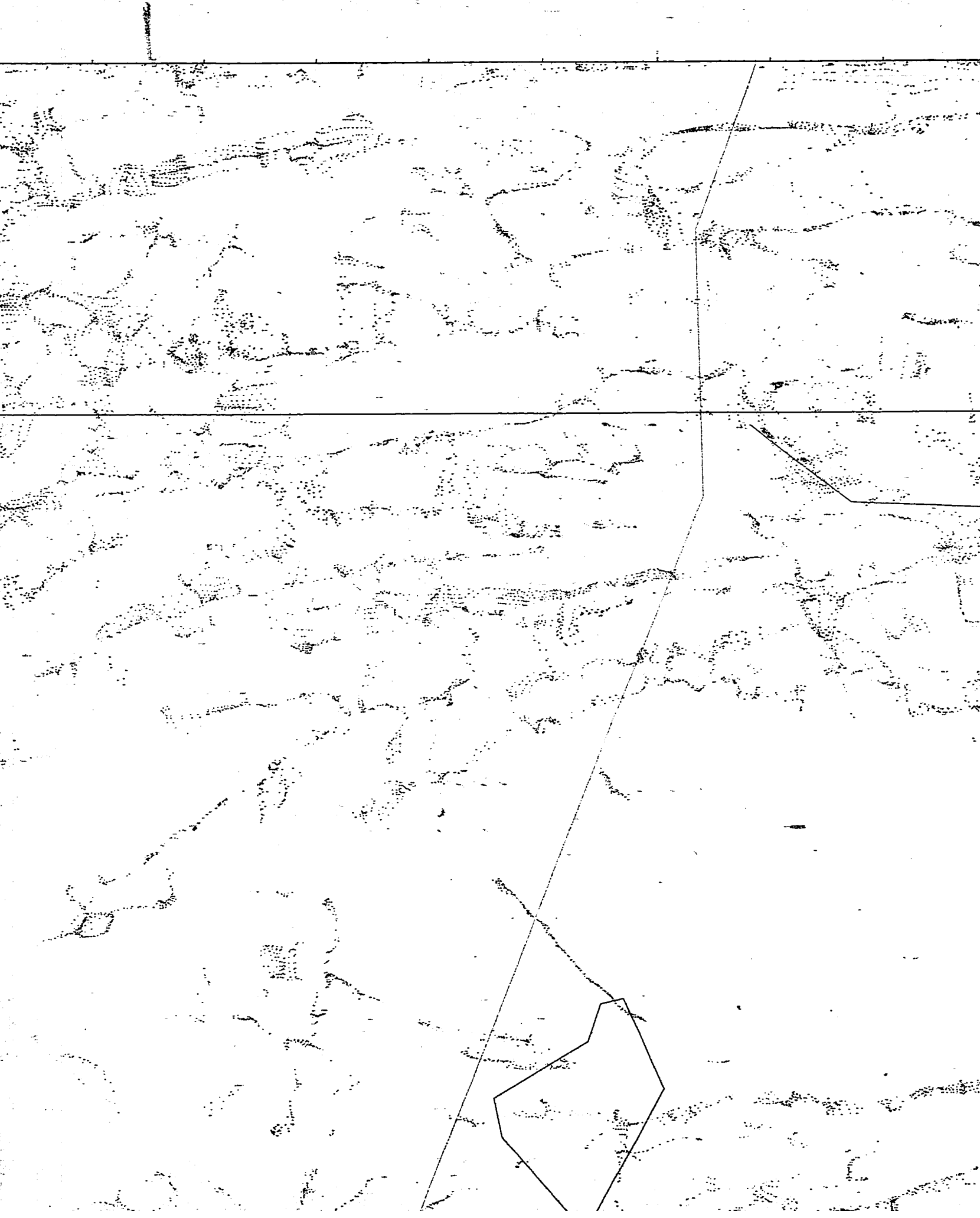

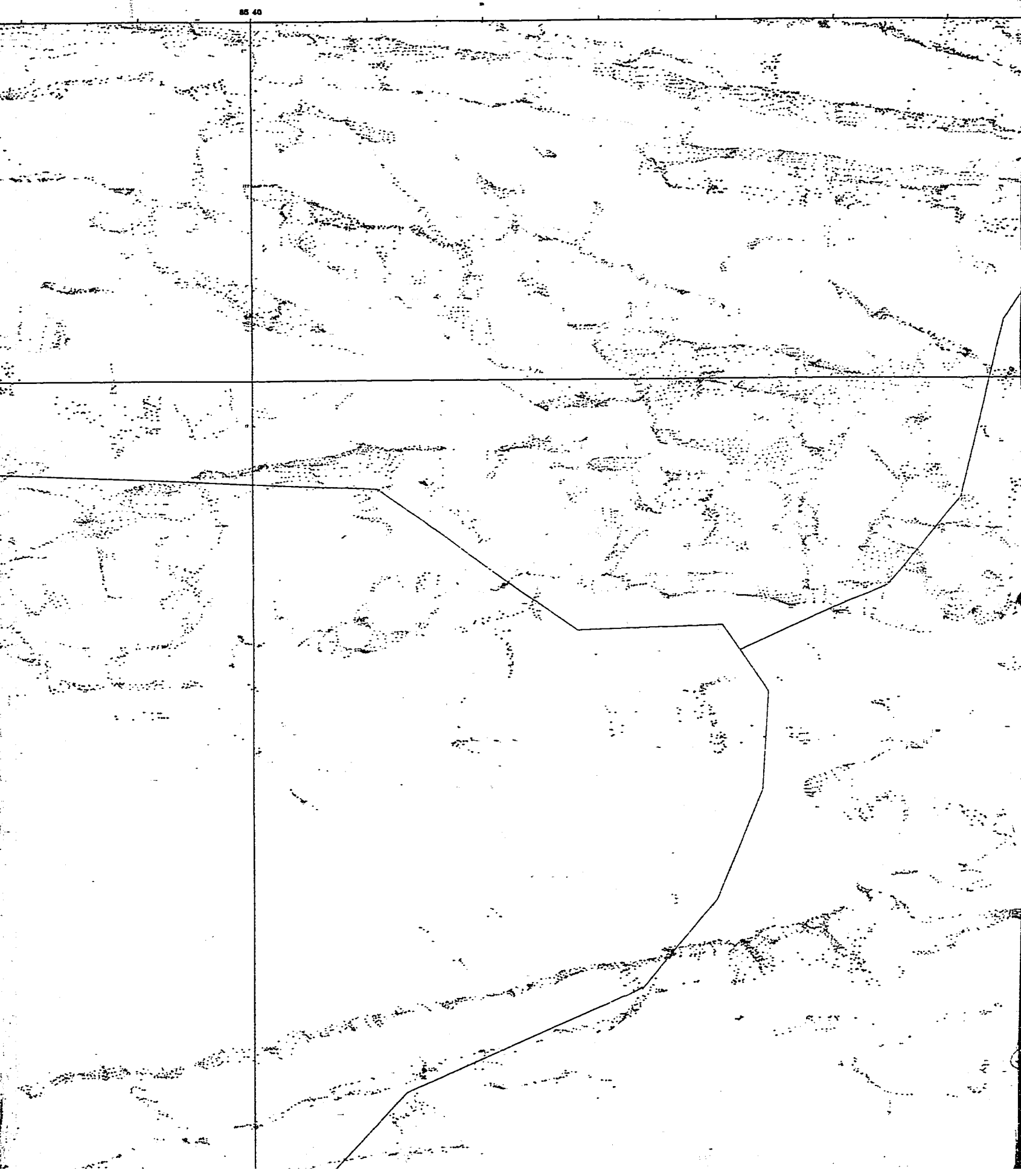
85 40

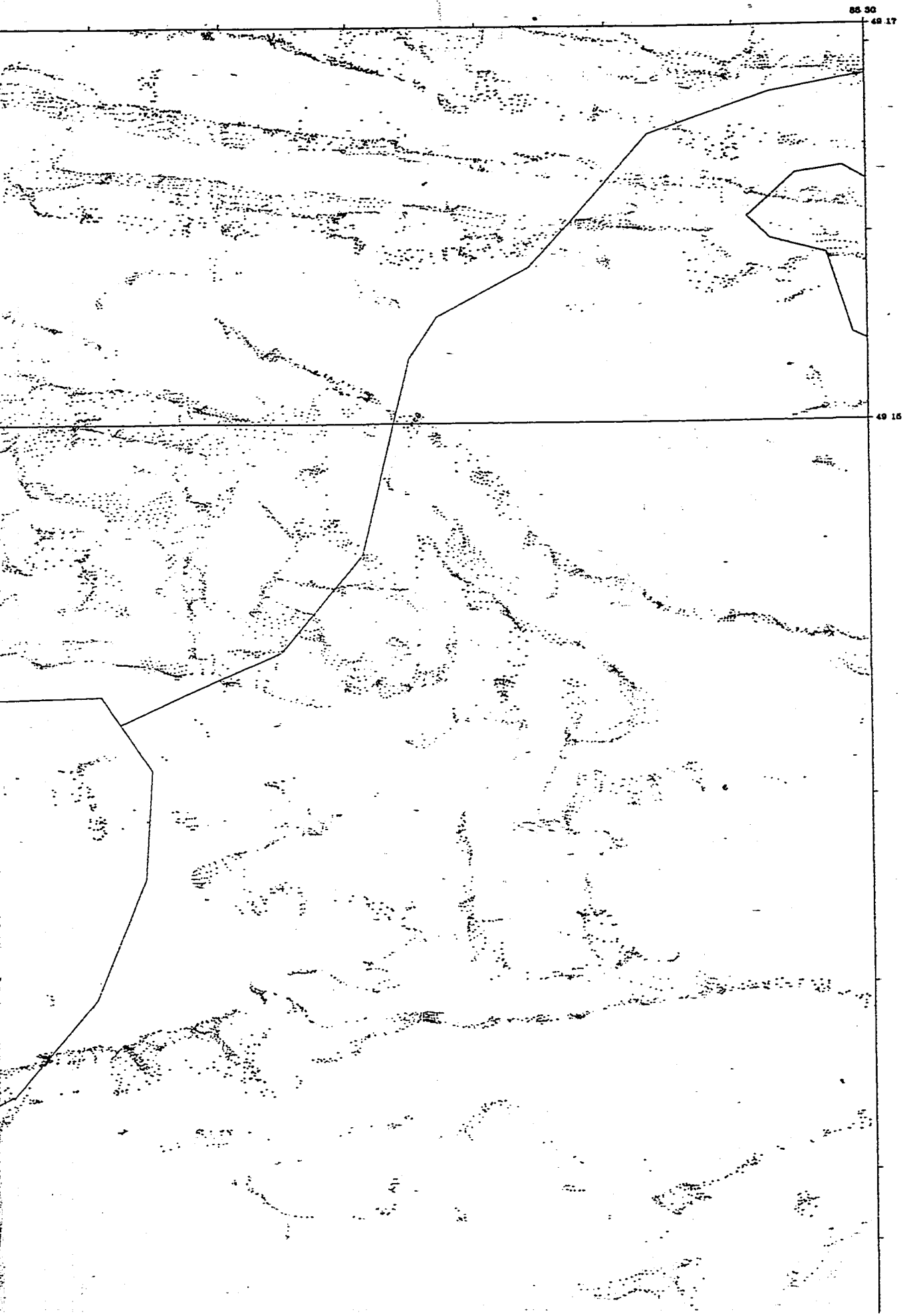
86 30
49 17
49 15

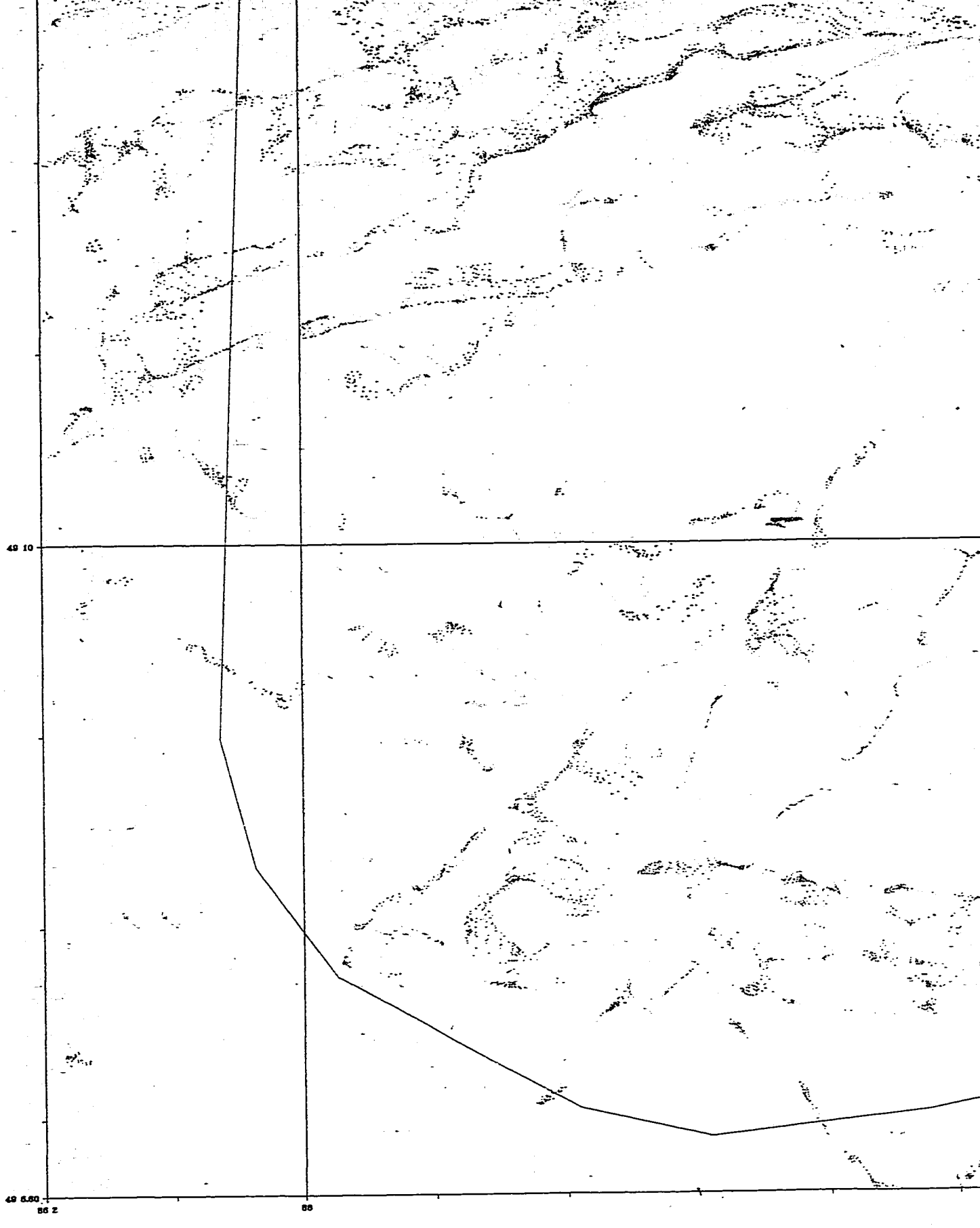

Map 5 - Eu

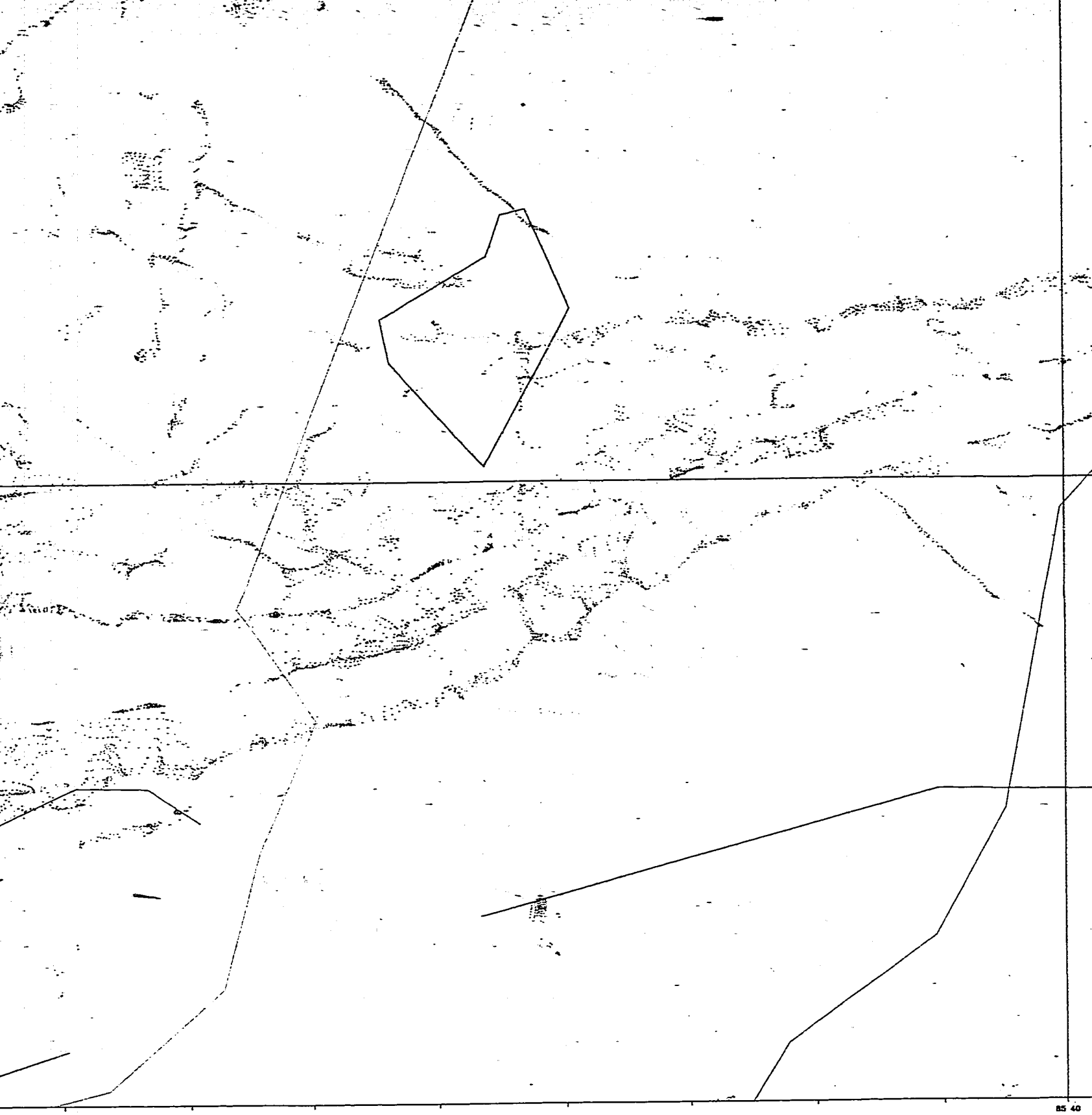

Map 5 - Euler deconvolution depth solutions - Manitouwadge study area.
Window=10, SI=1.0, tol=0.3, grid cell size=40m

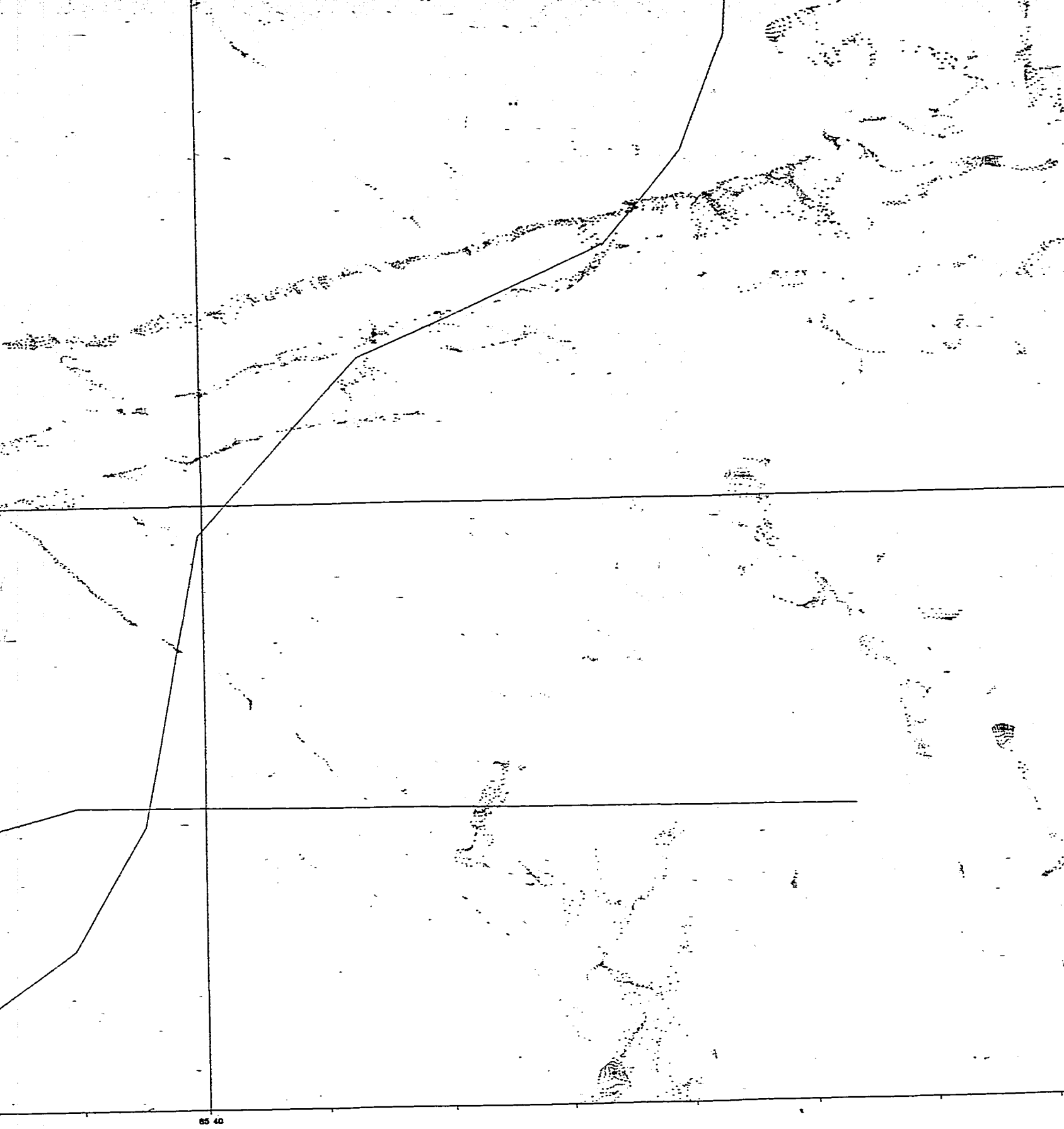
85 40

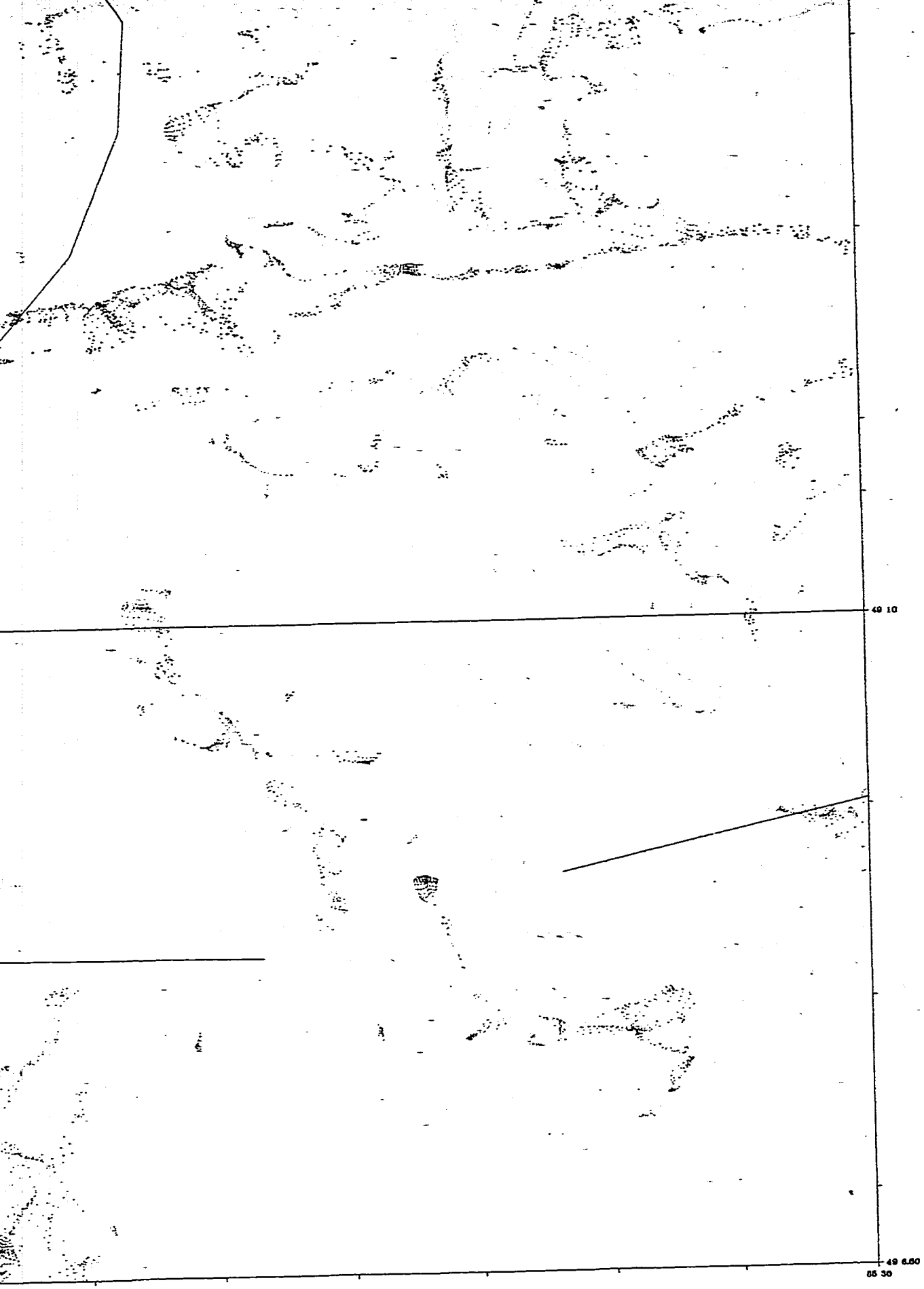

30m
67mm
134m
201m
269m
336m
403m
471m
538m
605m

NOTE TO USERS

Oversize maps and charts are microfilmed in sections in the following manner:

LEFT TO RIGHT, TOP TO BOTTOM, WITH SMALL OVERLAPS

The following map or chart has been microfilmed in its entirety at the end of this manuscript (not available on microfiche). A xerographic reproduction has been provided for paper copies and is inserted into the inside of the back cover.

Black and white photographic prints (17"x 23") are available for an additional charge.

UMI

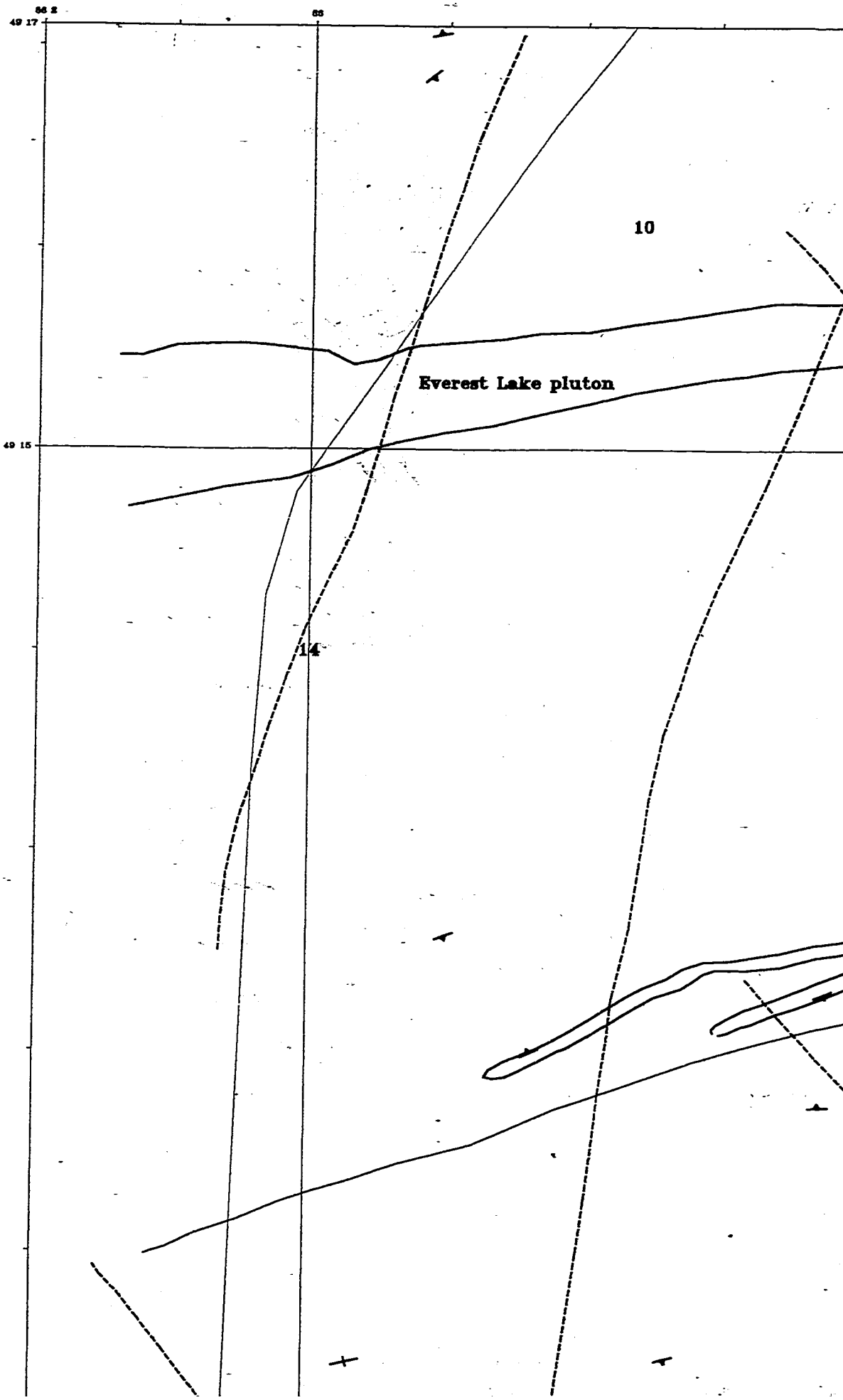


85 50
13a
9
4
9
4
12
9
13a
4

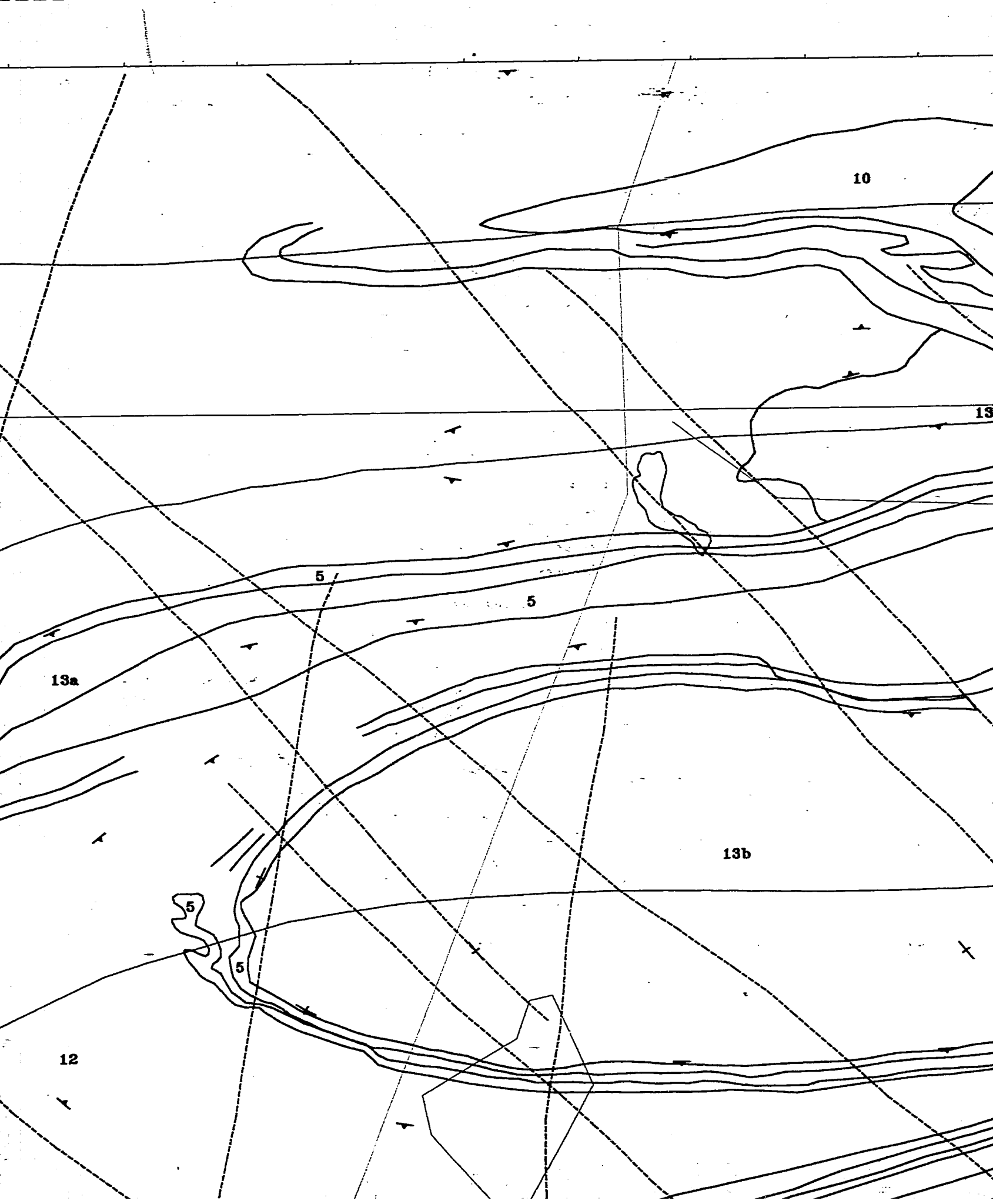
10
13
5
5
13a
13b
5
5
12

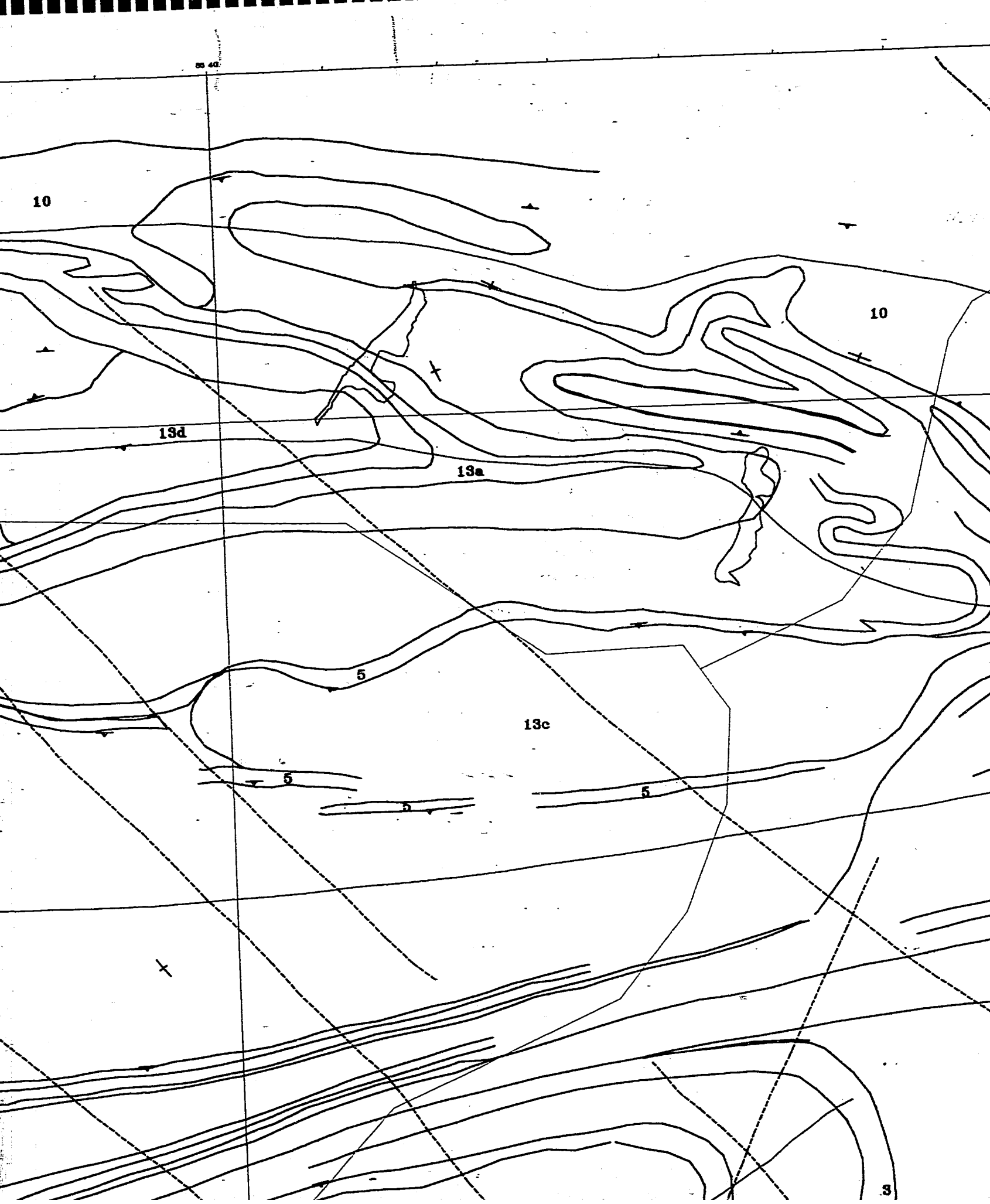
10
10
13d
13a
5
13c
5
5
5
3

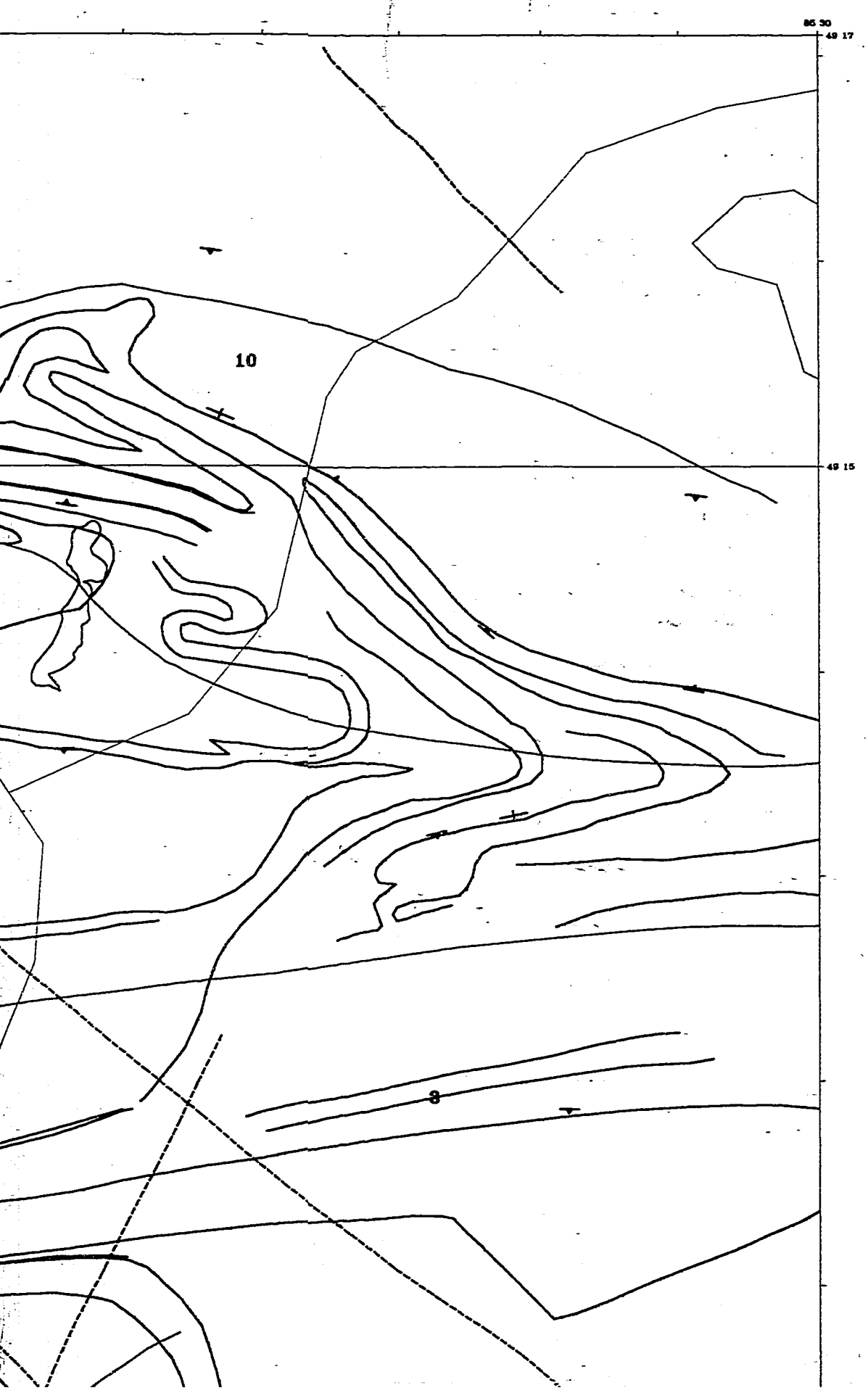
86 30
49 17
10
49 15
8

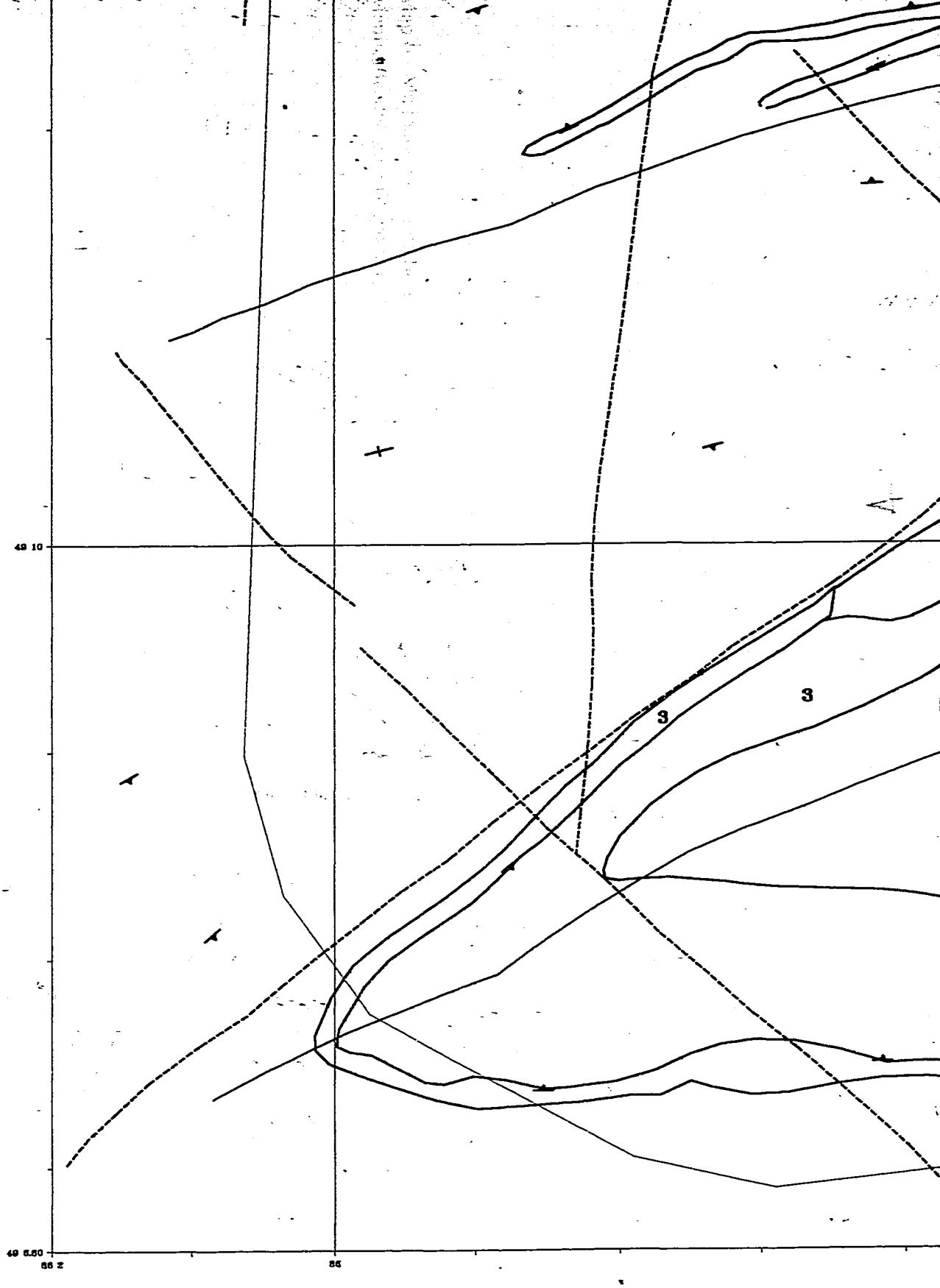

[Produced by PLOTSYS 5.15, created by Regional Geophysics/CGG/GIBONFR]

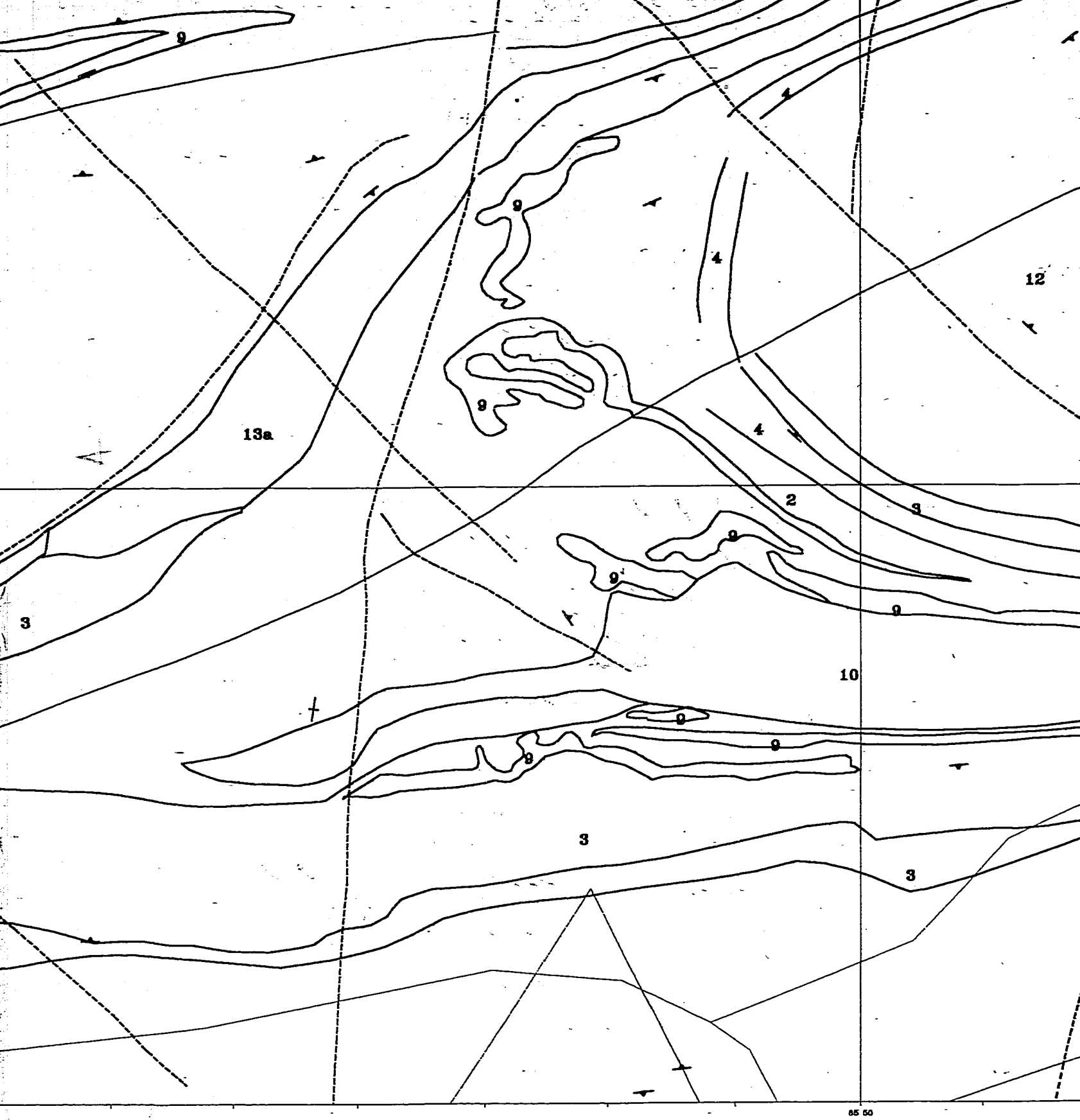
9
9
4
12
13a
4
2
3
9
9
9
3
10
9
9
9
3
3
85 50

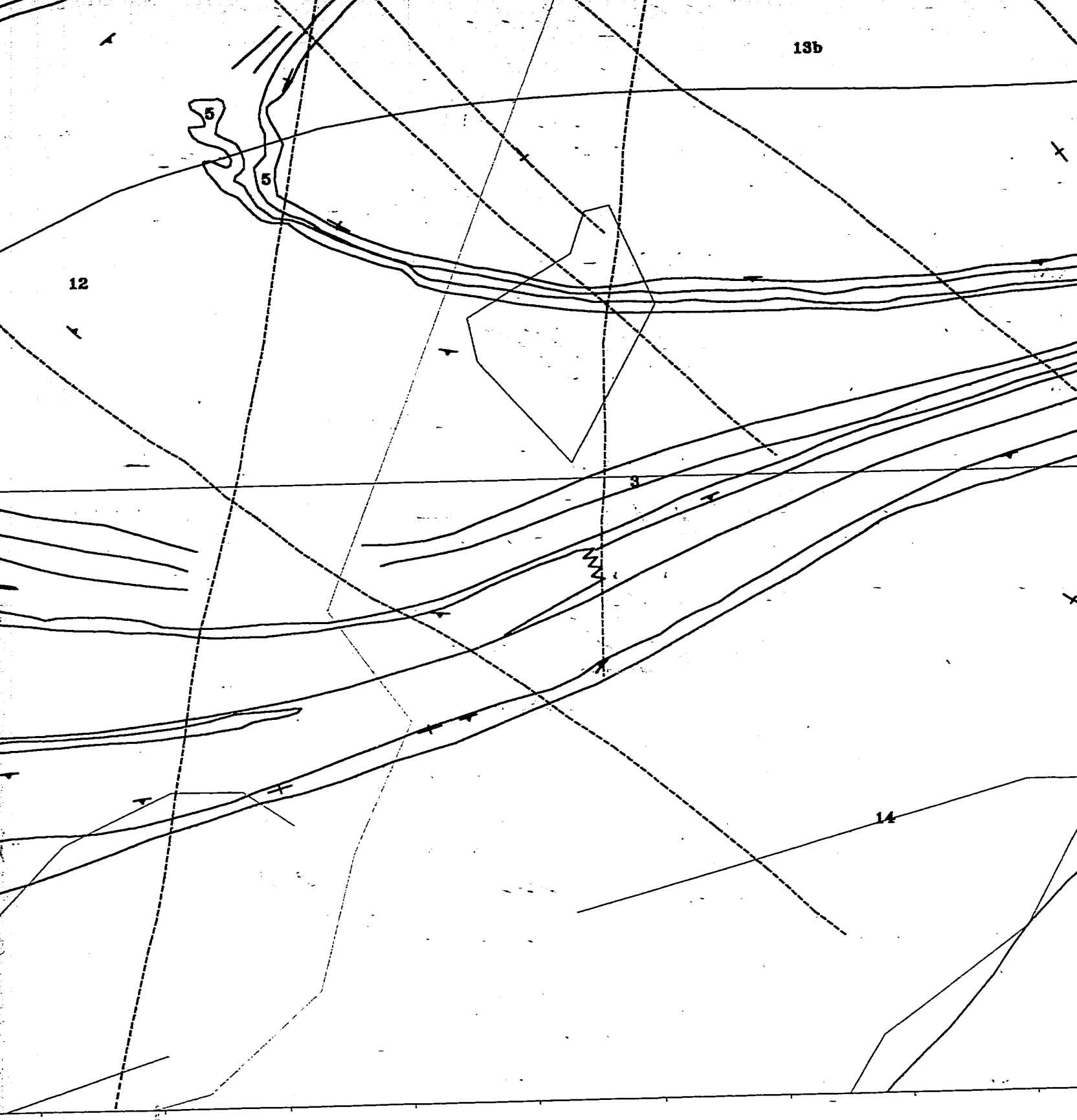

Map 6 - Magnetic Interpretation, Manitouwadge study area.

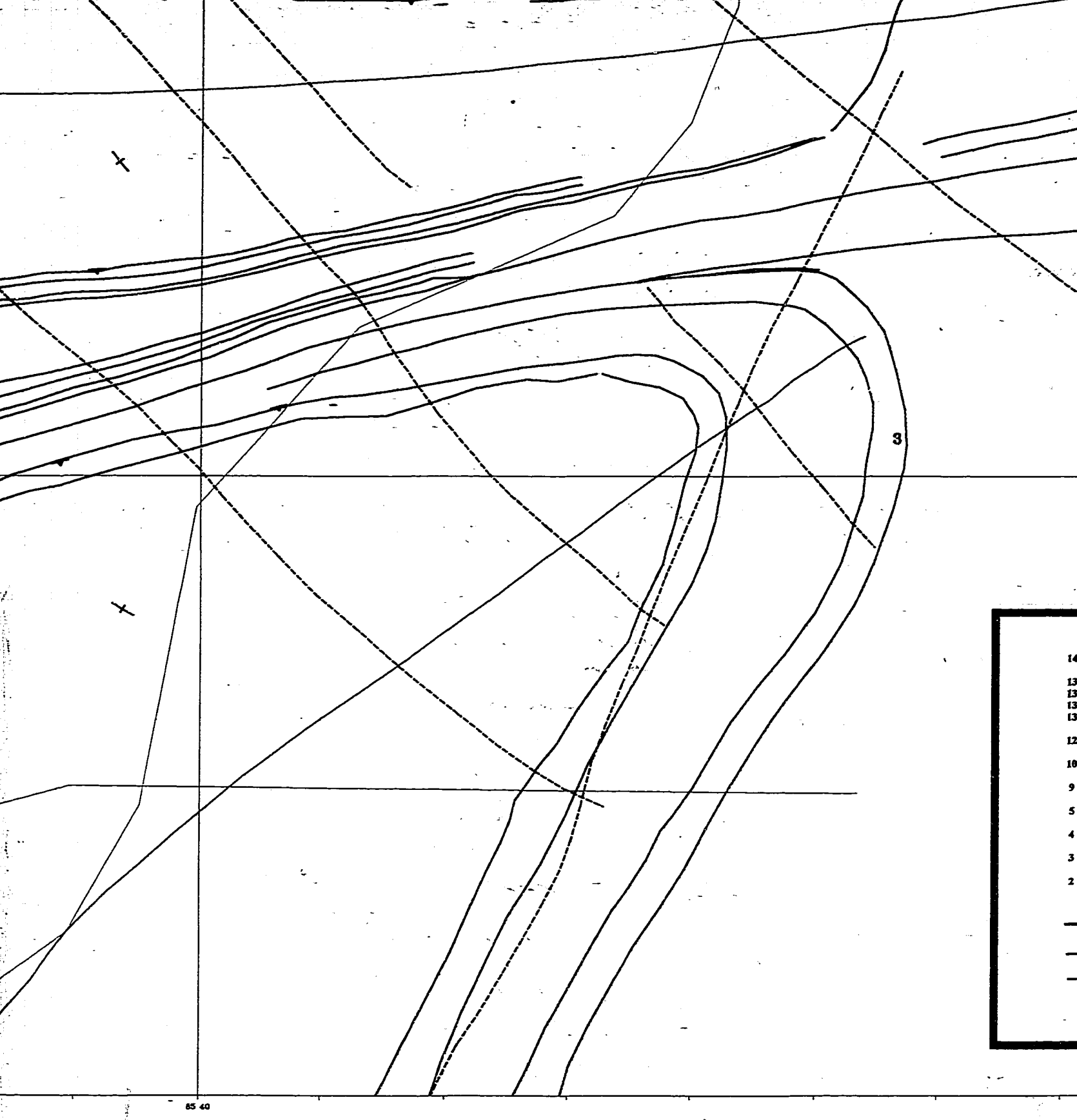
3
85 40

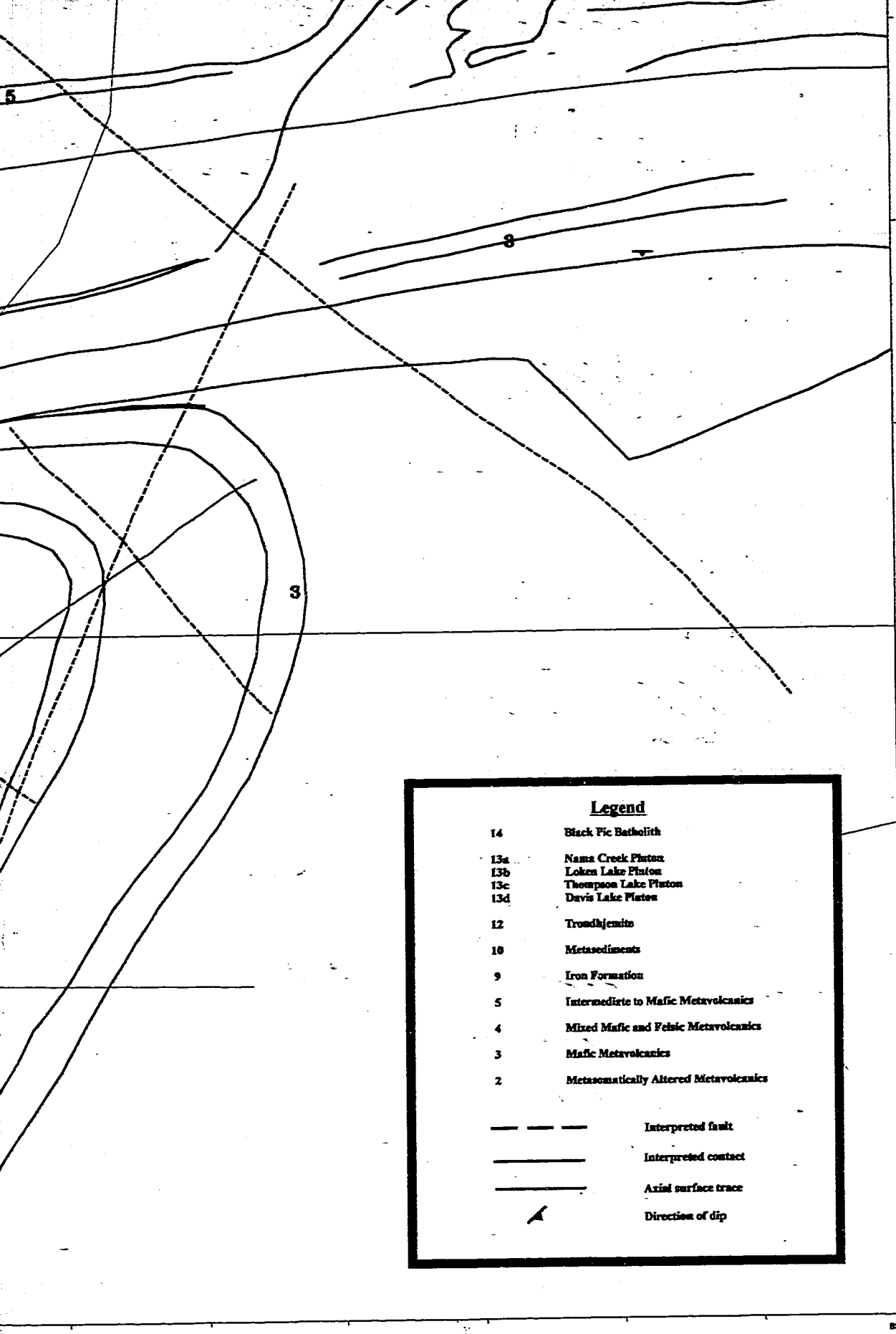

Legend

14	Black Pic Batholith
13a	Nama Creek Pluton
13b	Loken Lake Pluton
13c	Thompson Lake Pluton
13d	Davis Lake Pluton
12	Troudhjemite
10	Metasediments
9	Iron Formation
5	Intermediate to Mafic Metavolcanics
4	Mixed Mafic and Felsic Metavolcanics
3	Mafic Metavolcanics
2	Metasomatically Altered Metavolcanics

Interpreted fault

Interpreted contact

Axial surface trace

Direction of dip